Thesis presented for the degree of Doctor of Philosophy in Earth Sciences
in cotutelle between Université Jean-Monnet — Saint Etienne
Département de Géologie
&
University of Cape Town — South Africa
Faculty of Sciences — Department of Geological Sciences

CRATONIC ECLOGITE XENOLITHS — FORMATION AND EVOLUTION OF THE SUBCONTINENTAL LITHOSPHERIC MANTLE

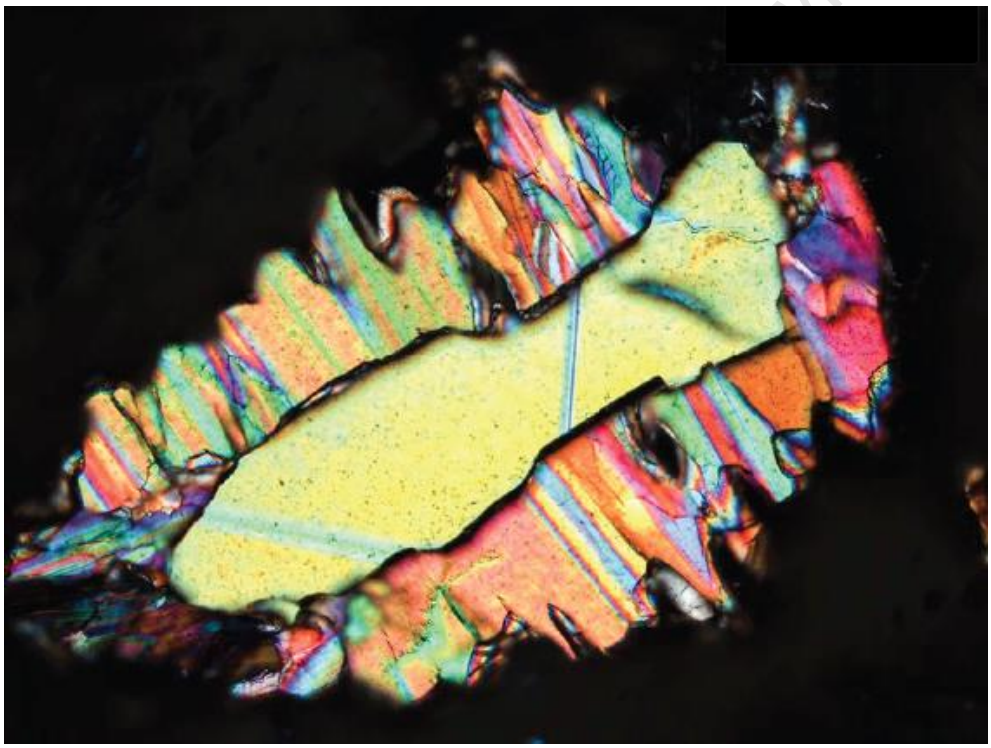

By Ioana-Bogdana RADU

April 2018

Under the supervision of **Prof. C. HARRIS, University of Cape Town**
Prof. J.-Y. COTTIN & Dr. B. N. MOINE, Université de Saint Etienne, France

N.B.: This version is to be submitted to University of Cape Town and is identical in content to the one submitted at Université Jean Monnet de Saint-Etienne

XENOLITES ECLOGITIQUES CRATONIQUES — ORIGINE ET EVOLUTION DU MANTEAU LITHOSPHERIQUE SOUS-CONTINENTAL

Soutenue en Avril 2018
devant le jury composé de:

Jean-Yves Cottin	**codirecteur**
Chris Harris	**codirecteur**
Bertrand Moine	**co-encadrant**
Michel Grégoire	**rapporteur**
Fanus Viljoen	**rapporteur**
Doritt Jacob	**rapporteur**
Gelu Costin	**invité**
Violaine Sautter	**examinatrice**
Nathalie Bolfan-Casanova	**examinatrice**

Plagiarism declaration

I know what the meaning of plagiarism and declare that all of the work in the thesis, save for that which is properly acknowledged, is my own.

Signed by candidate

Declaration of free licence

I hereby:

a) grant the University free license to reproduce the above thesis in whole or in part, for the purpose of research;

b) declare that:

I. the above thesis is my own unaided work, both in conception and execution, and that apart from the normal guidance from my supervisor(s), I have received no assistance except as stated below;

II. neither the substance nor any part of the thesis has been submitted in the past, or is being, or is to be submitted for a degree at this University or at any other University, except as stated below.

I am now presenting the thesis for examination for the Degree of PhD.

Signed by candidate

I dedicate this thesis to the memory of my grandmother,

Rîcu Constantina

TABLE OF CONTENTS

PART I

RÉSUMÉ ÉTENDU

Les éclogites sont des roches métamorphiques de hautes pressions (HP) de compositions largement basaltiques principalement associées aux zones de subductions. Les assemblages de minéraux qui les composent permet de regrouper les différents types d'éclogites en éclogites biphasées, éclogites à disthène, éclogites à coésite et éclogites à corindon. Historiquement et géographiquement, ces groupes varient dans la littérature. Le caractère « précieux » des minéraux qu'elles contiennent (grenat rose orangé à grains grossiers et roche porteuse d'omphacite verte) et leur dureté en ont fait un matériau hautement recherché. Les plus vieux indices de son utilisation remontent au Néolithique et à l'âge du Bronze dans les Alpes occidentales (D'Amico et al., 1995). De nos jours, ces pierres précieuses sont toujours utilisées grandement dans l'industrie de la pierre ornementale. Ces caractéristiques ont attiré l'attention des géologues à partir du XVIIIe siècle, ce qui a conduit aux découvertes des faciès métamorphiques (Eskola, 1920), des conditions de hautes pressions et *in fine* à une meilleure compréhension des processus de recyclage de la croute océanique dans les zones de subduction (Godard, 2001).

Les éclogites peuvent aussi être trouvées comme xénolites dans des kimberlites au sein des cratons précambriens (Hatton, 1978). Ces éclogites ont des compostions basiques à ultrabasiques et contiennent souvent des diamants. Depuis leur découverte, il y a deux cent ans, la présence de diamant au sein de ces éclogites a suscité de nombreux débats sur la pétrogenèse des roches mantelliques et leurs implications sur la formation des racines cratoniques. Pendant de nombreuse années, la genèse de ces éclogites a été base sur le consensus que les éclogites sont le résultat de la transformation subsolidus à haute pression du basalte/gabbro (Green et Ringwood, 1967a) et ainsi, que le manteau terrestre devait être fait d'éclogites en tant qu'équivalent haute pression de la croûte océanique (Fermor, 1912). Cette théorie a perduré

pendant plus de 50 ans jusqu'à ce qu'elle soit réfutée en faveur d'un manteau péridotitique (Green et Ringwood, 1967b) composé de corps éclogitiques isolés de forme inconnue.

Les éclogites cratoniques ramenées à la surface par les magmas kimberlitiques sont des échantillons uniques (> 1% des xénolites du manteau) sinon inaccessibles du manteau lithosphérique subcontinental (SCLM). Dans la littérature moderne (*p.ex*. Jacob *et al*., 2004 ; Schulze *et al*., 2000), ces éclogites cratoniques, sont vues comme la preuve la plus évidente de l'évolution de croûte basaltique primitive conservée à la base des racines continentales, de 140 à 200 km de profondeur.

Par définition, la minéralogie primaire des eclogites consiste en un assemblage minéral de haute pression : grenat (gt) + clinopyroxène omphacitique (omph). La plupart des xénolites éclogitiques comportent seulement deux ces minéraux (i.e. éclogites biphasées), avec comme phase accessoire principale le rutile. Moins fréquemment, elles peuvent contenir de la coésite (dont on observe généralement que le quartz en palissade en témoin), du diamant, du graphite, du disthène et du corindon. Peu d'échantillons montrent des textures d'exsolution telles que des lamelles topotactiques (contrôlées par la cristallographie) ; des lentilles de grenat et/ou de disthène dans du clinopyroxène, ou d'aiguilles de rutile.

Le travail présenté dans cette thèse est basé sur une collection très complète d'éclogites cratoniques, prélevées dans quatre localités principales au sein du craton Sibérien (Obnazhennaya, Udachnaya) et du craton du Kaapvaal (Jagersfontein, Roberts Victor). Les différentes xénolites éclogitiques varient en taille et en abondance entre les cratons Kaapvaal et Sibérien. À travers une collection de 208 nodules, j'ai identifié quatre principaux groupes de textures étroitement liés à leur paragenèse.

(1) Type I : éclogites biphasées dominées par des grenats arrondis avec des joints de grains dentés et une omphacite interstitielle contenant de nombreuses inclusions minérales et vitreuses. Ces échantillons ont généralement un aspect «poussiéreux» et contiennent de la

phlogopite comme principal minéral secondaire, souvent accompagné de sanidine interstitielle, rutile et une symplectite à diopside-plagioclase. Ces caractéristiques indiquent que les éclogites de Type I ont interagi avec des fluides métasomatiques dérivés de la kimberlite, précédant leur mise en place en surface.

(2) Type II : éclogites biphasées dominées par des grenats subhédraux et une omphacite avec des joints de grains nets et des fines inclusions d'aiguilles de rutile. Elles représentent un matériel "vierge" (non-métasomatique) provenant de la racine cratonique et peuvent être utilisés pour retracer la nature et l'origine du protolithe.

(3) Type III : éclogites à coésite et à disthène sont caractérisées par des grenats sub- à anhédrals et une matrice d'omphacite "spongieuse" blanche. Les reliques de coésite se trouvent sous forme de noyau xénomorphe, entourées de quartz α en palissade et associées à des veines riches en carbonates. Le disthène se présente sous la forme de grains subhédraux bleu clair, tabulaires ou arrondis. Certains échantillons montrent des signes de métasomatisme carbonaté.

(4) Type IV : éclogites à corindon ont un assemblage minéral dominé par une omphacite vert pâle (abondance modale ~ 60%), des grenats sous-idiomorphes à arrondis et du corindon subhédral rose. L'omphacite présente souvent des textures d'exsolution (lamelles fines, couronnes et chaînes granulaires). Les lamelles topotaxiales peuvent contenir du grenat, du disthène bordé de grenat ou d'un assemblage de grenat-zoïsite entrelacés. L'absence de minéraux-indice du métasomatisme ou de l'interaction avec des fluides, indique que les éclogites contenant du corindon sont donc potentiellement des échantillons "vierges" de la racine cratonique.

Les compositions chimiques associées aux observations pétrologiques offrent des informations clés sur l'origine des éclogites du manteau, en permettant de distinguer les xénolites d'éclogites métasomatisées par des fluides kimberlitiques/carbonés et les xénolites d'éclogites « vierges »

c'est à dire non-métasomatisées. Le plus souvent, l'enrichissement en alcalin indique une contribution de fluides dérivés de la kimberlite et donc la composition initiale de l'éclogite ne peut pas être retracée. Il est donc important d'analyser une large variété d'échantillons, de textures, afin d'obtenir une image complète de la gamme de compositions et des processus conduisant à la formation d'éclogites dans les racines cratoniques. Les variations de compositions des éléments majeurs dans 76 échantillons représentatifs montrent une corrélation positive globale entre Al_2O_3 et Na_2O (r = 2.03) et une corrélation négative entre MgO et Na_2O (r = -1.60) dans le clinopyroxène, associée à des grenats riches en pyrope-grossulaire.

Les eclogites de Type I ont une teneur plus élevé en Na_2O dans le grenat et K_2O dans l'omphacite. Elles comprennent une grande variété de compositions de grenat et de clinopyroxène, allant respectivement du riche en pyrope à riche en grossulaire et de riche en diopside à riche en jadéite. Les estimations géothermobarométriques montrent que le métasomatisme kimberlitique s'intensifie vers les basses pressions, mais est présent sur toute l'épaisseur de la racine.

Les éclogites de Type II comprennent deux sous-groupes dérivés de protolithes différentes. Le premier groupe (Type IIA) est plus magnésien et correspond à une zone de plus basse pression (3—3.5 GPa). Le second groupe (Type IIB) est plus sodique et alumineux et correspond à des échantillons équilibrés à plus haute pression (4—4.5 GPa).

Les éclogites à corindon et/ou disthène montrent des compositions similaires quel que soit le craton considéré et sont caractérisées par des grenats riches en grossulaire et des clinopyroxènes riches en composant jadéitique. Leurs conditions pression-température (P-T) d'équilibration sont plus élevées (4.0—7.0 GPa ; 950—1300° C) et correspondent à la partie la plus basse de la racine cratonique. Les éclogites portant le corindon montrent souvent des textures d'exsolution topotactique de grossulaire ± disthène/zoisite dans l'omphacite suggérant une diminution de la température et/ou une augmentation de la pression, bien avant l'échantillonnage par le magma kimberlitique.

Contrairement aux éléments majeurs, les compositions des éléments traces sont plus susceptibles aux changements en réponse aux variations des conditions P-T, aux interactions fluides-roches et aux processus métamorphiques. Le métasomatisme dérivé du magma kimberlitique est caractérisé par une teneur plus élevée en terres rares, en Ba, en Sr et en HFSE (High Field Strength Elements) (Gréau et al., 2011, Huang et al., 2012). L'analyse des éléments traces permet de mieux contraindre les différents types d'eclogites ainsi que la nature des différents protolithes (Neal et al., 1990). Les 62 échantillons analysés pour les compositions en éléments traces ne montrent aucune distinction marquée entre les xénolites d'éclogite du craton Kaapvaal et celles du craton Sibérien.

Les éclogites biphasiques de Type I (métasomatisées) enregistrent une gamme étroite de concentrations en LREE (Light Rare Earth Elements) et en LILE (Large Ion Lithophile Elements) dans l'omphacite et le grenat, avec des HREE (Heavy Rare Earth Elements) variables, ce qui permet de faire la distinction entre deux sous-groupes ; Type IA : grenats riches en HREE et Type IB : grenats pauvres en HREE.

Les éclogites de Type IIA (riches en MgO) possèdent une omphacite riche en LREE avec des anomalies positives en Sr, négativement corrélées dans le grenat. Les éclogites de Type IIB (pauvres en MgO), sont caractérisées par un clinopyroxène omphacitique appauvri en LREE avec des anomalies positives en Sr, négativement corrélées dans le grenat.

Les échantillons à coésite et à disthène ont des compositions en éléments traces similaires, avec généralement des spectres de distributions en REE concaves dans l'omphacite et des distribution fractionnées en LREE et plates en HREE dans le grenat adjacent. Dans l'ensemble des échantillons, le clinopyroxène est caractérisé par des inflexions positives en Eu, Sr, Pb et Hf. De même, le grenat est caractérisé par des inflexions positives en Eu et négative en Sr, Pb et Hf.

Les éclogites contenant du corindon ont des concentrations d'éléments traces significativement plus faibles par rapport aux autres types d'éclogites ou au manteau primitif et ont typiquement

des spectres de REE (Rare Earth Elements) concaves dans l'omphacite et des LREE fractionnés avec des distributions de HREE plats dans le grenat adjacent. La plupart des omphacites ont des anomalies positives en Eu et Sr, corrélées avec des anomalies positives en Eu et négatives en Sr du grenat. Dans les échantillons présentant des exsolutions lamellaires (grenat ± zoïsite) le long des plans de clivage de l'omphacite, le grenat exsolvé et (le cas échéant) la zoïsite ont des spectres fractionnés en MREE-HREE, de compositions intermédiaires entre celles du clinopyroxène et du grenat non-exsolvés. Les anomalies en Eu et Sr sont marquées à la fois dans les minéraux primaires et dans les exsolutions et sont typiquement interprété come héritées d'une protolithe riche en feldspath plagioclasique.

Des nombreuses études ont utilisé les isotopes de l'oxygène pour retracer l'histoire du protolithe des éclogites mantelliques, conduisant à une importante base de données sur les variations de $\delta^{18}O$ dans les éclogites du manteau. Néanmoins, de nombreuses études utilisent des échantillons entièrement (Garlick et al., 1971, Gréau et al., 2011, MacGregor et Manton, 1986, Schulze et al., 2000) ou partiellement métasomatisés (Riches et al., 2016). Seules quelques études ont été réalisées sur des éclogites non métasomatisées (Huang et al., 2016, Jacob et al., 2005, Viljoen et al., 2005).

Les xénolites d'éclogites étudiés comprennent à la fois des valeurs de $\delta^{18}O$ inferieures et supérieures par rapport aux valeurs admises du manteau (5.0±0.4 ‰, Mattey *et al*. (1994)) (1.1—4.8 ‰ ; 6.0—7.7 ‰ dans le grenat et 0.9—4.9 ‰ ; 6.0—7.5 ‰ dans le clinopyroxène omphacitique). Les éclogites biphasiques métasomatisées (Type I) ont des valeurs de $\delta^{18}O$ identiques ou supérieures au manteau. Parmi les éclogites biphasiques non-métasomatisés (Type II), on peut distinguer deux groupes : les $\delta^{18}O$ bas (2.3—3.9 ‰ dans le grenat) correspondent aux éclogites de Type IIB provenant de la partie inférieure de la racine cratonique, et les $\delta^{18}O$ plus haut (3.6—7.7 ‰ dans le grenat) correspondent aux éclogites de Type IIA, de la partie supérieure des formations éclogitiques. Les xénolites d'éclogites à corindon de Roberts Victor

ont des valeurs de $\delta^{18}O$ inférieures au manteau, parmi les plus faibles (1.1 ‰ valeur moyenne dans le grenat, n=4, 1σ=0.2), alors que les échantillons à corindon d'Obnazhennaya ainsi que les éclogites à disthène et à coésite ont des valeurs $\delta^{18}O$ dans la même gamme ou supérieures aux valeurs mantelliques.

Basé sur les compositions roches totales recalculées pour des éléments majeurs et traces et pour les rapports des isotopes de l'oxygène, les éclogites Type IIA et IIB, sont interprétées comme dérivant d'une croûte océanique Archéenne ou Paléoprotérozoïque de composition picritique évoluée, qui a subi une altération hydrothermale de basse à très haute température. Les éclogites de Type IIB enfouies à des profondeurs plus élevées ont probablement subi un épisode de fusion partielle avant ou pendant l'éclogitisation, menant à leurs appauvrissement en LREE. Cependant, il n'est pas clair si les deux types sont issus de la même croûte océanique, ou formés au cours de différents événements tectoniques.

Les éclogites à coésite et à disthène, d'une manière similaire aux éclogites biphasiques, montrent des anomalies positives en Sr et en Eu et, à partir de compositions de roches totales reconstituées, sont interprétées comme dérivées d'un composant gabbroïque issu d'une croute océanique, tandis que les éclogites à corindon correspondraient à un cumulat crustal à dominante pyroxénitique.

Les éclogites non-métasomatisées étudiées ont typiquement des rapports isotopiques de l'oxygène inférieurs au manteau asthénosphérique et une des éclogites à corindon de Roberts Victor a une valeur roche totale reconstruite de $\delta^{18}O$ de 1.4 ‰, qui est à ce jour le rapport le plus faible mesuré dans des éclogites mantelliques. Un agent métasomatique avec des valeurs $\delta^{18}O$ extrêmement basses, affectant la partie inférieure de la racine cratonique mais sans rééquilibration avec le manteau péridotitique environnant, est considéré comme peu probable. Il en est donc déduit que les rapports isotopiques de l'oxygène dans les éclogites non-métasomatisées sont hérités d'un protolithe d'âge Archéen ou Paléoprotérozoïque. Ceci implique

deux conséquences possibles selon lesquels les températures des interactions roche-eau de mer étaient beaucoup plus élevées et/ou que le manteau archéen avait des valeurs $\delta^{18}O$ inférieures à celles du manteau moderne.

Parmi les éclogites à corindon montrant des exsolutions topotactique de grossulaire ± disthène/zoïsite dans l'omphacite, et basé sur des profils de diffusion préservés pour Si, Al et Mg. J'ai interprété la composition des exsolutions comme étant contrôlée par des échanges dans un système isochimique. Cette interprétation est également soutenue par le fractionnement variable des HREE entre les grains exsolvés et l'omphacite hôte. La formation de la zoïsite (1.7% H_2O) à partir d'un clinopyroxène précurseur nécessite une quantité importante d'hydrogène (sous forme de H_2, OH^- ou H_2O) incorporée dans l'omphacite à hautes pressions.

Les minéraux nominalement anhydres (NAMs) du manteau supérieur, comme le clinopyroxène, pourraient incorporer plus d'eau que le grenat, l'olivine et l'orthopyroxène à hautes pressions (Bell et Rossman, 1992, Kovacs et al., 2012, Peslier, 2010). Par conséquence, l'abondance du clinopyroxène dans le SCLM peut jouer un rôle déterminant dans la distribution de l'eau au sein du manteau supérieur (Ingrin et Skogby, 2000). Jusqu'à présent, l'accès limité aux xénolites d'éclogite non-métasomatisées a rendu la détermination de leur capacité de stockage en eau mal contrainte. L'hydrogène peut être incorporé dans le clinopyroxène omphacitique comme OH^-, H_2 et H_2O. L'eau stockée sous forme d'hydroxyle est généralement structurellement liée à des défauts ponctuels (substitution d'atomes interstitiels ou structuraux, lacunes atomiques), linéaires (dislocations dans des réseaux déformés), défauts planaires (joints de grains) et de volume (inclusions associées à un cluster de points) et caractérisé par différentes bandes d'absorption dans le spectre infrarouge. L'incorporation d'eau ou d'hydrogène moléculaire (H_2O et H_2) est par contre encore mal contrainte et peut être drastiquement influencée par des facteurs d'oxydo-réductions tel que la stabilité du fer ferrique dans l'omphacite (composant jadéite).

Basé sur les analyses FTIR d'hydrogène type OH^-, la teneur en eau calculée dans les omphacites d'Obnazhennaya varie entre 929 et 1413 ppm en utilisant le coefficient d'absorption de Koch-Müller et al. (2007) et 1576—2398 ppm lors de l'utilisation du coefficient de Bell et al. (1995). Les grenats analysés par FTIR ne contiennent pas d'eau détectable. La teneur total en H_2O mesurée par ERDA est de ~1173 ± 38 ppm wt. dans les mêmes gammes de valeurs que l'estimation FTIR pour l'omphacite de l'échantillon Obn112/13. La teneur totale en eau mesurée par SIMS, basée sur le rapport H^+/Si mesuré dans l'omphacite de l'échantillon Obn110/13 varie entre ~3870 et 6170 ppm, en accord avec les résultats obtenus par TC/EA-MS, qui donnent une estimation de 2750—5400 ppm wt.

L'omphacite provenant des éclogites de Roberts Victor montre des bandes d'absorption FTIR similaires aux échantillons d'Obnazhennaya, mais avec des estimations d'eau significativement plus faibles. La teneur en eau calculée varie entre 124 ppm et 609 ppm lorsqu'on utilise le coefficient d'absorption de Koch-Müller et al. (2007) et entre 130 ppm et 1191 ppm lors de l'utilisation du coefficient de Bell et al. (1995). Les estimations d'eau totale mesurées par l'ERDA sont légèrement plus élevées (130—632 ppm wt. par FTIR et 428-795 ppm wt. par ERDA), tandis que les estimations totales par TC/EA-MS sont approximativement entre 2 et 20 fois plus élevées (1230—5500 ppm wt.).

Il en est déduit que la différence entre les méthodes utilisées pour la quantification de l'hydrogène peut être due à la nature intrinsèque de chaque technique et/ou aux différentes quantités d'eau structurelle et moléculaire dans l'omphacite.

La teneur recalculée en eau totale des roches varie entre 72 et 953 ppm wt. H_2O dans les éclogites de Roberts Victor et 459-1367 ppm dans les éclogites d'Obnazhennaya, calculés en utilisant les estimations d'hydroxyle, ou entre 241—4400 ppm et 633—3132 ppm respectivement, en utilisant les estimations totales TC/EA-MS. Les plus faibles estimations de l'eau (basées sur l'analyse FTIR) pour les éclogites mantelliques sont généralement supérieures à

la teneur maximale mesurée dans les péridotites environnantes, estimée entre <1 et 394 ppm wt. sous le craton Sibérien et entre 0 et 200 ppm wt. sous le craton Kaapvaal.

Cela implique que, malgré le fait qu'elles représentent seulement une petite fraction du manteau supérieur, les éclogites mantelliques peuvent constituer un réservoir majeur d'eau sur Terre. En outre, ces hautes teneurs en eau dans le SCLM ont des conséquences majeures sur la résistance mécanique des minéraux, la stabilité des racines cratoniques (Li et al., 2008), sur la diffusion des éléments, la déformation et la rhéologie du manteau lithosphérique (Kohlstedt, 1996), sur la fusion partielle, la conductivité thermique et électrique (Karato, 1990) ainsi que sur le cycle global de l'eau et son recyclage dans les zones de subduction.

ABSTRACT

The most extensive evidence for the evolution of the primitive crust is preserved at the base of the continental roots (140 to 200 km depth). However, this is completely inaccessible and hard to evaluate, except through the study of mantle xenoliths brought to the surface by kimberlite magmas. Most mantle xenoliths undergo kimberlitic/carbonaceous metasomatism prior to their entrapment, altering their primary composition. Despite a very complex history and a very low abundance (<1 % mantle xenoliths), cratonic eclogites are the oldest relics of the ancient crust and unique in allowing us to decipher the composition and evolution of the early continents.

This study is based on the most complete existing collection of cratonic eclogites (>180 nodules), sampled in four main localities from the Siberian (Obnazhennaya, Udachnaya) and South African (Jagersfontein, Roberts Victor) cratons. Major and trace element compositions have been analysed in representative bimineralic (garnet (gt)-omphacite (cpx)), coesite-, kyanite- and corundum-bearing eclogites. Metasomatized eclogites (Type I) have a higher alkali- (Na_2O in garnet and K_2O in omphacite) and LREE, LILE-content. Non-metasomatized (Type II) eclogites include two main compositional groups, derived from different protoliths. The first group (Type IIA) is typically more magnesian, enriched in LREE and has $\delta^{18}O$ values from 3.73 to 7.50 ‰, with positive Sr anomalies and corresponding to a low pressure-temperature layer. The whole-rock composition is consistent with a basaltic protolith. The second group (Type IIB) is more sodic and aluminous, depleted in LREE and has $\delta^{18}O$ values of 2.35 to 3.59 ‰, corresponding to equilibrium at high pressure and temperature. The whole-rock trace element composition is consistent with a pyroxenitic protolith. Eclogites that contain coesite, kyanite and corundum (coe-ky-cor) are typically characterized by jadeite-rich clinopyroxenes with positive Eu and Sr anomalies and grossular-rich garnets with corresponding positive Eu and negative Sr anomalies. Additionally, corundum-bearing samples are overall LREE-depleted. Pressure-

temperature estimates indicate coe-ky-cor-bearing eclogites equilibrated in the lowermost part of the cratonic keel, and the reconstructed whole-rock trace element composition corresponds to a very depleted gabbroic protolith.

Corundum-bearing eclogites often show topotactic exsolution textures hosted in omphacite, consisting of a more calcic garnet ± kyanite/zoisite. Based on Si, Al and Mg diffusion profiles it can be inferred that exsolution was controlled by chemical exchange in an isochemical system. Similarly, an interpretation can be made for the variable HREE fractionation of intermediate composition between the exsolutions and the host omphacite, as evidence for intermineral partitioning. The formation of zoisite (1.7 % H_2O) from a precursor clinopyroxene requires a significant amount of hydrogen (as H^+, OH^- or H_2O) incorporated in omphacite at mantle conditions. Calculated water content of omphacite, based on Fourier transform infrared spectrometry (FTIR) analyses, varies from ~930—1410 to ~1100—1680 ppm by weight H_2O, according to different absorption coefficients. Primary garnets are typically anhydrous (<7 ppm H_2O), whereas coarse exsolutions contain between 165—1950 ppm H_2O. Reconstructed estimates for whole-rock water content (~310—890 ppm H_2O) for the Obnazhennaya eclogites are significantly higher than those of the surrounding peridotites.

The variability of $\delta^{18}O$ in garnet among 41 xenoliths, shows a bi-modal distribution with median values at 3.57 ‰ and 5.68 ‰ and strong correlation (r = 0.96) between garnet and omphacite. The $\delta^{18}O$ values and the reconstructed whole-rock trace element compositions indicate an oceanic crustal protolith for mantle eclogite xenoliths. This is consistent with the subduction of a hydrothermally altered, basaltic to websteritic sequence of an incompatible-element-depleted oceanic crust.

Furthermore, although eclogites represent a small fraction of the upper mantle, they may be an important water reservoir at the base of the cratonic root. High water content in the lithospheric mantle would have major consequences for the longevity of the cratonic keel, for

physical and chemical properties in minerals, partial melting, mantle rheology and electrical conductivity and the global water cycle.

CHAPTER I.

INTRODUCTION

CHAPTER I. INTRODUCTION

1.1. Eclogites from the mantle: classification and petrogenesis

Eclogites are meta-igneous rocks characterized by a broadly basaltic composition; nevertheless their defining mineral assemblage and ideas of their petrogenesis has varied historically and geographically. Their beauty (coarse-grained orange-pink garnet and green omphacite – bearing rock) and hardness made them a common material used during the Neolithic-to-Bronze age in the western Alps (D'Amico et al., 1995) and, more recently, in the ornamental stone industry. The same beauty and particular mineral association has drawn the attention of geologists beginning with the XVIII century and has led to several discoveries such as high-pressure metamorphism of igneous rocks, the concept of metamorphic facies and the better understanding of Earth's interior and crustal recycling through subduction (Godard, 2001). Two centuries later since their first account, the association of eclogites with diamonds as xenoliths entrapped in kimberlitic pipes, has opened a new series of ongoing debates, concerning the petrogenesis of mantle eclogites and their implications for cratonic root formation.

1.1.1. Short history of eclogites

The first recorded description of an eclogite is that of Horace-Bénédict de Saussure in his *Voyages dans les Alpes*. He mentions a beautiful dense rock, not yet documented, constituted of garnet crystals in a green matrix made of jade and schorl (it should be noted that Saussure used the term "schorl" for any dark to green prismatic mineral, including amphibole, pyroxene and tourmaline (Godard, 2001)). He firstly described this in the vicinity of Geneva in Switzerland and later close to Chamonix, France and Montjovet, Italy: «we encounter rocks composed of a mixture of dark green schorl as glimmering needles and red garnet as mass or confusedly

crystallized. This stone seems in the sun to be of the utmost beauty» («*on rencontre des roches composés d'un mélange de schorl verd foncé en aiguilles brillantes & de grenat rouge en masse ou confusément crystallisé. Cette pierre paroît au soleil de la plus grande beauté.* »; (Saussure, 1779-1796)). At about the same time, a similar description was made by Déodat Gratet de Dolomieu: «we sometimes encounter in the primitive mountains, masses of rocks, of which one portion presents, for example, the contexture of schorl and on the other, that of garnet. The transition from one to the other, more or less suddenly, is not determined by a change in the rock composition; the results of the analysis are same for both parties; but on one hand it is the schorl, which has been the active and modifying substance, and on the other the garnet, and in the general mass the molecules of the two substances are almost equally mixed. » («*on rencontre quelquefois dans les montagnes primitives des masses de roches dont une portion présente, par exemple, la contexture de schorl, & l'autre celle du grenat. La transition de l'un à l'autre, plus ou moins subite, n'est pas déterminée par un changement dans la composition de la roche; les résultats d'une analyse sont les mêmes pour les deux parties; mais d'une côté c'est le schorl qui a été la substance active & modifiante, & de l'autre le grenat, &dans la masse en général les molécules des deux substances se trouvent mêlangées à-peu-près en égale quantité.*»;(Dolomieu, 1794)). It was only two decades later, that Abraham Gottlob Werner introduces the term "omphacite" (*«omphazit»*) as a replacement of the previously used smaragdite or dialage (by Saussure), from the Greek "omphax", as an analogy between the mineral and green unripen vine grapes. He signals its occurrence in association with "noble garnet and sky-blue cyanite" (kyanite) in rocks from the Saualpe, Austria and Zethau, Germany (*«mit edlem granat, eiene auch mit himmelblauem cyanit*»; (Werner, 1817)).

The notion of "eclogite" was introduced in 1822, by René-Just Haüy in his book *Traité de minéralogie*: «diallage can be found in three primitive rocks (…) In the former, diallage is considered the main mineral, and forms, with the garnet, a binary association to which kyanite, quartz, epidote and lamellar amphibole can be unevenly added. I have given to this rock the

name of eclogite, which means choice, election, because its constituents, which do not normally coexist together in primitive rocks, as do the feldspar, mica and amphibole, seem to have chosen themselves to form a distinctive association. This rock can be found in Carinthia, Saualpe and Styria, Austria. (*«La diallage fait partie de trois roches primitives, (...) Dans la première, la diallage est considérée comme faisant la fonction de base, et forme avec le grenat une combinaison binaire à laquelle sont censés s'unir accidentellement le disthène, le quarz, l'épidote et l'amphibole laminaire. J'ai donné à cette roche le nom d'éclogite, qui signifie choix, élection, parceque ses composans, n'étant pas de ceux qui existent communément plusieurs ensemble dans les roches primitives, comme le feldspath, le mica, l'amphibole, semblent s'être choisi pour faire bande à part. Cette roche se trouve en Carinthie, dans le Sau-Alpe, et en Styrie.»*;(Haüy, 1822-1823)). Later on, Lacroix (1891) elaborated one of the first graphic records of eclogite mineral assemblage, showing retrogressed kelyphitic and symplectitic textures (Figure I—1).

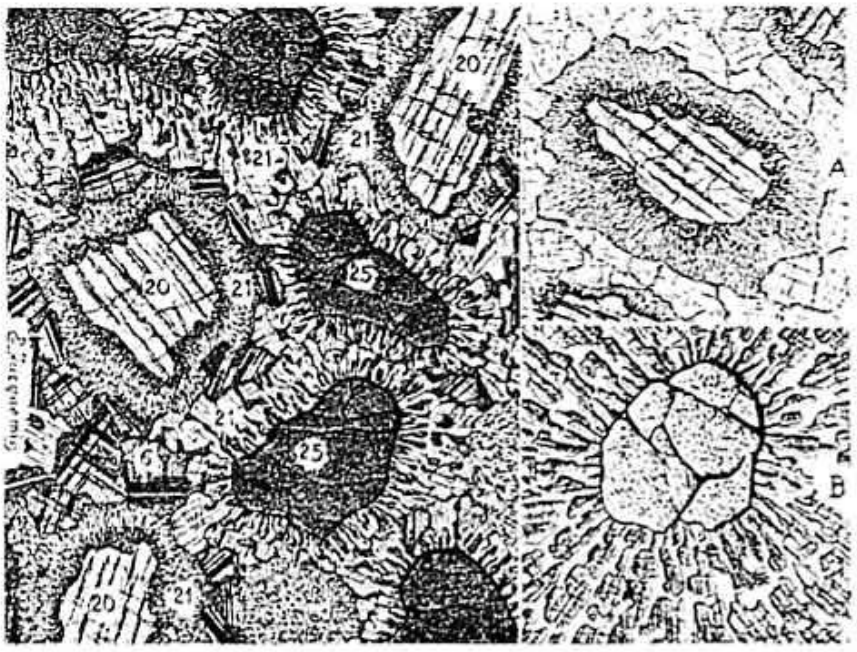

Figure I—1. Retrogressed textures in eclogites, after Alfred Lacroix (1981); one of the first graphic records of eclogite rocks. Garnet (25) is surrounded and consumed by an amphibole-plagioclase keliphitic rim (21) in an omphacitic mass (20) partially replaced by a fine pyroxene-plagioclase symplectite.

The later development of mineralogy and geochemistry allowed defining omphacite as a solid solution between jadeite and diopside. This was first recorded by Ludovic Mrazec in 1898 in his *Notes on jadeite from the Piedmont:* «A white pyroxene of similar chemical composition, found in an eclogite enclosed in the serpentine tuff of Jagersfontein (South Africa) (…) the

composition of the jadeite can vary and come close to that of the diopside, with which it shares all optical properties. (…) Since isomorphic mixtures can be formed in all possible proportions between the diopside and the jadeite terms, there will be varieties of pyroxene approaching diopside (omphacite) or jadeite.» (*«Un pyroxene blanc de composition chimique analogue, qui se trouve dans une eclogite enclavée dans le tuf serpentineux de Jagersfontein dans la republique d'Orange. (…) la composition de la jadeite peut varier et se rapprocher de celle du diopside dont elle partage d'ailleurs toutes les proprieties optiques. (…) Comme les melanges isomorphes se peuvent former dans toutes les proportions possibles entre le terme diopside et le terme jadeite, il existera des varieties de pyroxene se rapprochant du diopside (omphazite) ou de la jadeite.»*;(Mrazec, 1898)).

The defining mineral assemblage and petrogenesis has continued to be the subject of debate and, for many years, some geologists considered eclogites as metamorphic rocks according to the German and Austrian school, while others classified them as magmatic rocks, according to the Scandinavian theorists. This is due to their basaltic bulk rock composition and mineral assemblage, which could equally form through crystallization within the mantle or at deep crustal conditions. The connection between the two compositionally similar, yet mineralogically different rocks has been first made by Friedrich Becke who concluded that eclogite are the high pressure equivalent of gabbro. Subsequently Eskola further developed the concept of metamorphic facies, with the introduction of pressure in addition to temperature as a new independent, intensive variable. This allowed distinguishing between eclogites and eclogite-facies rocks, *i.e.* "olivine- and enstatite-rocks, olivine-pyrope-rocks, eclogites, chloromelanites and jadeitites" (Eskola, 1920).

The progress in experimental petrology and geochemistry over the years has led to the broad recognition of eclogites as the plagioclase-free, high-pressure product of metamorphosed mafic rocks, containing more than 75% vol. of omphacitic clinopyroxene and pyrope garnet as major constituents, with neither amounting to more than 75% of the rock by volume (International

Union of Geological Sciences Subcommission on the Systematics of Metamorphic Rocks). Nevertheless, confusion persists and often, garnet pyroxenites or grosspydites (grossular-clinopyroxene-kyanite) are misclassified as eclogites of high-pressure magmatic origin.

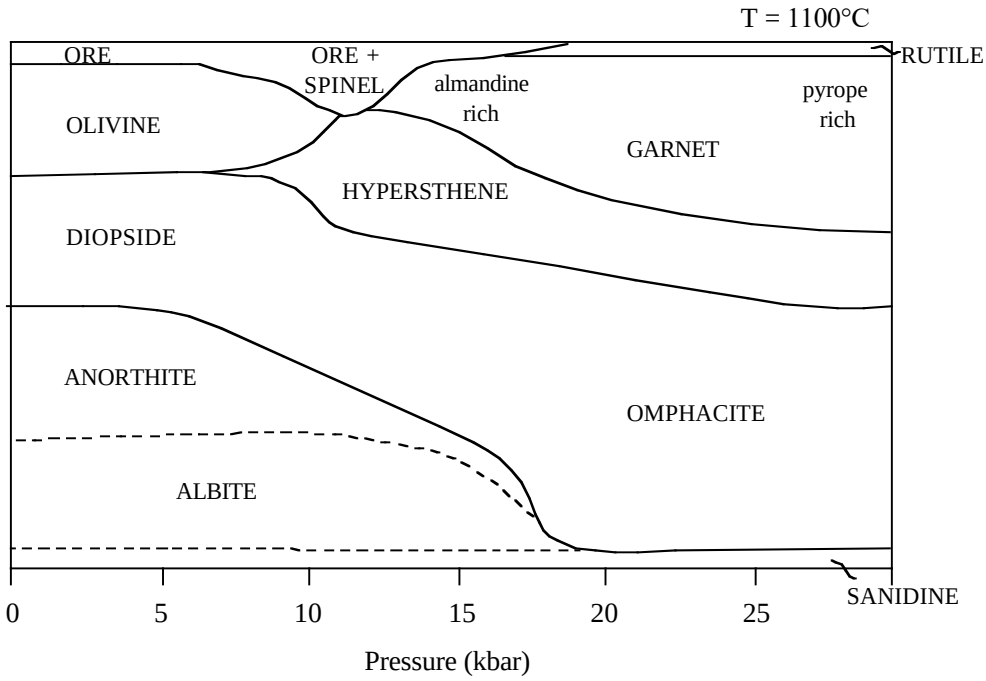

Figure I—2. Modal diagram showing variations in mineralogy with change in pressure, at 1100°C in a alkali olivine basalt composition, after Green and Ringwood (1967a).

The study of mantle eclogite began at the end of the XIX century, when eclogite xenoliths were found along with peridotites in diamond-bearing kimberlite. Their presence as xenoliths associated with diamonds indicates great depth of origin. According to the general consensus, eclogites have a basaltic composition and the subsolidus high-pressure transition of basalt/gabbro into eclogites (Figure I—2) has been demonstrated by Green and Ringwood (1967a). This has led to the hypothesis that the Earth's mantle is made of eclogites as high-pressure equivalent of basaltic crust (Fermor, 1912) («At present, petrologists regard the plutonic rocks, such as granite and gabbro, as the most deep seated known rocks. But, under the effects of enormous pressures, the granites should become garnetiferous and the gabbros be converted into eclogites, and the conclusion seems inevitably to follow that beneath the rocks now known as plutonic there must be a zone of garnetiferous rocks extending downwards in a plastic-solid form as far as the presumed metallic core of the earth.»;). This theory lasted for 50 years until it has

been disproved in favour of a dominantly peridotitic mantle (Green and Ringwood, 1967b) with isolated eclogites of unknown form.

1.1.2. Textural and compositional classifications

The first classification of eclogites (Table I) was made by Coleman et al. (1965) and divides them into three groups, based on their chemistry and type of occurrence (Figure I—3). Group A eclogites are found as inclusions in kimberlites, basalts or layers in ultramafic rocks and are interpreted as upper mantle material. They are characterized by pyrope-rich garnets (>55% vol.) and diopside-rich omphacites and may contain diamonds. Their bulk composition is similar to that of olivine basalts and they are believed to be of deep-seated igneous or metamorphic origin.

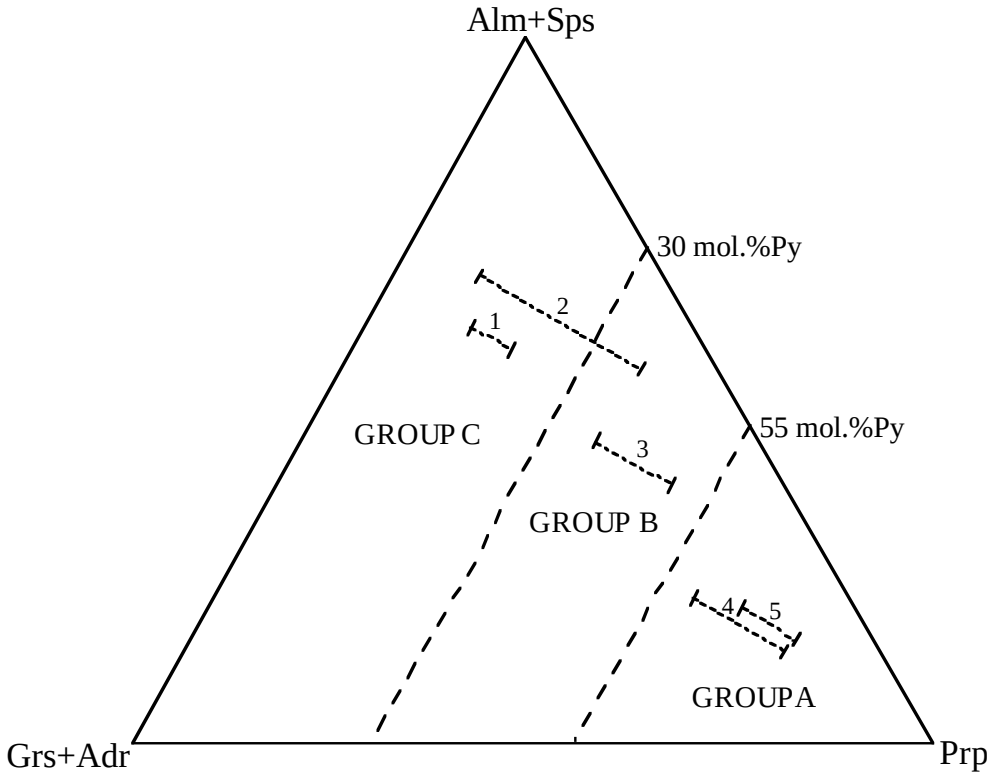

Figure I—3. Ternary diagram showing relative proportions of garnet end-members Alm = Almandine; Sps = Spessartine; Prp = Pyrope; Grs = Grossular; Adr = Andradite. 1—garnets from amphibolites; 2— garnet from charnockites and granulites; 3—garnets from eclogites in gneissic or migmatite metamorphic terrains; 4—garnets from eclogites found in kimberlite pipes; 5—garnets from eclogites within mafic rocks (i.e. dunite; peridotite). Figure after Coleman et al. (1965).

Group B eclogites are found as bands or lenses within migmatite gneissic terrains and are characterized by garnet (30—55% pyrope) and omphacite of intermediate composition. Group C eclogites are found as bands or lenses within alpine-Type metamorphic rocks and are characterized by pyrope-poor garnets (<30% vol.) and jadeite-rich omphacites. Group B and C eclogites have bulk composition similar to that of tholeiitic basalts and are interpreted to represent recrystallized material in deep orogens.

	MacGregor & Carter 1970	Hatton 1978	Jagoutz et al. 1984	McCandless & Gurney 1989	Huang et al. 2012		Radu et al. 2017
Group I	Coarse-grained, sub-hedral to rounded pyrope- xenomorphous, interstitial diopside Na_2O-rich garnet; K_2O-rich bulk Ky and Bimin.	Altered	Group A poikilitic textures ↑ bulk LREE, ↓ bulk HREE; $\delta^{18}O$ 7.2-7.3 ‰	Large, cloudy subhedral to rounded gt clinopyroxene matrix ≥ 0.09 wt% Na_2O garnet ≥ 0.08 wt% K_2O clinopyroxene	Type I - Metasomatized Coarse-grained, subhedral to rounded garnets, with irregular boundaries, in a matrix of xenomorphous to interstitial clinopyroxene many fluid inclusions - "dusty aspect" interstitial phlogopite, sulphides and rutile ≥ 0.09 wt% Na2O garnet ≥ 0.08 wt% K2O clinopyroxene	Type IA least altered, high FeO (>17 wt%) in garnet Type IB increasingly more altered; lower FeO (≤17 wt.%) in garnet Type IK most altered; CaO-rich garnets; jadeite-rich clinopyroxene (41-55%)	Type I - metasomatized In general agreement with Huang et al. 2012
Group II	Irregular, anhedral, pyrope-; interlocked jadeite Na2O-poor garnet, K_2O-poor bulk Oriented rutile inclusions	Fresh	Group B interlocking fabric rutile exsolutions $\downarrow_{bulk}$ LREE, $\uparrow_{bulk}$ HREE; $\delta^{18}O$ 4.1-5.7 ‰	Interlocking texture; anhedral gt + cpx; less altered < 0.09 wt% Na_2O garnet < 0.08 wt% K_2O clinopyroxene	Type II - Non-metasomatized Interlocking texture of garnet and clinopyroxene, delimited by straight grain boundaries fresh aspect. Rutile needle-like inclusions Rare interstitial phlogopite and/or spinel. < 0.09 wt% Na_2O garnet < 0.08 wt% K_2O clinopyroxene	Type IIA high-MgO in garnet (>12 wt%) Type IIB low-MgO in garnet (<12wt.%)	Type II - non-metasomatized In addition to Huang et al.2012 includes kyanite-bearing eclogites

Table I. Summary of geochemical and textural classifications of mantle eclogites.

Similarly, MacGregor and Carter (1970) divided eclogite xenoliths at Roberts Victor into two groups. The first group is characterized by coarse-grained, subhedral to rounded, pyrope-rich garnet, with higher NiO, Li_2O and Na_2O concentrations. The adjacent clinopyroxene is xenomorphous and interstitial, diopside-rich, with higher FeO and MnO content. The bulk rock composition has higher K_2O and Cr_2O_3 and lower CaO concentration. This group is further subdivided into kyanite and/or rutile-bearing and bimineralic and is interpreted to be the resulted cumulate of fractional crystallization in a high-pressure magma. The second group is characterized by irregular, anhedral, pyrope-poor garnets, significantly less altered, with lower Ni, Li and Na_2O content. The adjacent clinopyroxene is jadeite-rich, and lower FeO and MnO content, and it describes a tightly interlocking fabric. The bulk composition has higher CaO and lower K_2O and Cr_2O_3 concentration and often both garnet and clinopyroxene exhibit oriented

inclusions of rutile. The second group is interpreted as the product of the residual, successively cooled sets of liquids.

The first documented detailed description of eclogite xenoliths (nodules) was made by Hatton (1978). From a suite of 750 samples of mantle xenoliths from the Roberts Victor kimberlite in South Africa, he concluded that more than 95% are represented by eclogite, in agreement with the previous observations by MacGregor and Carter (1970). Their unusually high abundance in the xenolith suite has subsequently made Roberts Victor mine the unofficial type locality for mantle eclogites. Hatton identified three textural categories of eclogites associated to different petrogenetic processes, derived from a magmatic origin. He interpreted megacryst-bearing eclogites as the product of differential crystallization in a volatile-rich portion of eclogite magma, where clinopyroxene megacrysts are entrapped in bimineralic eclogites. Secondly, inhomogeneous kyanite-bearing eclogites were interpreted as the product of an immiscible liquid within the eclogite magma. Lastly, he interpreted chrome-rich eclogites as the product of a garnet lherzolite-derived melt, with variable volatile content during crystallization, accounting for their high compositional variability. Among the studied samples, Hatton also identified garnet websterites (Figure I—4), previously misclassified as orthopyroxene-bearing eclogites, as well as diamond and graphite-bearing eclogites. His observations supported the classification by MacGregor and Carter (1970) to which he added the importance of volatile and thermal input variability as cause for the observed textural diversity. Thus he inferred a low volatile content and high temperature melting would produce larger, homogeneous eclogite bodies, which he referred to as “Type I”, whereas high volatile content and low temperature melting would lead to heterogeneous eclogites which he named “Type II”.

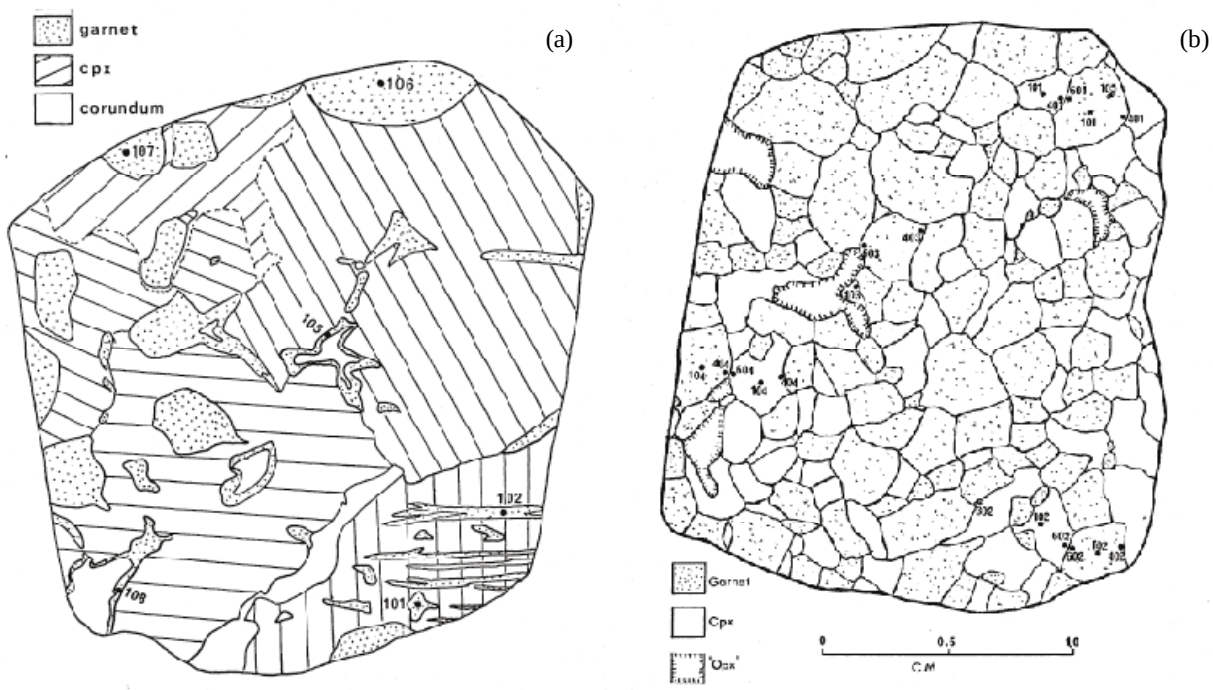

Figure I—4. Sketch of Roberts Victor xenoliths from Hatton (1978) showing different mineral assemblages and textural types: (a) Type II garnet websterite and (b) corundum eclogite.

In addition to major element chemistry, Jagoutz et al. (1984) identified two distinct eclogite Types based on trace elements and oxygen isotope analysis in mineral separates from Roberts Victor (South Africa) and Vissuri (Tanzania). Group A eclogites are characterized by poikilitic texture, with Ca-rich clinopyroxene showing orthopyroxene exsolution lamellae. They are overall LREE enriched and HREE depleted and show positive Eu-anomaly and 7.2—7.3 ‰ whole rock $\delta^{18}O$ values. Group B eclogites are characterized by an interlocking fabric and rutile exsolutions in both clinopyroxene and garnet. They are strongly LREE depleted and HREE enriched and reconstructed whole rock $\delta^{18}O$ values that range from 4.1—5.7 ‰. The study by Jagoutz et al. (1984) to some extent combines the previous interpretations of eclogite xenoliths and proposed a model based on magmatic differentiation at shallow depths within a subducting segment of lithosphere. The resulting felsic and mafic protoliths, previously hydrothermally altered, are subsequently metamorphosed into Group A and Group B eclogites respectively.

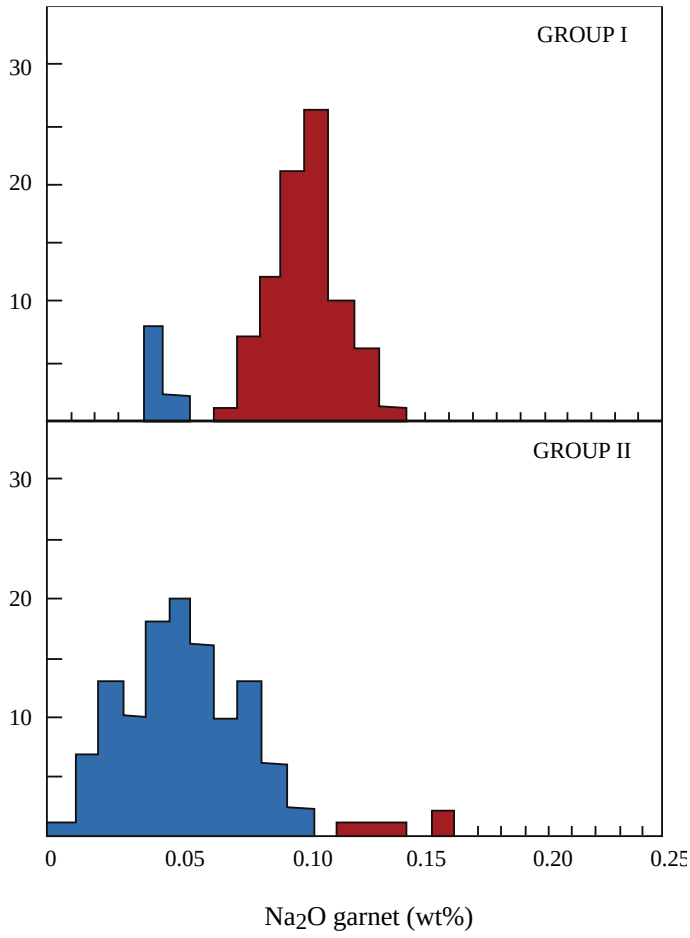

Figure I—5. Histogram showing sodium distribution in garnet in eclogite xenoliths from Roberts Victor kimberlite. (a) Group I eclogites have predominantly High Na_2O in garnet and represent metasomatized eclogites (red); (b) Group II eclogites have predominantly Low Na2O in garnet and represent non-metasomatized (pristine) eclogites (blue). After McCandless and Gurney (1989).

Integrating the two textural groups identified by MacGregor and Carter (1970) along with Hatton (1978) observations, McCandless and Gurney (1989) constrained eclogite xenoliths from Roberts Victor mine into two main groups (Figure I—5). Group I eclogites are characterized by clinopyroxene with values of or above 0.08wt.% K_2O and ≥ 0.09wt.% Na_2O in garnet, whereas eclogites with the lesser contents are referred to as Group II which have been subsequently interpreted by Gréau et al. (2011) as metasomatized by kimberlite-derived fluids and non-metasomatized material respectively. This classification is a stepping-stone in the study of eclogite xenoliths as it is applicable to more than 90% of the eclogite suite (McCandless and Gurney, 1989) and allows identifying pristine compositions, which are the only ones that can allow retracing the nature of the protolith and the petrogenesis of mantle eclogites.

This classification has been subsequently refined by Huang et al. (2012) who distinguished five textural and compositional eclogite groups (IA, IB, IK, IIA, IIB; Figure I—6). Type I eclogites are characterized by coarse-grained subhedral to rounded garnets, with irregular grain

boundaries, in a matrix of xenomorphous to interstitial clinopyroxene. Abundant fluid inclusions give them a “dusty” appearance. Accessory minerals such as phlogopite, sulphide and rutile are found both as inclusions and along grain boundaries and compositionally they are enriched in incompatible elements. From Type IA to Type IB and Type IK, eclogites show broader alteration. Type IA is characterized by high FeO content (>17 wt.%) in predominantly pyrope-almandine-rich garnets. The adjacent omphacite has low jadeite (10—30%) and high enstatite (14—26%) contents and has $\delta^{18}O$ values range from 4.9 ‰ to 7.3 ‰. Type IB eclogites are characterized by lower FeO content (≤ 17 wt.%) in typically pyrope rich garnets.

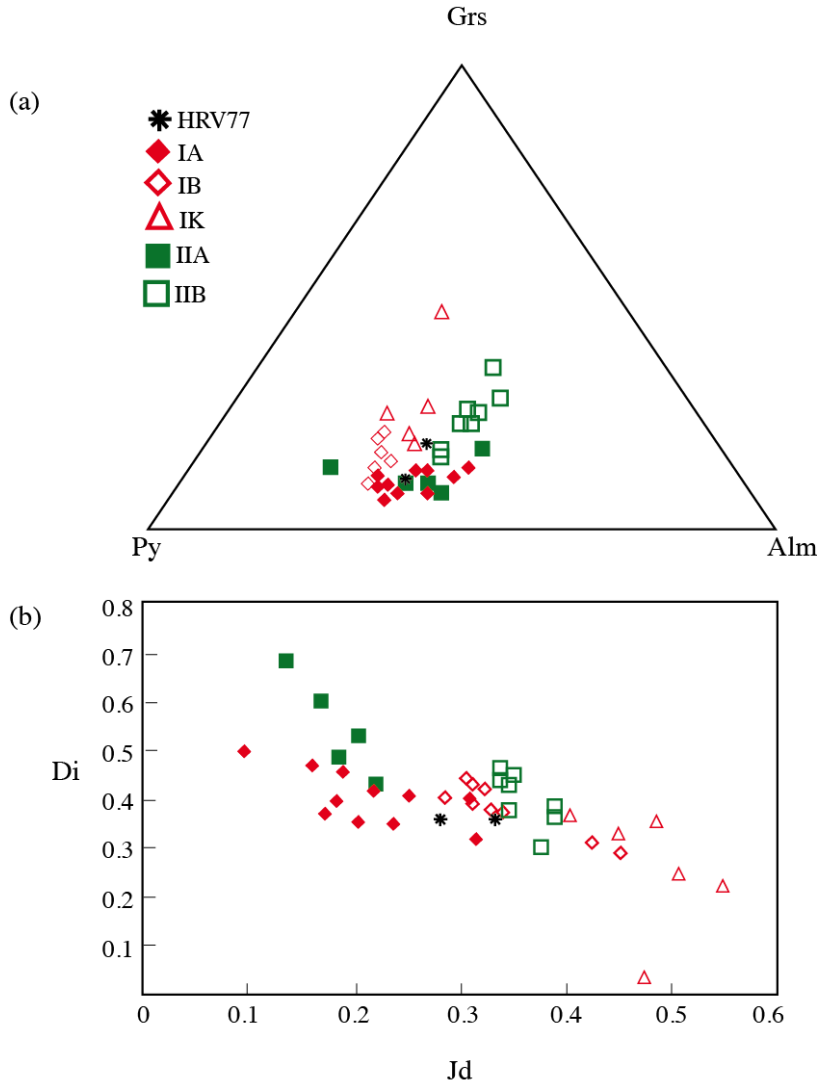

Figure I—6. Compositional variations in (a) garnet and (b) diopside vs. jadeite content per formula unit in clinopyroxene from Roberts Victor eclogites, after Huang et al. (2012). Py - Pyrope, Grs - grossular, Alm - Almandine, Di - diopside, Jd - jadeite.

The associated clinopyroxene is of intermediate composition. The $\delta^{18}O$ values range from 4.1 ‰ to 6.7 ‰The estimated equilibrium temperatures and depths for Type IA and Type IB are similar, within the ~1100—1160°C and ~180—190 km range. Type IK contains eclogites with typically higher grossular content in garnet and the highest Jadeite content in the adjacent omphacite (41—55%). Oxygen isotopic values range from 2.2 ‰ to 6.8 ‰The estimated equilibrium temperatures and depths are higher than for Type IA and Type IB, within the ~1140—1270°C and 186—196 km range.

Type II eclogites have an overall fresh appearance, with interlocking texture of garnet and clinopyroxene, delimited by straight grain boundaries. Rutile is typically found as needle-like inclusions throughout the samples, and when found, accessory phlogopite or spinel are restricted to grain boundaries. No petrographic distinctions are described between Type IIA and IIB. Type IIA eclogites are characterized by high MgO content in garnet (>12 wt.%) and clinopyroxene of intermediate composition (14—21% Jadeite (Jd); 44—67% Diopside (Di); 8—14% Enstatite (En)). The measured oxygen isotopic value is 3.52 ‰. The estimated equilibrium temperatures are within the 897—1063°C range, corresponding to depths of 168—180 km. Type IIB eclogites are characterized by low MgO garnets (≤12 wt.%) associated with Jadeite-rich omphacite (34—39% Jd; 32—46% Di; 3—8% En). The measured oxygen isotopic value is 3.9 ‰. The equilibrium estimates for Type IIB eclogites are significantly higher than for Type IIA, with individual estimates of 1183—1300°C corresponding to depths of 189—198 km.

The classification by Coleman et al. (1965) into Group A, Group B and Group C eclogite xenoliths, was refined by Taylor and Neal (1989) into the three groups based on major and rare earth element (REE) composition (Figure I—7). Group A eclogites (more commonly misclassified garnet pyroxenites) are characterized by Mg- and Cr- rich garnets (up to 21.0 wt.% MgO) and Na-poor, Mg-, Ca- rich clinopyroxene (~21 wt.% MgO; ~16 wt.% CaO). Whole rock compositions have high Mg# and oxygen isotopic values of 4.8—5.1 ‰, and estimated equilibrium temperatures are of 834—852°C. Group A eclogites are coarse-grained, with

clinopyroxene crystals having lamellar orthopyroxene exsolutions. The primary assemblage often contains olivine and orthopyroxene and secondary phlogopite within serpentinized grain boundaries. Eclogites belonging to this group are interpreted as product of fractional crystallization.

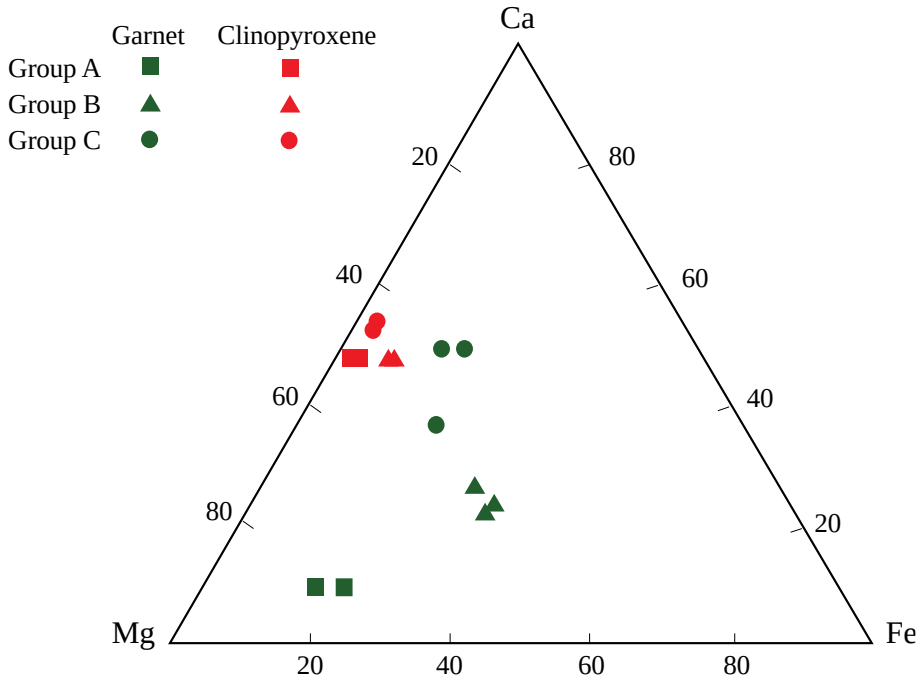

Figure I—7. Garnet and clinopyroxene compositions represented in a Ca-Mg-Fe ternary diagram, distinguishing the three A-B-C eclogite groups, after Taylor and Neal (1989).

Group B eclogites are characterized by LREE-depleted, HREE and Fe-rich garnets (up to 16.4 wt.% FeO) and LREE-depleted adjacent clinopyroxene of intermediate composition (~18—19 wt.% MgO; 12—13 wt.% CaO). Whole rock $\delta^{18}O$ values range between 3.0 ‰ and 3.3 ‰ and the rocks have overall low concentrations of incompatible elements. Estimated equilibrium temperatures range between 915 and 930°C. Group B eclogites contain clinopyroxene with massive unaltered cores and “spongy” or “crinkled” rims in association with fresh garnets. Altered grain boundaries are often associated with interstitial phlogopite and amphibole. The unaltered clinopyroxene cores seldom show exsolution lamellae. Group C eclogites are characterized by Ca-rich garnets (up to 18.8 wt.% CaO) in association with Na-rich, Mg-, Ca-poor clinopyroxene (7—8 wt.% MgO; 12—13 wt.% CaO), with systematic positive Eu anomaly throughout the mineral assemblage. Whole rock $\delta^{18}O$ values range from 4.3 ‰ to 4.9 ‰ and the

rocks have overall low REE abundance. Group C eclogites yield slightly higher equilibrium temperature estimates, of 921—1001°C, than Group A and Group B eclogites. Their mineral assemblage is dominated by coarse clinopyroxene and garnet, with poorly developed "spongy", altered grain boundaries. Kyanite may also be found as a primary mineral, whereas phlogopite and amphibole can be found as secondary minerals along fractures or altered grain boundaries. Eclogites belonging to Group B and Group C are interpreted to be the metamorphosed product of an ancient subducted oceanic crust, corresponding to the basaltic and a plagioclase-rich, plutonic segment respectively.

1.1.3. Petrogenesis of mantle eclogites

Eclogite xenoliths are believed to be a minor component (0-15%, (Schulze, 1989)) of the subcontinental lithospheric mantle (SCLM), nevertheless their understanding is key for retracing Earth's crust-mantle evolution and the origin and preservation of thick cratonic keels (Riches et al., 2010; Smyth et al., 1989). Despite eclogite xenoliths in kimberlite pipes having been studied for more than 50 years, their petrogenesis is still a strongly debated issue (Gréau et al., 2011; Schulze et al., 2000). There are currently three fundamental hypotheses for the petrogenesis of mantle eclogites: 1—mantle-derived high pressure cumulates (Hatton, 1978; MacGregor and Carter, 1970); 2—metamorphosed fragments of a subducted oceanic crust (Jacob et al., 1994; Schulze and Helmstaedt, 1988); and 3— subduction-derived melt residues (Rollinson, 1997; Shchipansky, 2012).

A magmatic origin for mantle eclogites was first suggested by MacGregor and Carter (1970), based on petrographical and major element compositional arguments. In this model it is proposed that mantle eclogites are the product of high-pressure igneous fractionation of a garnet peridotite-derived melt, and the model has been subsequently supported by Hatton (1978); Hatton and Gurney (1977), and experimental studies by O'Hara and Yoder (1967). A concurrent model was introduced by Harte and Gurney (1975) and later refined by Caporuscio and Smyth

(1990); Lappin (1978); Lappin and Dawson (1975); Smyth and Caporuscio (1984); Smyth et al. (1989), which presents a complex evolution of mantle eclogites as the product of high-pressure (>3GPa) igneous accumulation of hyperaluminous clinopyroxene (±garnet ±kyanite) from an eclogitic magma, followed by exsolution and low temperature re-equilibration.

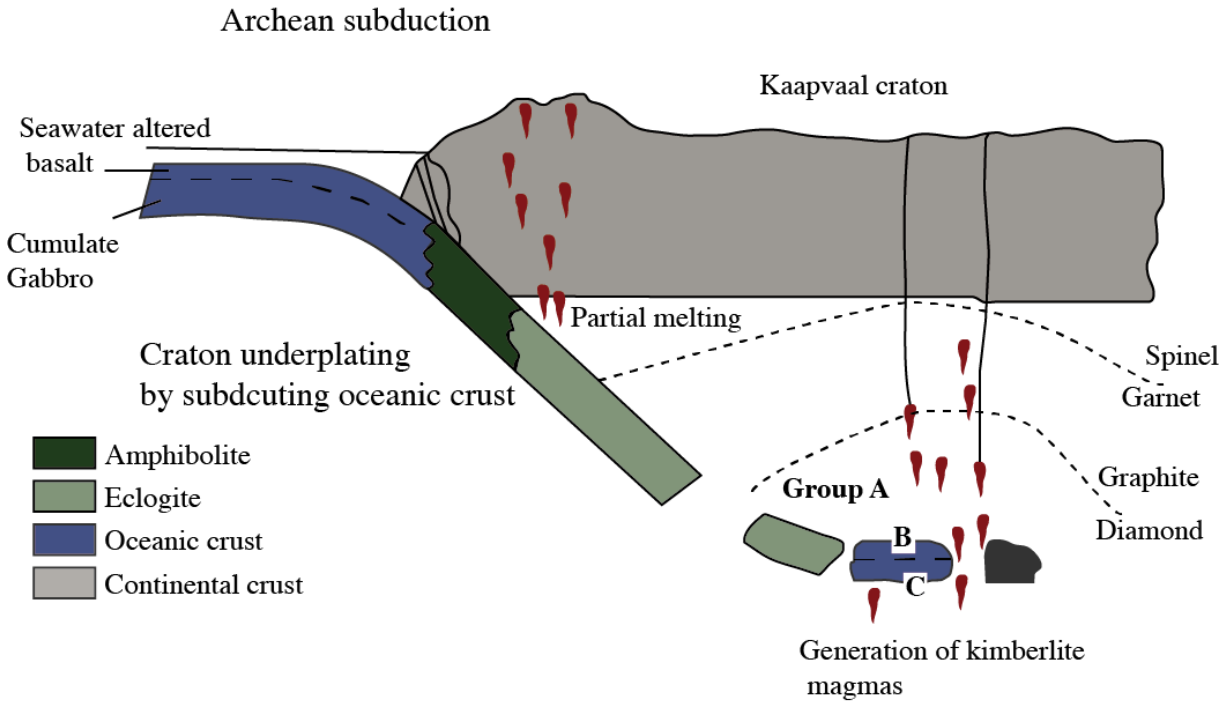

Figure I—8. Graphic representation of Bellsbank eclogite petrogenesis, after Neal et al. (1990) showing different protoliths and evolution of the three A-B-C eclogite types.

Most of the studies arguing for a magmatic origin of eclogite xenoliths are, however, based on misclassified grosspydites xenoliths. Moreover, this hypothesis fails to account for the presence of a parental basaltic melt at depths beyond 200 km, the large range in $\delta^{18}O$ values, or the absence of ubiquitous olivine (Jacob, 2004). Regarding the hypothesis of a hyperaluminous, high-pressure, pyroxene-rich cumulate, this could not account for the excess silica in order to produce kyanite for the entire range of bulk Mg#, the high jadeite content or the lack of correlation between Ca/Mg and Mg# (Ater et al., 1984).

Mixed origins for different eclogite types were first suggested by Coleman et al. (1965) and later supported by Neal et al. (1990); Taylor and Neal (1989). In this scheme, group A eclogites, including mostly misclassified garnet pyroxenites and grosspydites, are mantle cumulates,

however group B and group C eclogites are the metamorphosed product of a subducted oceanic crust (Figure I—8).

The crustal-derived hypothesis for the petrogenesis of mantle eclogites, first postulated by Coleman et al. (1965), has become strongly debated throughout the years and has emerged as two distinct models.

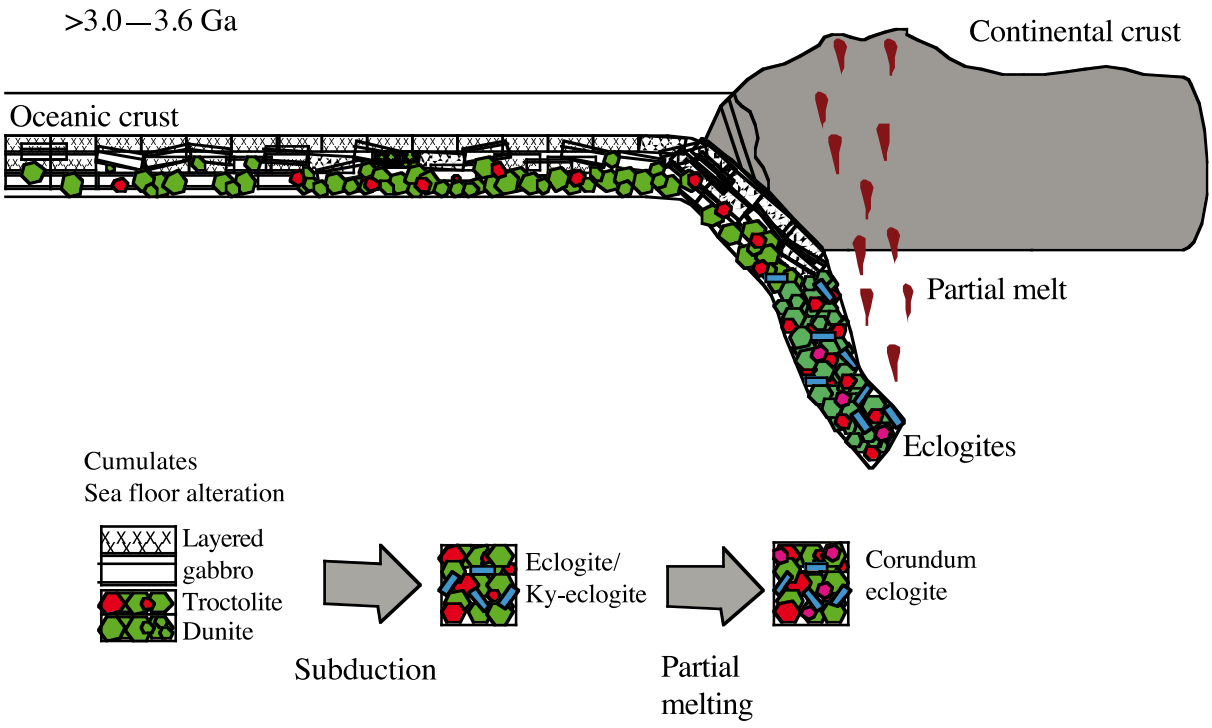

Figure I—9. Schematic representation of mantle eclogites petrogenesis after Shu et al. (2016)

One model interprets mantle eclogites as subducted relics (Figure I—9) of an Archaean, oceanic crust (Aulbach et al., 2016; Beard et al., 1996; Helmstaedt and Doig, 1975; Jacob, 2004; Jacob and Foley, 1999; Jacob et al., 1994; MacGregor and Manton, 1986; Riches et al., 2016; Schulze and Helmstaedt, 1988; Schulze et al., 2000; Shervais et al., 1988; Shu et al., 2016; Viljoen et al., 2005), where the compositional variability is explained via the heterogeneity of the protolith (altered oceanic basalts vs. low pressure cumulates). The second model suggests eclogite xenoliths are the melt residue of Archaean crust formation (Ireland et al., 1994; Shchipansky, 2012; Snyder et al., 1993). The crustal residue hypothesis (Figure I—10) is based on modelled complementary composition of whole rock eclogites and granitoid TTG (tonalite-

trondhjemite-granodiorite) magmas, as derived from a common basaltic parent rock (Rollinson, 1997).

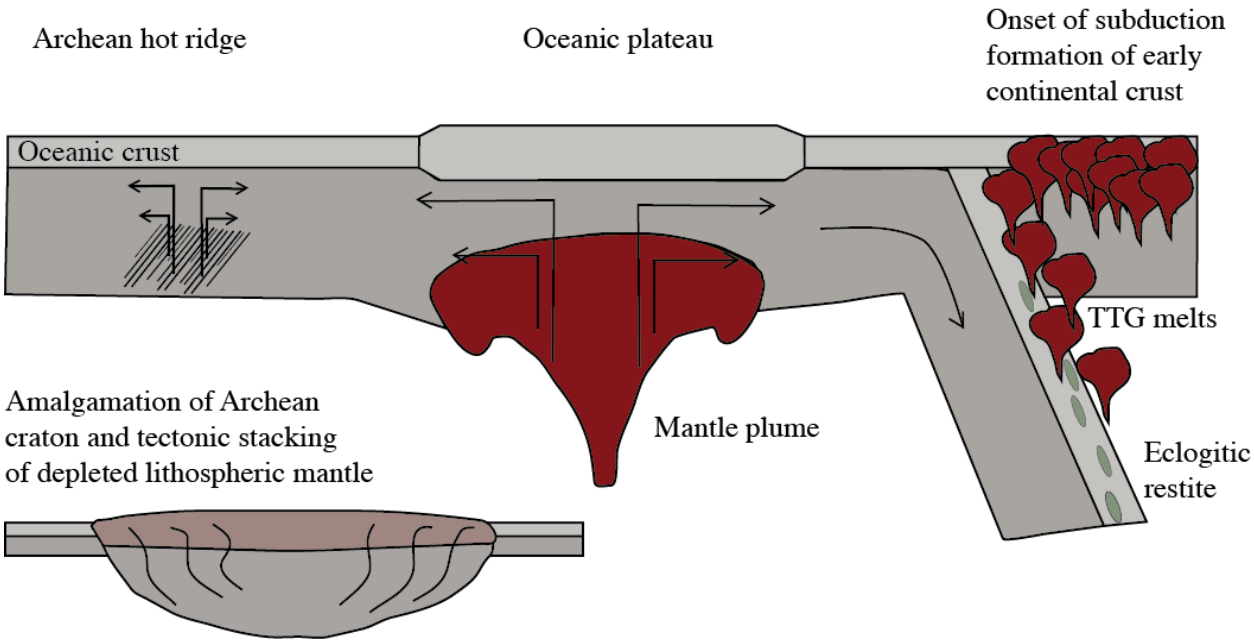

Figure I—10. Conceptual geodynamic model for early continental crust formation and mantle eclogites petrogenesis after Shchipansky (2012).

The main arguments supporting the Archaean crust hypothesis are the wide range of $\delta^{18}O$ values and the positive Eu and Sr anomalies in clinopyroxenes. Nevertheless, the influence of redox conditions and percolating metasomatism have been proposed as alternative mechanisms that could generate positive Eu anomalies, leading to strong debates (Griffin and O'Reilly, 2007). The robustness of oxygen isotopes as crustal tracers have been equally contested by (Huang et al., 2014) and attributed to carbonatite metasomatism (Gréau et al., 2011).

The pervasive metasomatism preceding their entrapment in the kimberlitic magma and the limited access to pristine samples (Figure I—11) have led to little consensus being reached regarding the possible protolith of eclogite xenoliths. Despite the numerous studies and the large amount of petrographical and geochemical data gathered, the origin of mantle eclogites remains uncertain.

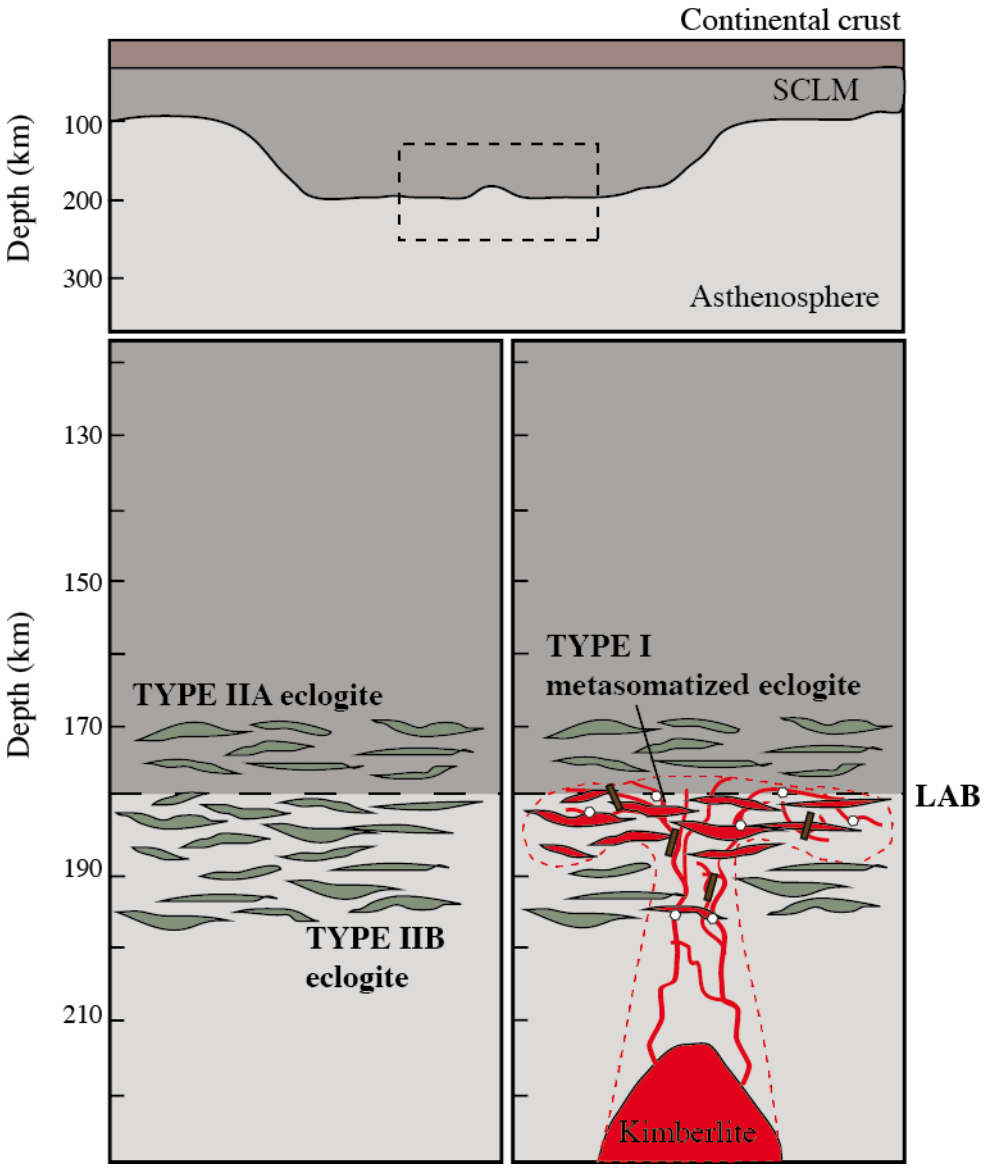

Figure I—11. Graphic representation of eclogite-rich subcontinental lithospheric mantle (SCLM) area around the lithosphere-asthenosphere boundary (LAB), showing distribution of Type IIA and Type IIB eclogites and formation of Type I eclogites through discrete mantle metasomatism by carbonattitic-kimberlitic melts/fluids. After Huang et al. (2014) and Gréau et al. (2011).

1.2. Aims of the thesis

This study aims to improve the understanding of mantle eclogite xenoliths and the subcratonic lithospheric mantle, through a more accurate and complete description of eclogite xenoliths from the South African and Siberian cratons. Based on a collection of more than 180 xenoliths, Part I of this study commences with a thorough account of mineral assemblages and textures present and identifying pristine, non-metasomatized eclogites. The subsequent chapters focus on the chemical compositions (major and trace elements; oxygen isotopes) characteristic for each eclogite Type and refining the textural and petrologic classification and determining their pressure-temperature equilibrium conditions. Through a combined petro-geochemical approach, the first part of this study discusses possible protoliths and petrogenesis behind mantle eclogites.

Part II focuses on "water" preservation in nominally anhydrous minerals at mantle conditions. It discuses hydrogen incorporation in omphacite and garnet and the differences and difficulties regarding "water" quantification. An equally important aspect is the stability of zoisite in the upper mantle and chemical reactions involved in exsolution of grossular-rich garnet and zoisite from a precursor clinopyroxene. Furthermore, the aim of this second part of the study is to determine the amount of "water" stored in mantle eclogites, and the implication of this on the stability of the cratonic root and on upper mantle properties.

1.3. South-African and Siberian cratons – a brief introduction

1.3.1. Origin of Archaean crust and subcontinental lithospheric mantle

A craton is a large, consolidated domain of Earth's continental crust, which has reached and maintained long-term stability, with little internal deformation, except in some cases the marginal zone due to interaction with neighbouring terranes (Bleeker and Davis, 2004). A craton is typically constituted of polydeformed and metamorphosed crystalline and metamorphic rocks that have attained steady density, compositional and thermal profile with the underlying lithosphere. There are currently ca. 35 large cratons (~7—11 million km^2 exposed; Figure I—12) representing a biased sample of Archaean crust and lithosphere (Bleeker, 2002). The Archaean to Proterozoic transition is marked by major geodynamic changes, from low-to-moderate pressure and moderate–to-high temperature, to high-to-ultra-high pressure and low-to-medium temperature (Brown, 2006). The survival of Archaean nuclei requires the presence of a thick crustal root, acting as buffer and protecting the base of the crust from being molten by the greater Archaean heat flux (Davies, 1979), nonetheless, geological processes and geodynamics in the Archaean, leading to early crust formation and craton accretion, are still poorly known. Moreover, sampling of the subcratonic mantle is limited to xenoliths and xenocrysts captured by kimberlite magmas from the Transition Zone (> 400 km depth) to the base of the lithosphere (Sautter et al., 1998).

Recent studies argue for a differentiated crust early (> 4Ga) in the Earth's history (Boyet and Carlson, 2005) likely catalysed by the presence of water and its consequences on mantle rheology and melting processes (Bleeker, 2002). In the context of a younger, hotter (~3 times greater heat flow rate than at present) Earth, heat loss thorough present tectonic mechanisms is insufficient(Davies, 1979), possibly leading to episodic mantle overturns and crust formation episodes (Davies, 1995). Alternative models for excess heat release have been suggested, such as heat advection by intrusion of partial melt from the lower levels of a thicker crust, to the higher

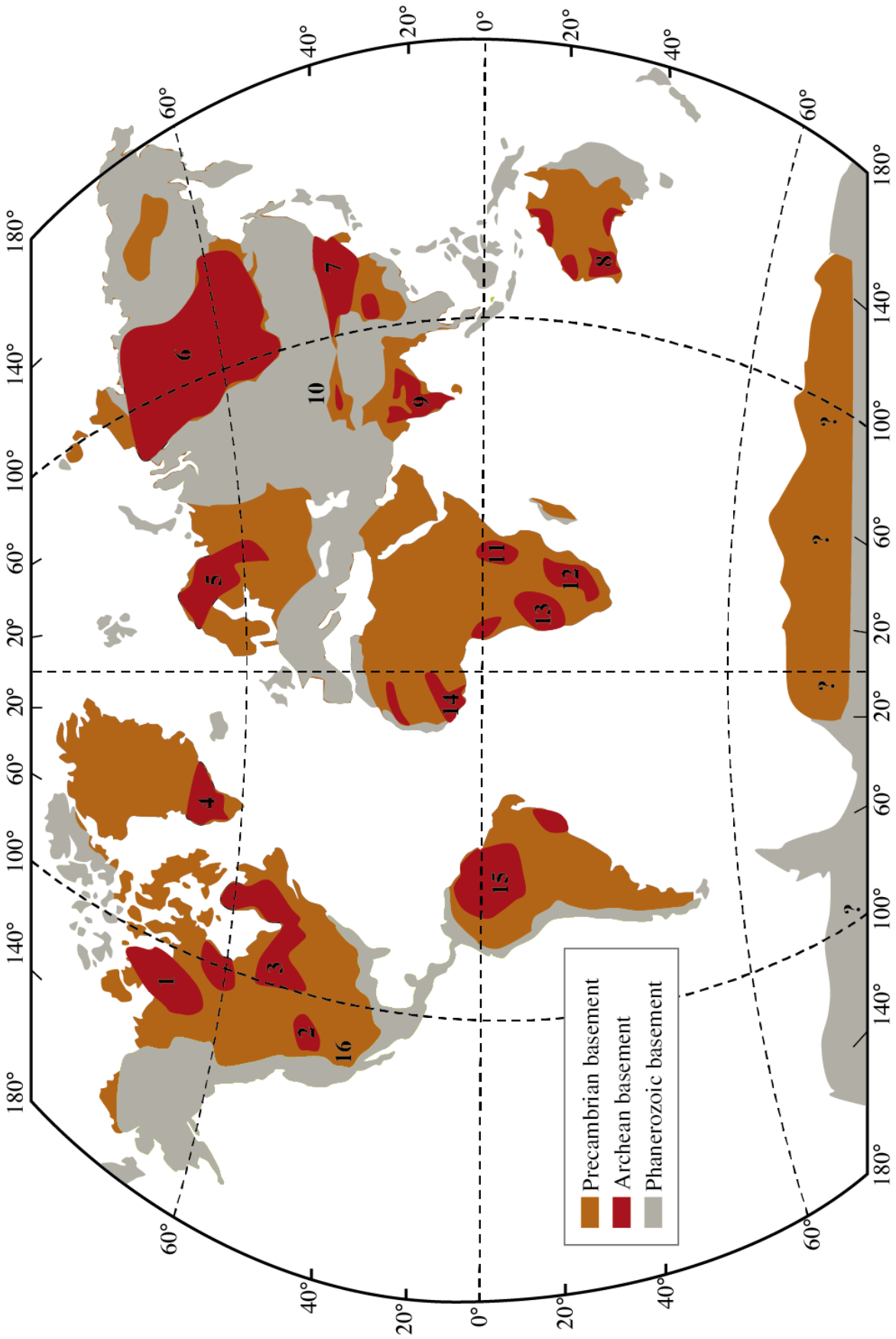

Figure I—12. Map showing Archean cratons and Precambrian and Phanerozoic basement distribution. Archean cratons are marked as follows: 1 - Slave; 2 - Wyoming; 3 -Superior;4 -Greenland;5 -Fennoscandian;6 -Siberian;7 -NorthChina;8 -westAustralian; 9 -Indian;10 - Tarim; 11 -Tanzanian; 12 -Kaapvaal; 13 - Congo; 14 - westAfrican;15 - Amazonia;16 – Colorado Plateau. After Lee et al. (2011)

levels (Zegers and van Keken, 2001). This model requires delamination of a lower eclogitic part of a thick oceanic proto-crust, which is replaced by decompression melts of a hot, depleted mantle. The third model involves mantle plumes from the mantle-core boundary, that lead to domal uplifts at surface with surrounding radial dike swarms, followed by gradual subsidence (Campbell, 2001) (Figure I—13).

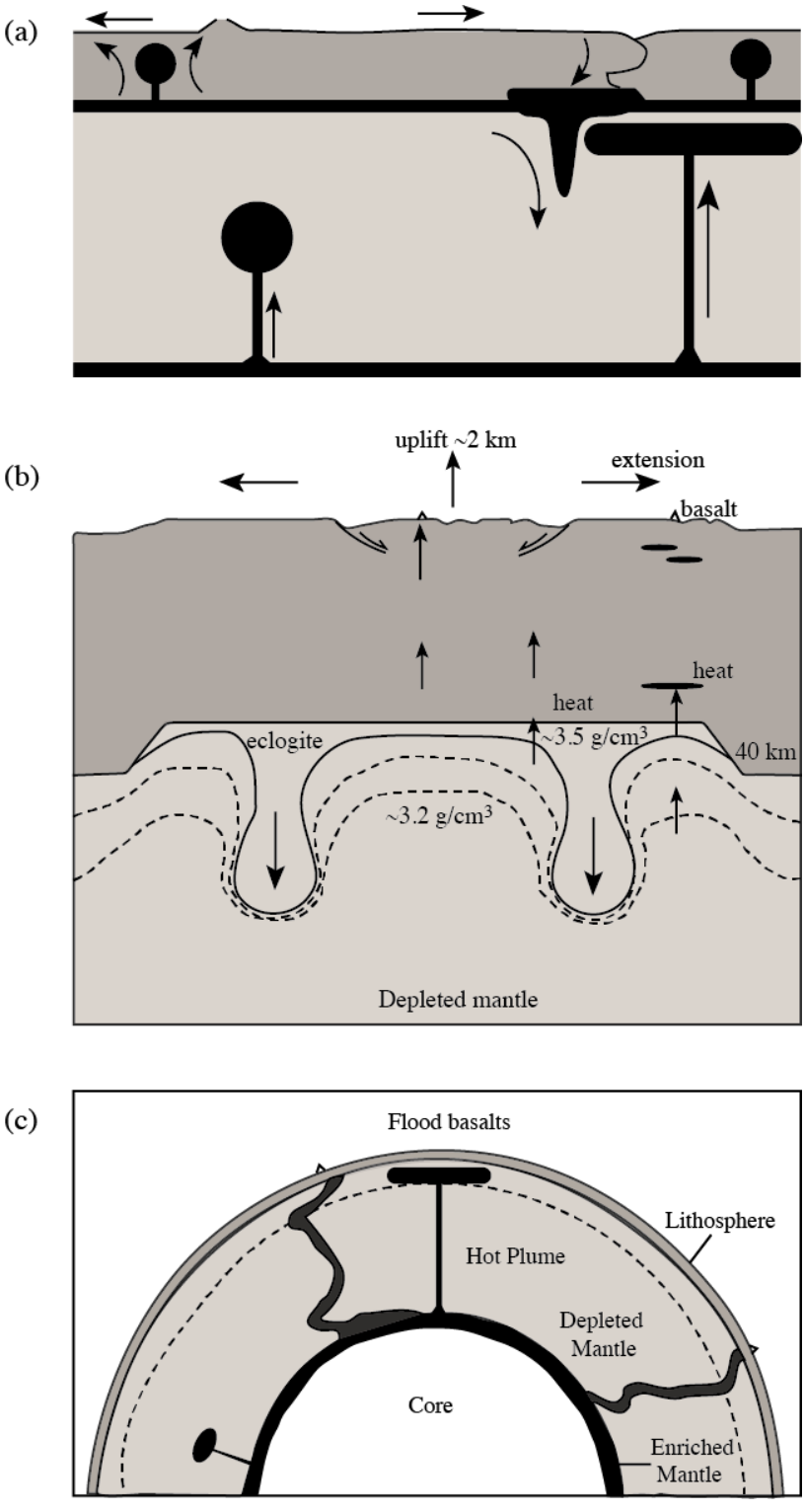

Figure I—13. Graphic representations of heat release during the Archean, in the context of a hotter Earth. (a) heat loss through upper mantle overturns leading to crust generation, after Davies (1995); (b) heat advection with lower eclogitic crust delamination, model after Zeger and van Keken (2001); (c) deep plume injection from the mantle-core boundary, model after Campbell (2001).

Many studies suggest that most of the crust was formed by the end of the Archaean (< 2.9 Ga) (Armstrong and Harmon, 1981; Griffin et al., 2014; Lee et al., 2011), whereas others state that maximum continental growth was reached between 2.5 — 2.0 Ga (Allègre and Rousseau, 1984). More recently, it has been accepted that the Archaean continental fragments found today, are biased samples of old continental cores, insulated from convergent plate margin erosion, therefore showing crustal preservation (Hawkesworth et al., 2009) and not episodic crustal production in time (Abouchami et al., 1990).

The primary focus for continental crust production is explained through a thicker oceanic arc context, implying a more buoyant oceanic crust, derived from a hotter, more extensively molten mantle. Subsequent collision/accretion geodynamics is believed to have led to oceanic plateaus and further to Archaean continents (Condie and Kröner, 2013).

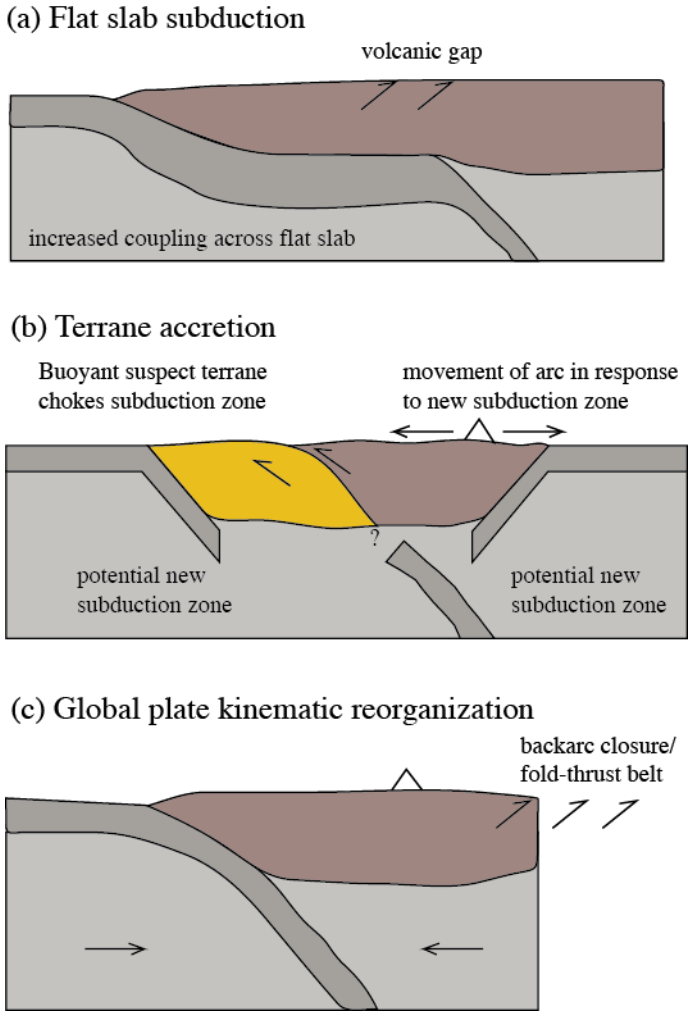

Figure I—14. Possible models for plate coupling, entailed by accretionary orogenesis (a) buoyant oceanic lithosphere subduction; (b) accretion of buoyant lithosphere (c) plate reorganization with increased convergence across boundaries. After Cawood et al. (2009).

Accretionary orogenesis occurs in the context of continuous plate convergence during stabilization and thickening of continental crust (Cawood et al., 2009), and the entailed plate coupling can result from buoyant oceanic lithosphere subduction (flatslab subduction); accretion of buoyant lithosphere (terrane accretion) or plate reorganization with increased convergence across the boundaries (Figure I—14). Accretionary orogens are however manifestations of horizontal tectonics (continuous, episodic or combined with other processes). The subduction-driven, horizontal tectonics model is comparable to the modern style of plate tectonics. The oldest evidence for a rigid oceanic lithosphere and lateral plate movements has been found in the EoArchaean Isua supracrustal belt (Komiya et al., 1999). On the basis of preserved duplex structures and oceanic plate stratigraphy in what is considered the oldest accretionary complex (Figure I—15), it has been inferred significant horizontal tectonic plate motions were operational 3.8—3.7 Ga.

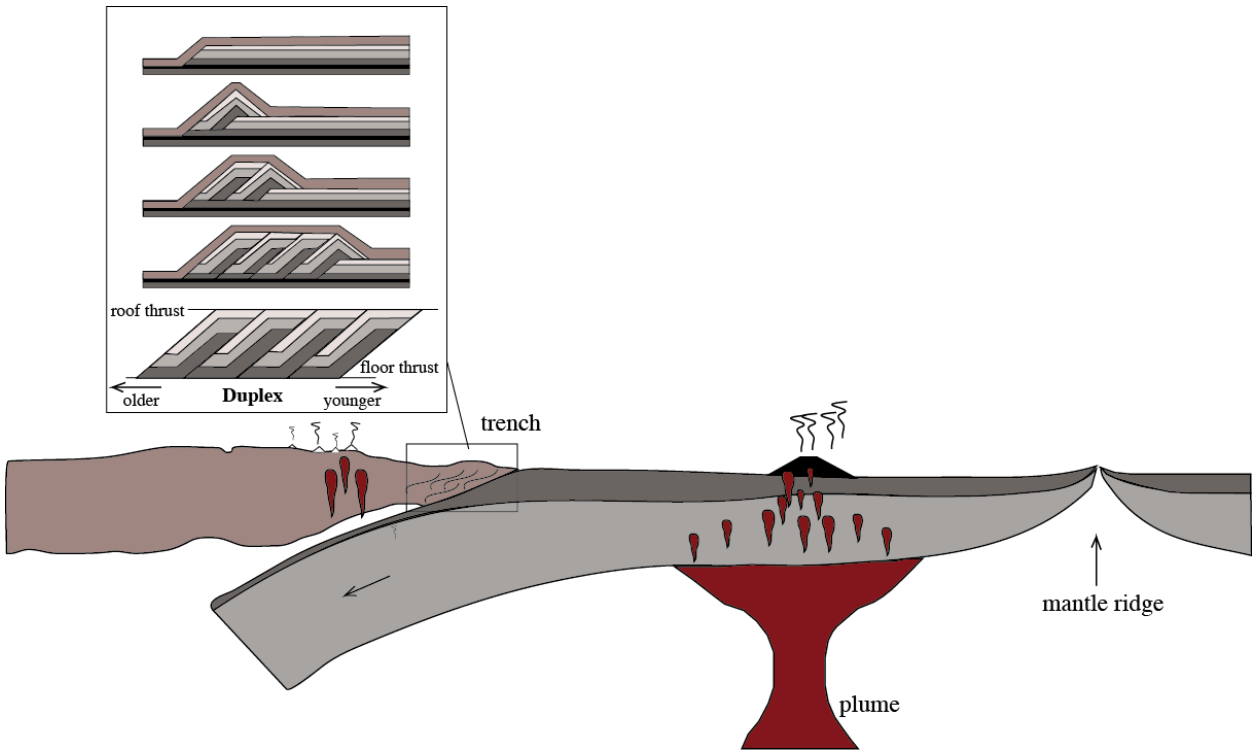

Figure I—15. Duplex structures as evidence for subduction driven horizontal tectonics, after Komyia et al. (1999)

This has been further supported by Martin et al. (2005)based on chemical changes in juvenile crust (~90% TTG) from Early Archaean (flat subduction) to Middle and Late Archaean (similar to modern subduction). This theory has been later disputed in the context of a hotter Archaean mantle with a lower mantle viscosity and higher plate buoyancy (Martin et al., 2014; van Hunen and Moyen, 2012). Some igneous rocks, such as high-pressure TTGs require deep burial of surface material and cannot be satisfactory explained through mechanisms as flat subduction or long-lived modern-style subduction.

An opposing model is the subduction stacking or underplating of oceanic lithosphere (Griffin and O'Reilly, 2007; Hoffman, 1990; Pearson and Witting, 2008), which is similar in complexity to deformed ophiolitic melange found in Phanerozoic orogenic belts (Helmstaedt and Schulze, 1989). Although this would explain the lack of systematic compositional stratification with depth and the formation of TTG melts from partial melts of underthrusting oceanic crust (Figure I—16), the negatively buoyant oceanic lithosphere is more likely to subduct than subcrete (Lee et al., 2011) and cratonic root longevity is questionable.

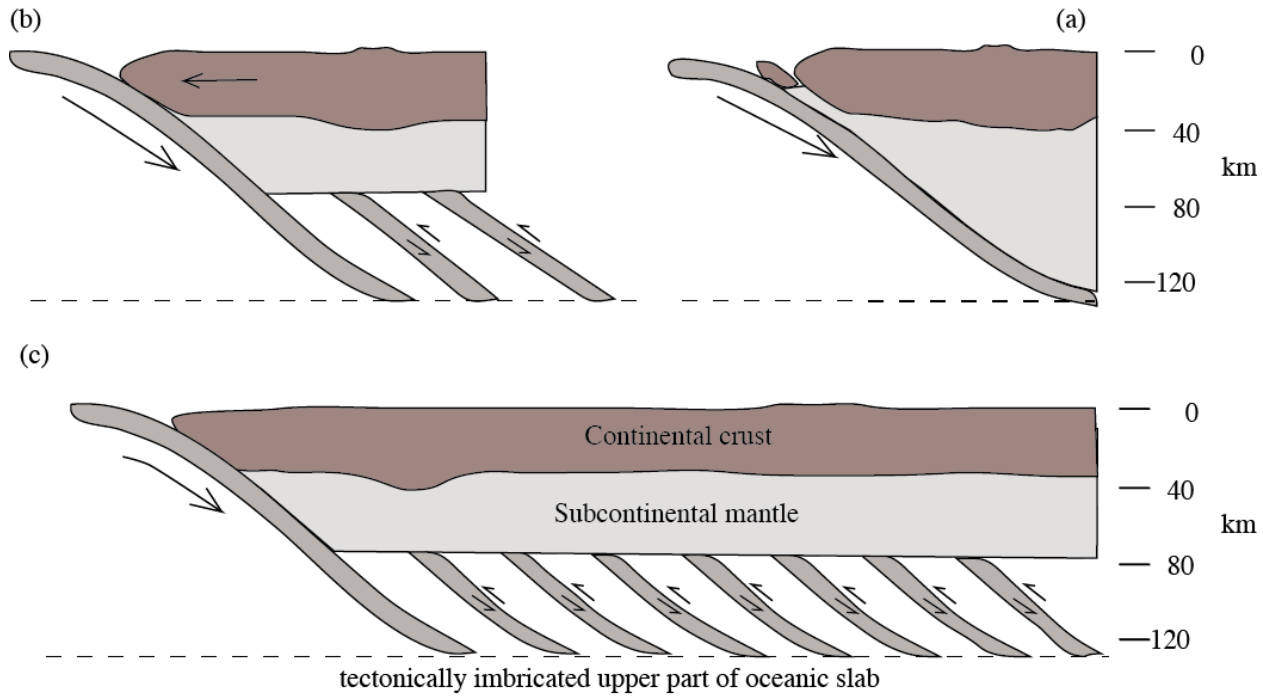

Figure I—16. Model of progressive imbrication of subducted slab during low angle subduction. (a) initial subduction zone with island arc; (b) and (c) subduction zone overridden by continental lithosphere after increased convergence rate. After Helmstaedt and Schulze (1989).

Another mechanism for building thick continental crust is the vertical or stagnant lid tectonics that implies tectonic evolution through episodic, partial convective overturn of the upper and middle crust (with an inverted crustal density profile; Figure I—17), releasing heat from the mantle to the surface (van Kranendonk et al., 2004). Partial melting of the granitoid, mid-crustal layer, subsequently crystalizing during ascent, would lead to long-lived, crustal-scale dome and syncline geometry.

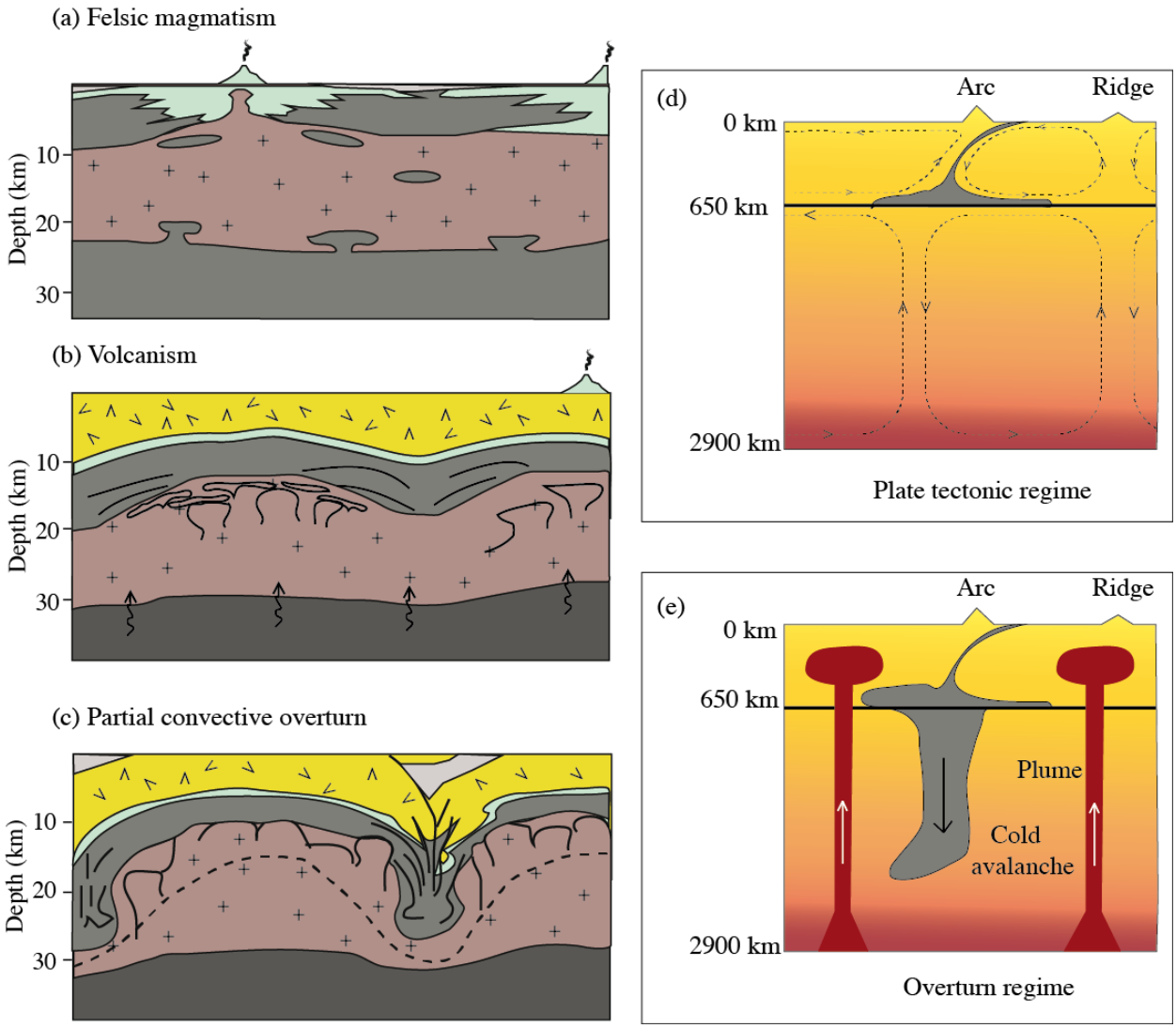

Figure I—17. Models for partial overturn (a—c) after van Krenendonk et al. (2004) and complete mantle overturn after Martin et al. (2014) through which cold, dense crustal material can sink into the mantle.

This model is supported by characteristic features of magmatic diapirism (e.g. chaotic internal geometry of domes, ring faults, inter-diapir syncline sediments) described in the Pilbara craton.

Similarly, (Griffin et al., 2014) suggest that the Earth's crust was under a stagnant lid regime with pulses of juvenile magmatic activity (i.e. mantle overturns or plume episodes) at 4.2 Ga, 3.8 Ga and 3.3—3.4 Ga, followed by a period of very rapid overturning in the mantle between 2.9—2.5 Ga, creating most of the Subcontinental Lithospheric Mantle and transitioning to the modern day tectonics.

More recently, a new tectonic model has been suggested, referred to as ultra-hot orogens (UHO), which combines vertical and horizontal advection, under long-lasting convergence (Chardon et al., 2009). This model envisages distributed orogenic shortening followed by homogenous thickening, driven by downward movements of supracrustal units and mass redistribution in the underlying viscous lithosphere. Tectonic shortening is the consequence of externally exerted compression, resulting in the depleted root from the middle of the domain to be pushed downwards, thereby creating the shortening and initial thickening of the cratonic root (Figure I—18).

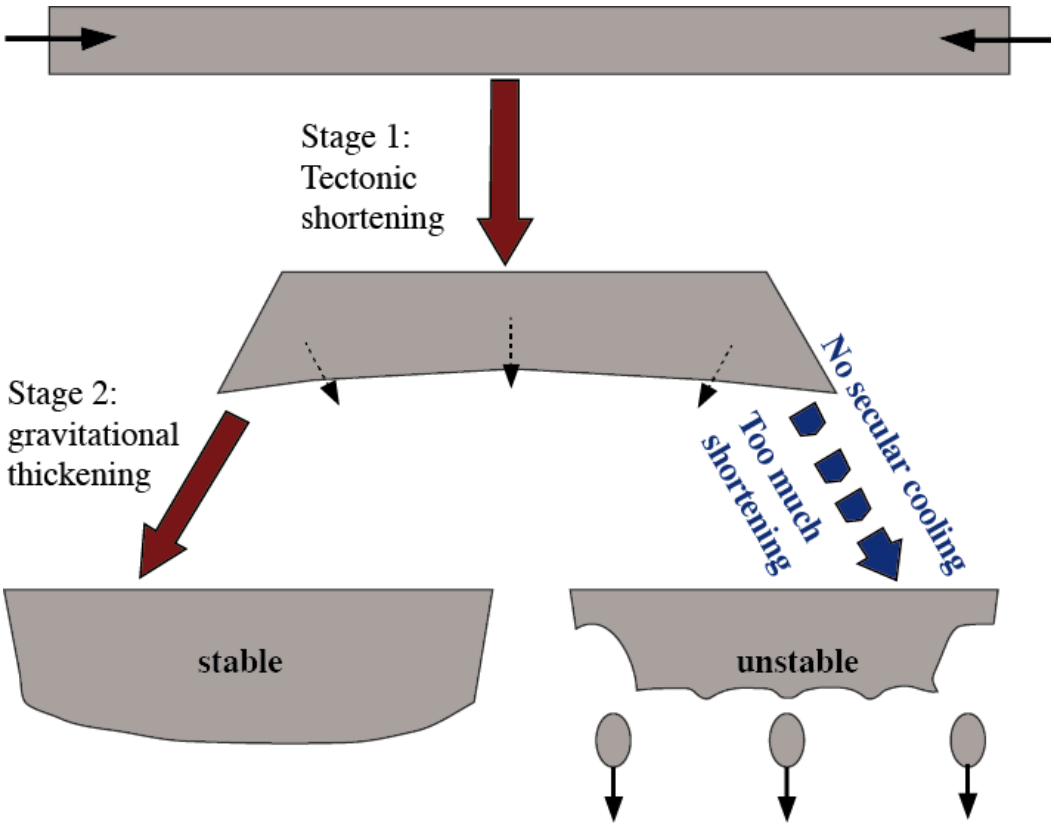

Figure I—18. Graphic representation of the two-stage thickening model for the formation of thick cratons, resulting from numerical simulations. Stage 1 — tectonic shortening is essential, followed by Stage 2 - gravitational thickening. After Wang et al. (2016).

This is considered essential for initiating the cratonization process, and according to computational modelling (Wang et al., 2016) the estimated crustal thickening is of ~43 km over 50 Ma. Subsequent gravitational self-thickening is driven by the diffusive cooling of the root, slowly embedding depleted lithospheric material. As the thickened root cools, it becomes denser and negatively buoyant, resulting in further thickening. Recycling of the root material is considered negligible (~20% in the compressive stage; ~6% in the self-thickening stage) and the modelled root growth estimate is of ~36 km/550 Ma (Wang et al., 2016). The steady self-driven thickening accommodated by a slowly cooling ambient mantle will stabilize a thick cratonic root and diminish the thermal buoyancy contrast between lithosphere and asthenosphere, ensuring the long-term survival of cratons and underlying lithospheric mantle.

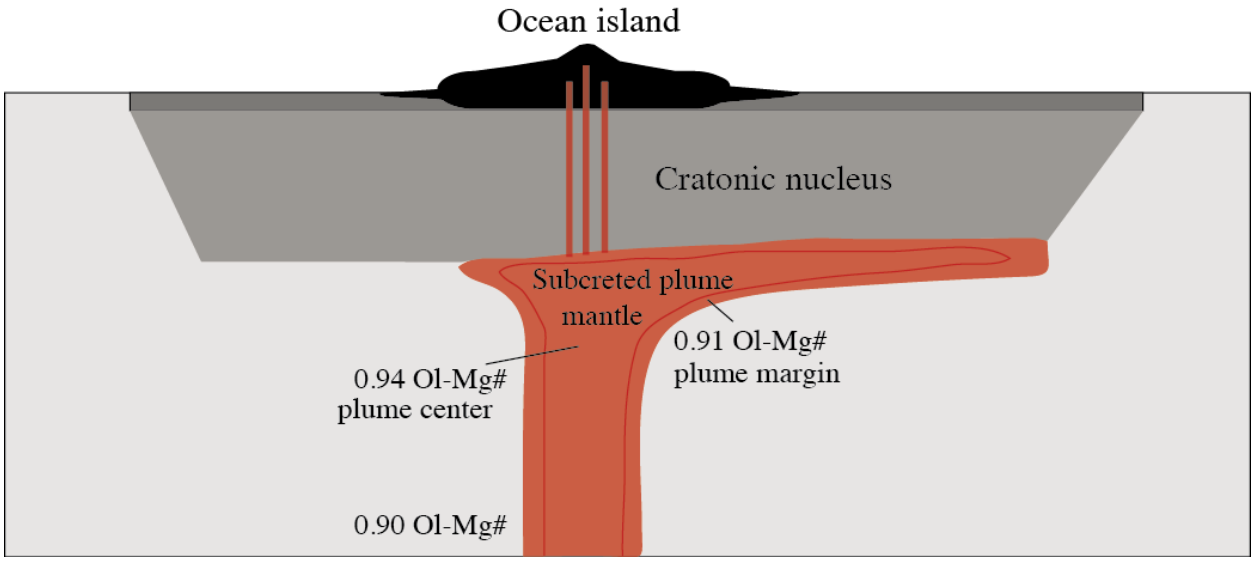

Figure I—19. Sketch of cratonic nucleus subcreted by upwelling plume mantle resulting in material flow laterally towards thinner craton margins. After Arndt et al. (2009) and Aulbach et al. (2017).

Alternatively a largely accepted hypothesis for crustal thickening and the preservation of long-lived cratonic roots is high-degree mantle melting in a plume setting (Figure I—19), followed by reworking of material to eliminate high-density, low viscosity lithologies (Arndt et al., 2009). This is supported by the dominant composition of the subcontinental lithospheric mantle (SCLM), rich in forsteritic olivine and magnesian orthopyroxene, as well as the FeO-MgO and Cr_2O_3-Al_2O_3 high-degree mantle melting residue at pressure >3 GPa (Aulbach, 2012). This

model accepts that any of the previous hypothesis (i.e. shallow plate interactions, vertical tectonics self-thickening) may have acted in the early history of the crust formation, however it argues that craton longevity and cratonic root are dominantly controlled by plume impingement.

1.3.2. Destroying continental mantle

The lack of cratons predominantly older than 3.5 Ga as well as evidence for Proterozoic and Phanerozoic continental lithospheric mantle (Saleeby et al., 2003) suggest many continents may have been destroyed and recycled throughout Earth history. There are several mechanisms through which continental lithosphere could be removed (Figure I—20).

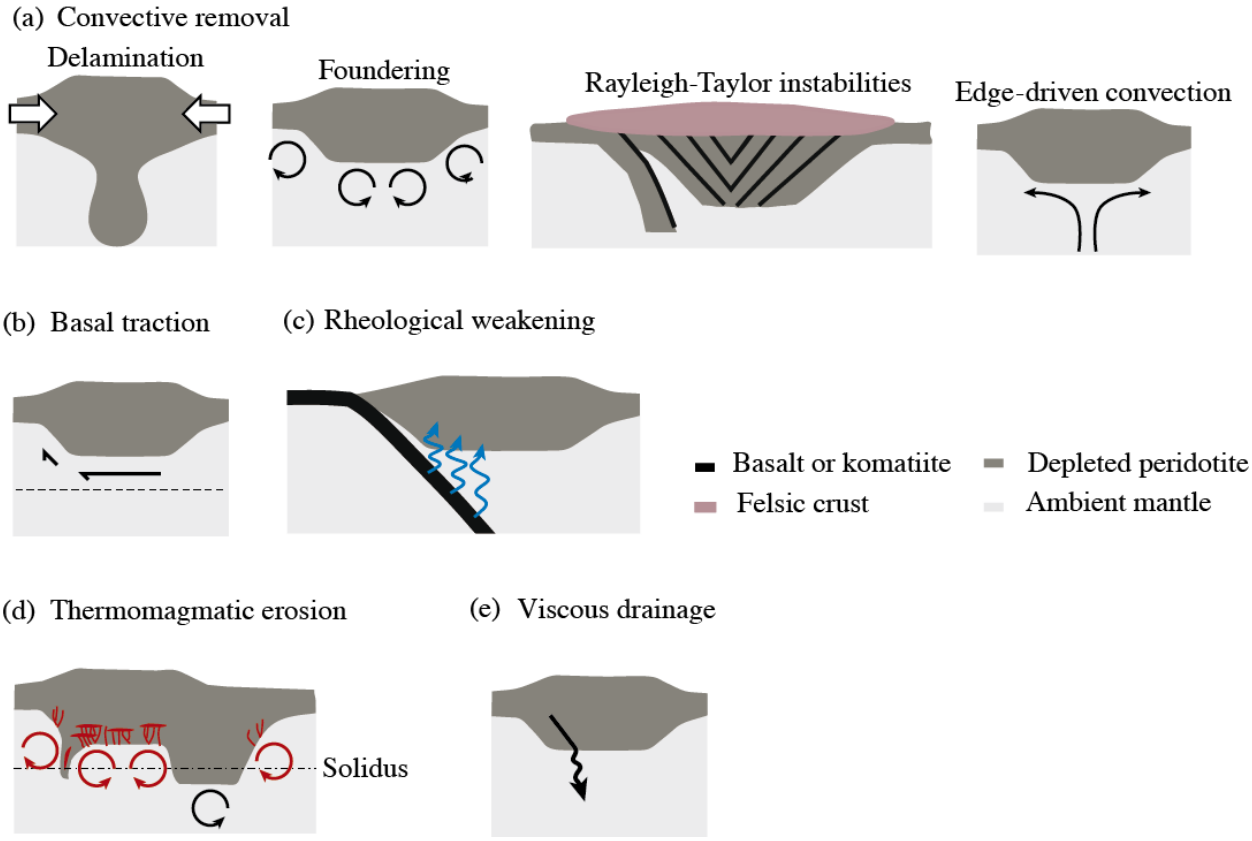

Figure I—20. Different models for destroying or recycling continental mantle, after Lee et al. (2011).

Without a compositional buffer, density contrasts due to thermal differences induce buoyancy-derived destabilization, whereas both vertical and horizontal thermal contrasts can lead to small-scale convective lithospheric removal (Huang et al., 2003). Another important factor that can

facilitate convective erosion is rheological weakening induced by infiltrating hydrous melts or supercritical fluids. Similarly, refertilization via melt intrusions or mantle plumes, increasing Fe and water content, could cause partial melting and could generate thermomagmatic erosion. To a lesser extent, erosion of continental lithosphere can be induced by basal mantle flow shear stress in the asthenosphere, however this could not account for craton destruction, as shear stress decreases rapidly with craton thickness (Lee et al., 2011). Although an untested model, continental mantle could be equally removed through viscous drainage, through the delamination of high-density, low-viscosity lithologies.

1.3.3. Kaapvaal Craton

The Kaapvaal and Zimbabwe Archaean cratons represent the nucleus of southern Africa (Kalahari craton). Kaapvaal Craton (Figure I—21) comprises an eastern (~3.5 Ga) and a western (~3.2 Ga) domain, believed to have generally formed and stabilized between 3.7—2.6 Ga (de Wit et al., 1992). The north-central part of the craton was later disrupted by the major intracrustal formation of the Bushveld large igneous province (James et al., 2003) at ~ 2.05Ga. The Kaapvaal Craton is delimited by the Limpopo belt (~2.7 Ga) to the north, the Namaqua-Natal Province mobile belt (~1.1—1.9 Ga) to the south and east and by the overthrusted Kheis belt (~2.0 Ga) to the west (van Reenen et al., 1992). Seismic investigation of the craton have been interpreted as indicating a thin crust, with an average to felsic composition at the base (contrasting with most continental lower crust which is mafic) and a sharp, almost flat Moho (Schmitz and Bowring, 2003). This was subsequently attributed to intensive re-melting of the lower crust, possibly related to the Ventersdorp extensional tectonics and magmatism (2.7 Ga). Ultrahigh-temperature metamorphism (in excess of 1000° C in the lowermost crust) may have affected the western part of the craton as well as the Kimberley area(Schmitz and Bowring, 2003). Partial melting and deep crustal ductile flow may lead to differentiation at the base of the crust and high-pressure-temperature (HP-HT) crystallization (James et al., 2003).

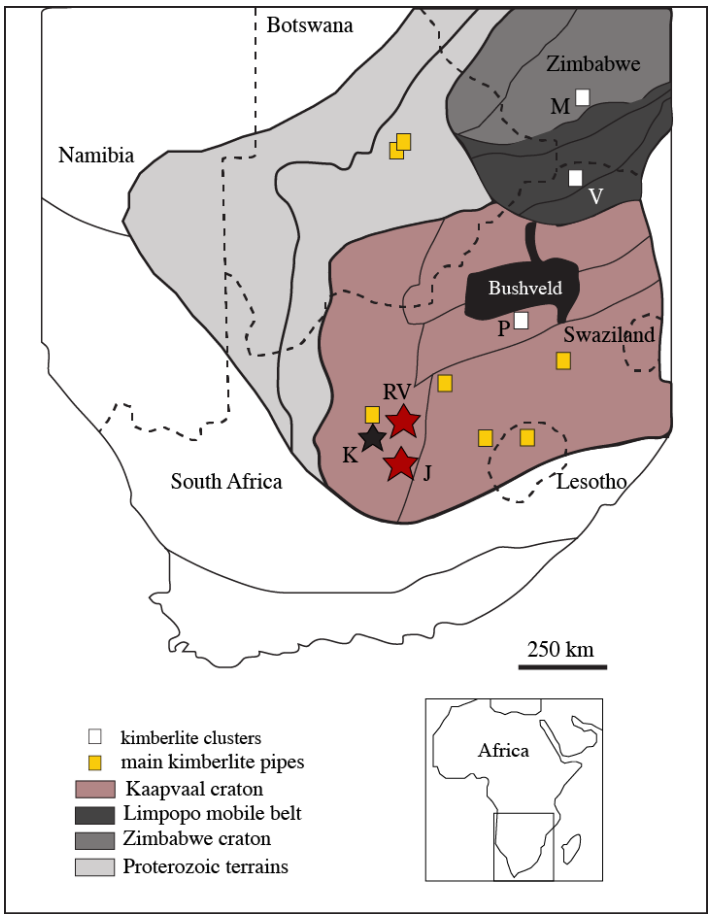

Figure I—21. Map of the Kalahari craton and separate terrains including the Kaapvaal and Zimbabwe cratons and the Limpopo Mobile Belt. K: Kimberly cluster; P: Premier/Cullinan cluster; M: Murowa/Sese kimberlite; V: Venetia kimberlite cluster; RV: Roberts Victor mine; J: Jagersfontein mine. After Van der Meer et al. (2013) and Katayama et al. (2009).

Roberts Victor mine (28° 29'S – 25° 33'E) is located ca. 95 km northeast of Kimberley, in the centre of the Kaapvaal craton. It consists of two small Group-2 kimberlite pipes, containing olivine, diopside, spinel, perovskite and apatite, in a phlogopite-dominated groundmass, in which potassium-rich minerals such as sanidine and K-richterite and leucite are also present (Field et al., 2008). Group-2 kimberlites have typically fine-grained textures; the chemical composition is enriched in SiO_2, K_2O, Pb, Rb, Ba and LREE-enriched and the eruption event is confined to a narrow geological period (114—200 Ma). Within this interval, Roberts Victor kimberlite has intruded ca. 128 Ma (Smith et al., 1985). The xenolith suite comprises Beaufort sandstone and Karoo basalt from the overlying formations, but is mostly dominated by mantle eclogites (> 95%), as well as xenocrysts and severely altered peridotites, often diamond-bearing (Hatton, 1978).

Jagersfontein mine (29° 46'S—25° 25'E) is located ca. 170 km southeast of Kimberly, close to the craton border. It is one of the large Group-1 kimberlite pipes, containing olivine, monticellite, calcite, phlogopite, ilmenite, spinel, perovskite and apatite in a micaceous

groundmass (Field et al., 2008). The texture is relatively coarse grained; with a Sr-Nd isotope composition slightly depleted with respect to bulk Earth and diverse radiometric ages (i.e. ranging from Proterozoic to Cretaceous). Jagersfontein kimberlite has been dated at ~ 85 Ma (Smith et al., 1985) and has intruded through sedimentary rocks of the Karoo Supergroup and a 245 m thick ~180 Ma Karoo dolerite sill. The xenoliths suit includes peridotites, eclogites, pyroxenites and megacrysts (Field et al., 2008). Both peridotite and eclogite xenoliths may contain diamonds. Some mantle xenoliths, exhibiting omphacite exsolutions in garnet have been interpreted as samples from the upper Transition Zone limit (Haggerty and Sautter, 1990).

1.3.4. Siberian Craton

The Siberian Craton (Figure I—22) comprises four Archaean to Paleoproteroizic terranes: Tungus, Anabar, Aldan and Olenek and occupies an estimate of 4 million km^2 of the Yakutian province and north-central Asia(Pisarevsky et al., 2008). It is delimited by Taimyr (Mid-Mesozoic) and Verkhoyansk (Cretaceous) sedimentary foldbelts in the north and east and by the Central-Asian (Late Mesoproterozoic – Triassic) and Mongol-Okhotsk (Late Palaeozoic – Early Triassic) volcanic orogenic belts in the west and south (Rosen, 2002). Based on Re-Os and Lu-Hf ages of sulphide inclusions in diamonds (Wiggers de Vries et al., 2013), refractory peridotite and eclogite xenoliths (Doucet et al., 2015; Ionov et al., 2015) respectively, it is believed that most of the underlying subcratonic mantle formed in two stages (3.5—2.8 Ga and 2.2—1.9 Ga). The mid-Proterozoic stage coincides with the amalgamation of the four crustal terrains, marked by granites and associated granulite suture belts, dated at ca. 1.9-1.8 Ga (Kobussen et al., 2006; Rosen et al., 2005). Seismic investigation of the craton and associated lithosphere show a variation in depth of the Lithosphere-Asthenosphere Boundary (LAB) from 200—240 km in the centre (Boyd et al., 1997; Goncharov et al., 2012) to 130—140km in the north and west (Griffin et al., 1999; Rosen et al., 1994).Three main events of kimberlite magmatism mark the Siberian Craton at 367—345Ma, 245—215Ma and 160—145Ma (Alifirova et al., 2012).

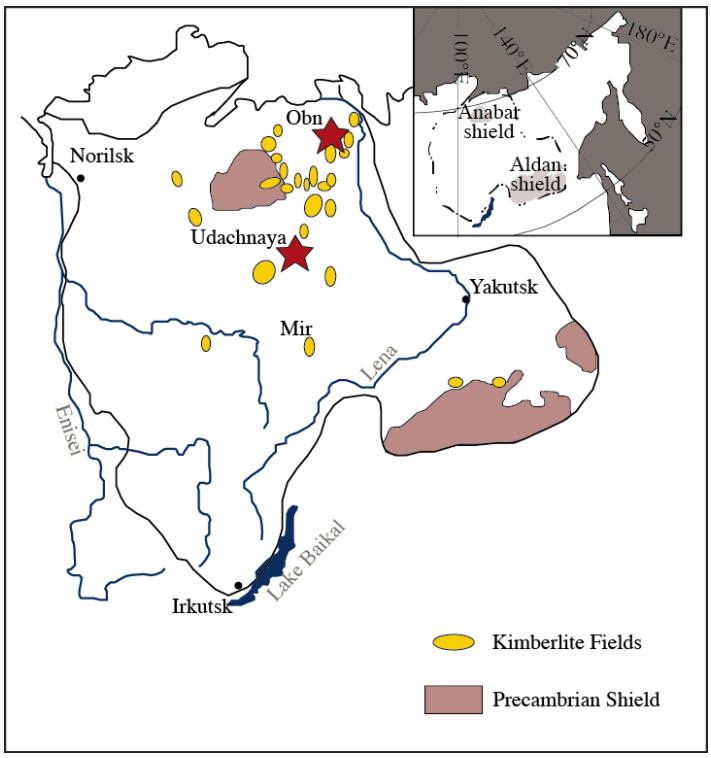

Figure I—22. Map of the Siberian craton with outcropping Precambrian Shields and main kimberlite pipes. Obnazhennaya (Obn) and Udachnaya pipes are marked with red star symbol. After Taylor et al. (2003).

Udachnaya pipe (66°26'N—112°19'E) is located just outside the Arctic Circle, in the southern part of the Anabar Province, in the centre of the Siberian craton. It is part of the Daldyn-Alakit field (Griffin et al., 1999) and is divided into two adjacent kimberlite bodies (Eastern and Western). It is classified as a Group-1 kimberlite (Kobussen et al., 2006), containing olivine, phlogopite, spinel group minerals, perovskite, monticellite, sulphides, chlorides, carbonates and K-bearing alkali-carbonates. However, the Udachnaya kimberlite has a unique composition among kimberlite intrusions in general, having high abundance of alkali carbonates and halides (Kamenetsky et al., 2014). The eruption has been dated to late Devonian (~367 Ma, (Ragozin et al., 2014)) and has intruded through the Daldyn terrain basement, mostly 3.3-3.0 Ga metabasites, granulite-facies rocks, reworked at 2.8 Ga and 1.94-1.80 Ga (Pisarevsky et al., 2008; Rosen, 2002) and overlying terrrigenous-carbonate and carbonate rocks. The xenolith suite contains a small fraction of sedimentary rocks (< 6 vol.%, (Kamenetsky et al., 2014)), xenocrysts and is dominated by peridotites and (to a lesser extent) eclogite xenoliths, often diamond bearing (Griffin et al., 1999; Ionov et al., 2010).

Obnazhennaya pipe (70°15'N—121°35'E) is a Group-1 kimberlite (Reguir et al., 2009), part of the Kuoyka kimberlite field in the Olenek province close to the northeastern craton border. Its

age is poorly defined (Late-Jurassic to Early Cretaceous), however most authors agree it erupted around ~160 Ma during the youngest kimberlite magmatic event (Smelov and Zaitsev, 2013) and it cuts across the Birekte terrane (Archaean granite – greenstone basement (Rosen et al., 1994), covered by Meso- Neoproterozoic and Phanerozoic sediments (Griffin et al., 1999)). The xenolith suite comprises xenocrysts, coarse-grained peridotite, eclogite, websterite and dunite mantle fragments (Taylor et al., 2003). Out of the known pipes (~100) that make up the Kuoyka field, Obnazhennaya is a "shallow pipe" and thus barren of diamonds (Smith et al., 2012).

Summary: The present study is based on a collection of more than 180 xenoliths from four kimberlite pipes, from the Kaapvaal and Siberian cratons, and it focuses on petro-geochemical variations among non-metasomatized eclogites. The origin of mantle eclogites has been controversial for more than a century and this study sets out to improve the understanding of mantle eclogites and their consequences on the subcratonic lithospheric mantle.

CHAPTER II.

ANALYTICAL TECHNIQUES

CHAPTER II. ANALYTICAL TECHNIQUES

Mineralogical and textural observations were performed with a Leica DM 4500P microscope at various magnifications at the Laboratoire Magmas et Volcans (LMV UMR CNRS 6524) in Saint-Etienne, France. Modal abundances of each mineral phase were estimated based on the thin sections.

2.1. Major and trace element analyses

Major elements analyses of individual minerals were performed at the Laboratoire Magmas et Volcans in Clermont Ferrand, France on a CAMECA SX 100 electron microprobe equipped with four WDS spectrometers and twelve diffraction crystals, using an accelerating voltage of 15keV and a current of 10nA, with a beam size of 1μm. The counting time was of 20 s for all elements, except K and Na (60 s), and 10 s for background. All data was processed using full ZAF (Cameca PAP) corrections. Supplementary data, major element profiles and distribution maps were performed at the Geology Department of Rhodes University, Grahamstown, South Africa on a JEOL JXA-8230 electron microprobe equipped with four WDS, one FCS and two L-Type spectrometers and twelve diffraction crystals. The distribution maps have been analysed using 15keV accelerating voltage and 20nA current, at 14x14 μm (XY) intervals, 1100x1750 points and the quantitative profiles at 0.99 μm steps, 2200 points.

Trace elements were analysed at the LMV Clermont Ferrand, France by laser ablation inductively coupled plasma spectrometry (LA-ICPMS). The ablation of minerals was done using a Resonetics Resolution M-50 laser powered by an ultra short pulse ATL AtlexExcimer laser system operating at a wavelength of 193 nm (detailed description in (Müller et al., 2009)). The spot diameter was of 73 μm associated to a repetition rate of 6 Hz. The ablated material is carried in helium, and then mixed with nitrogen and argon, before injection into a plasma source of an HR Element ICPMS. All data was corrected for fractionation occurring during laser sampling

and for instrumental mass discrimination (mass bias) by standard bracketing with repeated measurements of NIST610 standard. At the beginning and at the end of every run, repeated analyses of BCR-2g standard, treated as unknown control the reproducibility and accuracy of the analyses. Data reduction was carried out with the software package GLITTER® (Macquarie Research Ltd, 2001) van Achterbergh et al. (2001). For each analysis, the time resolved signal for each element was monitored to discard perturbations related to inclusions, fractures or mixing.

2.2. Oxygen isotope analysis

The O isotope analyses were performed at the Department of Geological Sciences, University of Cape Town (UCT), South Africa by the laser fluorination method described by Harris and Vogeli (2010). The laser fluorination method was originally described by Sharp (1990) and the UCT system uses a 20W New Wave CO_2 laser, mounted on a moveable stage. Mineral separates of garnet, omphacite, corundum and kyanite were handpicked under a binocular microscope from jaw-crushed material. The chosen grains showed no petrographical evidence for alteration, fractures or inclusions. Between 2.5 and 3.0 mg have been weighed of each mineral and placed in a pure Ni sample holder and left to degas at 110°C for a minimum of 30 minutes. Typically ten samples are loaded with two aliquots of the in-house standard MONGT Monastery garnet. Subsequently the sample holder was placed in the reaction chamber and within a closed, under vacuum system, all samples have been pre-fluorinated in the presence of ~10 kPa of BrF_5, at first for 30 seconds and second for a minimum of 12h (overnight). Each sample has been reacted in the presence of ~10kPa of BrF_5, with the excess removed cryogenically. The remaining gasses have been subsequently maintained for ~1 minute at 200°C in a KCl trap in order to remove possible F_2 compounds followed by the collection of the remaining fraction into a double-U trap

immersed in liquid N_2. The purified O_2 was afterwards collected onto molecular sieve contained within glass bottles.

Oxygen isotope ratios were analysed off-line with a Finnegan DeltaXP mass spectrometer, in dual inlet mode, on an O_2 reference gas. All values are reported relative to the SMOW scale, as $\delta^{18}O = (((^{18}O/^{16}O)\ \text{sample}/\ (^{18}O/^{16}O)\ \text{standard} - 1) \times 1000$. The long-term average difference between duplicates of MON GT is 0.11 ‰ (n = 216), which corresponds to a 1σ error of 0.075.

2.3. 'Water' analyses

2.3.1. Fourier Transform Infrared Spectroscopy (FTIR)

FTIR analyses were performed with a Bruker Vertex 70 spectrometer coupled with a Hyperion microscope at the Laboratoire Magmas et Volcans, in Clermont Ferrand, France. The individual, hand-picked crystals were mounted in discs of epoxy and double polished to a final thickness of 0.45—0.60 mm. They were analysed in the unpolarized method on randomly oriented grains. For each analysis 300 scans were collected in the 700—7500 cm^{-1} spectral range, with 100 scans for background, using a resolution of 2 cm^{-1}. The aperture size was adapted to avoid cracks or opaque areas, varying between 50x50 μm and 10x10 μm. The baseline for all spectra have been drawn with Bruker Opus 5.5 software and all surfaces integrated in the characteristic OH vibration interval for clinopyroxene 2800—3800 cm^{-1}(Peslier et al., 2002; Xia et al., 2010) and 3000—3800 cm^{-1} for garnet. The water concentrations are calculated through a modified equation of the Beer-Lambert law: $c = A^{tot}/\ \varepsilon \times t$, where c is the water content in ppm by weight, A^{tot} is the sum of the integrated absorbance measured along the three crystallographic axes (α, β, γ) expressed in cm^{-2}, t is the thickness in cm and ε is the specific absorption coefficient. In the unpolarized spectra a minimum of 10 measurements/sample is required for a ~20% estimated error and in the calculus formula for omphacite the total absorbance is replaced by 3 x A, where A is the average unpolarized absorbance (Kovacs et al., 2008). As garnet is isotropic, no such

correction was needed in the calculation. The absorption coefficient is composition and wavenumber dependent and therefore specific for each mineral (Bell et al., 1995; Huang et al., 2014). Comparative water contents have been calculated for omphacite with the 7.09±0.32 $ppm^{-1}cm^{-2}$ augite integral absorption coefficient by Bell et al. (1995), most commonly used for mantle clinopyroxene, and with the 65000±3000 L $mol^{-1}cm^{-2}$ omphacite coefficient given by Koch-Müller et al. (2007). Water concentration in garnet was calculated with the 1.39±0.14 $ppm^{-1}cm^{-2}$ pyrope absorption coefficient (Bell et al., 1995) and the hydrogrossular calibration of Rossman and Aines (1991) $c=0.786$ x A, where c is water expressed in ppm and A is the integrated absorbance per cm within the estimated error stated above.

2.3.2. Hydrogen content by Secondary Ion Mass Spectrometry (SIMS)

Hydrogen SIMS analyses were performed at CRPG-CNRS Nancy with a Cameca IMS1280 ion microprobe on double polished, gold-coated thin sections. Samples were degassed prior to analysis to eliminate adsorbed water. A 13keV, 5~10nA negative primary oxygen beam was focused onto omphacite crystals to a 30μm diameter spot. The secondary beam mass resolution was set at 2000, with an energy window of 55eV and no energy filtering. Secondary ions (for $^{1}H^{+}$, $^{2}H^{+}$, $^{28}Si^{+}$ and $^{30}Si^{+}$) have been measured by peak switching with 20 minutes ion counting time. Count rates on H^{+} varied between 1.105—2.105 counts/s with a statistical precision range of 5x—10x. Water content for background was inferior to 10 ppm. Sample water content was calculated with respect to the measured secondary hydrogen ion intensity (the secondary $^{1}H^{+}$ counts with respect to the primary ion intensity ratio) of several measurements on the augite standard (sample NSH3 (Xia et al., 2004)) as well as through the use of a working curve of H^{+}/Si^{+} vs. H_2O wt.% values. The estimated precision of standards was about 0.01 wt.% H_2O (1σ).

2.3.3. High Temperature Conversion Elemental Analysis (TC/EA)

Samples were analysed using a continuous flow elemental analyser (TC/EA) operating on-line with mass spectrometer (Gong et al., 2007a, b; Sharp et al., 2001) at the Laboratoire Magmas et Volcans of Jean Monnet University, in Saint-Etienne. The operating system used was a ThermoFisher Flash IRMS© coupled on-line with DeltaV+™ mass spectrometer monitored by ConflowIV™ diluter hosted. The DeltaV+™ used an electrostatic filter to prevent isobaric interferences between the helium carrier gas and the generated mass 3 of hydrogen. The elemental analyser was coupled with a pyrolysis line constituted by a glassy carbon tube filled with glassy carbon grains placed inside an alumina ceramic tube heated at 1450° C and flush by helium (100 ml/min). All hydrogenous gas were reduced by glassy carbon, H_2 was separated from other gas species (*i.e.* CO) by a chromatographic column heated at 90° C and transferred to the mass spectrometer. ConflowIV™ diluter monitored the flux and the 2 injections of H_2 reference gas. The duration of a complete analysis was of 300s.

Between 0.3 and 25 mg were analysed of each mineral separate, depending on their H_2O content previously measured through additional methods (*i.e.* FTIR, SIMS), crushed to <100µm as suggested by Gong et al. (2007b) to prevent incomplete extraction.

The relation between hydrogen contents and peak size (amplitude) detected by mass spectrometer was calibrated with benzoic acid (4.951 wt.% H) and then water concentrations were determined by mass H_2 peak amplitude and the uncertainty is estimated to be ±0.05 wt.%.

2.3.4. Elastic Recoil Detection Analysis (ERDA)

ERDA analyses were performed using a nuclear microprobe at Laboratoire d'Etudes des Elements Legers CEA Saclay, France, method described by Khodja et al. (2001) and analytical set-up is described into detail by Bureau et al. (2009). The measurements were performed

through three different sessions. Omphacite grains were hand-picked under a binocular microscope from jaw-crushed material and double polished, subsequently pressed into an indium plug of 12 mm diameter, contained within an aluminium sample holder of 22 mm diameter. The sample holder containing 9 omphacite crystals was gold-coated in the first session and carbon-coated in the following ones, and inserted into a stainless steel sample chamber. The coating does not influence the water measurement, however gold-coating creates a low energy tail in the ERDA spectrum, difficult to measure. Samples and standards may be tilted such that the polished surface is oriented perpendicular or at a low 'grazing' angle of 15° with respect to the incident ERDA beam.

The analysis uses a 3 MeV $^{4}He^{+}$ beam, produced by a single stage van de Graaf generator with beam size on the sample surface of 12 µm x 3 µm in the ERDA configuration. A set of standards such as Al_2O_3, $CaCO_3$, SiO_2, αFeS_2, SnBi Zr, ZrH and Kapton HN polymide ©Dupont Corp are used to calibrate the RBS solid angle (Withers et al., 2012), analysed at the beginning of each session for 15 min except for the Kapton, 30 min. The ERDA detector was positioned at 30° with respect to the incident beam and the RBS and ERDA energy spectra were modelled with the SIMNRA program (Mayer, 1999). The samples were analysed between 20 and 120 min and analysis areas were selected in order to avoid cracks, grain boundaries or secondary minerals, with the RISMIN software (Daudin et al., 2003). The H contents of the samples were calculated by simulation of the ERDA spectra using the SIMNRA program. The main uncertainty in the H estimates is derived from the detector counting statistics, however minor uncertainties may include contributions from sample tilt and RBS solid angles variation and ERDA energy calibration and spectra integration.

Whole rock compositions have been calculated based on individual mineral analyses and estimated modal abundance. The mineral proportions have been determined on thin sections scans and compositional maps, based on colour contrast between the different phases with the

use of the Adobe Photoshop CS6 program. Similarly, the composition of precursory clinopyroxene has been calculated based on the composition of the exsolved and host mineral phases and their estimated modal abundance. The errors in surface to volumetric conversions are negligible as all the minerals concerned have very similar densities.

CHAPTER III.

PETROGRAPHY and CLASSIFICATION

CHAPTER III. PETROGRAPHY and CLASSIFICATION

Eclogite xenoliths brought up to the surface by kimberlite magmas are unique, otherwise inaccessible samples from the Subcontinental Lithospheric Mantle (SCLM). By definition the primary mineralogy consists of a high-grade mineral assemblage of garnet and omphacitic clinopyroxene. Most eclogite xenoliths are bimineralic, with rutile as main accessory phase. Less frequently, they may contain coesite (typically found reverted to palisade quartz), diamond, graphite, kyanite and corundum as primary minor phases. Few samples show exsolution textures such as topotactic (crystallographically controlled) lamellae or lenses of garnet and/or kyanite in clinopyroxene, or needle-like rutile in both omphacite and garnet.

Petrological observations are a first-rate tool in identifying and classifying eclogite xenoliths based on their mineral assemblage and texture. This chapter sets out to offer a complete account of the different eclogite Types found in kimberlites from both Kaapvaal and Siberian cratons. For this purpose an ensemble of 182 samples from Roberts Victor, 11 from Jagersfontein, 11 from Udachnaya and 4 from Obnazhennaya kimberlites have been examined. Furthermore, this chapter aims to identify pristine eclogite xenoliths, which show no traces of contamination by kimberlite-derived fluids. Non-metasomatized eclogites can offer essential information about the nature of their protolith and represent the focus of the present study.

3.1. Bimineralic eclogites

Bimineralic eclogites comprise a garnet (gt) – omphacite (omph) assemblage often in association with rutile (ru). Samples showing interactions with kimberlitic/carbonaceous fluids typically contain phlogopite (phl), plagioclase feldspar (plg) and/or sanidine (sa) as index secondary minerals. Textures have variable grain size and grain boundaries, as well as modal abundance and colour.

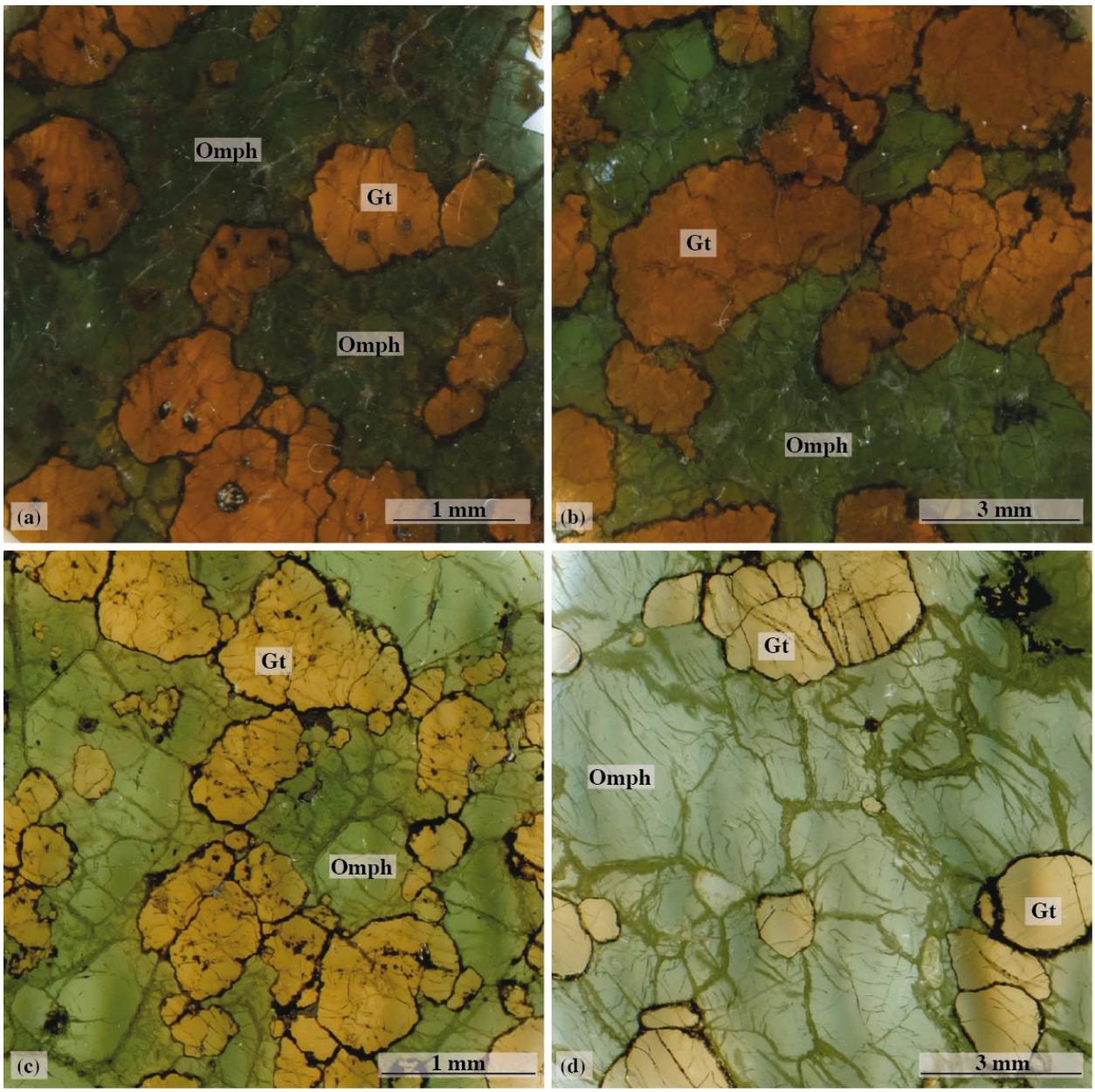

Figure III—1. Scanned thin sections of representative Type I (MacGregor & Carter, 1970) bimineralic eclogites from Roberts Victor Mine, South Africa. (a) — RV315; (b) —RV226; (c) — RV350; (d) — RV366. Garnet varies from rounded to «cauliflower» grains dark to pale orange, in dark to light green omphacitic mass. Numerous vitrous inclusions give an overall «dusty» appearance.

3.1.1. South African eclogites

Roberts Victor eclogite xenoliths range in size from ~2—20cm in diameter and are characterized by two main textural types. The most common type is defined by subhedral to rounded, or "cauliflower"-shaped garnet grains, with marked serrated grain boundaries (Figure III—1). These are enclosed in a finely crystallized, seemingly opaque, secondary rim. Garnet can be found as grain clusters, "necklaces" and less as isolated grains. They are irregularly fractured and with numerous scattered glass and melt inclusions that give a "dusty" appearance. Garnet ranges in size and modal abundance, with colour from dark to pale orange but showing no textural zoning. Omphacitic clinopyroxene is found as inequigranular, sub- to anhedral grains forming an interstitial matrix around garnet. Colour varies from dark to light green (in polarized light), with irregular grain boundaries doubled by simplectitic plagioclasic feldspar, diopside and fine-grained phlogopite. Rutile is interstitial and texturally bound to the fine-grained secondary minerals. This textural group will be hereinafter referred to as Type I eclogites after Gréau et al. (2011); MacGregor and Carter (1970) describing metasomatized eclogite xenoliths (Chapter 1.1.2). Less frequently, eclogite xenoliths have sub- to euhedral garnet (Figure III—2) bordered by a fine, opaque rim. The colour of the garnet varies from dark to pale orange, they are slightly less fractured and more systematically coarse-grained (size range) than the Type I. A few samples have fine, elongated anhedral garnet bordering clinopyroxene. Omphacite is found as a sub- to anhedral, inequigranular mass. Its colour ranges from dark to pale green, with translucent cores often surrounded by symplectitic rims. Rutile is found as needle-like exsolution spread throughout both garnet and omphacite. This textural group will henceforth be referred to as Type II, describing pristine, non-metasomatized eclogite xenoliths (Chapter 1.1.2).

Jagersfontein eclogite xenoliths are scarcer and range only few centimetres in size. Similarly, two textural groups are identified. Garnet is found as rounded anhedral grains with serrated grain boundaries, underlined by a fine-grained, opaque rim. Numerous intra-crystalline fine fractures associated with glass and melt inclusions give an overall "dusty" appearance (Figure III—3a-b).

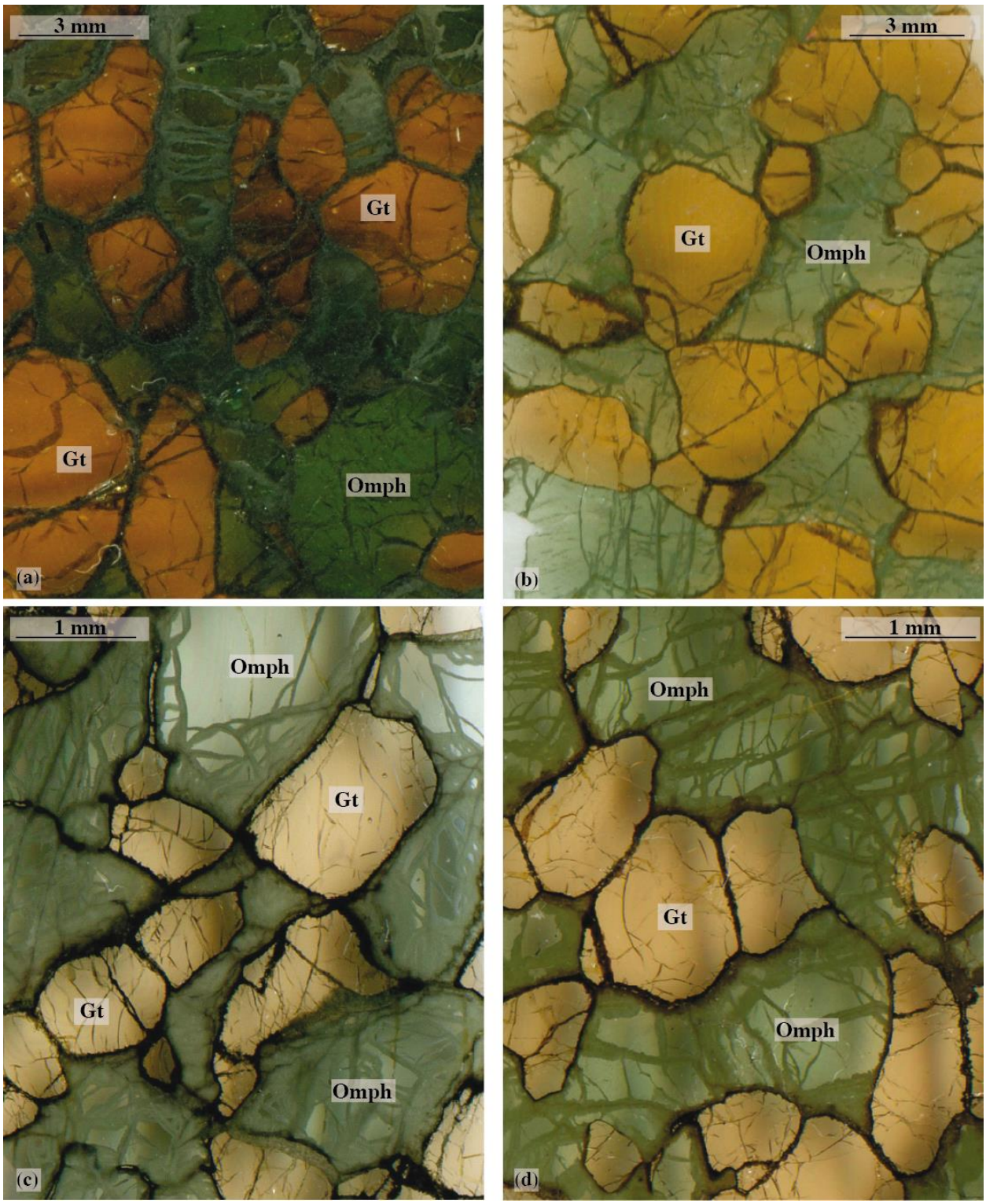

Figure III—2. Scanned thin sections of representative Type II (MacGregor & Carter, 1970) bimineralic eclogites from Roberts Victor mine, South Africa. (a) — RV220; (b) — RV232; (c) — RV398; (d) — RV469. Garnet varies from anhedral to subhedral and subrounded, dark to pale orange in a dark to light green omphacitic mass. Grain boundaries are straight, doubled by a fine-grained, opaque secondary rim around garnet and symplectite around the omphacite. Needle-like rutile exsolutions are spread throughout the sample.

Omphacite is destabilized into symplectite rims, with poorly preserved cores. The xenomorphous crystals are highly altered along irregular fractures by carbonate-rich fluids. This texture is consistent with the previously described “Type I” (metasomatized) eclogites. Less commonly, garnet is found as angular subhedral crystals with straight or slightly indented grain boundaries (Figure III—3c-d). Omphacite is xenomorphous and interstitial, with symplectitic rims of various thickness (give range) and well-preserved translucent cores. All grain boundaries are rimmed by carbonate-rich veinlets. This textural group is accordant with the prior explained “Type II” describing pristine, non-metasomatized eclogites.

3.1.2. Siberian eclogites

Siberian eclogites are typically only a few cm in diameter. Although they share textural similitudes with South African eclogite xenoliths, they are significantly less abundant than Roberts Victor eclogites, and more altered. Udachnaya bimineralic eclogite xenoliths are predominantly characterized by subrounded, anhedral, orange garnets (Figure III—4a-c). Grain boundaries are serrated and enclosed by secondary carbonate-rich coronae, with an outer fine-grained opaque rim. Omphacite is found as a xenomorphous, inequigranular, light green matrix. Symplectitic plagioclasic feldspar and diopside surround the grain boundaries and fractures, associated with carbonate-rich veinlets. Numerous melt inclusions spread throughout the samples, give an overall “dusty” appearance. This textural variety is consistent with the Type I eclogites. Less common, some Siberian eclogites have subhedral, light-coloured garnets, with straight grain boundaries doubled by secondary rims (Figure III—4d). Omphacite is found as a dark green interstitial matrix. Xenoblastic grain boundaries are preserved marking an inequigranular texture, underlined by fine symplectitic rims. The mineral assemblage is less fractured and inclusions-free, having an overall pristine appearance. Similarly, Obnazhennaya bimineralic eclogite (Figure III—5) is dominated by light coloured garnet, delimited by straight grain boundaries. Garnet ranges from small, rounded exsolved grains to large, subhedral crystals, underlined by a fine-grained, opaque secondary rim. Omphacite is found as xenoblastic, light

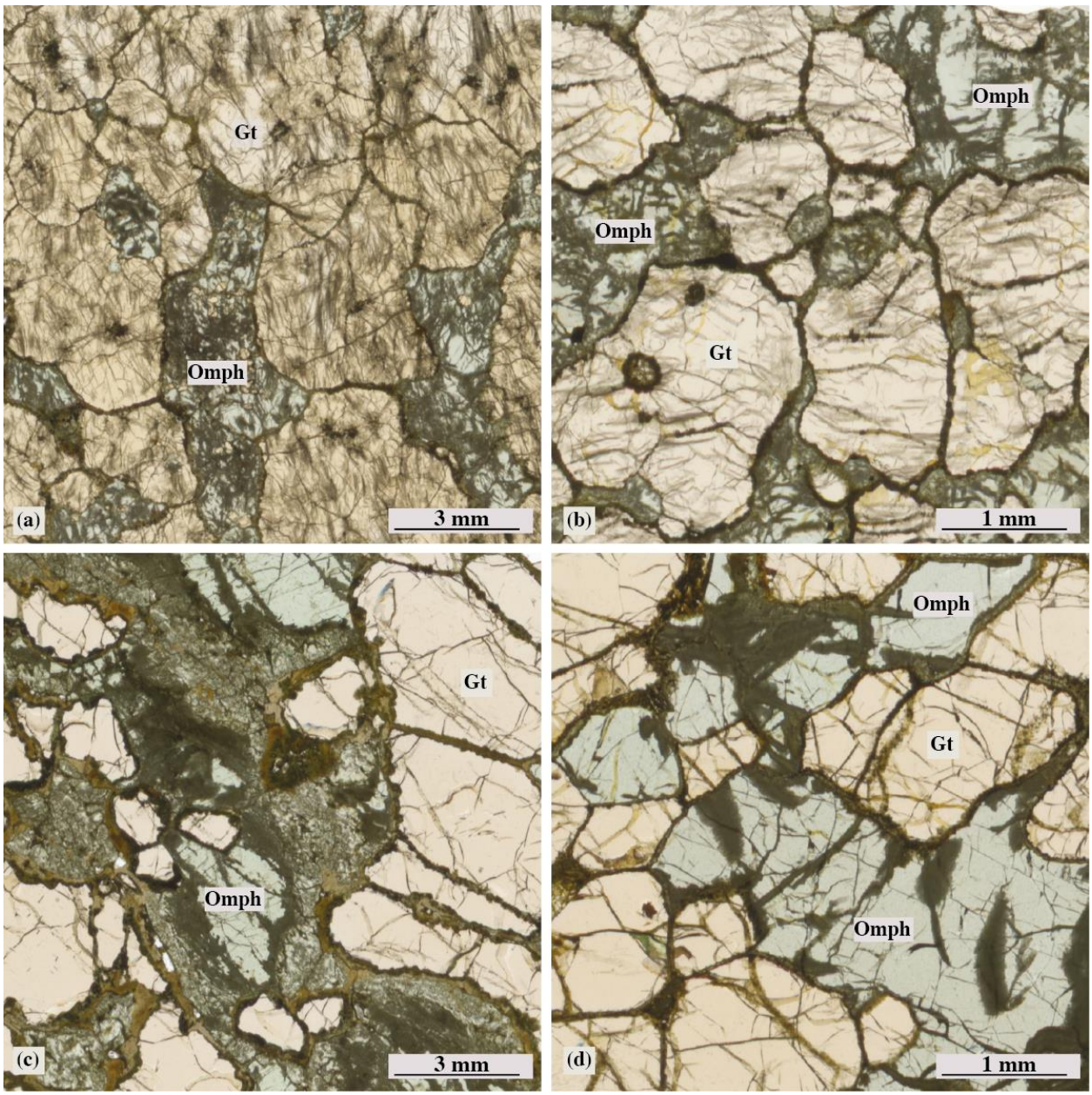

Figure III—3. Scanned thin sections of representativ bimineralic eclogites from Jagersfontein mine, South Africa. Type I: (a) — JG15-28; (b) — JG15-30 is characterized by rounded to «cauliflower» garnet grains, in an omphacitic mass. Numerous vitrous inclusions give an overall «dusty» aspect. Type II: (c) — JG15-29; (d) — JG15-32 is characterized by subhedral, inequigranular garnet in a light green omphacitic matrix. Grain boundaries are straight, underlined by carbonate-rich veinlets. Often omphacite rims are surrounded by symplectitic coronae.

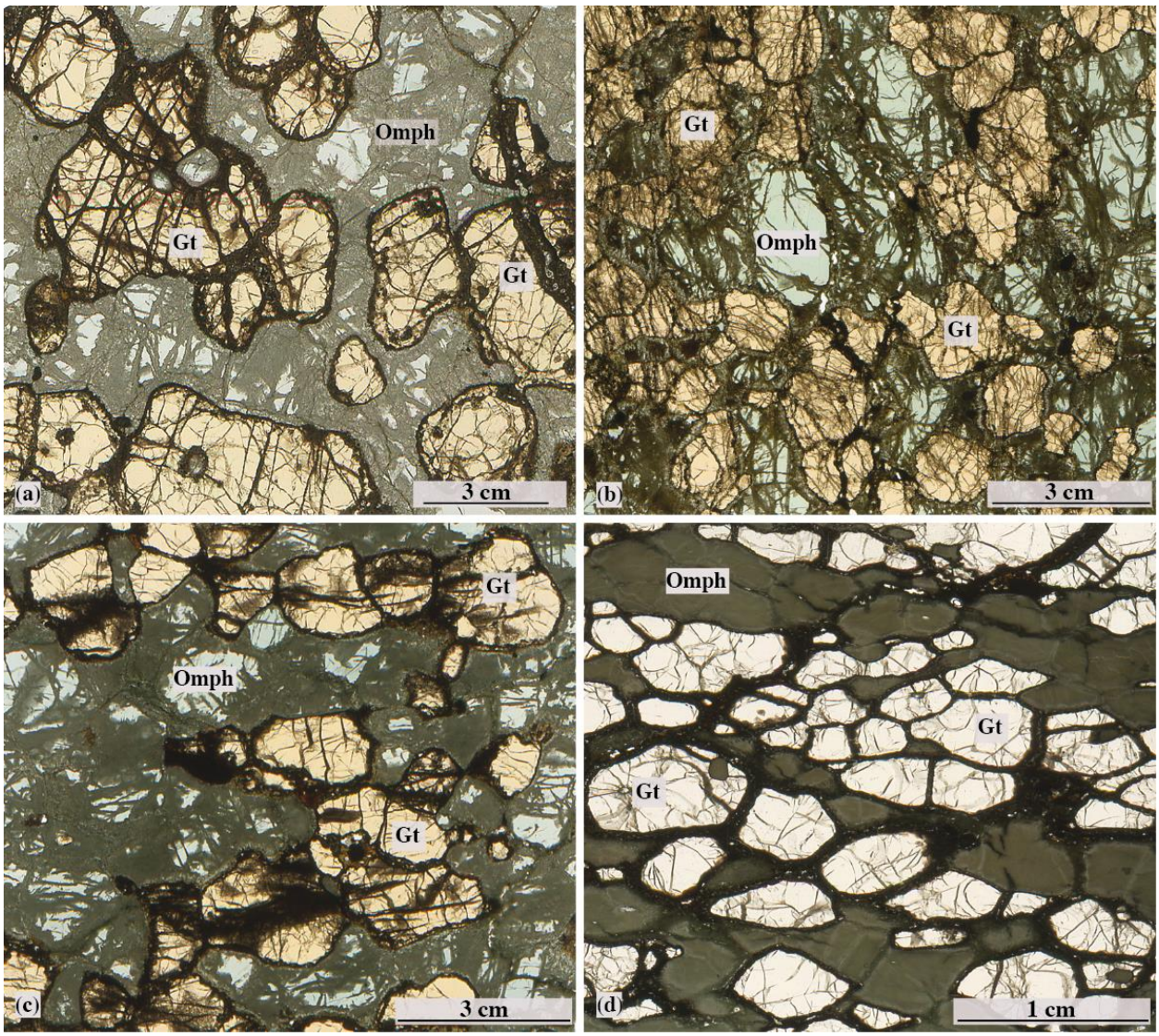

Figure III—4. Scanned thin sections of representative bimineralic eclogites from Udachnaya kimberlite.Type I: (a) — UV11-44; (b) — UV11-57; (c) — UV09-457 is characterized by subrounded to rounded orange garnets, highly fractured and rich in glass and melt inclusions giving an overall «dusty» appearance. Grain boundaries are indented, often surrounded by a secondry rim. Omphacite is found as xenomorphous, inequigranular, light green matrix. Carbonate-rich veinlets mark the numerous fractures and grain boundaries. Type II: (d)—UV09-434 is characterized by subhedral, inequigranular, light-coloured garnets with straight grain boundaries. Omphacite is found as a dark green interstitial matrix. Xenoblastic grain boundaries are preserved marking an inequigranular texture, underlined by fine symplectitic rims.

green, inequigranular grains. Often omphacite grains show strong cleavage planes, marked by oriented lens-shaped garnets or fine amphibole needle-like exsolutions (Figure III—5b). Where present, rutile is found as interstitial, xenoblastic grains, associated with interstitial carbonate-rich veinlets. This textural group is consistent with the previously described Type II, defined as non-metasomatized eclogite xenoliths.

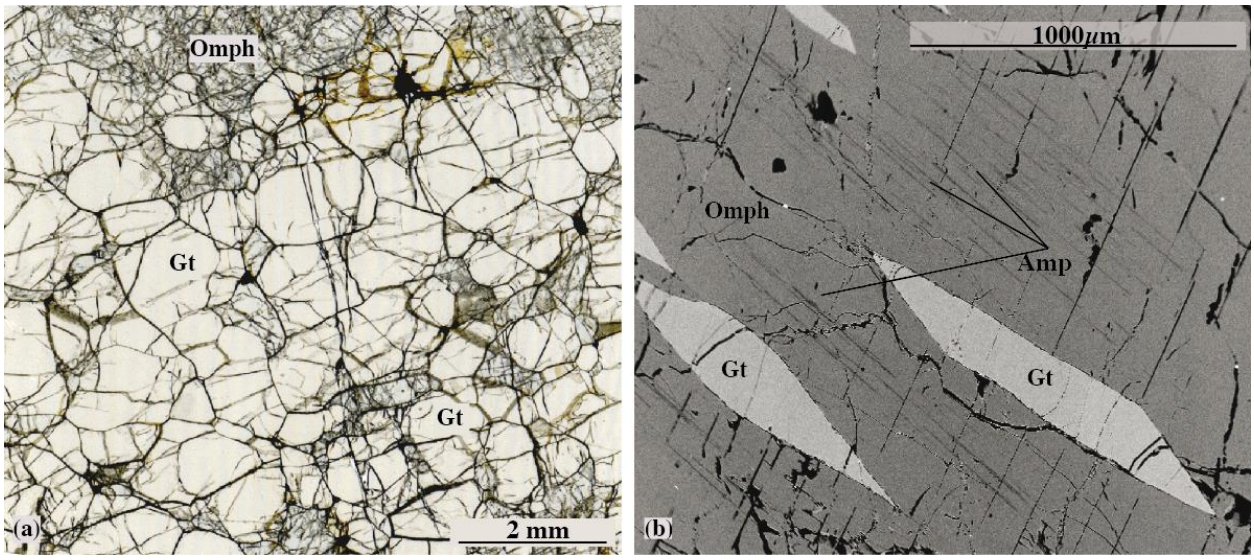

Figure III—5. (a) — Scanned thin section of one bimineralic eclogite from Obnazhennaya kimberlite: Obn108/13. Garnet is found as subhedral to rounded, inequigranular, light-coloured grains with straight grain boundaries. Omphacite is found as a xenoblastic light green, interstitial matrix. (b) — BSE (back-scattered electron) image of strong cleavage planes, marked by oriented lens-shaped garnets or fine amphibole needle-like exsolutions in host omphacite.

A few bimineralic eclogites preserve transitional textures from a garnet-dominated assemblage, with a cumulative appearance, to a balanced (50:50) omphacite-garnet assemblage (Figure III—6a). Garnets are typically “cauliflower”-shaped and the samples have an overall “dusty” appearance, surrounded by secondary rims, characteristic to the metasomatized Type I eclogites defined above. Similarly, a few xenoliths may show a transition from a classic bimineralic texture with green omphacite and orange garnet to a kyanite-bearing assemblage, characterized by a white omphacitic matrix with blue, tabular or xenomorphous, kyanite crystals, the latter often surrounded by garnet (Figure III—6b). The samples have an overall dusty and very fractured appearance, with irregular grain boundaries and show signs of a progressive, discrete metasomatism.

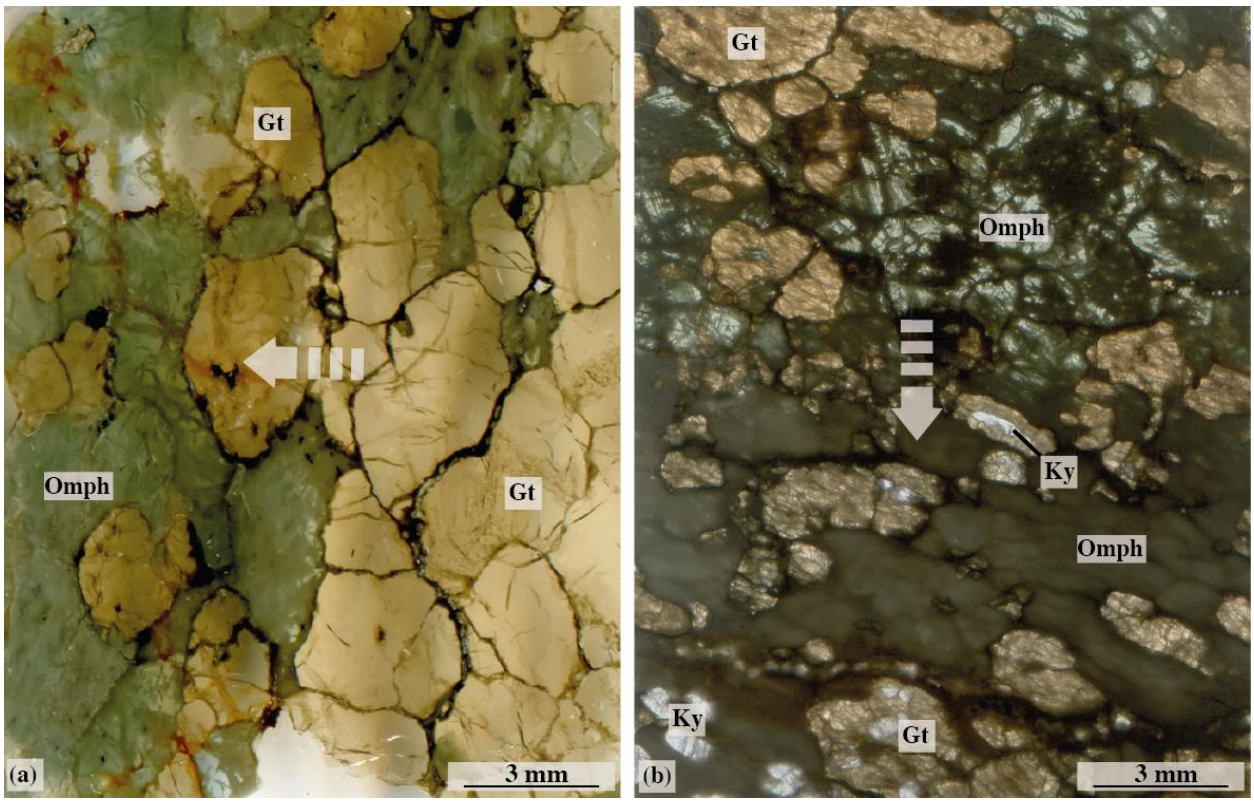

Figure III—6. Scanned thin sections of eclogite xenoliths from Roberts Victor mine, South Africa, preserving transitional textures and showing progressive degrees of metasomatic interaction: (a) — RV198 shows from from right to left the transition from a garnet-dominated eclogite with a cumulative textures to a classical bimineralic eclogite comprising a garnet (gt) - omphacite (omph) assemblage; (b) — RV153 shows from the top to bottom the transition from a bimineralic assemblage to a kyanite-bearing eclogite with a change in omphacite texture from green anhedral grains to a white «spongy» matrix.

3.2. Coesite-,Kyanite-, Corundum-bearing eclogites

3.2.1. Coesite-bearing eclogites

South African coesite-bearing eclogites are characterized by sub- to anhedral, pale orange garnets with straight to indented grain boundaries (Figure III—7). Omphacite is found as a white “cloudy” or “spongy” matrix, due to fast decompression breakdown of the clinopyroxene structure, with preserved xenoblastic grain boundaries. Fine-grained, carbonate-rich veinlets of variable thickness surround the garnet grains. Coesite (coe) is found as xenomorphous core relics surrounded by palisade α-quartz (qz). Smaller grains are fully inverted to quartz and often show radial fractures due to ~10% volume increase (Carswell and Zhang, 1999). Coesite is typically

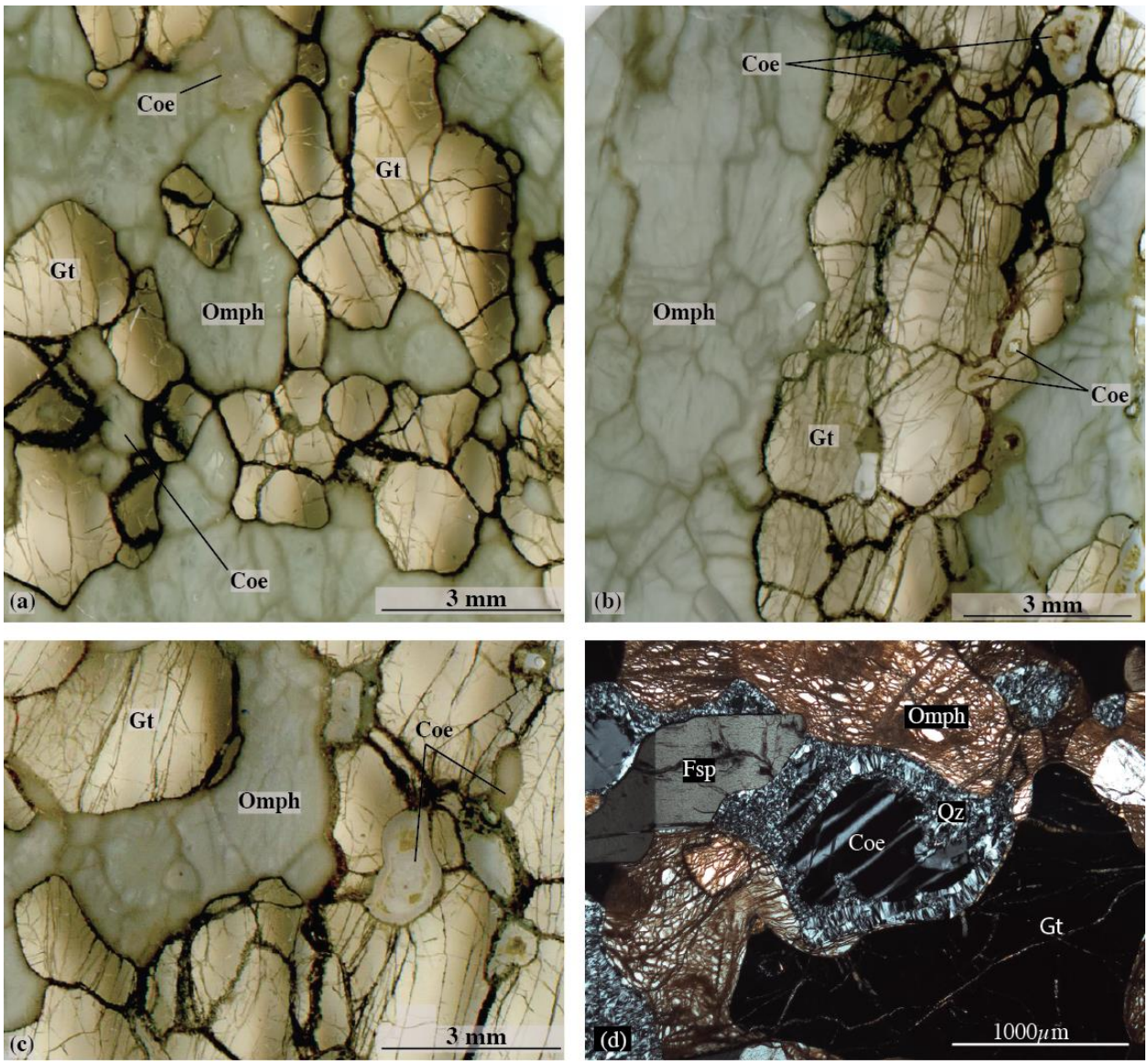

Figure III—7. Scanned thin sections (a—c) and photomicrograph (d) of representative coesite-bearing eclogites from Roberts Victor mine, South Africa. (a) —RV317; (b) — RV326; (c) — RV503; (d) — JJG4492. Anhedral, pale orange garnet is found typically clustered. Grain boundaries range from straight to indented and are doubled by a fine-grained, opaque, secondary rim. Omphacite is found as a white decompressional matrix, preserving xenoblastic grain boundaries. Relict xenomorphous coesite is surrounded by pallisade α-quartz and typically associated with kimberlitic/carbonaceous infiltration.

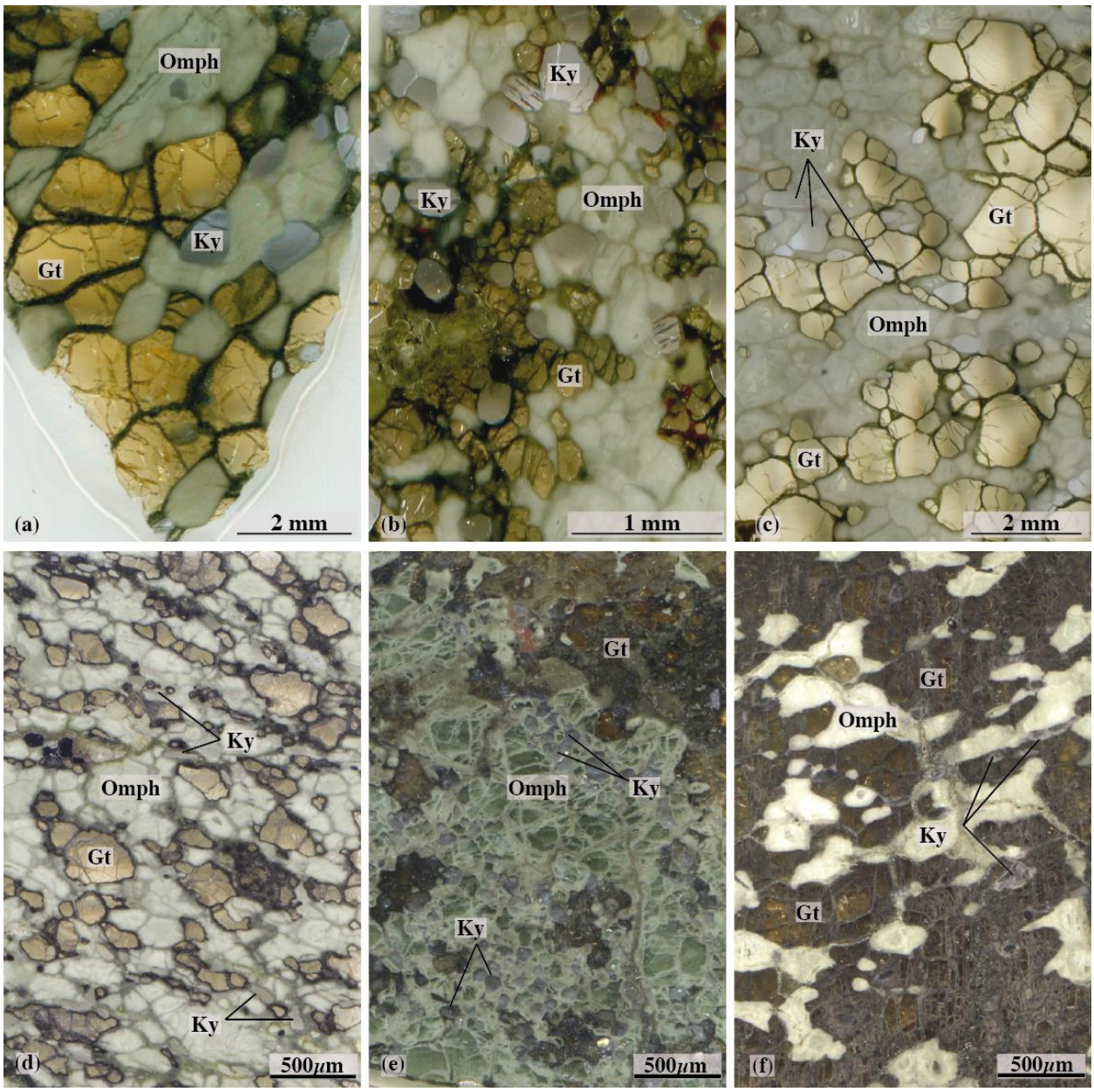

Figure III—8. Scanned thin sections of representative Scanned thin sections of representative kyanite-bearing eclogites from the Kaapvaal craton: (a)—RV195; (b)—RV209; (c) — RV320 and from the Siberian craton: (d) — UV09-487A; (e) — UV09-505; (f) — UV09-536. Garnet is found as subhedral to anhedral, inequigranular, dark to pale orange grains, with strainght or slightly indendted grain boundaries. Omphacite is found as a white matrix («cloudy»/«spongy» clinopyroxene). Some samples preserve translucent green core and xenoblastic grain boundaries. Kyanite is found as fine (30—40μm) subhedral, tabular, or rounded grains. Grain boundaries are surrounded by a fine-grained opaque rim.

found texturally bound to the carbonate-rich (cb) veinlets adjacent to garnet, associated with phlogopite, plagioclasic feldspar and/or sanidine.

3.2.2. Kyanite-bearing eclogites

Kyanite-bearing xenoliths, from both Siberian and Kaapvaal cratons, are characterized by sub- to anhedral, inequigranular garnets with straight to slightly indented grain boundaries (Figure III—8). The colour ranges from light to dark brown. Omphacite is broken down into a white "spongy" clinopyroxene matrix, sometimes with preserved translucent green cores and xenoblastic grain boundaries. Kyanite (ky) is found as small (30—40μm), subhedral to tabular or rounded, isolated or clustered grains. Microcrystalline, opaque rims surround grain boundaries.

3.2.3. Corundum-bearing eclogites

Omphacite is the dominant mineral (~60% modal abundance), ranging from small (~0.3cm) rounded grains to large (~2cm) subhedral light green crystals (Figure III—9). Garnet is found as subhedral and rounded inequigranular grains, with straight grain boundaries and of typically light brown colour. Corundum (cor) varies from ~2—17% modal abundance and is found as pale to intense pink, subhedral to anhedral crystals. Often corundum grains are surrounded by garnet or kyanite-garnet coronae (Figure III—9f). Rutile is scarce, mostly interstitial.

Three exsolution textures are present: fine oriented lamellae, coronae and granular clusters. The topotaxial lamellae (~50—300μm) consist of garnet; kyanite bordered by garnet or an intertwined garnet-zoisite assemblage (Figure III—10a-b-f). Some samples exhibit crosscutting garnet lamellae in-between the host omphacite cleavage planes (Figure III—10e). There is continuity between the lamellae and corona textures, as lamellae can be found blending into the coarse coronae (Figure III—10c-d). The coronitic texture is found around corundum grains and can be monophasic – consisting exclusively of garnet (Figure III—10c), or polyphasic –

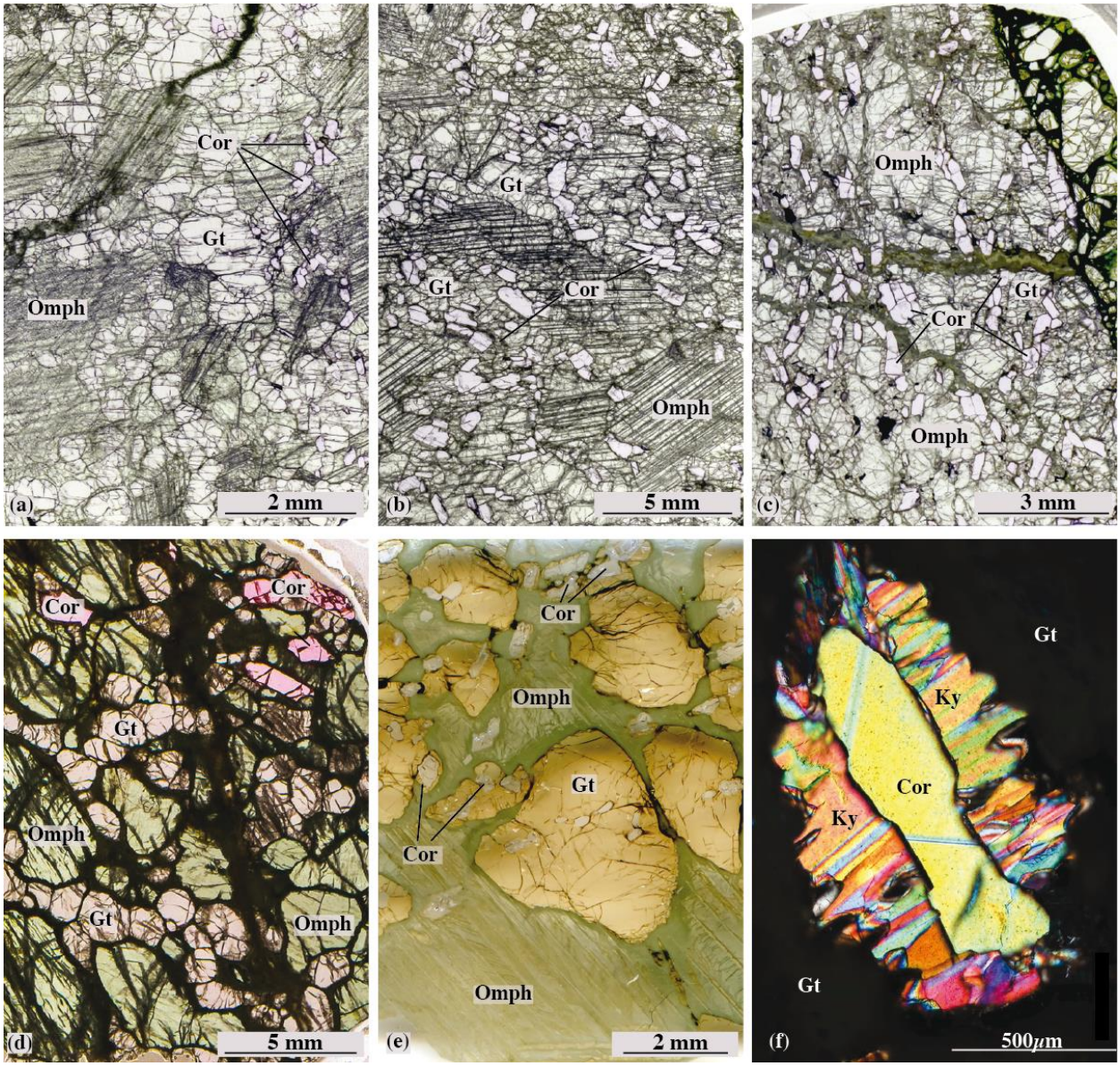

Figure III—9. Scanned thin sections and photomicrograph of representative corundum-bearing samples from the Siberian craton: (a) — Obn110/13; (b) — Obn111/13; (c) — Obn112/13 and Kaapvaal craton: (d) — RV179; (e-f) —RV344. Subhedral, light-green, inequigranular omphacite; large grains exhibit cleavage planes marked by thin exsolutions. Garnet ranges from subhedral to rounded, with straight grain boundaries and of ligh brown colour. Corundum is found as pale to intense pink sub- to anhedral grains. Garnet or kyanite-garnet coronae often surround xenomorphous corundum grains. Rutile is scarce and intestitial.

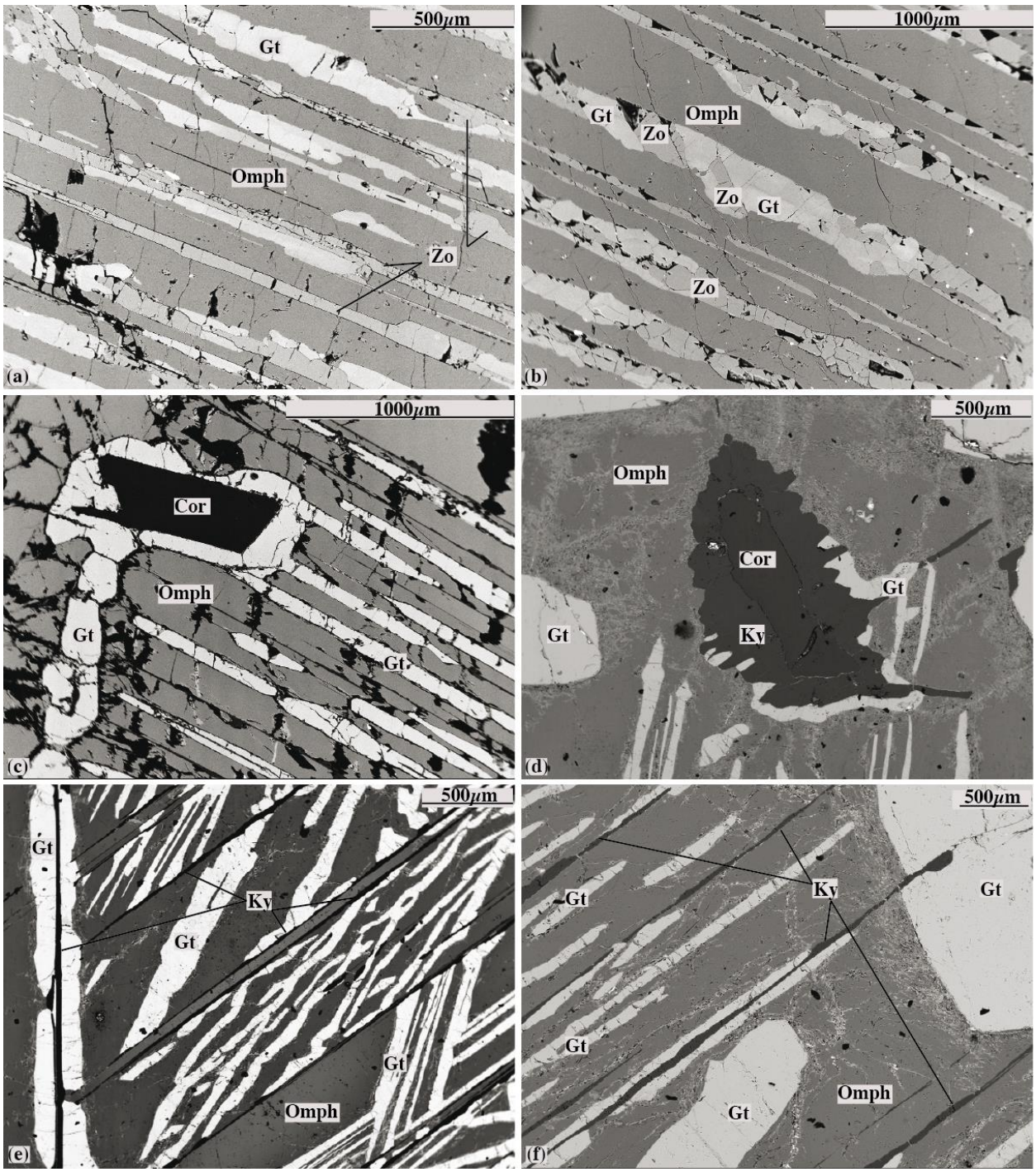

Figure III—10. BSE images of representative exsolution textures in corundum-bearing eclogites from the Siberian craton: (a-b) — Obn110/13; (c) — Obn111/13; and Kaapvaal craton: (d-f) — RV344. Large omphacite grains exhibit topotaxial garnet, garnet and kyanite or garnet-zoisite exsolution lamellae. Some samples contain crosscutting garnet lamellae inbetween the cleavaege planes. Corundum grains are often surrounded by monophasic (garnet) or polyphasic (kyanite and garnet) coronae.

consisting of a kyanite – garnet outward succession (Figure III—10d). The granular clusters consist of rounded, fine-grained (~0.1mm) garnet grains.

Summary: Eclogite xenoliths vary in size and abundance between the Kaapvaal and Siberian cratons. Throughout a collection of 208 nodules, we have identified four main textural groups closely related to their paragenesis. Bimineralic eclogites dominated by rounded garnets with serrated grain boundaries and interstitial omphacite, containing numerous inclusions are herein referred to as Type I. These samples typically have an overall "dusty" appearance and contain phlogopite as main secondary mineral, often accompanied by sanidine, interstitial rutile and a diopside-plagioclase symplectite. These features indicate Type I eclogites interacted with kimberlite-derived fluids during pervasive metasomatism preceding their entrainment. Bimineralic eclogites dominated by subhedral garnet, omphacite with net-grain boundaries and needle-like exsolution of rutile spread throughout, are referred to as Type II eclogites. They have a pristine aspect and it is believed they can be used for retracing the eclogite protolith.

Coesite- and kyanite-bearing eclogites are characterized by sub-to anhedral garnets and a white "spongy" clinopyroxene matrix. Coesite is found as xenomorphous core relics surrounded by palisade α-quartz and associated to carbonate-rich veinlets. Kyanite is found as light-blue subhedral, tabular or rounded grains. Some samples show signs of carbonaceous metasomatism. Corundum-bearing eclogites have a mineral assemblage dominated by light green omphacite (~60% modal abundance), subhedral to rounded inequigranular garnets and pink, subhedral corundum. Omphacite commonly exhibits exsolution textures (fine oriented lamellae, coronae and granular clusters). The topotaxial lamellae may contain garnet; kyanite bordered by garnet or an intertwined garnet-zoisite assemblage. The absence of metasomatic index minerals or fluid interaction indicates give corundum-bearing eclogites am overall pristine aspect.

CHAPTER IV.

MAJOR ELEMENT COMPOSITIONS

CHAPTER IV. MAJOR ELEMENT COMPOSITIONS

Chemical composition coupled with petrological observations offer key information on the origin of mantle eclogites. The major element composition in this thesis has been determined from mineral compositions and their modal proportions and allows a distinction to be made between eclogite xenoliths metasomatized by kimberlitic/carbonaceous fluids, from the pristine, non-metasomatized ones. Most commonly, alkali enrichment indicates a contribution from kimberlite-derived fluids and therefore the initial composition of the eclogite cannot be retraced. Significantly less abundant, pristine eclogites show no compositional input from the host kimberlite and offer information on their origin and protolith that is otherwise unobtainable. Chemical composition translates to the mineral assemblage and textures, and vice-versa. It is therefore important to analyse a broad textural variety of samples, in order to get a complete image of the compositional range and processes leading to eclogite formation in the cratonic keel.

This chapter aims to characterize compositional variations among all different textural types and mineral assemblages previously described (Chapter 3). For this purpose a selection of 76 representative samples has been chosen from the Kaapvaal (Roberts Victor and Jagersfontein) and Siberian (Udachnaya and Obnazhennaya) cratons. Through the use of estimated chemical composition, further specific trends for particular assemblages are shown and following previous classification criteria (Chapter 1), non-metasomatized samples are identified. Secondarily this chapter aims to establish the equilibrium pressure-temperature conditions of the eclogite xenoliths and their structural layout in the upper mantle.

4.1. Classification

Metasomatism that derives from interaction with the enclosing kimberlite magma is characterized by enrichment in the alkali content. As postulated by McCandless and Gurney (1989) and later refined by Huang et al. (2012), metasomatized eclogites have ≥ 0.8wt.% K_2O in clinopyroxene and/or ≥0.9wt.% Na_2O in garnet, referred to as "Type I", whereas pristine (non-metasomatized) eclogites have alkali contents lower than the above reference and are referred to as "Type II" (Chapter 1). Similarly, a correlation between different possible protoliths and Ca-Mg ratio in garnet and Na-content in clinopyroxene has been suggested by Taylor and Neal (1989). Mg-rich samples are interpreted as a cumulative product (group A) and samples with increasing jadeite and grossular contents (group B and respectively C) as relics of a subducted oceanic crust (Chapter 1).

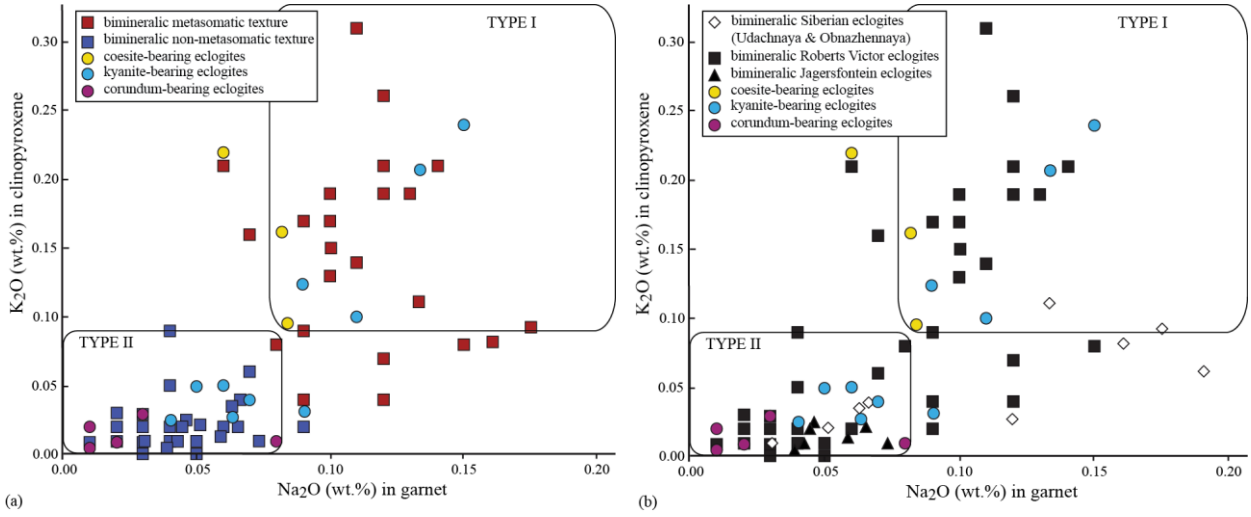

Figure IV—1. Na_2O in garnet vs. K_2O in clinopyroxene for eclogite xenoliths from the Siberian and Kaapvaal cratons. (a) Bimineralic eclogites showing metasomatic textural traits are marked in red and pristine samples in dark blue square symbols; (b) bimineralic eclogites from the Siberian craton comprise samples from Udachnaya (white diamonds) and Obnazhennaya kimberlites (White Square). Bimineralic eclogites from Kaapvaal craton comprise samples from Roberts Victor (solid black square) and Jagersfontein mines (solid black triangle). Si-Al-rich eclogites are marked with yellow (coesite-bearing), blue (kyanite-bearing) and violet (corundum-bearing) solid circle. The two types are delimited as defined by McCandless & Gurney (1989) and Huang et al. (2012): Type I — metasomatized eclogites (>0.8 wt.% Na_2O in garnet, >0.9 wt.% K_2O in clinopyroxene); Type II — pristine (non-metasomatized) eclogites (<0.8 wt.% Na_2O in garnet, <0.9wt.% K_2O in clinopyroxene).

4.1.1. Bimineralic eclogites

Representative major element compositions of garnet and clinopyroxene in bimineralic eclogites are shown in Table 2 (Kaapvaal) and Table 3 (Siberian craton). We identify Type I and Type II eclogites as well as transitional samples that fall outside the two predefined types (Figure IV—1). South African eclogites have a high variability in K_2O_{cpx} (~0.002—0.34wt. %) and Na_2O_{gt} (~0.01—0.16 wt. %), whereas Siberian samples have similar Na_2O_{gt} (~0.02—0.19 wt. %) and overall lower K_2O_{cpx} (~0.001—0.12wt. %). Due to their variable contents of FeO and MgO wt. % in garnet, the chosen bimineralic eclogites from both cratons are roughly equally distributed among the Types IA, IB and IIA, IIB respectively.

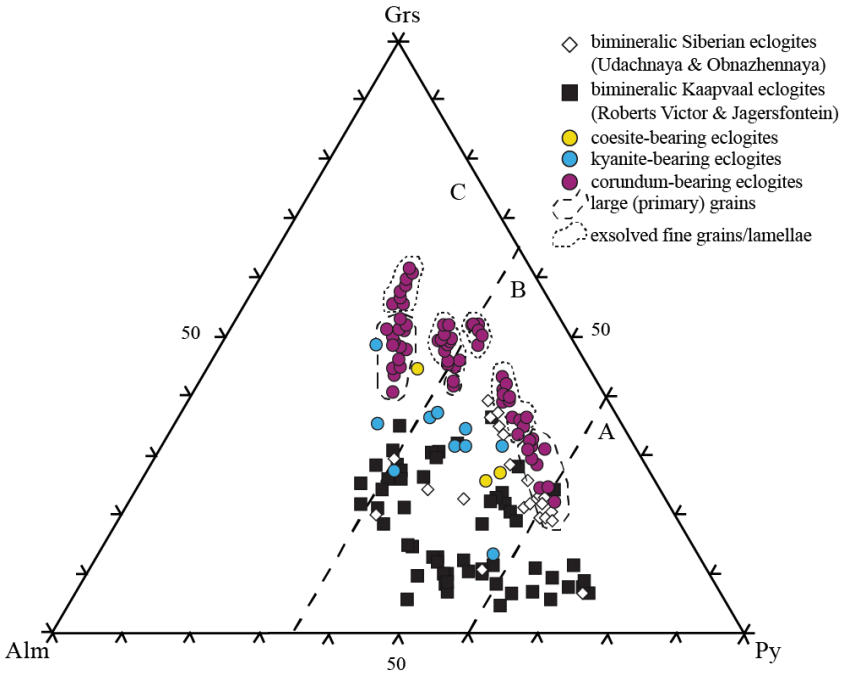

Figure IV—2. Ternary Grossular (Grs)-Pyrope (Py)-Almandine (Alm) plot (molar proportions) for eclogite xenoliths from the Siberian and Kaapvaal cratons. Bimineralic eclogites from the Siberian craton comprise samples from Udachnaya and Obnazhennaya kimberlites and are marked with white diamond symbols. Bimineralic eclogites from the Kaapvaal craton comprise samples from Roberts Victor and Jagersfontein mines and are marked with black solid square symbols. Si-Al-rich eclogites are marked with yellow (coesite-bearing), blue (kyanite-bearing) and violet (corundum-bearing) solid circle symbols. A, B, C groups are delimited as defined by Taylor & Neal (1989).

Sample	RV159		RV184		RV196		RV199		RV205		RV215		RV370		RV465		RV469		RV483		RV486		RV488		JG32		JG33		JG41	
	garnet	cpx	garnet	cpx	garnet	cpx	garnet	cpx	garnet	cpx	garnet	cpx	garnet	cpx	garnet	cpx	garnet	cpx	garnet	cpx	garnet	cpx	garnet	cpx	garnet	cpx	garnet	cpx	garnet	cpx
SiO_2	41.88	56.09	40.37	56.00	39.94	54.96	40.33	55.97	40.82	54.29	40.80	55.60	41.57	55.16	41.62	55.34	39.50	55.72	40.43	55.83	41.35	55.48	41.94	55.27	39.23	55.46	40.05	55.53	40.20	55.3
TiO_2	0.09	0.17	0.14	0.21	0.35	0.32	0.15	0.23	0.37	0.19	0.32	0.35	0.41	0.43	0.14	0.10	0.17	0.16	0.31	0.48	0.29	0.42	0.40	0.24	0.22	0.17	0.06	0.29	0.14	0.32
Al_2O_3	23.93	6.63	22.34	12.41	21.86	6.31	22.36	12.61	21.67	3.51	22.25	12.66	22.44	4.94	22.58	2.27	21.89	10.01	22.53	8.91	23.10	7.72	23.47	2.63	21.76	9.40	22.53	8.44	22.53	10.2
FeO	12.22	3.40	16.47	4.36	18.60	6.04	16.14	4.14	17.56	7.34	16.08	4.26	14.82	5.86	7.93	2.37	19.67	5.91	17.10	5.23	14.85	4.99	8.57	2.87	19.28	5.31	17.90	4.59	17.90	4.16
MnO	0.25	0.06	0.32	0.02	0.36	0.07	0.33	0.02	0.45	0.15	0.71	0.10	0.49	0.01	0.27	0.02	0.38	0.09	0.49	0.10	0.01	0.00	0.33	0.05	0.41	0.03	0.42	0.06	0.36	0.04
MgO	18.05	13.23	8.92	7.46	11.47	11.23	9.12	7.42	13.48	13.78	14.45	7.89	15.21	13.35	19.10	16.60	9.88	8.60	12.94	9.99	15.32	11.62	20.63	17.54	9.13	9.26	13.56	10.88	12.78	9.63
CaO	3.26	16.38	11.70	12.96	6.76	16.21	11.65	12.98	4.77	17.07	5.17	10.33	4.87	17.40	7.08	21.68	8.82	13.69	5.60	13.61	4.76	14.60	3.80	18.93	9.88	14.92	5.18	15.04	6.02	13.8
Na_2O	0.05	3.96	0.05	6.58	0.13	4.33	0.04	6.59	0.06	2.54	0.15	8.81	0.09	3.55	0.03	1.49	0.03	5.81	0.16	5.52	0.10	4.66	0.07	1.93	0.03	5.18	0.03	4.75	0.07	6.07
K_2O	0.02	0.08	0.01	0.01	0.05	0.26	0.00	0.01	0.00	0.23	0.02	0.08	0.00	0.04	*bdl*	0.03	*bdl*	0.00	0.02	0.24	0.01	0.17	0.01	0.05	*bdl*	0.03	*bdl*	0.03	*bdl*	0.03
Cr_2O_3	0.14	0.24	0.01	0.05	0.15	0.14	0.06	0.00	0.52	0.34	0.07	0.00	0.06	0.03	1.17	0.50	0.10	0.04	0.16	0.10	0.16	0.12	0.77	0.40	0.04	0.06	0.21	0.18	0.04	0.03
Total	99.96	100.24	100.49	100.11	99.67	99.92	100.19	100.02	99.73	99.52	100.00	100.10	99.99	100.97	99.92	100.40	100.43	100.04	99.74	100.21	100.03	99.77	100.01	100.00	99.99	99.82	99.93	99.78	100.04	99.6
Mg#	72.46	87.42	49.11	75.30	52.36	76.82	50.17	76.15	57.77	76.98	61.57	76.76	64.66	80.23	81.10	92.58	47.24	72.17	57.44	77.32	64.77	80.58	81.10	91.59	45.76	75.66	57.46	80.86	56.00	80.47
Si	3.01	1.91	3.02	1.91	3.01	1.88	3.02	1.91	3.04	1.85	3.01	1.90	3.04	1.88	2.98	1.89	2.98	1.90	3.01	1.90	3.02	1.89	2.97	1.89	2.98	1.89	2.98	1.89	2.99	1.89
Ti	0.01	0.004	0.01	0.01	0.02	0.01	0.01	0.01	0.02	0.005	0.02	0.01	0.02	0.01	0.01	0.003	0.01	0.004	0.02	0.01	0.02	0.01	0.02	0.01	0.01	-	0.004	0.01	0.01	0.01
Al	2.02	0.27	1.97	0.50	1.94	0.29	1.97	0.51	1.90	0.20	1.94	0.52	1.93	0.23	1.90	0.12	1.95	0.41	1.97	0.37	1.99	0.33	1.96	0.13	1.95	0.40	1.97	0.36	1.98	0.44
Cr	0.01	0.01	-	0.001	0.01	0.004	0.003	-	0.03	0.01	0.004	-	0.003	-	0.07	0.01	0.01	-	0.01	0.003	0.01	0.003	0.04	0.01	0.003	0.001	0.01	0.005	0.002	0.001
Fe	0.73	0.10	1.03	0.12	1.17	0.17	1.01	0.12	1.09	0.21	0.99	0.12	0.91	0.17	0.47	0.07	1.24	0.17	1.06	0.15	0.91	0.14	0.51	0.08	1.23	0.15	1.11	0.13	1.11	0.12
Mn	0.02	0.002	0.02	-	0.02	0.002	0.02	-	0.03	0.004	0.04	0.003	0.03	-	0.02	-	0.02	0.003	0.03	0.003	-	-	0.02	0.001	0.03	0.001	0.03	0.002	0.02	0.001
Mg	1.93	0.67	1.00	0.38	1.29	0.57	1.02	0.38	1.49	0.70	1.59	0.40	1.66	0.68	2.04	0.84	1.11	0.44	1.43	0.51	1.67	0.59	2.18	0.89	1.03	0.47	1.50	0.55	1.42	0.49
Ca	0.25	0.60	0.94	0.47	0.54	0.59	0.93	0.47	0.38	0.62	0.41	0.38	0.38	0.64	0.54	0.79	0.71	0.50	0.45	0.50	0.37	0.53	0.29	0.69	0.80	0.55	0.41	0.55	0.48	0.51
Na	-	0.26	-	0.44	-	0.29	-	0.44	-	0.17	-	0.58	-	0.24	-	0.10	-	0.38	-	0.37	-	0.31	-	0.13	-	0.34	-	0.31	-	0.40
K	-	0.003	-	-	-	0.01	-	-	-	0.01	-	0.003	-	0.002	-	0.001	-	-	-	0.01	-	0.01	-	0.002	-	0.001	-	0.001	-	0.001
Total	7.97	3.83	7.99	3.83	8.00	3.81	7.99	3.83	7.98	3.78	8.00	3.92	7.97	3.84	8.03	3.82	8.03	3.81	7.98	3.82	7.97	3.82	8.00	3.83	8.03	3.81	8.02	3.82	8.01	3.85

Table 2. Representative major element compositions and cation proportions in garnet and clinopyroxene (cpx) in bimineralic eclogites from the Kaapvaal craton. Samples marked with «RV» are from Roberts Victor mine and samples marked with «JG» are from the Jagersfontein mine, South Africa

South African garnets show three main compositional clusters: $Py_{35—40}Alm_{20—40}Grs_{20—35}$; $Py_{40—45}Alm_{15—30}Grs_{20—40}$ and $Py_{45—75}Alm_{20—45}Grs_{5—15}$ and range from groups A to C after Taylor and Neal (1989) (Figure IV—2). Among Siberian bimineralic samples, Udachnaya garnets show a more narrow compositional range in grossular content, with a wider spread for pyrope and almandine contents ($Py_{33—59}Alm_{19—42}Grs_{12—33}$) and are classified as group B, except for sample UV09-423 ($Py_{72}Alm_{20}Grs_{8}$) that belongs to group A. Obnazhennaya garnets show a particular compositional trend, low in almandine ($Py_{45—65}Alm_{15—20}Grs_{20—45}$) and progressively enriched in grossular with exsolutions (Figure IV—2), showing a transition from the lower to upper limit of group B eclogites.

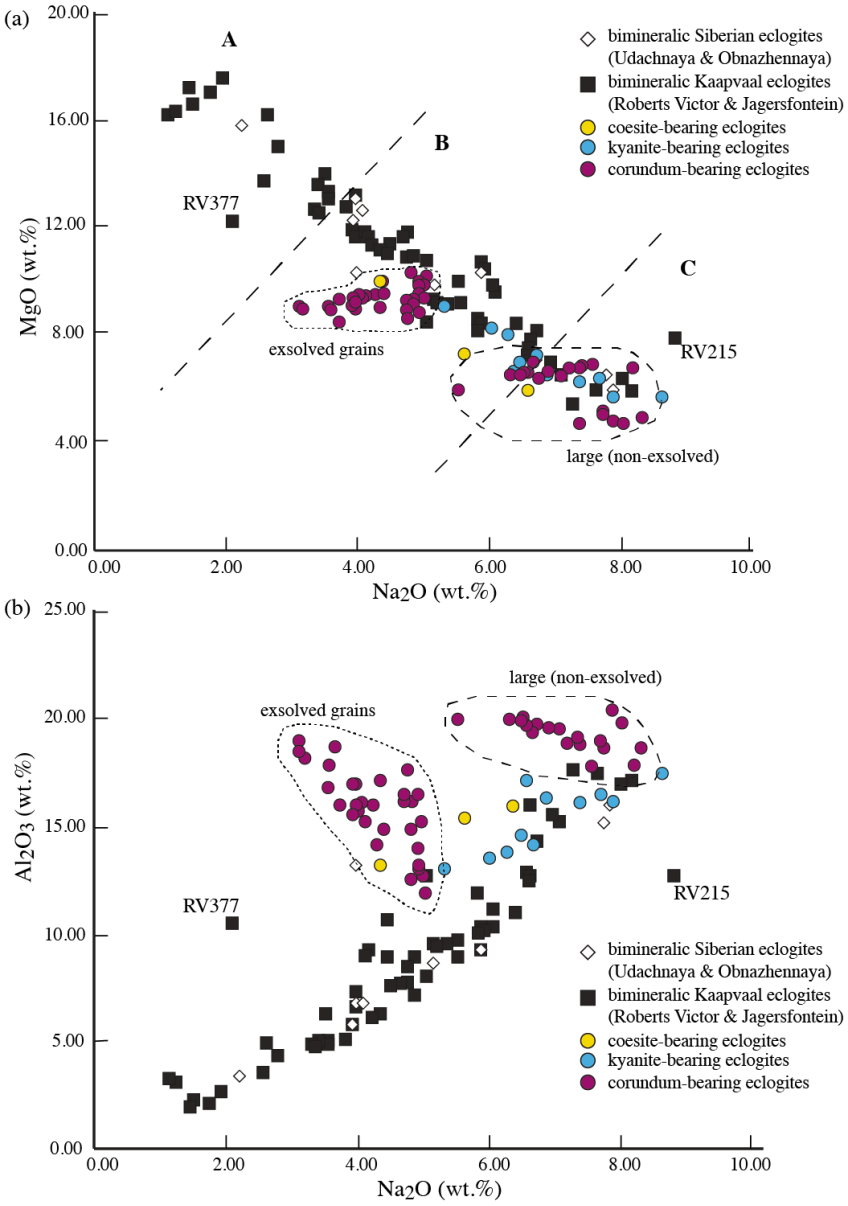

Figure IV—3. Plots of Na_2O vs. MgO (a) and Al_2O_3 (b) in clinopyroxenes for eclogite xenoliths from the Siberian and Kaapvaal cratons. Bimineralic eclogites from the Siberian craton comprise samples from Udachnaya and Obnazhennaya kimberlites and are marked with white diamond symbols. Bimineralic eclogites from the Kaapvaal craton comprise samples from Roberts Victor and Jagersfontein mines and are marked with black solid square symbols. Si-Al-rich eclogites are marked with yellow (coesite-bearing), blue (kyanite-bearing) and violet (corundum-bearing) solid circle symbols. A, B, C groups are delimited as defined by Taylor & Neal (1989).

Sample	Obn108/13			UV04-29		UV09-423		UV09-434		UV09-457		UV09-467		UV11-44		UV11-57		UV11-127b	
	primary gt	exsolution gt	exsolved cpx	gt	cpx	gt	cpx	gt	cpx	gt	cpx	gt	cpx	gt	cpx	gt	cpx	gt	cpx
SiO_2	41.04	41.24	51.39	40.56	55.52	42.01	55.57	39.96	56.70	38.98	55.53	39.40	56.68	40.74	55.54	40.49	55.93	40.77	55.29
TiO_2	0.08	0.04	0.26	0.32	0.16	0.21	0.31	0.14	0.24	0.45	0.27	0.16	0.15	0.64	0.35	0.37	0.42	0.79	0.48
Al_2O_3	23.48	23.39	13.26	22.19	5.82	23.16	3.40	22.79	15.06	21.43	8.67	22.53	15.94	22.24	6.84	22.41	9.19	22.52	6.85
FeO	8.72	6.56	1.56	14.54	4.74	10.49	2.63	16.38	2.49	20.36	5.20	17.08	2.84	11.23	3.71	16.50	4.92	10.58	3.44
MnO	0.18	0.12	0.02	0.41	0.04	0.30	0.05	0.34	0.01	0.32	0.05	0.29	0.00	0.21	0.06	0.34	0.05	0.22	0.03
MgO	15.43	12.21	10.40	12.08	12.31	19.68	15.82	10.56	6.55	8.92	9.88	8.58	6.00	14.64	12.64	14.80	10.29	15.57	13.13
CaO	11.06	16.90	19.35	10.46	17.87	3.96	19.78	10.50	10.81	8.97	15.32	12.13	10.26	9.82	16.94	5.28	13.37	9.29	16.79
Na_2O	0.02	0.02	3.97	0.13	3.92	0.06	2.21	0.06	7.75	0.14	5.15	0.06	7.85	0.15	4.07	0.15	5.87	0.19	3.96
K_2O	*bdl*	*bdl*	*bdl*	*bdl*	0.02	*bdl*	0.02	*bdl*	0.05	*bdl*	0.12	*bdl*	0.04	*bdl*	0.08	*bdl*	0.08	*bdl*	0.04
Cr_2O_3	0.08	0.08	0.15	0.11	0.06	0.27	0.22	0.06	0.06	0.05	0.04	0.02	0.03	0.04	0.06	0.07	0.11	0.15	0.08
Total	100.14	100.57	100.40	100.80	100.45	100.15	100.00	100.80	99.71	99.63	100.23	100.25	99.80	99.71	100.29	100.39	100.23	100.08	100.10
Mg#	75.93	76.85	92.23	59.69	82.24	76.97	91.47	53.47	82.43	43.84	77.20	47.24	78.99	69.91	85.86	61.52	78.85	72.40	87.17
Si	2.97	2.98	1.75	2.99	1.89	3.00	1.90	2.97	1.93	2.98	1.89	2.97	1.93	2.99	1.89	2.98	1.91	2.97	1.89
Ti	0.004	0.002	0.01	0.02	0.004	0.01	0.01	0.01	0.01	0.03	0.01	0.01	0.004	0.04	0.01	0.02	0.01	0.04	0.01
Al	2.00	1.99	0.69	1.93	0.25	1.95	0.15	2.00	0.61	1.93	0.37	2.00	0.64	1.92	0.29	1.94	0.37	1.93	0.30
Cr	0.004	0.005	0.004	0.01	0.002	0.02	0.01	0.003	0.002	0.003	0.001	0.001	0.001	0.003	0.002	0.004	0.003	0.01	0.002
Fe	0.53	0.40	0.04	0.90	0.14	0.63	0.08	1.02	0.07	1.30	0.15	1.08	0.08	0.69	0.11	1.02	0.14	0.64	0.10
Mn	0.01	0.01	-	0.03	0.001	0.02	0.001	0.02	-	0.02	0.002	0.02	-	0.01	0.002	0.02	0.001	0.01	0.001
Mg	1.66	1.32	0.53	1.33	0.63	2.09	0.80	1.17	0.33	1.02	0.50	0.96	0.31	1.60	0.64	1.62	0.52	1.69	0.67
Ca	0.86	1.31	0.71	0.83	0.65	0.30	0.72	0.84	0.40	0.74	0.56	0.98	0.38	0.77	0.62	0.42	0.49	0.72	0.61
Na	-	-	0.26	-	0.26	-	0.15	-	0.51	-	0.34	-	0.52	-	0.27	-	0.39	-	0.26
K	-	-	-	-	0.001	-	0.001	-	0.002	-	0.01	-	0.002	-	0.004	-	0.004	-	0.002
Total	8.03	8.02	4.00	8.02	3.83	8.01	3.81	8.02	3.86	8.02	3.83	8.02	3.86	8.02	3.84	8.03	3.84	8.02	3.85

Table 3. Representative major element compositions and cation proportions in garnet and clinopyroxene (cpx) in bimineralic eclogites from the Siberian craton. Samples marked with «Obn» are from Obnazhennaya mine and samples marked with «UV» are from the Udachnaya mine, Russia.

Clinopyroxene composition among bimineralic eclogites from both cratons show a wide spread in Na_2O and MgO, negatively correlated, ranging from group A to group C (Figure IV—3a). Similarly, they cover a broad compositional range in Al_2O_3 and Na_2O (jadeite component), with a positive correlated trend (Figure IV—3b). There are two exceptions from these main tendencies, represented by samples RV215 and RV377, which have high-Na,Mg—low-Al and low-Na—high-Mg,Al respectively.

4.1.2. Coesite-, kyanite-, corundum-bearing eclogites

Representative major element compositions of garnet and clinopyroxene in coe-, ky-, cor-bearing eclogites are shown in Table 4. All coesite-bearing samples have high K_2O_{cpx} (~0.09—0.24 wt.%) and belong either to the Type I, or plot outside the two fields (Figure IV—1). FeO content in garnet is low (~9.5—10.7 wt.%) and clinopyroxene has medium to high-jadeite content ($Jd_{33—55}$Dp-$Hd_{51—38}$En-$Fs_{16—7}$), characteristic of Type IB eclogites as defined by Huang et al. (2012). Sample JJG4492 has grossular-rich garnet (~$Py_{30}Alm_{20}Grs_{50}$) and jadeite-rich clinopyroxene and belongs to group C eclogites, whereas the other two coesite-bearing samples have pyrope-rich garnets (~$Py_{50}Alm_{20}Grs_{30}$) and clinopyroxene of intermediate jadeitic composition, classified as group B (Figure IV—2; Figure IV—3). All coesite-bearing samples have clinopyroxene of more aluminous composition with respect to bimineralic eclogites (Figure IV—3b) and more K-rich compositions.

Kyanite-bearing samples cover a wide compositional range and fall both in the metasomatized – Type I and pristine – Type II categories, as well as in the transitional area. Garnet is typically MgO poor (~4.6—11.4wt.%) except for sample RV333 and intermediate RV153 eclogite (~12.9—15.1wt.%). All metasomatized kyanite-eclogites are characterized by low FeO_{gt} (~10.8—14.4wt.%) and jadeite-rich clinopyroxene ($Jd_{50—57}$Dp-$Hd_{33—48}$En-$Fs_{2—9}$) classified as Type IB and IK. Non-metasomatized samples belong to the Type IIB group, except for RV333, which is a Type IIA. All kyanite-bearing eclogites are classified as group B and group C (Figure

Sample	JIG4492		RV326		RV153		RV319		RV333		UV09-487A		UV180/13		Obh110/13					Obn112/13			RV179				RV344			
	coe-bearing		coe-bearing		ky-bearing		ky-bearing		ky-bearing		ky-bearing		ky-bearing		cor-bearing					cor-bearing			cor-bearing				cor-bearing			
	garnet	cpx	garnet	cpx	garnet	cpx	garnet	cpx	garnet	cpx	garnet	cpx	garnet	cpx	non-ex gt	ex gt	non-ex cpx	ex cpx	ex gt	non-ex cpx	ex cpx	non-ex gt	ex gt	non-ex cpx	ex cpx	non-ex gt	ex gt	non-ex cpx	ex cpx
SiO_2	40.13	56.93	41.74	56.84	40.42	57.06	40.85	56.10	41.58	55.94	39.19	56.60	39.09	56.23	41.53	40.59	52.10	53.95	40.41	48.14	51.18	41.80	41.77	50.78	49.82	39.45	39.52	53.19	49.51
TiO_2	0.12	0.06	0.15	0.22	0.28	0.32	0.18	0.23	*bdl*	0.02	0.13	0.27	0.33	0.19	0.09	0.07	0.07	0.04	0.03	*bdl*	0.04	*bdl*	0.02	*bdl*	0.02	0.19	0.28	0.30	0.52
Al_2O_3	22.71	17.20	23.42	15.38	23.04	16.60	22.80	13.65	23.61	13.11	22.52	16.20	21.92	14.57	23.66	23.58	16.51	14.03	23.14	18.36	15.26	23.28	23.03	19.96	15.98	22.41	22.00	20.42	19.91
FeO	10.70	1.63	9.47	1.60	14.43	1.88	10.19	1.72	8.17	1.35	17.21	2.77	12.50	2.55	8.05	6.24	0.80	0.77	5.69	1.37	1.21	6.86	6.23	0.75	1.98	13.30	6.99	1.77	2.33
MnO	0.22	*bdl*	0.16	0.04	0.43	0.01	0.17	0.03	0.01	0.03	0.32	*bdl*	0.17	*bdl*	0.19	0.14	0.01	0.02	0.09	*bdl*	0.01	0.13	0.14	0.01	0.04	0.30	0.06	*bdl*	*bdl*
MgO	7.41	6.02	13.61	7.38	15.11	6.46	10.76	8.28	12.92	9.15	8.67	5.75	4.90	7.06	16.50	11.63	8.84	9.59	8.15	9.07	9.47	14.94	11.77	6.59	9.53	6.88	4.59	4.82	5.97
CaO	18.94	11.70	11.75	12.49	6.79	10.33	15.03	14.08	13.86	14.94	12.21	9.97	21.20	13.55	10.77	17.43	17.71	17.53	22.50	20.54	18.82	12.79	16.88	15.04	17.79	17.01	26.11	11.31	16.11
Na_2O	0.08	6.58	0.06	5.61	0.14	7.68	0.05	6.00	0.03	5.32	0.05	7.87	0.09	6.47	0.02	0.01	4.91	4.90	0.02	3.07	4.07	0.04	0.02	6.50	4.24	0.07	0.10	7.87	5.51
K_2O	*bdl*	0.16	0.01	0.24	*bdl*	0.04	*bdl*	0.04	*bdl*	0.04	*bdl*	0.03	*bdl*	0.04	*bdl*	*bdl*	*bdl*	0.01	*bdl*	0.02	*bdl*	0.01	0.03	0.02	0.01	0.01	*bdl*	0.01	*bdl*
Cr_2O_3	0.01	0.04	0.04	0.05	0.06	0.04	0.10	0.10	0.06	0.04	*bdl*	0.02	0.07	0.01	*bdl*	0.07	0.04	0.09	0.10	0.07	0.05	0.12	0.14	0.13	0.24	0.07	0.11	*bdl*	0.06
Total	100.31	100.32	100.44	99.97	100.68	100.42	100.42	100.42	100.22	100.00	100.32	99.48	100.27	100.68	100.81	99.78	101.08	101.05	100.12	100.67	100.11	99.96	100.01	99.88	99.85	99.77	100.00	99.82	99.99
Mg#	55.23	86.79	71.93	89.16	65.11	85.96	65.31	89.59	73.81	92.36	47.32	78.76	41.11	83.15	78.52	76.87	95.16	95.70	71.85	92.20	93.32	79.51	77.09	93.98	89.58	47.98	53.91	82.90	82.03
Si	2.99	1.94	3.02	1.94	2.95	1.95	3.00	1.91	3.01	1.91	2.96	1.93	2.97	1.92	2.97	2.96	1.78	1.84	2.98	1.64	1.75	3.01	3.03	1.73	1.70	2.98	2.98	1.81	1.69
Ti	0.01	0.001	0.01	0.01	0.02	0.01	0.01	0.01	-	-	0.01	0.01	0.02	0.005	0.005	0.004	0.002	0.001	0.001	-	0.001	-	0.001	-	-	0.01	0.02	0.01	0.01
Al	1.99	0.69	1.99	0.62	1.98	0.67	1.98	0.55	2.01	0.53	2.00	0.65	1.96	0.59	1.99	2.03	0.80	0.64	2.01	1.01	0.78	1.97	1.97	0.98	0.86	2.00	1.95	0.92	1.02
Cr	0.001	0.001	0.002	0.001	0.003	0.001	0.01	0.003	0.003	0.001	-	0.001	0.004	-	-	0.004	0.001	0.003	0.01	0.002	0.001	0.01	0.01	0.004	0.01	0.004	0.01	-	0.002
Fe	0.67	0.05	0.57	0.05	0.88	0.05	0.63	0.05	0.49	0.04	1.09	0.08	0.79	0.07	0.48	0.38	0.02	0.02	0.35	0.04	0.03	0.41	0.38	0.02	0.06	0.84	0.44	0.05	0.07
Mn	0.01	-	0.01	0.001	0.03	-	0.01	0.001	-	0.001	0.02	-	0.01	-	0.01	0.01	-	0.001	0.01	-	-	0.01	0.01	-	0.001	0.02	0.004	-	-
Mg	0.82	0.31	1.47	0.38	1.65	0.33	1.18	0.42	1.39	0.47	0.98	0.29	0.55	0.36	1.76	1.27	0.45	0.49	0.89	0.46	0.48	1.60	1.27	0.34	0.48	0.78	0.52	0.25	0.30
Ca	-	0.43	0.91	0.46	0.53	0.38	1.18	0.51	1.07	0.55	0.99	0.36	1.72	0.50	0.82	1.36	0.65	0.64	1.77	0.75	0.69	0.99	1.31	0.55	0.65	1.38	2.11	0.41	0.59
Na	-	0.44	-	0.37	-	0.51	-	0.40	-	0.35	-	0.52	-	0.43	-	-	0.32	0.32	-	0.20	0.27	-	-	0.43	0.28	-	-	0.52	0.36
K	-	0.01	-	0.01	-	0.002	-	0.002	-	0.002	-	0.001	-	0.002	-	-	-	-	-	0.001	-	-	-	0.001	-	-	-	-	-
Total	8.01	3.86	7.98	3.82	8.04	3.89	8.00	3.86	7.98	3.85	8.04	3.85	8.03	3.87	8.03	8.02	4.02	3.96	8.02	4.11	4.00	8.00	7.98	4.06	4.04	8.01	8.02	3.97	4.05

Table 4. Representative major element compositions and cation proportions in garnet and clinopyroxene (cpx) as non-exsolved (non-ex) and exsolution/exsolved (ex) grains, in Si,Al-rich eclogites from the Kaapvaal and Siberian cratons. Samples marked with «JIG» and «RV» are from Roberts Victor mine, South Africa, samples marked with «UV» are from the Udachnaya mine and samples marked with «Obn» are from Obnazhennaya mine, Russia. Coesite-bearing eclogites are abbreviated with «coe-», kyanite -bearing with «ky-» and corundum-bearing with «cor-».

IV—2) after Taylor and Neal (1989) and with the exception of the two pyrope-rich samples, they are typically characterized by grossular-rich garnet and high-Na,Al—low-Mg clinopyroxene (Figure IV—3).

Corundum-bearing eclogites are restricted to the Type II – pristine eclogites (Figure IV—1) and have very low K_2O_{cpx} (0.01—0.02wt.%). The large, primary garnet grains have higher MgO (14.9—16.5 wt.%), specific to Type IIA, with respect to garnet exsolutions (4.59—11.8wt.% MgO), classified as Type IIB. Corundum-eclogites have typically grossular-rich garnets, specific to groups B and C (Taylor and Neal, 1989), with distinct trends towards Ca-enrichment for the exsolutions (Figure IV—2). Clinopyroxene exhibiting exsolution textures are typically more magnesian (~5.97—9.98) and less sodic and aluminous (~4.07—5.51wt.% Na_2O; 14.0—19.9wt.% Al_2O_3), with lower Ca-Tschermack (Ca-Ts) (~0.11—0.37) than non-exsolved, primary grains (~4.82—9.07wt.% MgO; 3.07—7.87wt.% Na_2O; 16.5—20.4wt.% Al_2O_3; 0.16—0.51 CaTs). The sodium and magnesium ratios place corundum-eclogites in the groups B and C after Taylor and Neal (1989), with similar particular compositional correlations as seen for the garnet, proportional to their degree of exsolution (Figure IV—3).

4.2. Pressure-Temperature estimation

Temperature estimates have been calculated with the garnet-clinopyroxene Fe-Mg geothermometer proposed by Krogh (1988). The partitioning of Fe^{2+} and Mg between garnet and clinopyroxene is related to temperature, pressure and composition. Conversely, determining the equilibration temperature is composition and pressure dependent. Several core and rim measurements have been deployed to ensure chemical homogeneity and temperatures have been calculated for 1 GPa, 3 GPa and 6 GPa. We have used the intercept of the calculated temperature trend lines with the local conductive model geotherms (Pollack and Chapman, 1977) corresponding to surface heat flow of 39mW m^{-2} for the Kaapvaal craton (Griffin et al., 2003)

and of 35—40mW m^{-2} for the Siberian craton (Ionov et al., 2010). The equilibration conditions obtained for the different eclogite types are shown in Figure IV—4.

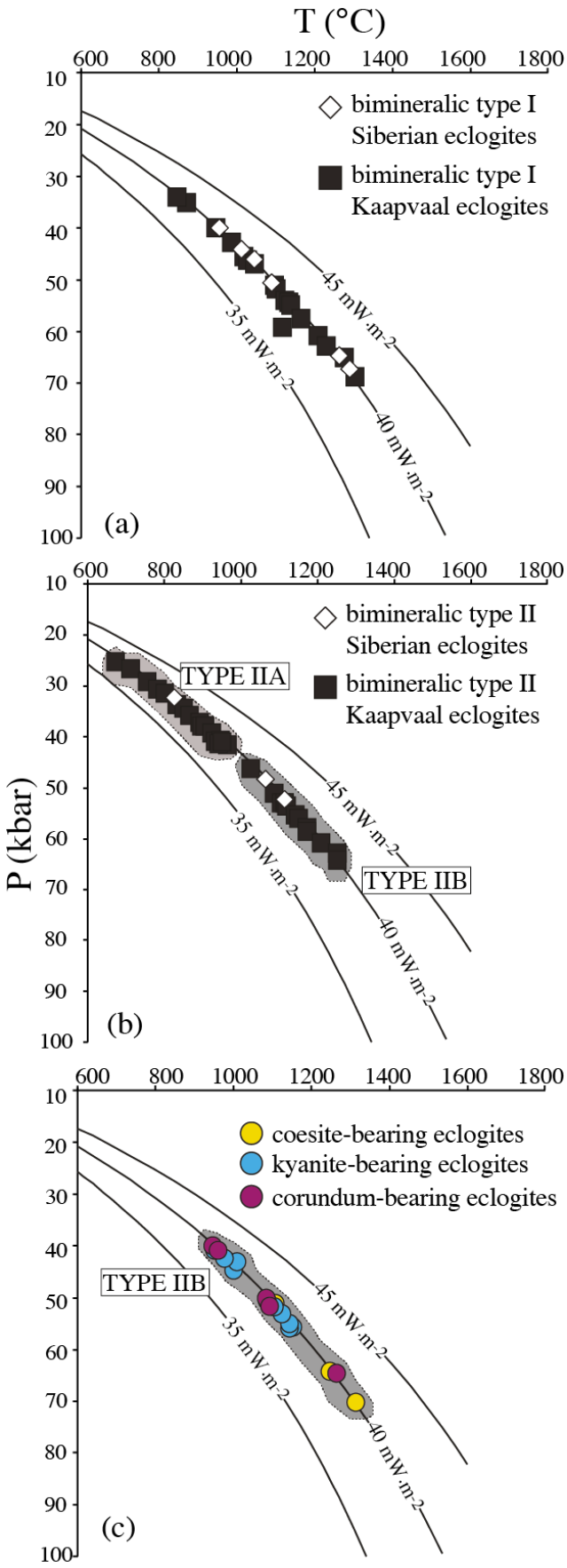

Figure IV—4. T (°C) — P (kbar) diagrams showing equilibrium conditions of eclogite xenoliths from the Siberian and Kaapvaal cratons. Bimineralic eclogites from the Siberian craton (Udachnaya; Obnazhennaya) are marked with white diamond symbols. Bimineralic eclogites from the Kaapvaal craton (Roberts Victor; Jagersfontein) are marked with black solid square symbols: Type I (a); Type II (b). Si-Al-rich (c) marked with yellow (coesite -), blue (kyanite -) and violet (corundum-bearing) solid circle symbols. Conductive model geotherms after Pollack & Chapman (1977) are shown for reference, corresponding to 35 mW.m^{-2}, 40 and 45 mW.m^{-2} surface heat flow.

Metasomatized (Type I) samples from both cratons cover a wide range in pressure-temperature conditions (~800—1300°C; ~3.2—6.5 GPa, Figure IV—4a), as metasomatism occurred through upward migration of kimberlitic fluids preceding the eruption.

The non-metasomatized, bimineralic eclogites (Figure IV—4b) show a bi-modal distribution, where the previously described Type IIA corresponds to lower PT conditions (~650—1000°C; ~2.0—4.5 GPa) than Type IIB (~1000—1300°C; ~4.5—6.5 GPa). This indicates two different depths for two chemically different eclogite Types within the eclogite formation. Coe-, ky-,cor-bearing eclogites appear to have equilibrated at high-PT conditions (Figure IV—4c): ~1010—1290°C; 5.0—7.0GPa the coesite-bearing; ~960—1150°C; 4.1—5.6GPa the kyanite-bearing and ~950—1300°C; 4.0—6.5GPa the corundum-bearing eclogites, specific for the lowermost part of the cratonic keel.

As the lithospheric thickness varies from the centre to the borders of craton, the inferred equilibration depths of mantle eclogites correspond to 150—200km for the center of the Kaapvaal craton, 210—240km for Udachnaya pipe in the center of the Siberian craton and 130—140km for Obnazhennaya pipe from the NE cratonic border, systematically coinciding with the lithosphere-asthenosphere boundary (LAB) estimates.

Summary: The variations in major element compositions show a wide sampling of the eclogite suite from the Kaapvaal and Siberian cratons, described by the 76 chosen samples. All samples show an overall positive correlation between Al_2O_3 and Na_2O (r = 2.03) and a negative correlation between MgO and Na_2O (r = -1.60) in the clinopyroxene, associated with pyrope-grossular rich garnets.

Eclogite xenoliths, which have been metasomatized by kimberlite-derived fluids (Type I), can be identified based on their higher alkali-content (Na_2O in garnet and K_2O in omphacite). They include a broad variety of garnet and clinopyroxene compositions, from pyrope- to grossular-rich and diopside- to jadeite-rich respectively. Geothermobarometry shows kimberlite

metasomatism was induced upward, across the entire thickness of the eclogite formation. Similarly bimineralic non-metasomatized eclogites have variable composition, characterized by a more magnesian, lower-PT layer (Type IIA) residing on top of a Na,Al-rich layer, characterized by high-PT equilibration conditions (Type IIB).

The coe-, ky-, cor-bearing eclogites show similar compositions regardless of the craton of their emplacement and are typically characterized by grossular-rich garnets and jadeite-rich clinopyroxenes. Their equilibration PT-conditions indicate the highest pressures and temperatures, corresponding to the lowermost part of the cratonic keel. Corundum-bearing eclogites often show topotactic exsolution textures hosted in omphacite, consisting of a more calcic garnet ± kyanite/zoisite, suggesting temperature decrease and/or pressure increase, prior to the eclogite entrapment in the kimberlite.

CHAPTER V.

TRACE ELEMENT COMPOSITIONS

CHAPTER V. TRACE ELEMENT COMPOSITIONS

Mineralogy and chemical composition are intrinsically connected parameters, controlled by pressure-temperature conditions. Unlike major elements, trace element compositions are more prone to change as a response to variations in pressure and temperature conditions, fluid interaction and metamorphic processes. Kimberlite-derived metasomatism is characterized by a higher LREE, Ba, Sr, and HFSE content (Gréau et al., 2011; Huang et al., 2012). This is a refinement of the textural and major element-based classification between metasomatized and pristine eclogites. Furthermore, trace element composition allows further constraints to be placed on the nature of the eclogite protolith and an understanding of their petrogenesis (Neal et al., 1990).

The aims of this chapter are to characterize the trace element composition and possible fluid interaction of eclogite xenoliths from the Kaapvaal and Siberian cratons and improve the previous textural (Chapter 3) and chemical (Chapter 4) classification of the sampled eclogite xenoliths. For this purpose a total of 62 samples were chosen for analysis, from the previously described eclogite assemblages (Chapter 3). Positive anomalies in clinopyroxene and garnet have been defined as $Sr^* \geq 1$ and $Eu^* \geq 1$ and negative anomalies as $Sr^* < 1$ and $Eu^* < 1$ respectively, with $Sr^* = Sr_N / sqrt(Sm_N * Nd_N)$ and $Eu^* = Eu_N / sqrt(Sm_N * Gd_N)$.

5.1. Bimineralic eclogites

Selected trace element compositions of garnet and clinopyroxene in bimineralic eclogites, pyrolite-normalized (McDonough and Sun, 1995), are given in Table 5 (Kaapvaal) and Table 6 (Siberian craton). The corresponding REE and extended incompatible elements patterns are shown in Figure V—1 and Figure V—2, with markedly overlapping trace elements distribution of the South African and Siberian eclogite xenoliths.

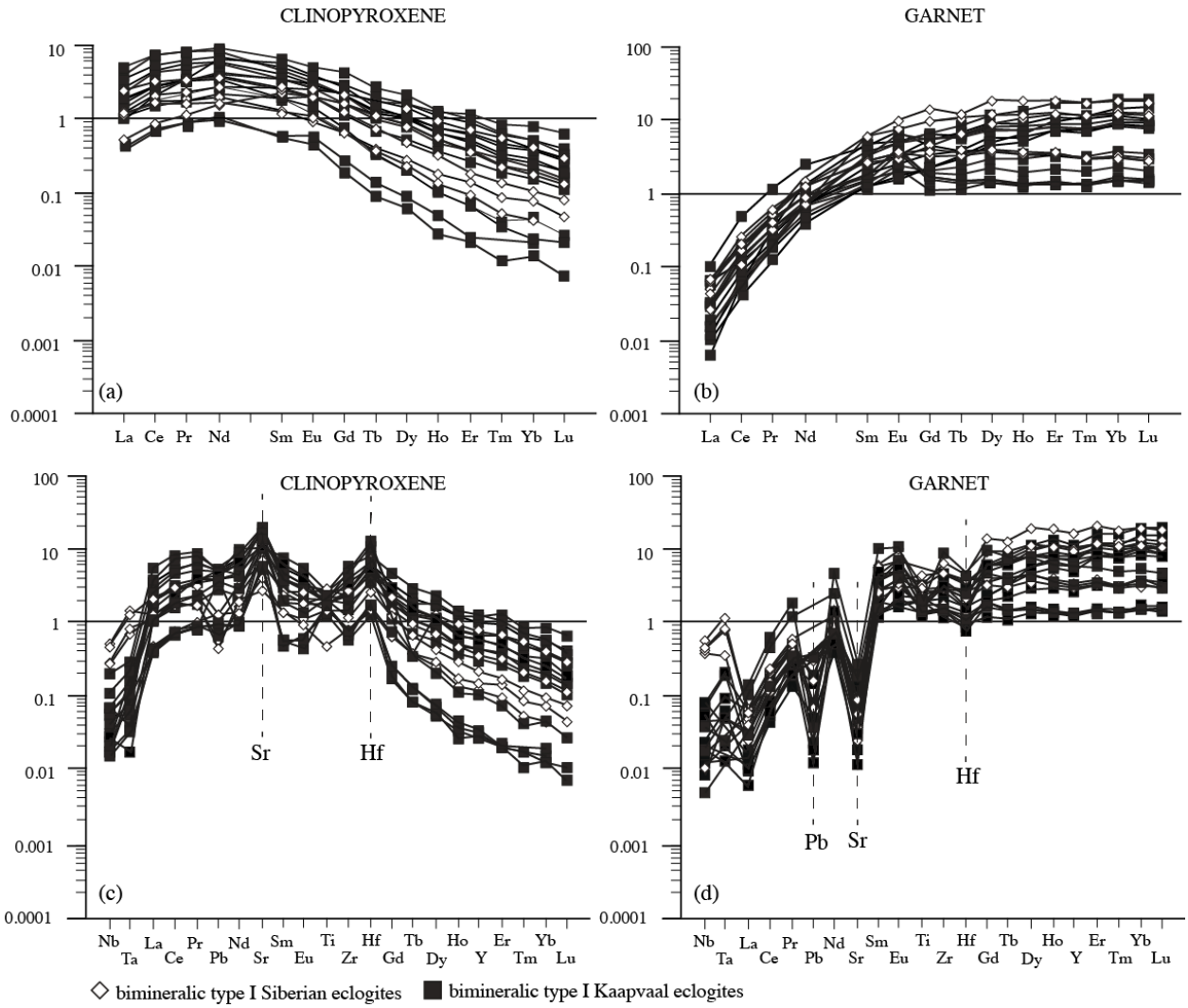

Figure V—1. REE (a—b) and extended trace elements patterns (c—d) in clinopyroxene and garnet in bimineralic, type I (metasomatized) eclogites from the Siberian and Kaapvaal cratons. Samples from the Siberian craton comprise eclogites from Udachnaya and Obnazhennaya kimberlites and are marked with white diamond symbols. Samples from the Kaapvaal craton comprise eclogites from Roberts Victor and Jagersfontein mines and are marked with black solid square symbols.

5.1.1. Type I

The previously described Type I (metasomatized) eclogites are characterized by a narrow LREE and LILE concentration range, with variable degrees of fractionation for HREE. Clinopyroxene has REE spoon-shaped patterns (Figure V—1a), with $(La/Nd)_N$ of 0.16—0.56 and $(Nd/Yb)_N$ of 5.33—76.2 ("N" shows pyrolite-normalized concentrations (McDonough and Sun, 1995)). The normalized Sr clinopyroxene concentration ranges between 2.5—19.9, roughly overlapping the ~5.0—15.1 estimated values for eclogitic clinopyroxene (Jacob et al., 2003). All samples have positive Sr (1.48—24.3 Sr*) and Hf anomalies in clinopyroxene (Figure V—1c)

Sample	RV159		RV174		RV218		RV226		RV233		RV236		RV315		RV349		RV355		RV360		RV370		RV377		RV451		RV465		RV469		RV483		RV486		RV488		JG32		JG33	
Type	II A		IIB		IB		IA		IIB		II B		IA		II A		II A		II A		IB		IIA		IIB		II A		IIB		IA		IB		II A		IIB		II A	
	garnet	cpx	garnet	cpx	garnet	cpx	garnet	cpx	garnet	cpx	garnet	cpx	garnet	cpx	garnet	cpx	garnet	cpx	garnet	cpx	garnet	cpx	garnet	cpx	garnet	cpx	garnet	cpx	garnet	cpx	garnet	cpx	garnet	cpx	garnet	cpx	garnet	cpx
Li	0.273	3.77	0.112	2.54	1.24	20.28	0.671	4.11	0.359	5.77	0.238	6.31	-	-	0.061	0.290	-	-	0.200	0.059	-	-	0.571	16.76	0.027	3.10	0.045	0.101	0.396	4.43	-	-	-	-	0.162	0.614	0.303	6.37	0.579	8.10
Sc	2.33	0.657	4.53	0.553	2.19	0.265	3.79	1.59	4.20	1.59	2.94	0.306	3.15	1.29	2.96	0.638	5.92	1.45	28.27	0.254	3.47	1.48	4.80	0.733	1.48	0.420	3.02	0.281	3.75	0.709	3.91	1.38	4.66	1.68	4.88	1.16	4.49	1.32	3.64	1.14
Ti	0.599	1.14	0.515	0.376	1.92	1.73	2.30	2.12	0.773	1.49	0.750	1.40	1.93	2.12	1.74	0.806	0.635	0.665	8.38	0.233	2.42	2.43	0.460	0.519	0.134	0.109	0.908	0.218	0.850	0.731	1.56	2.42	1.67	2.54	2.55	1.58	0.855	1.18	0.729	1.39
V	0.545	2.55	1.21	2.02	0.821	1.98	1.87	5.33	2.05	5.51	1.26	3.14	1.74	4.52	1.29	1.69	1.81	3.34	8.62	0.684	1.95	5.13	1.16	2.57	0.995	2.13	1.33	0.622	2.12	3.63	1.27	4.82	1.66	5.88	3.01	5.25	2.12	5.63	0.970	4.99
Cr	0.482	0.496	0.489	0.455	0.147	0.185	0.330	0.388	0.145	0.154	0.238	0.341	0.334	0.240	0.800	0.351	0.737	0.451	8.78	0.188	0.200	0.170	0.635	0.602	0.052	0.077	4.33	0.588	0.187	0.133	0.424	0.587	0.358	0.359	1.98	1.14	0.107	0.125	0.341	0.471
Co	0.787	0.282	0.702	0.307	0.583	0.145	0.643	0.383	0.737	0.376	0.618	0.185	0.636	0.368	0.680	0.382	0.774	0.412	2.71	0.060	0.656	0.316	0.820	0.364	0.287	0.127	0.733	0.107	0.963	0.248	0.635	0.332	0.558	0.321	0.460	0.248	0.706	0.385	0.562	0.243
Ni	0.019	0.205	0.044	0.456	0.040	0.174	0.019	0.150	0.016	0.225	0.019	0.161	0.020	0.165	0.047	0.383	0.030	0.569	0.145	0.060	0.027	0.248	0.032	0.341	0.023	0.226	0.036	0.101	0.019	0.151	0.023	0.191	0.018	0.139	0.036	0.262	0.010	0.164	0.006	0.066
Rb	*bd.*	*bd.*	0.055	0.238	0.009	1.08	0.032	0.024	0.039	*bd.*	0.025	*bd.*	*bd.*	0.033	0.009	0.012	0.013	*bd.*	0.050	*bd.*	0.031	*bd.*	*bd.*	0.292	*bd.*	0.006	*bd.*	0.002	0.022	*bd.*	0.015	0.030	0.137	0.034	0.028	0.025	0.041	0.009	0.025	*bd.*
Sr	0.025	39.04	0.040	0.993	0.193	5.11	0.032	15.03	0.005	1.22	0.008	0.299	0.029	11.88	0.021	18.40	0.001	0.512	0.046	2.09	0.012	9.58	0.003	0.709	0.001	0.055	0.017	6.95	0.003	0.361	0.068	19.14	0.067	16.27	0.014	8.55	0.005	0.742	0.027	20.74
Y	1.98	0.283	1.86	0.050	3.11	0.027	6.04	0.856	15.83	0.384	6.73	0.101	4.72	0.656	1.79	0.364	3.85	0.312	10.28	0.061	9.30	1.18	2.18	0.051	0.520	0.006	0.712	0.155	8.57	0.135	7.32	0.614	7.04	0.751	8.54	1.54	13.10	0.384	5.67	0.371
Zr	0.401	1.16	0.080	0.023	3.02	0.652	2.33	2.59	0.389	0.715	0.099	0.024	1.20	1.77	2.02	2.08	0.130	0.092	12.57	0.223	2.70	5.52	0.066	0.052	0.025	0.004	0.727	1.14	0.052	0.054	3.69	1.88	3.60	5.71	6.52	2.79	0.244	0.410	1.01	1.97
Nb	0.020	0.022	0.148	0.186	0.038	0.032	0.033	0.062	*bd.*	*bd.*	0.011	0.016	0.024	0.042	0.208	0.200	0.013	0.010	1.63	0.168	0.089	0.193	0.031	0.042	0.003	*bd.*	0.635	0.070	*bd.*	0.002	0.014	0.026	0.107	0.067	0.106	0.126	0.005	0.005	0.045	0.098
Ba	*bd.*	0.480	0.213	0.437	*bd.*	1.21	0.003	0.097	*bd.*	*bd.*	*bd.*	0.018	*bd.*	0.058	*bd.*	0.123	*bd.*	*bd.*	*bd.*	0.016	*bd.*	0.055	*bd.*	0.424	*bd.*	0.001	*bd.*	0.031	*bd.*	*bd.*	*bd.*	0.068	0.182	0.072	*bd.*	0.054	*bd.*	*bd.*	*bd.*	*bd.*	0.008
La	0.029	20.68	0.194	0.404	0.106	0.421	0.016	3.24	*bd.*	0.005	*bd.*	*bd.*	0.011	1.93	0.029	7.76	*bd.*	0.010	0.064	1.35	0.021	5.25	*bd.*	0.002	0.003	*bd.*	0.059	2.88	*bd.*	*bd.*	0.011	1.81	0.208	3.00	0.013	3.56	*bd.*	0.005	0.009	2.06
Ce	0.134	24.11	0.126	0.269	0.468	0.724	0.086	5.41	0.003	0.042	*bd.*	*bd.*	0.065	2.91	0.143	13.41	*bd.*	0.054	0.284	1.86	0.088	7.90	0.001	0.009	0.002	0.001	0.266	4.74	*bd.*	*bd.*	0.053	2.76	0.276	5.34	0.080	8.72	0.002	0.028	0.065	4.27
Pr	0.351	19.72	0.088	0.117	1.17	0.879	0.248	6.02	0.030	0.194	0.003	0.003	0.174	3.48	0.284	11.70	*bd.*	0.195	0.778	1.58	0.243	8.89	0.008	0.044	0.002	*bd.*	0.656	4.97	*bd.*	0.003	0.213	3.23	0.334	6.88	0.322	12.91	0.022	0.093	0.233	5.30
Nd	0.793	17.24	0.100	0.109	2.42	1.00	0.657	7.03	0.212	0.553	0.026	0.013	0.478	3.98	0.573	10.67	0.038	0.546	1.94	1.55	0.652	9.59	0.061	0.111	0.011	0.005	1.38	4.77	0.023	0.028	0.761	4.02	0.811	*bd.*	1.08	17.72	0.176	0.309	0.748	6.29
Sm	1.56	6.81	0.463	0.199	4.50	0.544	1.94	5.01	2.21	1.33	0.571	0.107	1.30	2.76	1.39	5.04	0.606	1.18	5.53	0.904	2.58	6.82	0.482	0.218	0.094	*bd.*	2.31	2.44	0.695	0.192	3.59	3.59	1.85	4.77	3.55	13.13	1.88	0.897	2.58	4.10
Eu	2.06	4.73	1.09	0.285	6.92	0.439	2.47	3.62	3.88	1.26	1.79	0.190	1.72	2.13	1.74	3.27	1.29	1.40	7.30	0.638	3.81	5.23	1.28	0.388	0.245	0.016	2.40	1.52	1.95	0.322	5.05	3.03	3.18	3.36	4.18	8.62	3.27	0.908	3.88	3.49
Gd	1.97	2.44	1.06	0.144	4.56	0.186	3.28	2.84	6.83	1.27	2.37	0.161	2.17	1.69	1.75	2.08	2.06	1.13	8.86	0.424	5.79	4.34	1.31	0.193	0.272	0.016	1.38	0.974	3.05	0.280	5.76	2.17	4.14	2.50	5.64	6.88	5.44	0.906	4.01	1.91
Tb	1.82	1.06	1.38	0.112	3.72	0.085	3.97	1.78	9.90	0.899	3.66	0.151	2.87	1.18	1.75	1.08	2.75	0.754	9.54	0.207	7.03	2.73	1.59	0.127	0.376	*bd.*	0.993	0.500	4.97	0.245	6.01	1.34	4.92	1.57	6.21	3.93	7.37	0.695	4.44	1.04
Dy	2.26	0.671	1.94	0.087	3.93	0.059	5.83	1.55	14.38	0.716	5.95	0.158	4.44	1.05	2.09	0.773	4.04	0.617	11.91	0.140	9.72	2.24	2.31	0.101	0.510	*bd.*	0.887	0.318	7.73	0.226	7.85	1.09	7.05	1.27	8.59	3.03	11.34	0.650	5.76	0.737
Ho	2.05	0.332	2.05	0.066	3.40	0.026	6.38	1.02	16.84	0.462	6.63	0.125	5.09	0.762	1.91	0.432	4.33	0.379	11.13	0.078	9.74	1.42	2.43	0.067	0.523	0.007	0.831	0.174	9.20	0.163	7.32	0.667	7.58	0.891	8.88	1.85	12.54	0.440	5.77	0.426
Er	2.30	0.234	2.40	0.049	3.39	0.021	8.13	0.833	20.29	0.302	8.33	0.098	6.89	0.664	2.05	0.309	5.12	0.279	13.15	0.052	11.46	1.07	2.81	0.043	0.600	*bd.*	0.822	0.111	11.19	0.124	8.70	0.552	9.82	0.744	10.53	1.41	15.82	0.368	6.83	0.315
Tm	2.11	0.115	2.29	0.038	2.98	0.011	8.10	0.584	20.50	0.203	8.29	0.065	6.91	0.478	1.85	0.180	4.76	0.181	12.50	0.031	10.26	0.682	2.62	0.030	0.578	*bd.*	0.740	0.059	11.65	0.090	8.00	0.350	9.94	0.546	10.06	0.896	15.47	0.228	6.74	0.213
Yb	2.32	0.103	2.70	0.026	3.27	0.013	9.93	0.496	23.56	0.135	10.25	0.058	8.64	0.424	2.15	0.160	5.40	0.150	14.78	0.025	11.75	0.556	3.23	0.017	0.687	*bd.*	0.819	0.042	13.76	0.082	9.41	0.311	12.20	0.482	12.06	0.705	18.87	0.209	7.98	0.178
Lu	2.18	0.061	2.39	0.013	2.91	0.007	9.51	0.363	23.71	0.087	9.76	0.040	8.24	0.304	2.00	0.091	5.14	0.065	14.52	0.017	10.98	0.357	2.91	0.016	0.656	*bd.*	0.756	0.023	13.66	0.057	8.62	0.219	11.90	0.330	11.63	0.517	18.22	0.145	7.81	0.107
Hf	0.170	1.60	0.119	0.086	2.38	1.68	1.59	5.41	0.507	2.46	0.275	0.156	0.866	3.43	1.50	2.99	0.346	0.437	7.83	0.452	1.53	7.11	0.087	0.145	0.046	0.013	0.523	1.98	0.131	0.380	2.24	3.56	2.73	12.83	4.15	5.16	0.274	1.36	0.430	3.28
Ta	*bd.*	*bd.*	0.067	0.129	0.024	0.062	0.013	0.061	*bd.*	*bd.*	*bd.*	0.016	*bd.*	0.053	0.295	0.287	*bd.*	*bd.*	1.70	0.238	0.195	0.310	*bd.*	*bd.*	*bd.*	*bd.*	1.13	0.084	*bd.*	*bd.*	*bd.*	*bd.*	0.130	0.163	*bd.*	0.046	0.012	*bd.*	*bd.*	0.069
Pb	0.014	71.73	0.161	1.07	*bd.*	0.645	*bd.*	4.61	0.065	0.052	*bd.*	*bd.*	*bd.*	3.68	*bd.*	18.42	*bd.*	*bd.*	*bd.*	1.55	*bd.*	5.06	*bd.*	0.014	0.025	0.034	*bd.*	3.09	0.024	*bd.*	*bd.*	4.87	0.144	4.50	0.016	6.03	0.013	0.016	*bd.*	2.09
Th	0.053	3.04	0.319	0.194	0.037	0.022	0.008	0.105	*bd.*	*bd.*	*bd.*	*bd.*	*bd.*	0.056	0.084	0.438	*bd.*	*bd.*	0.455	0.355	0.088	0.436	0.002	0.009	0.014	*bd.*	0.308	0.202	*bd.*	*bd.*	*bd.*	0.076	0.455	0.080	0.017	0.279	*bd.*	*bd.*	0.002	0.102
U	0.333	1.09	0.371	0.056	0.320	0.016	0.067	0.096	*bd.*	*bd.*	0.004	*bd.*	*bd.*	*bd.*	0.656	0.403	0.941	*bd.*	2.76	0.184	0.552	0.388	0.001	0.005	*bd.*	*bd.*	2.07	0.139	*bd.*	*bd.*	*bd.*	0.064	0.601	0.106	0.135	0.261	*bd.*	*bd.*	0.078	0.200
Eu*	1.18	1.16	1.56	1.69	1.53	1.38	0.982	0.958	1.00	0.969	1.54	1.45	1.02	0.985	1.12	1.01	1.16	1.21	1.04	1.03	0.987	0.961	1.61	1.89	1.54	-	1.34	0.987	1.34	1.39	1.11	1.08	1.15	0.975	0.933	0.908	1.02	1.01	1.21	1.25
Sr*	0.020	6.02	0.124	7.96	0.058	11.83	0.022	3.36	0.004	1.46	0.030	6.54	0.029	4.58	0.021	3.90	0.003	0.650	0.011	2.58	0.006	1.48	0.012	4.85	0.021	6.11	0.013	3.23	0.012	4.10	0.033	6.48	0.037	-	0.006	0.775	0.015	5.98	0.015	5.98

Table 5. Representative incompatible elements compositions of garnet and clinopyroxene (cpx) in bimineralic eclogites from the Kaapvaal craton. Samples marked with «RV» are from Roberts Victor mine and samples marked with «JG» are from the Jagersfontein mine, South Africa. All values are normalized to primitive mantle values (McDonough and Sun, 1995). $Eu^* = Eu_N/sqrt(Sm_N*Gd_N)$. $Sr^* = Sr_N/sqrt(Sm_N*Nd_N)$.

and negative Sr and Hf anomalies in garnet (0.01—0.17 Sr*). Negative Pb anomalies are also present in most samples (Figure V—1d), less marked in the clinopyroxene. Garnet REE spectra have strongly fractionated LREE ($(La/Nd)_N$ of 0.005—0.26) and generally flat MREE-HREE ($(Nd/Yb)_N$ of 0.03—0.89). We distinguish two compositional groups (Figure V—1b), characterized by HREE-rich garnet (between 8 and 11 times the primitive mantle) and HREE-poor garnet (between 1.5 and 3 times the primitive mantle (McDonough and Sun, 1995)).

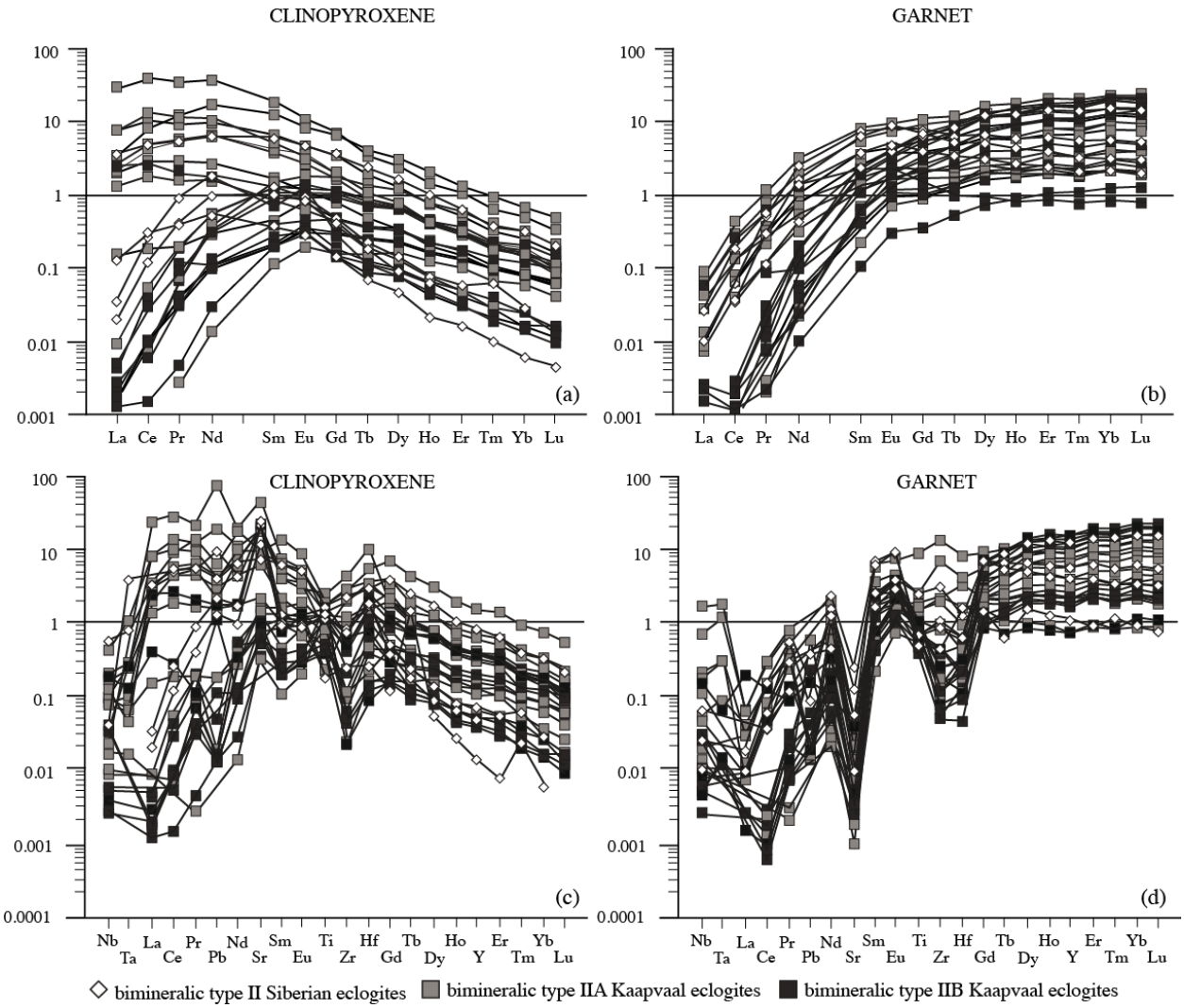

Figure V—2. REE (a—b) and extended trace elements patterns (c—d) in clinopyroxene and garnet in bimineralic, type II (non-metasomatized) eclogites from the Siberian and Kaapvaal cratons. Samples from the Siberian craton comprise eclogites from Udachnaya and Obnazhennaya kimberlites and are marked with white diamond symbols. Samples from the Kaapvaal craton comprise eclogites from Roberts Victor and Jagersfontein mines and are marked with grey (type IIA) and black (type IIB) solid square symbols.

Sample	Obn108/13										UV04-29		UV09-423		UV09-434		UV09-457		UV09-467		UV11-44		UV11-57		UV11-127b	
Type	IIA										IB		IIA		IIB		IA		IIB		IB		IA		IB	
	non-exsolved garnet			exsolved garnet			non-ex cpx	exsolved clinopyroxene			garnet	cpx	garnet	cpx	garnet	cpx	garnet	cpx	garnet	cpx	garnet	cpx	garnet	cpx	garnet	cpx
Li	-	-	-	-	-	-	-	-	-	-	0.156	0.412	0.260	0.462	0.470	9.63	0.745	4.80	0.368	9.54	0.373	1.89	0.919	5.90	0.307	0.711
Sc	0.640	1.45	1.88	0.246	0.277	0.298	0.185	0.082	0.110	0.050	6.01	0.703	13.43	2.15	3.15	0.625	3.37	1.54	2.53	0.667	3.00	1.07	4.62	1.37	2.83	0.459
Ti	0.213	0.433	0.639	0.297	0.327	0.310	1.49	1.45	1.33	0.766	1.70	0.463	2.28	1.58	0.664	1.14	2.42	2.04	0.662	1.30	2.99	2.22	3.37	2.95	4.08	1.42
V	0.923	1.43	1.90	1.62	1.61	1.56	3.52	3.63	4.05	2.23	3.62	3.33	3.77	5.04	1.12	4.03	3.23	7.91	1.10	4.21	1.43	2.98	2.44	6.08	1.44	1.31
Cr	0.149	0.176	0.232	0.204	0.203	0.212	0.161	0.229	0.259	0.132	0.244	0.074	1.56	0.428	0.144	0.185	0.116	0.119	0.030	0.043	0.271	0.231	0.312	0.418	0.341	0.143
Co	0.571	0.921	1.28	0.464	0.481	0.521	0.208	0.184	0.191	0.112	30.49	1.88	1.18	0.195	0.487	0.135	0.809	0.560	0.442	0.154	0.600	0.393	1.24	0.435	0.622	0.196
Ni	0.019	0.022	0.034	0.019	0.022	0.020	0.217	0.264	0.269	0.153	0.035	0.160	0.024	0.116	0.008	0.067	0.015	0.186	0.007	0.063	0.029	0.182	0.041	0.214	0.043	0.123
Rb	*bd.*	0.010	*bd.*	*bd.*	*bd.*	*bd.*	*bd.*	*bd.*	*bd.*	*bd.*	0.020	0.009	0.044	*bd.*	0.012	*bd.*	0.036	0.038	*bd.*	*bd.*	0.013	0.071	0.048	0.027	*bd.*	0.026
Sr	0.043	0.115	0.056	0.208	0.208	0.087	23.92	16.97	17.46	9.72	0.025	2.58	0.010	6.75	0.243	21.28	0.095	15.13	0.124	11.70	0.059	7.13	0.039	6.61	0.055	3.71
Y	0.440	0.798	1.13	0.085	0.131	0.158	0.024	0.003	0.003	0.002	9.48	0.154	10.85	0.788	5.63	0.072	9.83	0.394	3.81	0.047	3.06	0.234	16.38	0.760	3.32	0.117
Zr	0.143	0.321	0.482	0.095	0.094	0.101	0.188	0.083	0.078	0.043	1.74	0.823	2.87	2.18	1.08	0.794	3.07	3.174	0.836	0.690	3.05	1.22	6.55	2.83	4.59	0.763
Nb	0.018	0.021	0.025	0.037	0.037	0.035	0.574	0.681	0.634	0.316	0.565	0.295	0.062	0.040	0.010	*bd.*	0.010	*bd.*	*bd.*	*bd.*	0.476	0.486	0.397	0.529	0.409	0.273
Ba	*bd.*	*bd.*	*bd.*	*bd.*	*bd.*	*bd.*	0.038	0.016	0.003	0.001	0.007	0.009	*bd.*	0.023	*bd.*	*bd.*	*bd.*	0.013	*bd.*	*bd.*	*bd.*	0.056	*bd.*	0.013	*bd.*	0.023
La	0.025	0.024	0.018	0.067	0.082	0.064	3.40	2.25	2.42	1.19	0.050	1.10	*bd.*	3.59	0.010	0.034	0.042	0.534	*bd.*	0.021	0.062	2.25	0.026	1.28	0.066	1.24
Ce	0.191	0.153	0.162	0.436	0.536	0.442	5.74	4.33	4.59	2.40	0.218	1.73	0.035	4.75	0.061	0.253	0.162	0.857	0.036	0.116	0.250	3.05	0.113	1.93	0.211	1.70
Pr	0.463	0.467	0.562	1.03	1.23	1.13	5.79	4.30	4.34	2.32	0.548	1.81	0.111	5.40	0.508	0.881	0.526	1.15	0.289	0.404	0.620	3.32	0.331	2.26	0.415	1.63
Nd	0.684	1.02	1.29	1.60	1.85	1.82	4.48	2.91	2.90	1.59	1.20	1.90	0.415	6.17	2.28	1.77	1.50	1.51	1.51	0.942	1.26	3.46	0.712	2.54	0.892	1.63
Sm	0.665	1.20	1.61	1.18	1.32	1.27	0.993	0.495	0.473	0.263	2.59	1.28	2.29	5.96	6.69	1.30	5.84	2.16	6.16	0.978	2.80	2.42	6.24	2.64	2.70	1.24
Eu	1.29	2.24	2.94	1.65	1.83	1.84	0.928	0.353	0.373	0.202	2.88	0.916	3.84	4.70	8.52	0.933	7.28	1.98	8.77	0.845	3.45	1.93	10.19	2.44	3.64	1.06
Gd	0.724	1.14	1.61	0.610	0.728	0.735	0.268	0.082	0.103	0.054	4.49	0.651	6.12	3.68	7.08	0.494	9.34	1.59	6.76	0.369	3.34	1.27	14.72	2.11	3.82	0.653
Tb	0.645	1.02	1.49	0.349	0.423	0.479	0.119	0.025	0.028	0.015	6.23	0.394	8.11	2.35	6.30	0.228	10.23	1.08	5.18	0.172	3.30	0.729	12.37	0.385	3.82	0.370
Dy	0.645	1.04	1.51	0.211	0.279	0.336	0.057	0.007	0.009	0.004	9.11	0.281	11.23	1.65	6.53	0.142	11.57	0.766	4.91	0.089	3.64	0.463	19.30	1.34	4.09	0.239
Ho	0.513	0.868	1.29	0.103	0.156	0.198	0.028	*bd.*	*bd.*	*bd.*	10.13	0.181	12.34	1.01	6.06	0.078	11.32	0.517	4.19	0.064	3.48	0.307	19.07	0.958	3.71	0.135
Er	0.422	0.788	1.13	0.057	0.095	0.112	0.014	0.003	*bd.*	0.002	11.76	0.137	13.68	0.648	6.22	0.056	11.96	0.349	3.88	*bd.*	3.50	0.176	19.38	0.699	3.63	0.093
Tm	0.357	0.631	0.921	0.036	0.060	0.067	0.008	0.001	0.001	*bd.*	11.25	0.086	13.49	0.362	5.56	0.058	11.16	0.228	3.24	*bd.*	3.05	0.132	18.01	0.560	3.00	0.052
Yb	0.270	0.624	0.896	0.019	0.038	0.048	0.006	*bd.*	*bd.*	*bd.*	12.74	0.076	14.67	0.315	5.93	0.028	11.61	0.178	3.16	*bd.*	3.30	0.104	19.30	0.413	3.13	0.042
Lu	0.205	0.550	0.776	0.013	0.027	0.043	*bd.*	*bd.*	0.001	0.001	12.49	0.047	14.47	0.204	5.59	*bd.*	11.04	0.129	3.07	*bd.*	3.05	0.080	18.46	0.295	2.85	*bd.*
Hf	0.161	0.252	0.445	0.076	0.056	0.075	0.251	0.159	0.162	0.090	1.37	1.47	1.20	2.87	0.663	1.678	2.17	6.89	0.625	1.80	2.28	2.66	4.52	7.04	3.65	1.57
Ta	*bd.*	*bd.*	*bd.*	*bd.*	0.029	*bd.*	0.816	0.819	0.778	0.396	1.13	0.830	*bd.*	*bd.*	*bd.*	*bd.*	*bd.*	*bd.*	*bd.*	*bd.*	0.878	1.34	0.357	1.47	0.759	0.654
Pb	0.017	0.104	0.089	0.059	0.060	0.020	9.28	5.89	6.61	3.25	0.072	0.445	0.360	3.88	*bd.*	2.21	0.168	1.40	*bd.*	1.27	*bd.*	1.36	0.305	1.01	0.070	0.549
Th	0.052	0.024	0.013	0.121	0.173	0.161	1.43	1.10	1.18	0.546	*bd.*	0.112	*bd.*	0.692	*bd.*	*bd.*	*bd.*	*bd.*	*bd.*	*bd.*	0.068	0.258	*bd.*	0.113	0.065	0.157
U	0.564	0.572	0.454	1.37	1.70	1.58	1.36	0.818	0.946	0.464	0.670	0.169	*bd.*	0.315	*bd.*	*bd.*	*bd.*	*bd.*	*bd.*	*bd.*	0.695	0.182	*bd.*	0.236	0.404	0.094
Eu*	1.86	1.92	1.83	1.95	1.87	1.91	1.80	1.75	1.69	1.70	0.845	1.00	1.03	1.00	1.24	1.16	0.986	1.07	1.36	1.41	1.13	1.10	1.06	1.03	1.13	1.17
Sr*	0.061	0.106	0.039	0.210	0.179	0.075	21.83	34.72	31.97	33.20	0.011	2.32	0.006	1.42	0.060	22.75	0.025	9.75	0.039	19.83	0.029	3.40	0.012	2.86	0.030	3.59

Table 6. Representative incompatible elements compositions of garnet and clinopyroxene (cpx) in bimineralic eclogites from the Siberian craton. Samples marked with «UV» are from Udachnaya mine and samples marked with «Obn» are from the Obnazhennaya mine, Siberia. All values are normalized to primitive mantle values (McDonough and Sun, 1995). $Eu^* = Eu_N/sqrt(Sm_N*Gd_N)$. $Sr^* = Sr_N/sqrt(Sm_N*Nd_N)$.

5.1.2. Type II

Type II (non-metasomatized) eclogites comprise two compositional groups and associated LREE and LILE distribution patterns, for both garnet and clinopyroxene. The first group predominantly consists of Type IIA eclogites (Chapters 4—5) and is characterized by clinopyroxene with LREE concentrations higher than the primitive mantle values (between 1 and 30 times primitive mantle). The clinopyroxene REE patterns have flat LREE distribution ($(La/Nd)_N$ of 0.20—1.38) and strongly fractionated MREE-HREE $(Nd/Yb)_N$ of 3.43—167.1 (Figure V—2a). The normalized clinopyroxene Sr concentration ranges between 1.42 and 39.0. All clinopyroxene extended trace element spectra have strongly fractionated, $(Nb/La)_N$ ratio (0.001—0.50) and show positive Sr anomalies (1.71—30.0 Sr*) except for sample RV488 (Figure V—2c). Similarly, garnet compositions (Figure V—2b) have high and slightly fractionated LREE composition, $(La/Nd)_N$ of 0.01—0.05, and flat MREE-HREE distribution ($(Nd/Yb)_N$ of 0.08—1.68). The extended trace elements spectra have $(Nb/La)_N$ of 0.68—25.6 and negative Sr anomalies, complementary to the clinopyroxene patterns (Figure V—2d). Weak positive Zr inflections are observed in garnet.

The second compositional group contains both Type IIA and IIB eclogites and is defined by sub-primitive mantle LREE concentrations in clinopyroxene (>9 times lower than pyrolite values). REE patterns typically have fractionated LREE ($(La/Sm)_N$ of 0.03—0.01) and, less pronounced, HREE ($(Sm/Yb)_N$ of 4.04—13.2) (Figure 17a). Sr content in clinopyroxene (0.51—1.22 Sr_N) is lower than the LREE-rich group and typical eclogitic values. Although less pronounced, all LREE-poor clinopyroxene have positive Sr anomalies (Sr* 1.40—7.95), except for sample RV355 (Figure 17c). The extended trace element spectra have inversely fractionated, $(Nb/La)_N$ ratio in both clinopyroxene and garnet ~1.06—22.2. Similarly, garnet composition is LREE-depleted, with strongly fractioned $(La/Eu)_N$ of 0.001—0.02 and flat or slightly enriched HREE distribution ($(Eu/Yb)_N$ of 0.25—2.93). The extended trace elements spectra show

negative Sr anomalies, complementary to the clinopyroxene patterns and additional negative inflections are observed for Zr and Hf.

Sample	JIG4492		RV153	RV168		RV209		UV09-487A		UV09-502b		UV09-505		UV09-536		UV180/13	
	coe-bearing		ky-bearing	ky-bearing		ky-bearing		ky-bearing		ky-bearing		ky-bearing		ky-bearing		ky-bearing	
	garnet	cpx	garnet	garnet	cpx	garnet	cpx	garnet	cpx	garnet	cpx	garnet	cpx	garnet	cpx	garnet	cpx
Li	0.648	72.34	-	0.309	12.14	0.244	17.66	0.404	11.87	0.476	8.74	0.397	8.16	0.617	13.22	1.06	12.91
Sc	1.48	0.218	1.95	1.89	0.773	0.823	0.824	2.60	0.649	0.940	0.382	1.31	0.481	0.682	0.327	1.52	0.633
Ti	0.711	0.033	1.52	0.601	1.32	0.393	1.50	0.538	1.07	1.00	1.11	0.562	0.836	0.753	0.573	1.89	1.29
V	0.412	0.020	0.724	0.566	2.62	0.039	0.076	0.924	3.75	0.675	1.71	0.559	1.54	0.296	0.723	1.63	2.53
Cr	0.104	0.001	0.108	0.081	0.151	0.195	0.349	0.042	0.066	0.876	0.077	0.048	0.054	0.009	0.009	0.047	0.037
Co	0.416	0.043	0.504	0.429	0.309	0.006	0.223	0.470	0.168	0.356	0.167	0.374	0.181	0.656	0.196	0.372	0.221
Ni	0.014	0.020	0.027	0.015	0.254	0.005	0.140	0.006	0.062	0.026	0.239	0.006	0.089	0.035	0.199	0.017	0.228
Rb	0.039	7.72	0.009	0.009	0.008	0.010	0.025	*bd.*	*bd.*	0.011	*bd.*	*bd.*	*bd.*	*bd.*	0.072	0.010	*bd.*
Sr	0.426	5.35	0.199	0.126	16.22	0.195	0.366	0.281	22.36	0.234	10.86	0.082	8.99	0.237	6.50	0.128	5.10
Y	1.32	0.247	1.37	1.90	0.042	0.162	0.824	4.47	0.052	2.75	0.043	2.32	0.022	0.588	0.005	2.39	0.022
Zr	2.81	0.033	1.32	0.687	0.987	0.148	0.861	1.03	0.826	3.22	2.21	0.655	0.977	1.42	0.212	1.55	2.30
Nb	0.157	0.029	0.027	0.007	0.011	0.757	1.65	*bd.*	*bd.*	0.005	*bd.*	*bd.*	*bd.*	0.516	0.160	0.005	0.003
Ba	0.020	2.23	*bd.*	0.005	0.022	1.96	1.98	*bd.*	*bd.*	*bd.*	0.013	*bd.*	*bd.*	*bd.*	*bd.*	*bd.*	0.001
La	0.289	4.05	0.054	0.109	1.77	0.042	2.69	*bd.*	0.050	0.027	0.175	0.010	0.164	0.154	0.332	0.025	0.127
Ce	0.794	4.24	0.263	0.580	2.96	3.82	1.94	0.107	0.339	0.314	0.673	0.202	0.897	0.655	0.546	0.182	0.304
Pr	1.54	2.76	0.698	1.47	3.12	0.148	10.53	0.783	0.965	1.37	1.36	0.860	1.43	1.55	0.596	0.541	0.407
Nd	2.86	1.83	1.48	2.80	2.78	*bd.*	*bd.*	2.90	1.71	3.95	2.01	2.00	1.47	2.88	0.617	1.33	0.507
Sm	5.18	0.975	1.95	3.91	1.03	5.188	0.574	7.81	1.26	9.46	1.55	3.67	0.717	4.18	0.331	3.76	0.364
Eu	7.70	0.578	3.83	5.08	0.869	0.445	0.836	9.73	0.994	8.92	0.919	5.95	0.608	5.13	0.231	4.82	0.286
Gd	3.78	0.686	1.53	0.420	2.06	0.370	0.789	7.83	0.476	7.48	0.494	3.64	0.214	2.46	0.101	3.86	0.142
Tb	2.35	0.532	1.34	2.83	0.290	0.304	1.93	6.14	0.174	5.10	0.180	3.07	0.110	1.40	*bd.*	3.20	0.071
Dy	1.73	0.318	1.50	2.27	0.134	2.068	0.202	5.80	0.117	4.24	0.112	3.01	0.062	0.939	*bd.*	3.15	0.046
Ho	1.37	0.293	1.53	2.29	0.084	1.365	0.066	5.01	0.085	3.14	0.046	2.58	0.020	0.647	*bd.*	2.62	0.021
Er	1.44	0.195	1.65	2.11	0.043	1.298	0.043	4.77	0.047	2.65	0.034	2.41	0.021	0.553	*bd.*	2.47	0.016
Tm	1.30	0.138	1.56	2.16	0.031	1.168	0.046	4.10	*bd.*	2.07	*bd.*	2.05	*bd.*	0.436	*bd.*	2.05	0.010
Yb	1.66	0.145	1.81	1.98	0.034	1.012	0.019	4.08	*bd.*	2.10	*bd.*	2.11	*bd.*	0.445	0.049	2.20	0.006
Lu	1.63	0.093	1.80	2.05	0.030	1.183	0.046	3.85	*bd.*	1.82	*bd.*	1.94	*bd.*	0.441	*bd.*	1.88	0.004
Hf	1.56	0.065	0.909	1.97	0.034	1.099	0.085	0.721	2.25	1.96	3.84	0.417	1.65	0.905	0.550	0.969	4.00
Ta	0.414	0.168	*bd.*	0.095	0.100	1.277	0.070	*bd.*	*bd.*	*bd.*	*bd.*	*bd.*	*bd.*	0.611	0.597	0.019	*bd.*
Pb	0.187	0.810	0.029	0.046	4.90	1.201	0.157	*bd.*	2.56	*bd.*	1.65	*bd.*	2.43	*bd.*	0.337	0.062	8.92
Th	0.187	0.081	*bd.*	0.323	0.673	0.526	0.633	*bd.*	*bd.*	*bd.*	*bd.*	*bd.*	*bd.*	*bd.*	*bd.*	0.002	0.004
U	0.990	0.350	0.124	2.59	0.749	2.857	0.453	*bd.*	*bd.*	*bd.*	*bd.*	*bd.*	*bd.*	1.06	*bd.*	*bd.*	*bd.*
Eu*	1.74	0.707	2.22	3.97	0.596	0.321	1.24	1.24	1.28	1.06	1.05	1.63	1.55	1.60	1.27	1.27	1.26
Sr*	0.130	4.78	0.133	0.116	6.77	-	-	0.059	24.76	0.043	10.90	0.030	16.04	0.089	26.10	0.056	19.00

Table 7. Representative incompatible element compositions of garnet (gt) and clinopyroxene (cpx) in Si,Al-rich eclogites from the Kaapvaal and Siberian cratons. Samples marked with «JIG» and «RV» are from Roberts Victor mine, South Africa, and samples marked with «UV» are from the Udachnaya mine, Russia. Coesite-bearing eclogites are abbreviated with «coe-», kyanite -bearing with «ky-».All values are normalized to primitive mantle values (McDonough&Sun, 1995).
Eu*= Eu_N/sqrt(Sm_N*Gd_N). Sr*=Sr_N/sqrt(Sm_N*Nd_N).

5.2. Coesite-, kyanite-, corundum-bearing eclogites

Representative trace elements composition of garnet and clinopyroxene in coe-,ky-,cor-bearing eclogites, primitive mantle-normalized (McDonough and Sun, 1995), are given in Table 7 (coesite- and kyanite-bearing eclogites) and Table 8 (corundum-bearing eclogites). The corresponding REE and extended incompatible elements patterns are shown in Figure V—3 (coesite- and kyanite-bearing) and Figure V—4 (corundum-bearing eclogites), with homogeneous compositions among the Siberian and Kaapvaal samples.

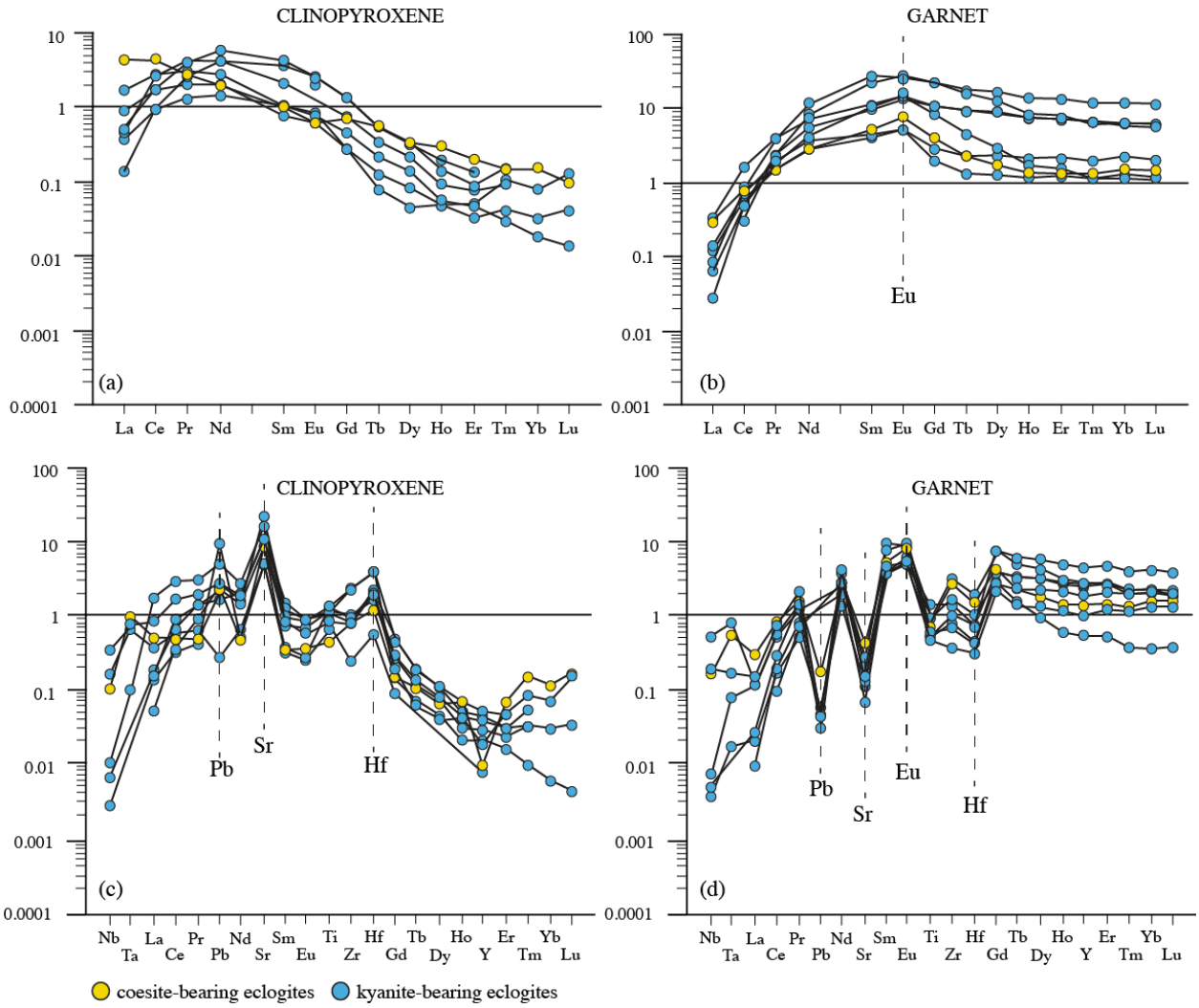

Figure V—3. REE (a—b) and extended trace elements patterns (c—d) in clinopyroxene and garnet in kyanite-bearing eclogites from the Siberian (Udachnaya, Obnazhennaya) and Kaapvaal (Roberts Victor, Jagersfontein) cratons. Coesite-bearing eclogites are marked with solid yellow circle symbols and kyanite-bearing eclogites with blue solid circle symbols.

Coesite and kyanite-bearing eclogites have similar compositional range and distribution of incompatible elements. Clinopyroxene REE patters are spoon shaped (Figure V—3a), with fractioned LREE (0.03—9.39 $(La/Nd)_N$) and HREE (19.6—114 $(Nd/Lu)_N$). Sr_N concentrations are typically between ~5 and 22 times higher than primitive mantle values. Garnet REE spectra have fractionated LREE (0.003—0.06 $(La/Sm)_N$) and flat HREE (Figure V—3b) with 0.21—2.33 $(Gd/Lu)_N$ except for samples UV09-502b and UV09-536, which are more fractionated (4.10—5.58 $(Gd/Lu)_N$). All samples have positive Sr anomalies in clinopyroxene (Sr^*_{cpx} vary between 4.78—26.1), negatively correlated in garnet (Sr^*_{gt} range of 0.03—0.13) (Figure V—

Sample	Obh110/13									Obn111/13								Obn112/13				RV179												RV344			
	non-ex gt	non-ex cpx	exsolved clinopyroxene				exsolved zoisite			non-ex garne		ex garnet		non-ex cpx		exs cpx	non-exs		exs gt	non-ex cpx	exsolved clinopyroxer		garnet					clinopyroxene					garnet		clinopyroxene	
Li	*bd.*	2.89	3.30	3.22	3.28	3.56	1.13	4.78	0.250	-	-	-	-	-	-	-	0.156	0.462	0.093	5.81	4.35	4.81	4.99	-	-	-	-	-	-	-	-	-	-	-	-	-	-	-
Sc	2.92	0.215	0.101	0.104	0.102	0.117	0.970	0.826	0.876	2.53	3.56	0.909	0.714	0.313	0.376	0.157	53.13	46.13	12.17	3.96	7.33	4.96	4.67	2.84	2.70	2.68	2.83	3.09	2.69	0.337	0.344	0.354	0.325	0.315	3.19	3.06	2.91	0.371	0.386	0.385	0.351
Ti	0.158	0.324	0.320	0.360	0.318	0.429	0.192	0.218	0.183	0.120	0.105	0.123	0.118	0.203	0.231	0.215	198.7	195.3	171.7	454.5	335.8	377.6	380.7	0.098	0.096	0.093	0.096	0.112	0.098	0.090	0.092	0.090	0.095	0.088	1.25	1.20	1.12	1.24	1.61	1.29	1.42
V	1.01	1.77	2.24	2.07	2.12	2.72	1.33	1.57	1.29	0.795	0.659	0.844	0.875	1.27	1.24	1.46	74.90	75.66	101.7	160.6	131.6	143.4	143.0	0.738	0.749	0.690	0.723	0.875	0.716	1.08	1.04	1.04	1.12	1.03	2.00	1.87	1.86	2.79	3.41	3.00	2.80
Cr	0.151	0.139	0.143	0.142	0.135	0.166	0.165	0.175	0.179	0.120	0.117	0.100	0.111	0.105	0.107	0.107	347.6	363.5	312.8	375.8	350.4	357.3	355.2	0.338	0.347	0.320	0.331	0.352	0.319	0.302	0.350	0.347	0.382	0.337	0.062	0.059	0.057	0.048	0.054	0.052	0.048
Co	1.19	0.236	0.218	0.219	0.226	0.210	0.674	0.628	0.710	0.751	0.909	0.443	0.475	0.216	0.212	0.218	45.72	48.68	27.36	14.79	17.47	12.06	16.51	0.704	0.707	0.628	0.681	0.774	0.640	0.118	0.125	0.124	0.127	0.115	0.691	0.658	0.586	0.210	0.195	0.184	0.206
Ni	0.070	0.429	0.393	0.428	0.442	0.540	0.057	0.155	0.044	0.040	0.046	0.028	0.029	0.381	0.379	0.442	25.94	21.32	14.97	253.3	192.6	194.2	240.7	0.072	0.077	0.064	0.070	0.082	0.065	0.347	0.324	0.331	0.347	0.327	0.019	0.019	0.014	0.091	0.112	0.083	0.104
Rb	*bd.*	*bd.*	*bd.*	*bd.*	*bd.*	*bd.*	0.055	0.211	0.025	*bd.*	*bd.*	0.011	*bd.*	*bd.*	*bd.*	0.007	*bd.*	0.012	0.006	*bd.*	323	0.013	*bd.*	0.010	*bd.*	0.014	*bd.*	*bd.*	0.010	0.017	0.021	0.014	0.018	0.435	0.014	0.016	0.020	*bd.*	4.02	*bd.*	*bd.*
Sr	0.005	0.578	0.363	0.520	0.450	0.426	0.077	0.233	0.021	0.004	0.004	0.008	0.005	0.455	0.446	0.356	0.049	0.139	0.045	5.10	3.94	4.67	4.65	0.018	0.019	0.019	0.017	0.019	0.017	0.922	0.813	0.798	1.00	1.43	0.028	0.027	0.030	0.474	1.29	0.515	0.540
Y	0.835	0.002	0.002	0.001	0.002	0.002	0.192	0.172	0.195	0.538	0.819	0.157	0.237	0.002	0.002	0.001	4.43	3.09	0.420	0.014	0.154	0.049	0.049	0.483	0.472	0.439	0.463	0.516	0.402	0.018	0.026	0.024	0.015	0.018	5.96	6.05	4.02	0.084	0.047	0.109	0.069
Zr	0.086	0.011	0.012	0.012	0.012	0.015	0.033	0.031	0.028	0.024	0.030	0.029	0.018	0.005	0.006	0.006	0.212	0.146	0.069	0.034	0.049	0.236	0.051	0.233	0.184	0.184	0.196	0.245	0.193	0.015	0.017	0.017	0.012	0.012	0.507	0.497	0.346	0.054	0.046	0.054	0.044
Nb	0.018	0.405	0.752	0.726	0.641	1.76	0.704	1.09	0.573	0.008	0.008	0.301	0.007	0.011	0.013	0.013	0.004	0.026	0.003	0.009	0.008	0.153	0.004	0.060	0.089	0.070	0.060	0.082	0.064	0.153	0.147	0.128	0.193	0.169	*bd.*	*bd.*	*bd.*	*bd.*	0.009	*bd.*	*bd.*
Ba	*bd.*	0.005	0.002	0.002	0.003	0.002	0.222	0.615	0.012	*bd.*	*bd.*	0.021	0.005	0.001	0.001	0.003	*bd.*	0.318	*bd.*	0.100	323	0.436	*bd.*	*bd.*	*bd.*	0.012	*bd.*	*bd.*	*bd.*	0.061	0.065	0.061	0.061	0.226	*bd.*	*bd.*	*bd.*	*bd.*	84.77	*bd.*	*bd.*
La	*bd.*	0.005	0.002	*bd.*	0.003	*bd.*	0.006	0.026	0.002	0.001	*bd.*	0.002	*bd.*	0.004	0.003	0.001	0.001	0.003	*bd.*	0.005	0.005	0.016	0.005	0.038	0.056	0.056	0.039	0.031	0.032	0.196	0.151	0.147	0.220	0.268	*bd.*	*bd.*	0.005	0.005	0.013	0.009	0.007
Ce	0.004	0.018	0.001	0.007	0.004	0.004	0.010	0.028	0.003	0.003	0.003	0.004	0.004	0.012	0.013	0.005	0.003	0.006	0.004	0.018	0.013	0.046	0.016	0.103	0.104	0.115	0.102	0.093	0.103	0.178	0.176	0.167	0.189	0.205	0.021	0.020	0.027	0.022	0.029	0.028	0.030
Pr	0.035	0.047	0.006	0.026	0.015	0.018	0.025	0.033	0.027	0.024	0.023	0.025	0.033	0.033	0.031	0.014	0.003	0.003	0.003	0.006	0.006	0.010	0.006	0.160	0.141	0.171	0.153	0.161	0.167	0.152	0.184	0.167	0.159	0.159	0.130	0.128	0.141	0.061	0.062	0.071	0.076
Nd	0.155	0.085	0.008	0.039	0.026	0.036	0.118	0.105	0.143	0.116	0.106	0.111	0.131	0.058	0.064	0.032	0.092	0.081	0.086	0.053	0.065	0.073	0.068	0.228	0.196	0.220	0.205	0.220	0.211	0.137	0.150	0.146	0.124	0.131	0.475	0.523	0.486	0.149	0.122	0.180	0.147
Sm	0.754	0.072	0.014	0.027	0.024	0.025	0.416	0.329	0.397	0.401	0.409	0.427	0.478	0.040	0.044	0.022	0.149	0.138	0.080	0.021	0.034	0.029	0.027	0.246	0.206	0.249	0.249	0.273	0.219	0.066	0.075	0.075	0.055	0.090	2.33	2.22	1.95	0.254	0.138	0.317	0.232
Eu	1.99	0.093	0.021	0.043	0.024	0.027	0.895	0.777	1.00	1.23	1.34	0.943	1.12	0.047	0.054	0.036	0.208	0.190	0.082	0.008	0.028	0.016	0.017	1.10	1.05	1.05	1.12	1.28	1.04	0.248	0.312	0.285	0.181	0.226	3.62	3.44	2.90	0.290	0.184	0.329	0.231
Gd	0.983	0.027	*bd.*	*bd.*	0.012	0.014	0.438	0.325	0.412	0.537	0.680	0.388	0.494	0.012	0.014	0.007	0.435	0.387	0.132	0.005	0.047	0.028	0.029	0.320	0.307	0.311	0.333	0.381	0.307	0.039	0.050	0.052	0.040	0.040	4.31	4.16	3.18	0.225	0.140	0.277	0.215
Tb	1.03	0.019	0.006	0.006	0.008	0.011	0.336	0.272	0.387	0.524	0.742	0.295	0.387	0.005	0.006	*bd.*	0.093	0.072	0.019	0.001	0.007	0.002	0.003	0.410	0.346	0.357	0.365	0.421	0.323	0.038	0.043	0.068	*bd.*	0.031	5.00	4.94	3.49	0.171	0.076	0.200	0.166
Dy	1.05	0.007	0.004	0.004	0.006	0.004	0.344	0.239	0.315	0.613	0.936	0.247	0.380	0.004	0.003	0.001	0.836	0.622	0.121	0.005	0.046	0.020	0.017	0.518	0.513	0.506	0.507	0.574	0.436	0.039	0.045	0.042	0.034	0.026	6.29	6.35	4.15	0.147	0.077	0.185	0.119
Ho	0.958	*bd.*	*bd.*	*bd.*	*bd.*	*bd.*	0.244	0.227	0.244	0.569	0.940	0.193	0.246	*bd.*	*bd.*	*bd.*	0.175	0.125	0.019	0.001	0.008	0.003	0.002	0.576	0.544	0.499	0.526	0.581	0.466	*bd.*	0.029	0.033	*bd.*	0.032	6.50	6.69	4.01	0.101	0.054	0.126	0.078
Er	0.890	0.004	0.004	*bd.*	*bd.*	*bd.*	0.176	0.152	0.184	0.616	1.01	0.132	0.235	0.001	0.001	0.001	0.599	0.393	0.045	0.002	0.017	0.004	0.004	0.605	0.600	0.548	0.589	0.678	0.482	*bd.*	0.022	0.026	*bd.*	0.017	7.10	7.37	4.31	0.068	0.027	0.101	0.053
Tm	0.760	0.003	0.004	0.003	0.001	*bd.*	0.071	0.111	0.143	0.562	0.988	0.107	0.185	0.001	*bd.*	*bd.*	0.078	0.054	0.004	0.000	0.001	0.001	*bd.*	0.575	0.534	0.469	0.547	0.603	0.488	*bd.*	*bd.*	bd.	0.030	*bd.*	6.66	6.99	3.99	0.058	*bd.*	0.047	*bd.*
Yb	0.696	*bd.*	*bd.*	*bd.*	*bd.*	*bd.*	0.127	0.077	0.094	0.642	1.08	0.099	0.122	*bd.*	*bd.*	*bd.*	0.530	0.344	0.021	*bd.*	0.008	*bd.*	0.002	0.635	0.596	0.565	0.528	0.692	0.503	*bd.*	0.027	bd.	*bd.*	*bd.*	7.21	7.64	4.34	0.028	*bd.*	0.039	*bd.*
Lu	0.582	0.001	*bd.*	*bd.*	*bd.*	0.003	0.083	0.063	0.059	0.572	1.01	0.064	0.092	0.001	0.001	*bd.*	0.073	0.047	0.002	*bd.*	0.001	*bd.*	*bd.*	0.554	0.572	0.458	0.511	0.591	0.436	0.049	*bd.*	bd.	*bd.*	*bd.*	6.83	7.05	4.07	0.026	*bd.*	0.031	*bd.*
Hf	0.127	0.062	0.052	0.040	0.061	0.076	*bd.*	0.053	0.030	0.035	0.041	0.018	0.022	0.031	0.029	0.033	0.010	0.010	0.004	0.010	0.008	0.013	0.006	0.237	0.222	0.205	0.249	0.316	0.172	0.040	0.037	0.040	0.035	0.038	1.08	1.09	0.746	0.278	0.337	0.299	0.316
Ta	*bd.*	0.056	0.091	0.067	0.097	0.303	0.089	0.113	*bd.*	*bd.*	*bd.*	0.115	*bd.*	*bd.*	*bd.*	*bd.*	*bd.*	0.001	*bd.*	*bd.*	*bd.*	0.009	*bd.*	*bd.*	*bd.*	*bd.*	*bd.*	*bd.*	*bd.*	0.084	*bd.*	*bd.*	*bd.*	*bd.*	*bd.*	*bd.*	*bd.*	*bd.*	*bd.*	*bd.*	*bd.*
Pb	0.068	0.085	0.268	0.131	0.241	0.379	0.249	0.327	*bd.*	0.049	0.062	0.049	*bd.*	0.057	0.058	0.069	0.003	0.059	*bd.*	0.082	0.108	0.087	0.088	0.067	0.038	*bd.*	0.059	*bd.*	0.059	0.640	0.620	0.593	0.673	0.660	*bd.*	0.039	*bd.*	0.044	0.121	0.049	0.059
Th	0.004	*bd.*	*bd.*	*bd.*	*bd.*	0.001	0.082	0.165	0.002	*bd.*	*bd.*	0.078	0.005	*bd.*	0.035	0.001	*bd.*	0.001	*bd.*	*bd.*	*bd.*	0.003	*bd.*	0.167	0.296	0.270	0.196	0.150	0.157	0.136	0.208	0.189	0.233	0.187	*bd.*	*bd.*	*bd.*	*bd.*	*bd.*	*bd.*	*bd.*
U	*bd.*	*bd.*	0.003	0.014	0.008	*bd.*	0.066	0.522	0.012	*bd.*	0.003	0.087	0.004	0.003	*bd.*	*bd.*	*bd.*	0.001	*bd.*	*bd.*	*bd.*	0.002	*bd.*	0.236	0.305	0.305	0.286	0.315	0.232	*bd.*	*bd.*	*bd.*	*bd.*	*bd.*	*bd.*	*bd.*	*bd.*	*bd.*	0.133	*bd.*	*bd.*
Eu*	2.31	2.10	-	-	1.41	1.43	2.10	2.37	2.48	2.65	2.54	2.32	2.31	2.16	2.20	2.95	0.794	0.823	0.818	0.779	0.703	0.567	0.613	3.93	4.16	3.79	3.88	3.97	4.02	4.91	5.07	4.56	3.87	3.77	1.14	1.13	1.17	1.22	1.32	1.11	1.03
Sr*	0.014	12.03	-	-	25.51	18.86	0.339	1.26	0.085	0.015	0.014	0.036	0.019	17.42	15.11	24.45	0.425	0.785	0.246	322.8	70.95	103.4	105.8	0.068	0.079	0.073	0.064	0.067	0.067	12.66	9.37	9.17	14.25	19.73	0.019	0.019	0.024	2.60	9.84	2.31	3.04

Table 8. Representative incompatible elements compositions of garnet (gt), clinopyroxene (cpx) and zoisite (zo) as non-exsolved (non-ex) and exsolution/exsolved (ex) grains in corundum-bearing eclogites from the Kaapvaal and the Siberian cratons. Samples marked with «RV» are from Roberts Victor mine and samples marked with «Obn» are from the Obnazhennaya mine. All values are normalized to primitive mantle values (McDonough&Sun, 1995). Eu*= EuN/sqrt(SmN*GdN). Sr*=SrN/sqrt(SmN*NdN).

3c—d). Similarly, both clinopyroxene and garnet have positive Eu anomalies (Eu^*_{cpx} 1.05—1.55, Eu^*_{gt} 1.06—3.97), except for samples JIG4492 and RV168 where they are preserved only in the garnet fraction. The extended incompatible elements patterns show additional positive inflections for Pb and Hf in clinopyroxene and equivalent negative inflections in garnet.

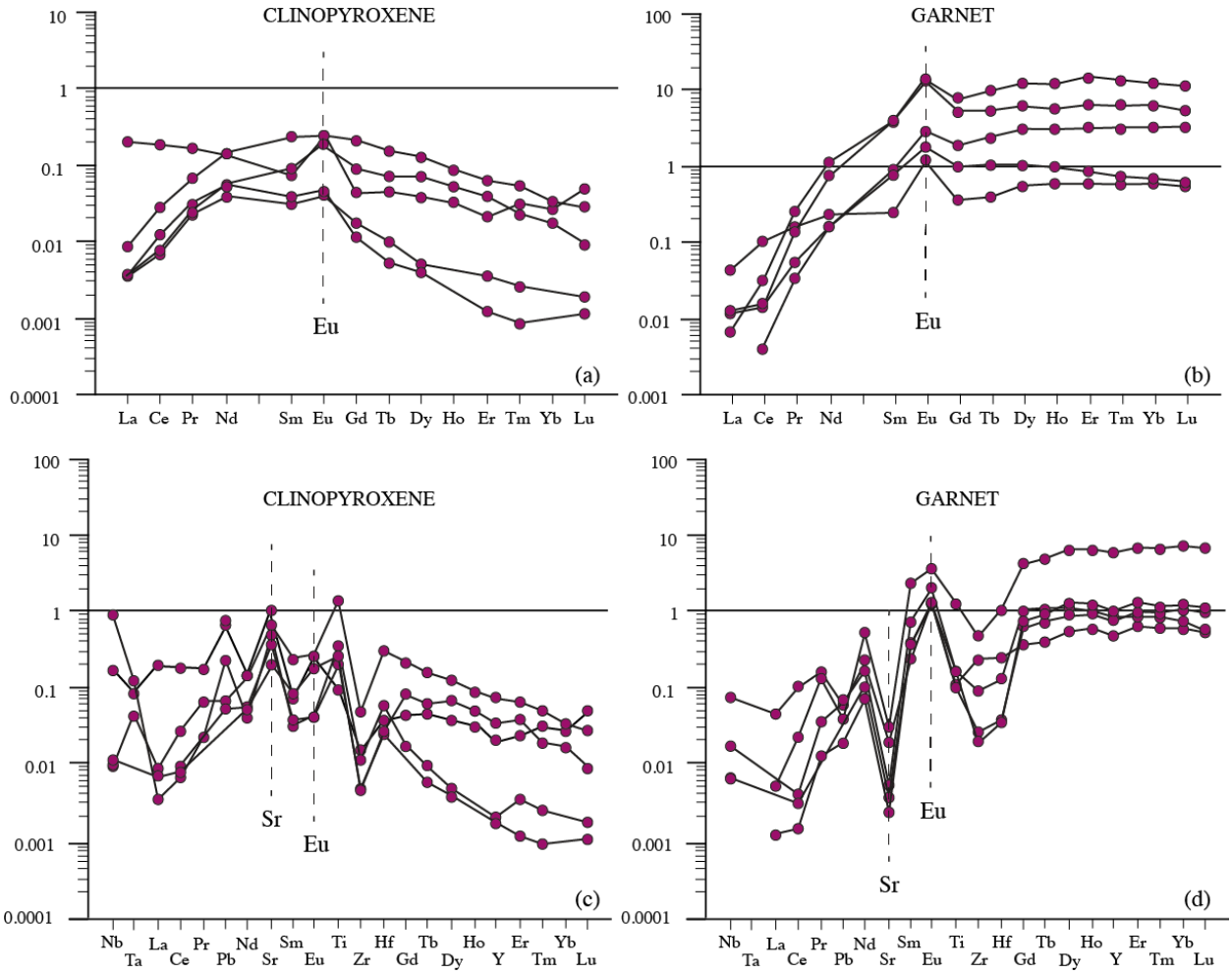

Figure V—4. REE (a—b) and extended trace elements patterns (c—d) in clinopyroxene and garnet in corundum-bearing eclogites from the Obnazhennaya and Roberts Victor mines.

Corundum-bearing eclogites have clinopyroxene REE concentrations lower than the primitive mantle (>5 times less than pyrolite values) (Figure V—4a), with typically convex-downward fractionated LREE (0.02—0.25 $(La/Sm)_N$) and HREE (8.71—31.3 $(Gd/Lu)_N$). One exception is sample RV179 which is slightly LREE-enriched ($(La/Sm)_N$ ~2.79). Sr_N concentrations vary between 0.45—0.58, much lower than the coesite- and kyanite-bearing eclogites. Similarly, garnet REE spectra have fractionated LREE (0.002—0.02 $(La/Sm)_N$) and flat or slightly

fractionated HREE (Figure V—4b) with 0.54—6.06 $(Gd/Lu)_N$. All samples have positive Sr (2.31—322.8 Sr^*_{cpx}) and Eu (Eu^*_{cpx} 1.03—5.07) anomalies in clinopyroxene (Figure V—4c) and corresponding negative Sr (Sr^*_{gt} 0.01—0.08) and positive Eu (Eu^*_{gt} 1.13—4.16) anomalies in garnet (Figure V—4d). An exception is made in sample Obn112/13 that has weak negative Eu anomaly in clinopyroxene and garnet (Eu^*_{cpx} 0.67, Eu^*_{gt} 0.81). The extended incompatible elements patterns show additional weak positive inflection for Pb and negative for Zr in clinopyroxene and corresponding weak positive inflection for Pb and negative for Zr and Hf in garnet (Figure V—4d).

5.3. Compositional variations and exsolution textures

Exsolution textures are present in all corundum-bearing samples and in the bimineralic Type IIA eclogite Obn108/13. REE and extended incompatible elements patterns in coarse exsolutions, host crystals and in the primary assemblage are shown in Figure V—5.

Bimineralic sample Obn108/13 is characterized by typical convex-downward clinopyroxene patterns (Figure V—5a), with average $(La/Nd)_N$ of 0.78 and increasingly fractionated HREE with the degree of exsolution ($(Nd/Tm)_N$ ~564 in non-exsolved grains, 2194—3960 in exsolved clinopyroxene). Primary garnets have general saucer-shaped LREE patterns (average $(La/Nd)_N$ of 0.02) and flat MREE-HREE distribution (average $(Nd/Tm)_N$ ~1.64). Similarly, exsolved garnets have LREE concentrations up to three times higher than primary garnets and are more fractionated (average $(La/Nd)_N$ of 0.04), markedly for MREE-HREE ($(Nd/Tm)_N$ of 27.2—43.8). Both primary and exsolved clinopyroxene have positive Sr (Sr* ~30.4) and Eu anomalies (Eu* ~1.74) correlated to negative Sr (Sr* ~0.11) and positive Eu (Eu* ~1.89) anomalies in garnet (Figure V—5b).

The analyzed corundum eclogites (Obn110/13, Obn111/13 and Obn112/13) have sub-primitive mantle LREE concentrations in clinopyroxene (~5—30 times lower than primitive

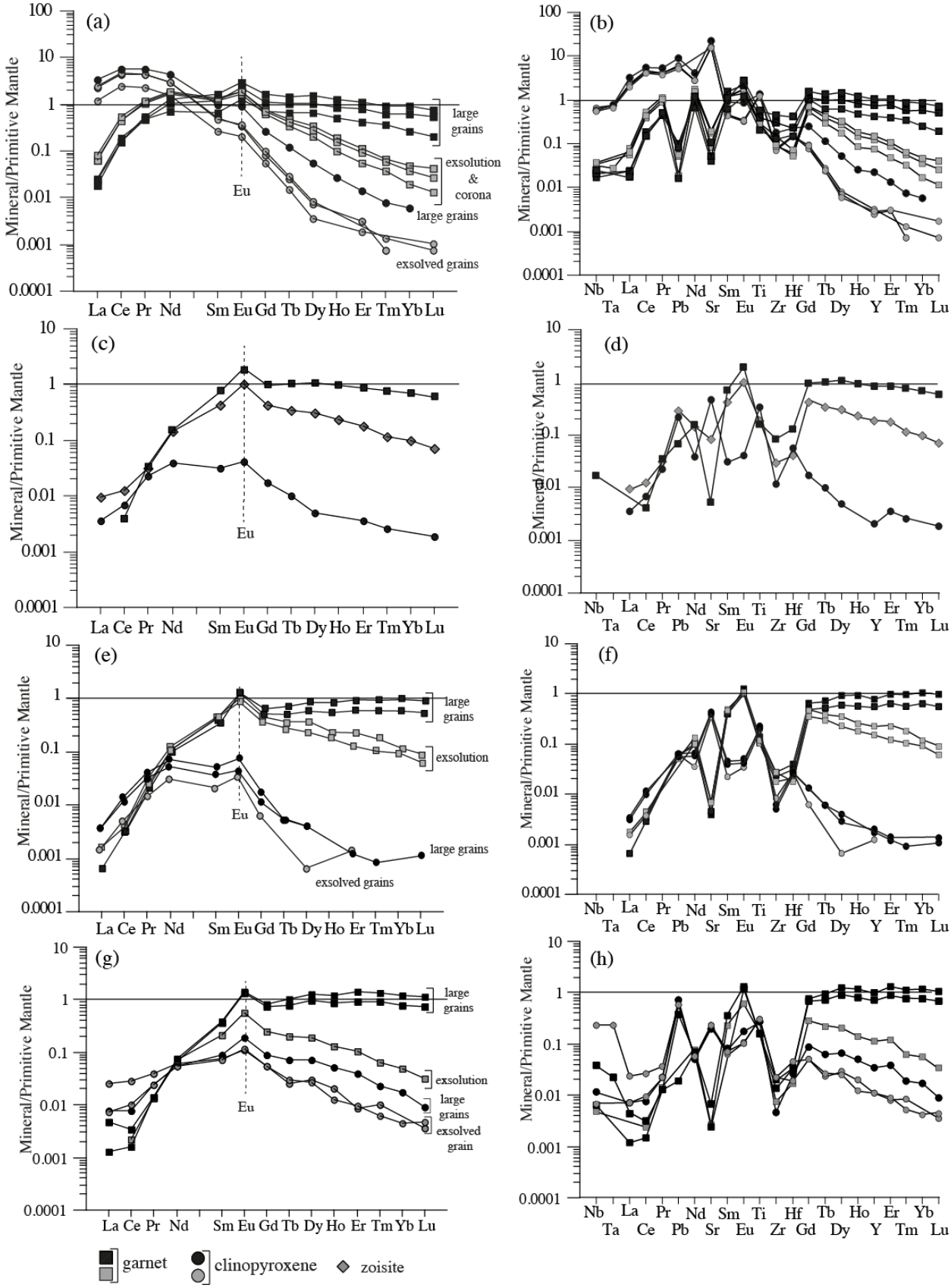

Figure V—5. REE and extended trace element patterns in clinopyroxene, garnet and zoisite as primary, host and exsolved grains in eclogite xenoliths from Obnazhennaya, Siberia.

mantle values). Clinopyroxene REE patterns are typically asymmetric bell shaped (Figure V—5c-h), with variably fractionated MREE-HREE in the exsolved grains ($(Sm/Lu)_N$ vary between 9.98 and 122). Primary (large) garnets have typically fractionated LREE and flat HREE ($(Sm/Lu)_N$ 0.04—2.05), whereas exsolved garnet and (where present) zoisite have fractionated MREE-HREE of intermediate composition towards the non-exsolved clinopyroxene ($(Sm/Lu)_N$ 5.02—39.8). Where present, positive Eu and Sr anomalies are marked both in primary and exsolved clinopyroxene. Similarly, extended trace element spectra for garnet show corresponding positive Eu and negative Sr anomalies in primary and exsolved grains, as well as additional Zr and Hf negative anomalies (Figure V—5d-h).

Summary: A set of 62 samples has been analyzed for trace element compositions and no pronounced distinction has been observed between eclogite xenoliths from the Kaapvaal and the Siberian cratons. Type I (metasomatized) bimineralic eclogites register a narrow LREE and LILE concentration range in both omphacite and garnet, with variable HREE, leading to the distinction between two groups, defined by HREE-rich and HREE-poor garnets.

Type II (non-metasomatized) bimineralic eclogites are similarly subdivided into two compositional groups. The first group is constituted exclusively by Type IIA (Mg-rich) eclogites and have LREE-rich omphacite with positive Sr anomalies, negatively correlated in garnet. The second compositional group is dominated by Type IIB (Mg-poor) eclogites, but includes also some Type IIA samples. It is characterized by LREE-depleted clinopyroxene with positive Sr anomalies, negatively correlated in garnet.

Coesite- and kyanite-bearing samples have similar trace element compositions, with generally spoon shaped REE patterns in omphacite and fractionated LREE with flat HREE patterns in the adjacent garnet. All samples have positive Eu, Sr, Pb and Hf inflections in clinopyroxene correlated with positive Eu and negative Sr, Pb and Hf in garnet. Corundum-bearing eclogites have significantly lower trace element concentrations with respect to the other eclogite types or

to the primitive mantle values and have typically convex-downward REE patterns in omphacite and fractionated LREE with flat HREE patterns in the adjacent garnet. Most omphacite have positive Eu and Sr anomalies correlated with positive Eu and negative Sr anomalies in garnet, except for sample Obn112/13. In samples exhibiting lamellar exsolutions (garnet ± zoisite) along the omphacite cleavage planes, the exsolved garnet and (where present) zoisite have fractionated MREE-HREE of intermediate composition towards the non-exsolved clinopyroxene, whereas the Eu and Sr anomalies are marked both in primary and exsolved minerals.

CHAPTER VI.

OXYGEN ISOTOPE COMPOSITIONS

CHAPTER VI. OXYGEN ISOTOPE COMPOSITIONS

Oxygen is the most abundant element in the Earth's crust and mantle and dominates the composition of silicate rock-forming minerals. It exists in the form of three isotopes: ^{16}O (99.76%), ^{17}O (0.04%) and ^{18}O (0.2%) and their weight difference leads to different physical and chemical properties and further to mass-dependent isotopic variations. These are expressed as $^{18}O/^{16}O$ or $\delta^{18}O$, where $\delta^{18}O$ is defined as:

$$\delta^{18}O = [(^{18}O/^{16}O)_{sample}/(^{18}O/^{16}O)_{standard} - 1] * 1000$$

The reference standard commonly used for reporting oxygen isotopic abundance ratio is the Vienna Mean Standard Ocean Water (VSMOW) with a $\delta^{18}O$ value of 2.0052 ‰ (Baertschi, 1976).

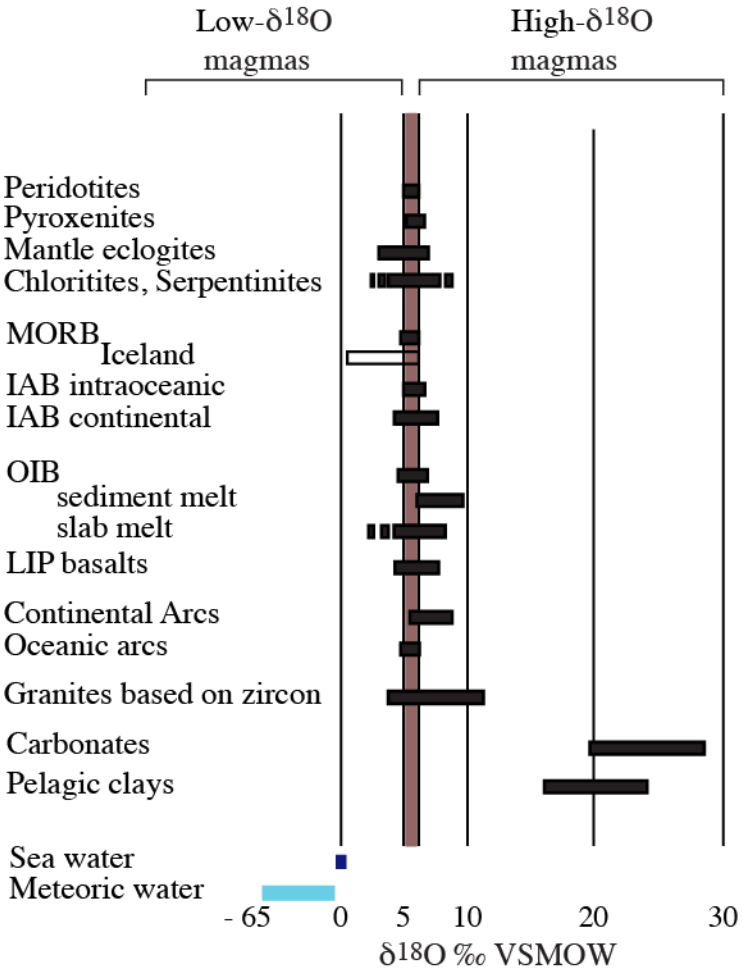

Figure VI—1. Oxygen isotopic variations in common terrestrial rocks and magmas, reported to the Vienna Mean Standard Ocean Water (VSMOW). Red band represents «normal» δ18O values (+5.5±0.4 ‰; Mattey et al. 1994) of mafic and basaltic magmas, interpreted as equivalent for the predominant mantle and mantle-derived rocks. Low- and high-$\delta^{18}O$ are defined with respect to the normal mantle values. Data compilation after Bindeman (2008).

Oxygen isotopic variations on Earth cover a wide range of values (Figure VI—1). Among them, meteoric waters have the highest variability and most negative values, caused by Rayleigh

fractionation during evaporation and condensation. Isotopic fractionation refers to the enrichment in one isotope (*i.e.*^{16}O) relative to another (*i.e.* ^{18}O.) during a physical process or a chemical reaction, between two components (*i.e.* A and B). This is expressed by the fractionation factor, α (alpha), defined as:

$$\alpha_{A-B} = R_A/R_B = (1000 + \delta^{18}O)_A/(1000 + \delta^{18}O)_B$$

Unaltered basaltic and ultramafic rocks typically have oxygen isotope compositions in the 5.1—5.9 ‰ range (Mattey et al., 1994), that replicate the predominant mantle and mantle-derived composition ("normal-mantle value"). Felsic rocks and magmas have more variable and higher δ^{18}O values, whereas authigenic sedimentary rocks such as limestones and cherts have the highest δ^{18}O values. Low-temperature precipitation of secondary minerals and rock-seawater exchange at low temperatures, with a high mineral-fluid isotope fractionation factor, will lead to high-δ^{18}O values. Exchange between rock and fluids at high temperatures or assimilation of materials that interacted with strongly negative meteoric waters at high temperatures, will result in low-δ^{18}O rocks and magmas (Bindeman, 2008). As the bulk mantle and mantle-derived rocks have a narrow range of δ^{18}O values (+5.5±0.4 ‰; Mattey et al. (1994)), the oxygen isotopic variation among basaltic magmas and mantle xenoliths can be used to retrace potential oceanic crust recycling (Gurenko et al., 2011). Under this premise, mantle rocks and magmas with high δ^{18}O value contain a crustal component, which has undergone low-temperature alteration or fluid exchange typically constrained to the upper part of the crust (Bindeman, 2008; Eiler, 2001). Similarly, magmatic rocks with δ^{18}O values lower than the normal mantle contain a high temperature, hydrothermally altered crustal component, typically corresponding to the lower part of the oceanic crust (McCulloch et al., 1981). The variability of oxygen isotopic composition with depth in oceanic crust has been studied by Gregory and Taylor (1981) for the Samail ophiolite, as a complete representative of modern oceanic crust (Figure VI—2).

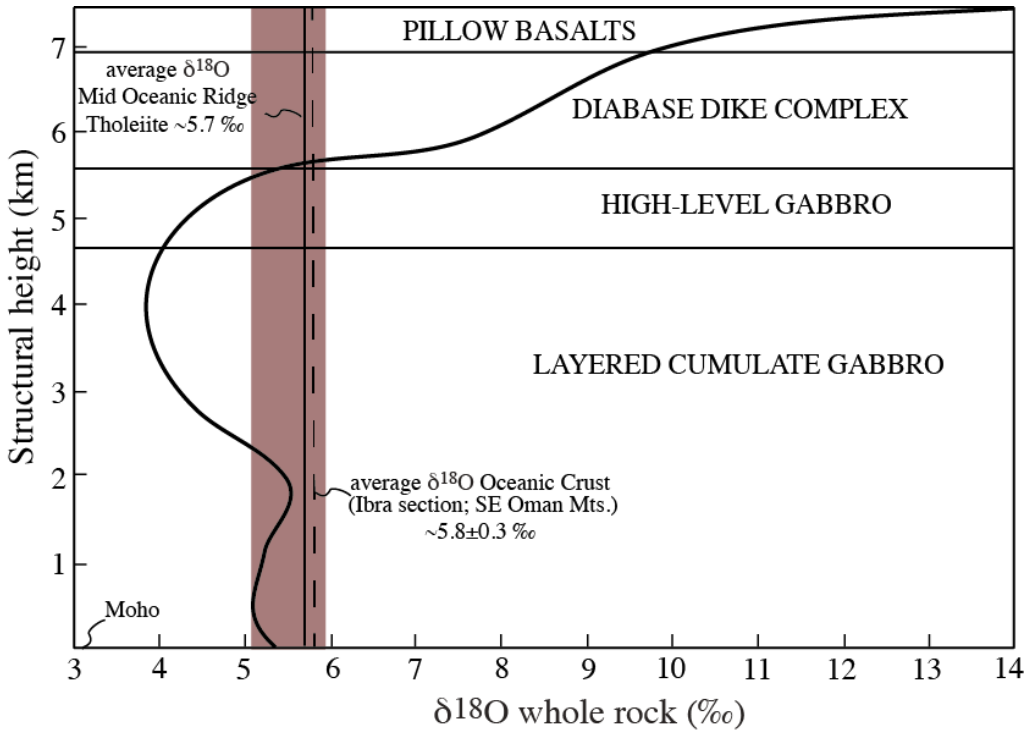

Figure VI—2. Material balance calculation for the generalized oxygen isotopic profile displayed by the Ibra section (marked by solid curve). Figure after Gregory and Taylor (1981), with calculated average $\delta^{18}O$ value of mature, altered oceanic crust at 5.8 ± 0.3 ‰. «Normal-mantle» values are marked with a red band at 5.5 ± 0.4 ‰ (Mattey et al. 1994). Pillow lavas $\delta^{18}O$ values vary between 10.7—14 ‰ and the underlying dike complex range between 5.7 and 10.7 ‰. The gabbro crustal formations have lower $\delta^{18}O$ values, ranging between ~4.0 and 5.5 ‰.

The section comprising pillow basalts and dolerite dike complex, marking the upper crustal part, have $\delta^{18}O$ values ranging between 10.7—14 ‰ and 5.7—10.7 ‰ respectively. The middle section comprising vari-textured and upper cumulate gabbro have $\delta^{18}O$ values lower than the average oceanic crust, ranging roughly between 4.0 and 5.5 ‰, typically below normal mantle values. And the lowest section of cumulate gabbro has normal or close to normal oxygen isotopic values. Unlike other geochemical tracers (i.e. incompatible elements) Oxygen isotopes are robust and recycled crustal material preserves its $\delta^{18}O$ values and variability when subducted at mantle conditions (Neal et al., 1990). This makes the oxygen isotopic system very useful for differentiating rocks of crustal origin from mantle-derived rocks.

The origin of eclogite xenoliths as derived from an ancient subducted oceanic crust or mantle magma has been debated for more than 40 years (Chapter 1.1). Numerous studies have used oxygen isotopes to retrace the history of their protolith, leading to an important database of $\delta^{18}O$

variations in mantle eclogites. Nevertheless, many of them are focused on fully (Garlick et al., 1971; Gréau et al., 2011; MacGregor and Manton, 1986; Schulze et al., 2000) or partly metasomatized (Riches et al., 2016) material and only few include oxygen isotopic composition of non-metasomatized eclogites (Huang et al., 2016; Jacob et al., 2005; Viljoen et al., 2005).

This chapter aims to identify first hand the $\delta^{18}O$ values of non-metasomatized eclogite xenoliths from the Siberian and Kaapvaal cratons. For this purpose a set of 41 samples has been analysed using laser fluorination and between 1 and 4 minerals have been carried out per sample mineral (garnet, clinopyroxene, kyanite, corundum). Secondly, this chapter focuses on the difference in $\delta^{18}O$ value in co-existing clinopyroxene and garnet. If the measured $\delta^{18}O$ values result from the re-equilibration of a sample with a metasomatic fluid, isotopic disequilibrium is expected between the clinopyroxene and garnet, as each would be characterized by different mineral-fluid fractionation factors. The permil difference between two minerals, e.g. clinopyroxene and garnet, expressed as Δ, is defined as:

$$\Delta_{cpx\text{-}gt} = \delta^{18}O_{clinopyroxene} - \delta^{18}O_{garnet}$$

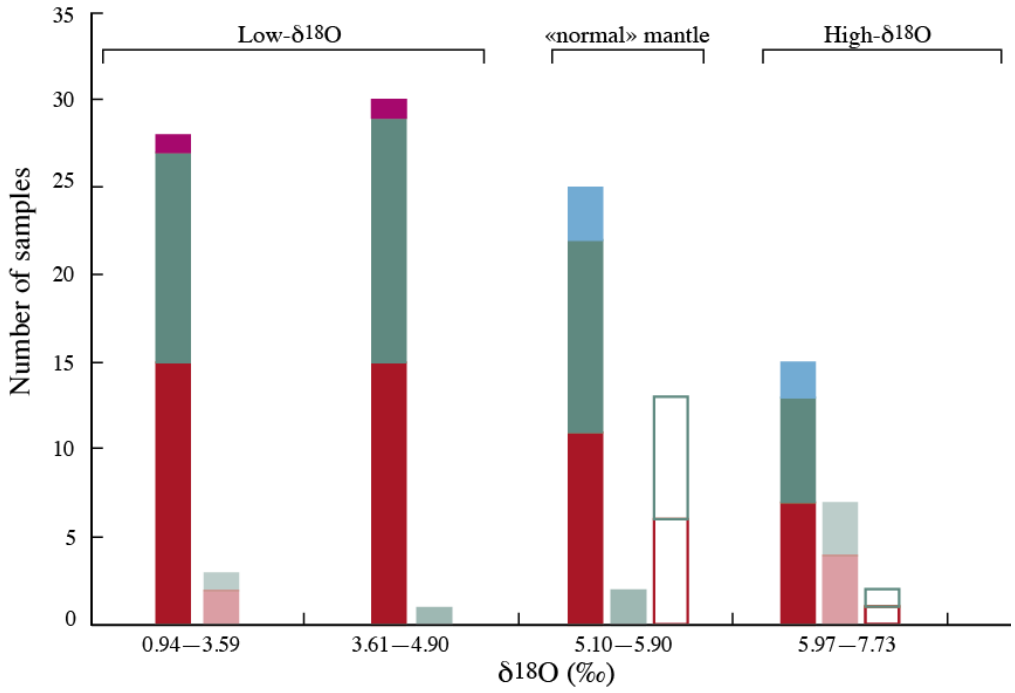

Figure VI—3. Histogram showing oxygen isotopic variations from this study, in garnet (red), clinopyroxene (green), kyanite (blue) and corundum (violet) in eclogites from Roberts Victor (solid bars), Jagersfontein (shaded bars) and Obnazhennaya (clear bars) kimberlite mines. Their range in δ18O values shows a bi-modal distribution with respect to the normal mantle (5.5 ± 0.4 ‰; Mattey 1994), having both lower and higher values.

and is a good indicator for the inherited or metasomatic character of the oxygen isotope ratio.

Oxygen isotope compositions of garnet, clinopyroxene, kyanite and corundum are reported in Table 9 and Figure VI—3. The calculated whole rock $\delta^{18}O$ values, estimated from the modal abundances, vary widely from 1.37 ‰ to 7.54 ‰. The oxygen isotope compositions of individual minerals show $\delta^{18}O$ values higher and lower than the mantle (+5.5±0.4 ‰; Mattey et al. (1994)) (Figure VI—4).

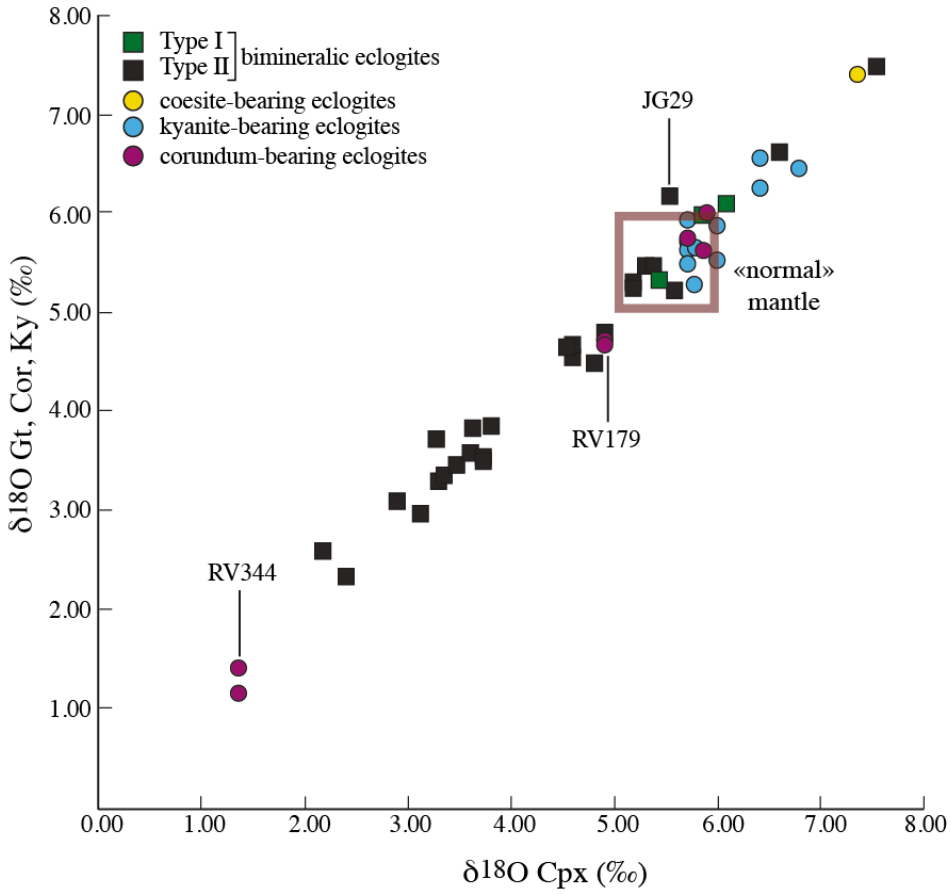

Figure VI—4. Plot of $\delta^{18}O$ values of garnet (gt), corundum (cor) and kyanite (ky) vs. clinopyroxene (cpx) from this study. Metasomatized (Type I) bimineralic eclogites (Roberts Victor mine) are marked with green solid square symbol. Non-metasomatized (Type II) bimineralic eclogites comprise samples from Kaapvaal (Roberts Victor, Jagersfontein mines) and Siberian craton (Obnazhennaya kimberlite) are marked with black solid square symbol. Coe-ky-cor-bearing samples are marked with solid yellow (coesite-), blue (kyanite-) and violet (corundum-) solid circle symbols. Red square marks normal mantle values 5.5 ± 0.4 ‰ (Mattey et al., 1994).

Three metasomatized (Type I) samples have been analyzed for reference. The $\delta^{18}O$ values of garnet range from 5.35 ‰ and 6.12 ‰. Among the non-metasomatized eclogites, we distinguish low-$\delta^{18}O$ eclogites, which have garnet values ranging from 1.1 ‰ to 4.8 ‰ in agreement with

the coexisting clinopyroxene (1.4—4.9 ‰), and high-$\delta^{18}O$ eclogites, with garnet $\delta^{18}O$ values ranging within normal mantle values, between 5.2—6.0 ‰ in garnet and 5.2—6.0 ‰ in clinopyroxene, as well as higher, 6.0—7.5 ‰ and 5.5— 7.5 ‰ respectively.

The low-$\delta^{18}O$ group includes bimineralic samples, garnet values between 2.3—3.9 ‰ and between 4.5—4.8 ‰ (Figure VI—5). The lowermost values typically correspond to the low-magnesium (Type IIB) eclogites characterized by high pressure-temperature equilibrium conditions, whereas the higher $\delta^{18}O$ values correspond exclusively to the magnesium-rich, Type IIA eclogites (Chapter 4), characterized by lower-PT conditions (Figure VI—5). Similarly, the high-$\delta^{18}O$ group with mantle-like or higher $\delta^{18}O$ values corresponds strictly to Type IIA eclogites.

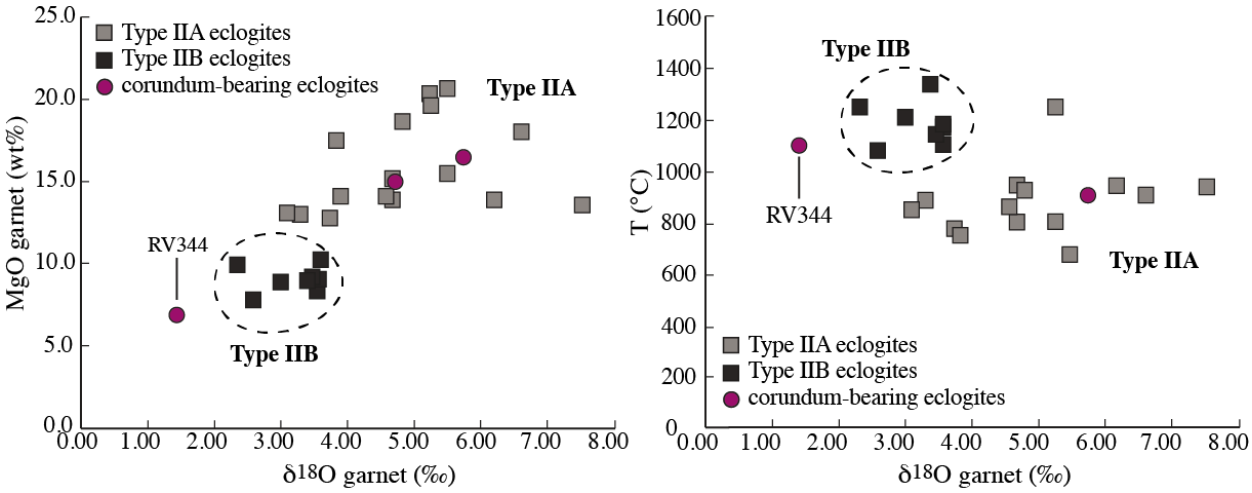

Figure VI—5. $\delta^{18}O$ in garnet vs. (a) MgO in garnet and (b) T (°C) calculated based on Fe-Mg exchange between garnet and clinopyroxene after Krogh (1988) in bimineralic Type II (non-metasomatized) and corundum-bearing eclogites fromt his study. Pristine eclogites with Mg-rich garnets (Type IIA) have generally higher $\delta^{18}O$ values and correspond to lower P-T conditions. Non-metasomatized eclogites with Mg-poor garnets (Type IIB) have lower $\delta^{18}O$ values and correspond to higher P-T equilibrium conditions. Type IIA is marked with grey solid square symbols, Type IIB with black solid square symbols and corundum-bearing eclogites are marked with violet solid circle symbols.

Among the corundum-bearing eclogites, xenoliths from the Roberts Victor mine have $\delta^{18}O$ values lower than the normal mantle (whole rock estimates of 1.4 and 4.8 ‰) , whereas eclogites from the Obnazhennaya pipe have mantle isotopic composition (5.5—5.9 ‰). Moreover, sample RV344 has the lowest $\delta^{18}O$ values recorded so far in mantle eclogites, with a garnet average of

Sample	Mineral				Type	wr $\delta^{18}O$	Occurrence	Δ cpx-gt
	garnet	cpx	kyanite	corundum				
JG29	6.52	5.78	-	-	IIA	6.15	Jagersfontein	0.74
JG29	6.18	5.54	-	-	IIA	5.86	Jagersfontein	0.64
JG32	3.55	3.73	-	-	IIB	3.64	Jagersfontein	0.17
JG32	3.14	3.49	-	-	IIB	3.31	Jagersfontein	0.35
JG33	7.73	7.47	-	-	IIA	7.49	Jagersfontein	0.27
JG33	-	7.28	-	-	IIA	-	Jagersfontein	-
JG33	7.50	7.54	-	-	IIA	7.54	Jagersfontein	0.04
JJG4492	7.41	7.35	-	-	coe-bearing	7.37	Roberts Victor	0.06
JJG4492	7.03	-	-	-	coe-bearing	-	Roberts Victor	-
Obn108/13	5.58	5.35	-	-	cor-bearing	5.53	Obnazhennaya	0.23
Obn108/13	5.48	5.39	-	-	cor-bearing	5.46	Obnazhennaya	0.09
Obn110/13	5.88	5.49	-	-	cor-bearing	5.65	Obnazhennaya	0.39
Obn110/13	5.74	5.71	-	-	cor-bearing	5.72	Obnazhennaya	0.03
Obn111/13	6.01	5.91	-	-	cor-bearing	5.94	Obnazhennaya	0.10
Obn111/13	5.61	5.81	-	-	cor-bearing	5.75	Obnazhennaya	0.20
Obn112/13	5.64	5.86	-	-	cor-bearing	5.79	Obnazhennaya	0.22
Obn112/13	-	5.23	-	-	cor-bearing	-	Obnazhennaya	-
RV159	6.60	6.59	-	-	IIA	6.59	Roberts Victor	0.01
RV168	6.27	6.41	6.58	-	ky-bearing	6.45	Roberts Victor	0.14
RV174	4.67	4.60	-	-	IIA	4.64	Roberts Victor	0.07
RV177	3.29	3.30	-	-	IIA	3.29	Roberts Victor	0.01
RV179	4.72	4.89	-	4.77	cor-bearing	4.84	Roberts Victor	0.17
RV179	5.34	5.11	-	-	cor-bearing	-	Roberts Victor	0.23
RV180	3.10	2.89	-	-	IIA	3.00	Roberts Victor	0.21
RV186	2.99	3.12	-	-	IIB	3.05	Roberts Victor	0.13
RV197	4.67	4.56	-	-	IIA	4.61	Roberts Victor	0.11
RV199	3.37	3.33	-	-	IIB	3.35	Roberts Victor	0.04
RV203	3.73	3.28	-	-	IIA	3.50	Roberts Victor	0.45
RV203	3.05	-	-	-	IIA	-	Roberts Victor	-
RV208	5.97	5.87	-	-	I A/B	5.92	Roberts Victor	0.11
RV209	5.32	5.76	5.69	-	ky-bearing	5.62	Roberts Victor	0.44
RV213	5.72	5.70	5.52	-	ky-bearing	5.69	Roberts Victor	0.03
RV213	5.72	-	-	-	ky-bearing	-	Roberts Victor	-
RV218	6.48	6.78	-	-	ky-bearing	6.71	Roberts Victor	0.30
RV219	5.35	5.42	-	-	I A/B	5.39	Roberts Victor	0.08
RV220	2.59	2.17	-	-	IIB	2.38	Roberts Victor	0.42
RV220	2.12	2.54	-	-	IIB	2.33	Roberts Victor	0.42
RV221	3.69	4.09	-	-	IIB	3.89	Roberts Victor	0.40
RV221	3.55	3.75	-	-	IIB	3.65	Roberts Victor	0.20
RV226	6.12	6.08	-	-	IA	6.10	Roberts Victor	0.04
RV233	3.61	3.69	-	-	IIB	3.65	Roberts Victor	0.08
RV233	3.59	3.61	-	-	IIB	3.60	Roberts Victor	0.01
RV234	3.48	3.47	-	-	IIB	3.47	Roberts Victor	0.01
RV319	5.65	5.71	5.95	-	ky-bearing	5.75	Roberts Victor	0.06
RV320	5.54	5.99	5.89	-	ky-bearing	5.76	Roberts Victor	0.45
RV344	0.98	0.86	-	-	cor-bearing	-	Roberts Victor	0.12
RV344	1.43	1.36	-	1.17	cor-bearing	1.37	Roberts Victor	0.07
RV344	0.94	-	-	-	cor-bearing	-	Roberts Victor	-
RV344	1.08	-	-	-	cor-bearing	-	Roberts Victor	-
RV347	4.82	4.90	-	-	IIA	4.86	Roberts Victor	0.08
RV355	3.84	3.63	-	-	IIA	3.71	Roberts Victor	0.22
RV355	3.99	3.63	-	-	IIA	3.78	Roberts Victor	0.36
RV356	4.50	4.81	-	-	IIA/B	4.66	Roberts Victor	0.31
RV360	5.25	5.18	-	-	IIA	5.24	Roberts Victor	0.07
RV377	3.88	3.80	-	-	IIA	3.83	Roberts Victor	0.08
RV377	3.84	3.63	-	-	IIA	3.71	Roberts Victor	0.21
RV469	-	2.40	-	-	IIB	-	Roberts Victor	-
RV469	2.35	2.40	-	-	IIB	2.38	Roberts Victor	0.05
RV488	5.47	5.19	-	-	IIA	5.39	Roberts Victor	0.28
RV488	-	5.29	-	-	IIA	-	Roberts Victor	-
RV508	4.37	-	-	-	IIA	-	Roberts Victor	-
RV508	4.56	4.59	-	-	IIA	4.58	Roberts Victor	0.03
RV508	4.43	-	-	-	IIA	-	Roberts Victor	-
RV513	5.23	5.58	-	-	IIA	5.40	Roberts Victor	0.35
RV580	5.32	5.17	-	-	IIA/B	5.24	Roberts Victor	0.15

Table 9. $\delta^{18}O$ values of garnet (gt), clinopyroxene (cpx), kyanite, corundum and recalculated bulk (wr) based on mineral modal abundance in eclogite xenoliths from Kaapvaal and Siberian cratons from this study. Samples marked with «RV» and «JJG» are from Roberts Victor mine, samples marked with «JG» are from the Jagersfontein mine South Africa and samples marked with Obn are from Obnazhennaya kimberlite, Siberia. Δ cpx-gt is the permil difference calculated by the formula Δ cpx-gt = $\delta^{18}O$ cpx - $\delta^{18}O$ gt.

1.1 (n=4, 1σ=0.22). By contrast, kyanite- (~5.6—6.7 ‰) and coesite-bearing (~7.4 ‰) samples have mantle or above normal mantle $\delta^{18}O$ values.

The per mil difference (Table 9) between clinopyroxene and garnet ($\Delta^{18}O$) ranges mostly from 0.01 ‰ to 0.31 ‰ (n=16) and -0.22 ‰ to -0.01 ‰ (n=19) except for samples: JG29 (-0.64 — -0.74 ‰), RV203 (-0.45 ‰), RV209 (0.44 ‰), RV220 (0.42 ‰), RV320 (0.45 ‰) and RV513 (0.35 ‰).

6.1. Equilibrium oxygen isotope fractionation

The fractionation associated with the equilibrium exchange between minerals is best expressed by the isotope fractionation factor, in this case:

$$10^3\ln \alpha_{cpx-gt} = 10^3\ln (10^3 + {}^{18}O/{}^{16}O)_{clinopyroxene} / (10^3 + {}^{18}O/{}^{16}O)_{garnet}$$

For minerals with $\delta^{18}O$ values relatively small in magnitude and permil difference lower than 10 ‰, $\Delta^{18}O \approx 10^3\ln \alpha$ (Hoefs, 2004).

Isotopic fractionation is strongly controlled by temperature and chemical bond-strength. At constant high temperatures, the isotope fractionation factor can be described as:

$$10^3\ln \alpha = A^* 10^6/T^2$$

where *A* is a simple factor, dependent on the coexisting minerals and T is Kelvin temperature (Urey, 1947). According to this theory, intermineral equilibrium fractionation would tend to 0 with infinitely increasing temperature.

Furthermore, oxygen isotope enrichment is believed to decrease from minerals dominated by Si-O bonds, Al-O to M^{2+}-O (Bindeman, 2008). Subsequently, substitutions of cations with identical charge (*i.e.* Na-K; Ca-Fe^{2+}-Mg) will play a negligible role on oxygen fractionation, whereas NaAl-Ca(Mg,Fe) substitutions in pyroxene and Al-Fe^{3+} substitutions in garnet will have a larger effect on oxygen enrichment (Sharp, 2017). In this case pyroxenes would have higher $\delta^{18}O$ values than the coexisting garnet, however some of this study's measured garnets have

slightly higher $\delta^{18}O$ than the coexisting clinopyroxene. The effects of octahedral cation substitution on isotope equilibrium fractionation between garnet and clinopyroxene have been discussed to generate crossovers in the values of the mineral-dependent *A* factor (Kohn& Valley, 1998). Similarly, Kieffer (1982) and Neal et al. (1990) argue that at different temperatures, crossovers in fractionation factors between chemically variable clinopyroxene and garnet are observed. This influence of mineral variations on the oxygen fractionation coefficient have been calculated by (Zheng, 1993) as:

$$10^3 \ln \alpha_{cpx-gt} = (A*10^6/T^2 + B*10^3/T + C)_{clinopyroxene} - (A*10^6/T^2 + B*10^3/T + C)_{garnet}$$

where A, B and C are mineral-dependent factors, however this does not support the previous hypothesis of crossovers in the fractionation factor at realistic temperatures (for the present samples, crossovers are to be expected at temperatures above 2500°C).

Studies by Ongley et al. (1987) and Neal et al. (1990) discuss the per mil difference between garnet and omphacitic clinopyroxene in eclogite xenoliths, concluding values less than 0.3 ‰ would indicate chemical equilibrium while higher values would suggest metasomatic disequilibrium. Taking into account the measurement error, the range for the permil difference between garnet and clinopyroxene at equilibrium should be 0.3±0.2 ‰, which is applicable to the majority of the analyzed samples

Summary: The investigated eclogite xenoliths comprise both high- and low-$\delta^{18}O$ examples (1.1—4.8 ‰; 6.0—7.7 ‰ garnet and 0.9—4.9 ‰; 6.0—7.5 ‰ clinopyroxene respectively; Figure VI–3). Metasomatized (Type I) bimineralic eclogites have mantle or higher $\delta^{18}O$ values. Among the non-metasomatized (Type II) bimineralic eclogites we can discriminate between two $\delta^{18}O$ groups. The lowest values (2.3—3.9 ‰ in garnet) correspond to the high-PT layer (Type IIB eclogite) from the lower part of the cratonic root, with calculated temperature estimates of ~1000—1300°C. The higher $\delta^{18}O$ range (3.6—7.7 ‰) corresponds to the upper, low-PT layer (Type IIA eclogite), with corresponding temperature estimates of ~650° and 1000°C. Corundum-

bearing eclogites from Roberts Victor have lower than mantle $\delta^{18}O$ values, including the lowest registered (1.1 ‰ garnet average, n=4, 1σ=0.2), whereas the corundum-bearing samples from Obnazhennaya and ky-coe-bearing eclogites have mantle or above normal mantle $\delta^{18}O$ values.

CHAPTER VII.

DISCUSSION PART I

CHAPTER VII. DISCUSSION PART I

Mantle eclogite xenoliths accommodate various textures and span over a broad range of compositions, most of which were subjected to various degrees of metasomatism. In this context, all compositional and textural aspects can be subject to different interpretations of on whether they can be indicative of the protolith composition and whether they are representative for the subcratonic mantle.

Major element composition of coexisting garnet and clinopyroxene are a critical point, allowing pressure – temperature estimates and influencing the concentrations and partitioning of trace elements. In agreement with previous classifications, extensively metasomatized eclogites can be distinguished from non-metasomatized eclogites (Chapter III and Chapter IV). This further allows investigating the petrogenesis of mantle eclogites based on the chemical composition of pristine xenoliths.

As discussed in Chapter 1 there are three fundamental petrogenetic models for mantle eclogites currently under debate: (i) mantle-derived high pressure cumulates (Hatton, 1978; MacGregor and Carter, 1970) and (ii) products of a buried Archean oceanic crust (as metamorphosed fragments after Jacob et al. (1994); Schulze and Helmstaedt (1988) or (iii) as melt residues after Rollinson (1997); Shchipansky (2012)). In order to test these three hypotheses, the reconstructed whole-rock compositions in major and incompatible elements as well as $\delta^{18}O$ values have been compared to possible protolith compositions. In the case of a crustal-derived petrogenesis in the context of a hotter Archean Earth, the overall oceanic crustal protolith is assumed to be compositionally equivalent to picrite. Subsequently for comparison, a basaltic composition corresponding to modern day oceanic crust is assumed, as well as gabbro for low pressure, plagioclase-rich cumulate, with granophyre as the most evolved term of an evolving mafic magma (GEOROC compilation: http://georoc.mpch-mainz.gwdg.de/georoc/).

7.1. Metasomatized eclogites

Type I, metasomatized eclogites have textural aspects consistent with fluid interaction: numerous inclusions leading to a dusty appearance, indented crystal boundaries and subrounded to rounded grains. They include bimineralic, coesite- and kyanite-bearing eclogites, often associated with phlogopite, symplectite and interstitial rutile. All samples studied in this thesis are "true eclogites", with Na/(Na + Ca) > 0.20 clinopyroxene (Clark and Papike, 1968), characterized by high alkali-content (Na_2O in garnet and K_2O in omphacite) and a variable garnet and clinopyroxene end-members composition (from pyrope- to grossular- rich and diopside- to jadeite-rich respectively). The high potassium content in the coesite-bearing eclogites could be due to high equilibrium pressure, attested by the thermobarometric calculations.

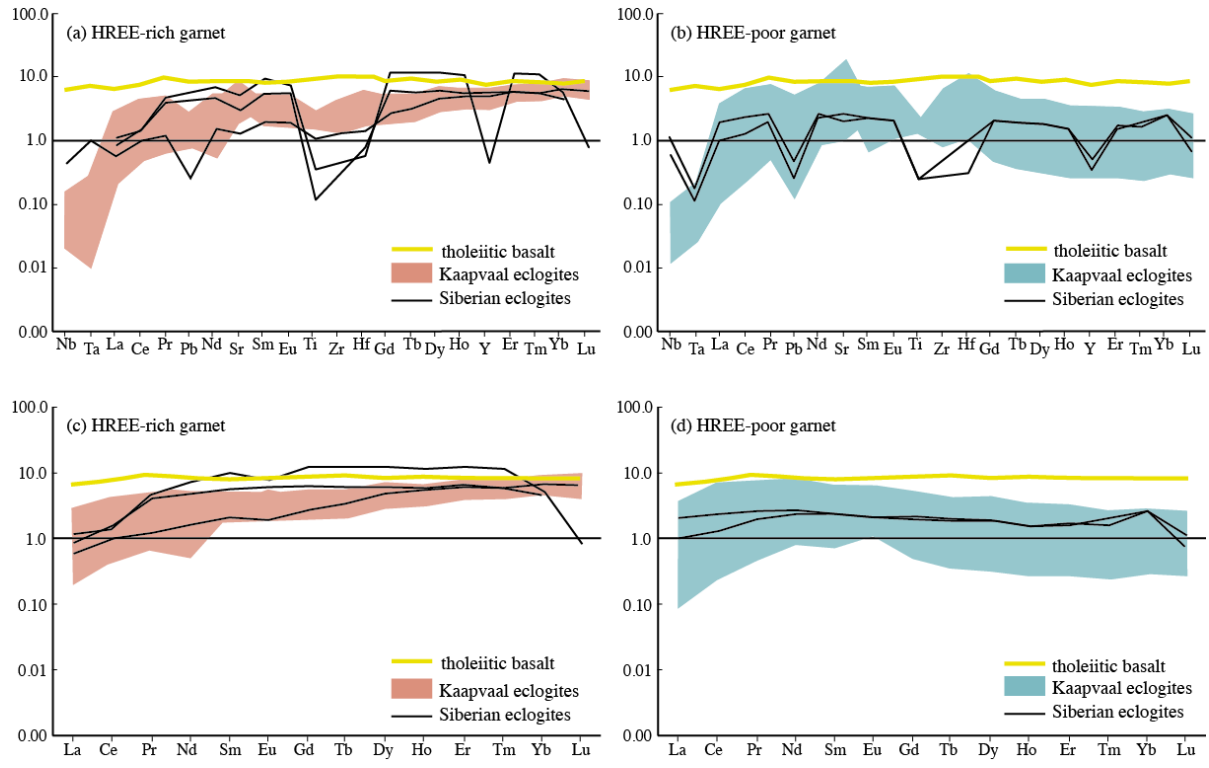

Figure VII—1. Reconstructed whole-rock extended trace (a—b) and REE patterns (c—d) in bimineralic Type I (metasomatized) eclogites from the Siberian and Kaapvaal cratons compared to tholeiitic basalt composition (GEOROC compilation) and the primitive mantle (McDonough and Sun, 1995).

Bimineralic (metasomatized) eclogites have narrow LREE and LILE concentrations, with variable HREE most pronounced in garnet (Figure V—1b). Reconstructed whole rock trace elements composition duplicates the two previously observed compositional groups characterized by HREE-rich (8—11 times pyrolite) and HREE-poor (1.5—3 times pyrolite) garnets (Figure VII—1).

The former shows typically flat REE spectra with slightly fractionated LREE, $(La/Sm)_N$ of 0.10—0.56 and $(Sm/Lu)_N$ of 0.31—0.83, similar to a tholeiitic basalt composition (Figure VII—1a, c). The latter group shows comparable LREE distribution, $(La/Sm)_N$ of 0.05—0.55 and more fractionated HREE, $(Sm/Lu)_N$ of 1.53—3.73, with significantly lower MREE-HREE concentrations (Figure VII—1b, d).Negative Ti, Zr, Hf and Y anomalies mark the reconstructed whole rock trace element distribution of the Siberian eclogites. There is a distinct correlation between the amount of HREE (Sm-Lu) and the FeO and CaO content in garnet (Figure VII—2). Eclogites containing garnets with low-CaO and high-FeO composition typically have higher bulk ΣHREE, whereas samples bearing Ca-rich, Fe-poor garnets have lower bulk ΣHREE composition. This is most probably due to preferential incorporation of HREE in the Fe-site in the garnet structure, controlled by similar ionic radii (Shannon and Prewitt, 1969).

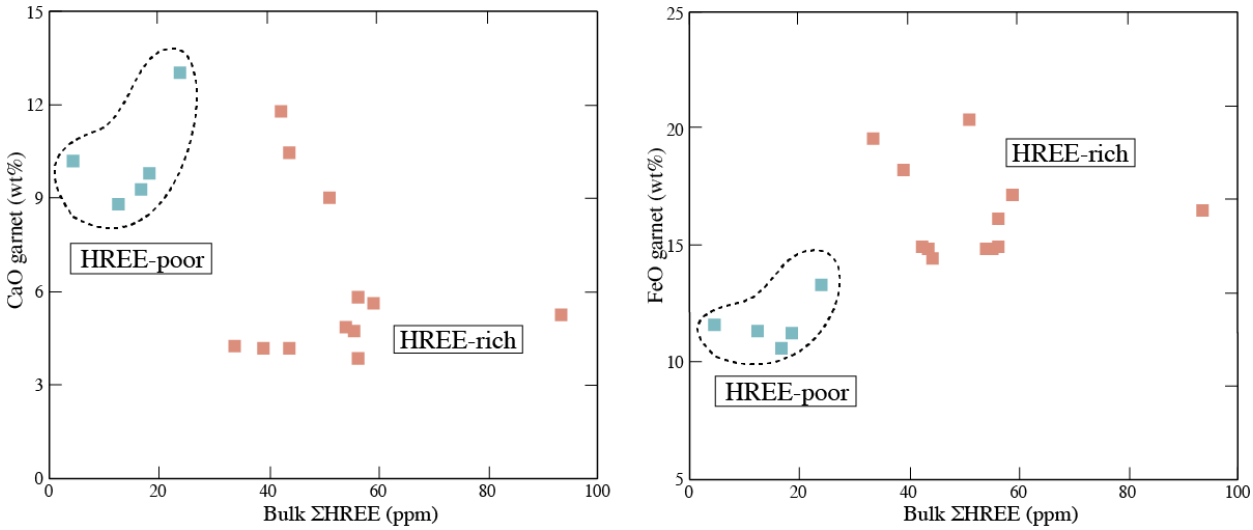

Figure VII—2. Reconstructed whole-rock ∑HREE (ppm) content as a function of CaO (wt%) and FeO (wt%) in garnet in Type I eclogites from the Kaapvaal and Siberian cratons. Eclogites containing HREE-rich garnets are marked with pink square symbols and HREE-poor eclogites are marked with pale blue symbols.

According to pressure-temperature equilibrium estimates (Chapter IV), ranging between 3.2 and 6.5 GPa and 800° and 1300°C, Type I eclogites from this study have been sampled throughout the eclogite formation underlying the cratonic keel. Nevertheless, the extensive carbonaceous/kimberlitic metasomatic imprint on the Type I eclogites, establishing the protolith composition and eclogite petrogenesis, as well as assessing their representativeness in the subcratonic lithospheric mantle.

7.2. Non-metasomatized eclogites

By contrast, non-metasomatized Type II eclogite xenoliths from this study are in apparent textural equilibrium, with translucent subhedral grains, showing no evidence of extensive metasomatism. Nevertheless, despite their overall pristine appearance, secondary minerals and veinlets often double grain boundaries. Non-metasomatized eclogites include bimineralic, kyanite- and corundum-bearing eclogites, often with needle-like rutile exsolutions. Most samples classified as Type II are “true eclogites”, except for bimineralic: RV349, RV355, RV360, RV377, RV465, RV488, RV509 and UV09-423, which contain clinopyroxene with Na/(Na+Ca) < 0.20.Non-metasomatized eclogites are characterized by garnet with Na_2O < 0.09 wt.% and K_2O in omphacite < 0.08 wt.% (Chapter 4).

7.2.1. Bimineralic eclogites

Two main compositional groups are individualized among non-metasomatized bimineralic eclogites (Chapter IV and Chapter V). Type IIA is characterized by Mg-rich garnets associated with Na,Al-poor clinopyroxene and overall LREE concentrations in clinopyroxene higher than the primitive mantle (1—30 times pyrolite), whereas Type IIB comprises Mg-poor garnets with adjacent Na,Al-rich omphacites and overall sub-primitive mantle LREE concentrations in clinopyroxene (>9 times less than pyrolite).

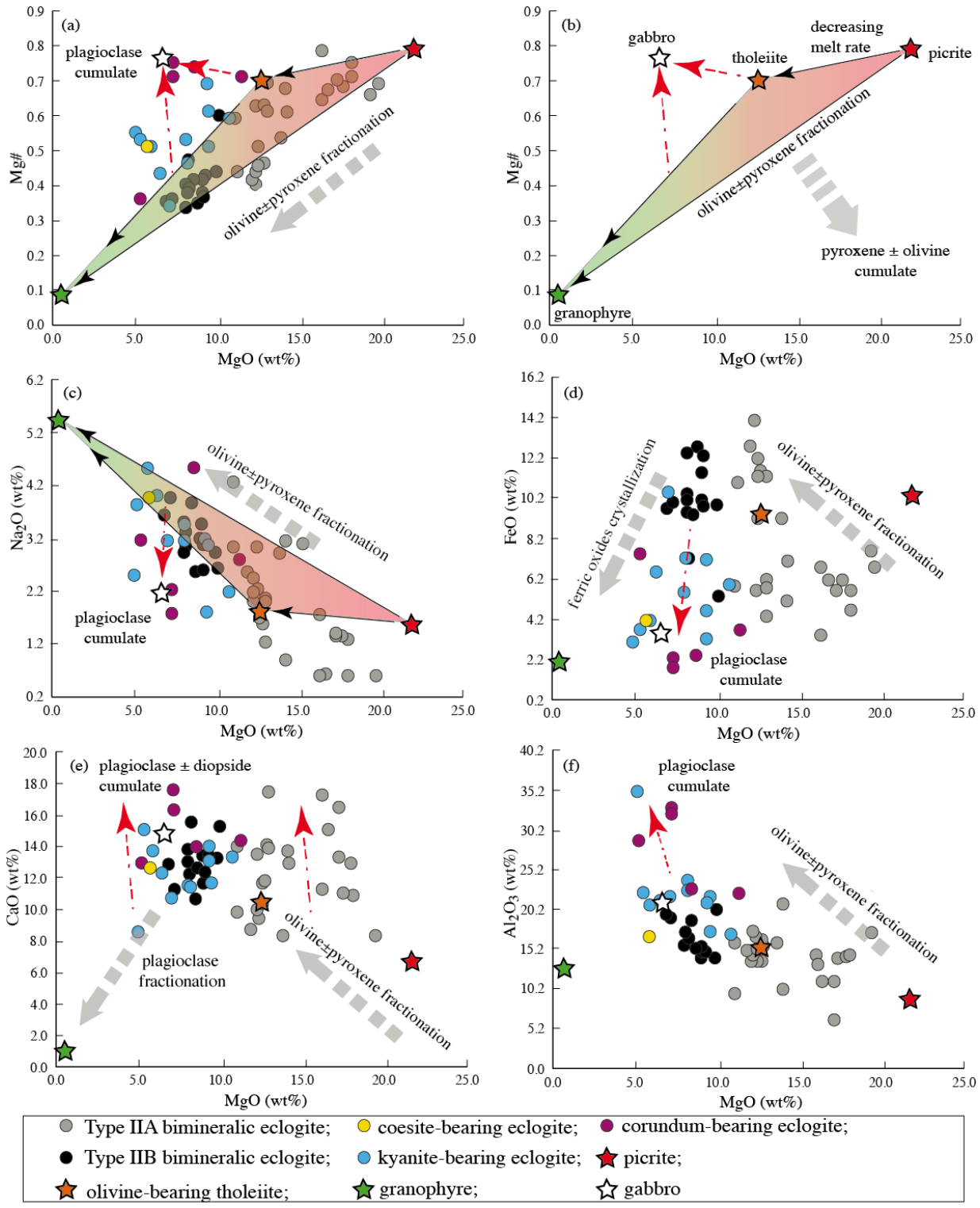

Figure VII—3. Relationships between major element in reconstructed whole rock compositions of bimineralic Type II (non-metasomatized) eclogites; coesite-, kyanite- and corundum-bearing eclogites from the Kaapvaal and Siberian cratons and magma series end-members (from GEOROC compilation). The ultramafic pole is represented by Icelandic picrite (red star) and the mafic pole by olivine-bearing tholeiite (orange star), whereas the felsic end-member is represented by granophyre (green star) and a plagioclase cumulate composition is represented by gabbro (white star symbol). Red arrows indicate plagioclase accumulation, thin grey arrows plagioclase or olivine ± pyroxene fractionation and thick grey arrows olivine ± pyroxene accumulation in the parental protolithic melt.

7.2.1.1. High-magnesium eclogites

Reconstructed whole rock Type IIA eclogite compositions have high MgO (11.15—19.71 wt.%) and broad variation from low to high, CaO (5.85—17.52 wt.%), Al_2O_3 (6.23—22.18 wt.%) and Na_2O (0.17—4.27 wt.%) content (Figure VII—3). The decreasing Mg# could be following olivine (±pyroxene) fractionation in an oceanic crustal protolith, translated also by the increasing FeO content (Aulbach and Viljoen, 2015). Furthermore, Type IIA eclogites systematically show an inverse correlation between Na_2O and Al_2O_3content with respect to MgO (Figure VII—3c, f), which can be equally accounted for by progressive fractional crystallization of olivine ± pyroxene in an evolving "basaltic" liquid (Aulbach et al., 2016). The high CaO content at relatively constant MgO is interpreted as evidence for a small fraction of plagioclase (± diopsidic clinopyroxene) accumulation, as main mineral phases preferentially incorporating Ca with respect to Mg (Beard et al., 1996).

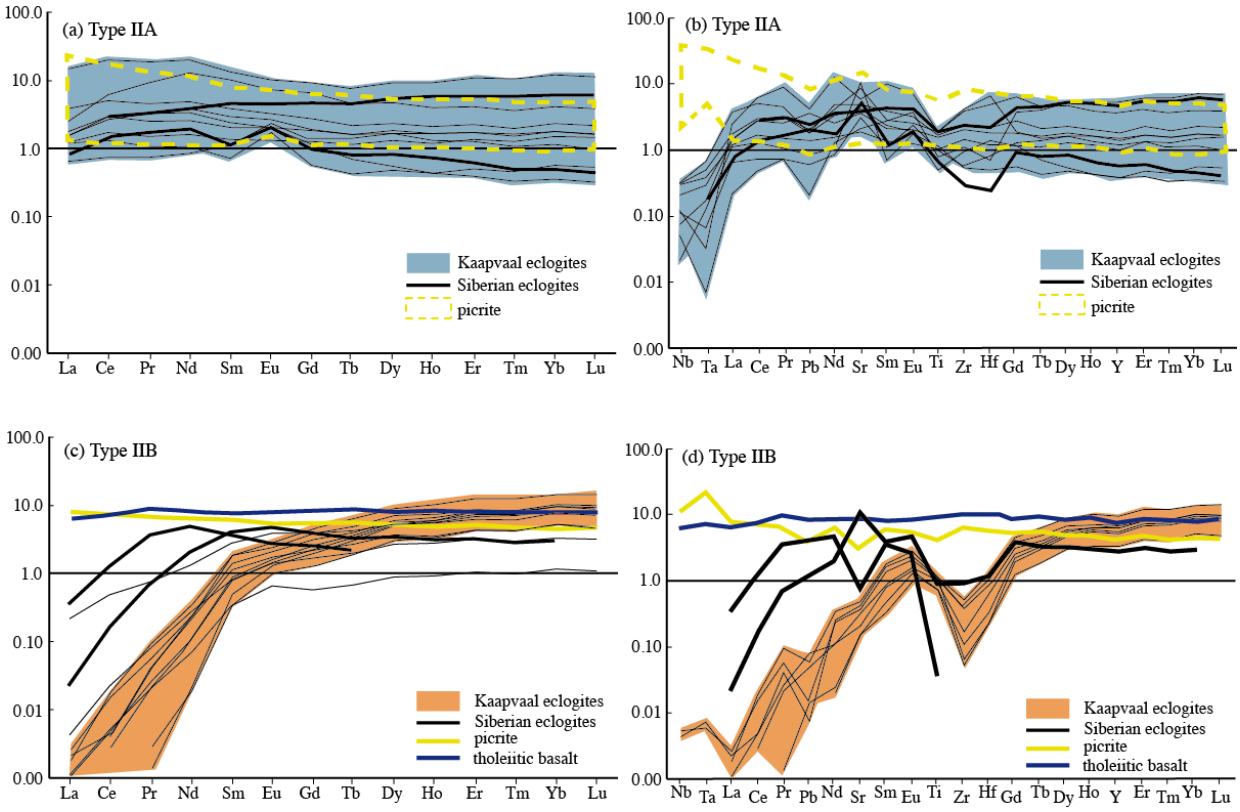

Figure VII—4. Reconstructed whole-rock REE (a, c) and extended trace elements patterns (b, d) in bimineralic Type II (non-metasomatized) eclogites from the Siberian and Kaapvaal cratons, compared to tholeiitic basalt and picrite compositions (GEOROC compilation) reported to the primitive mantle (McDonough and Sun, 1995)

REE and extended incompatible trace elements patterns of reconstructed whole-rock compositions (Figure VII—4 a-b), normalized to the primitive mantle (McDonough and Sun, 1995) are predominantly flat and higher than primitive mantle values (0.8—20 times

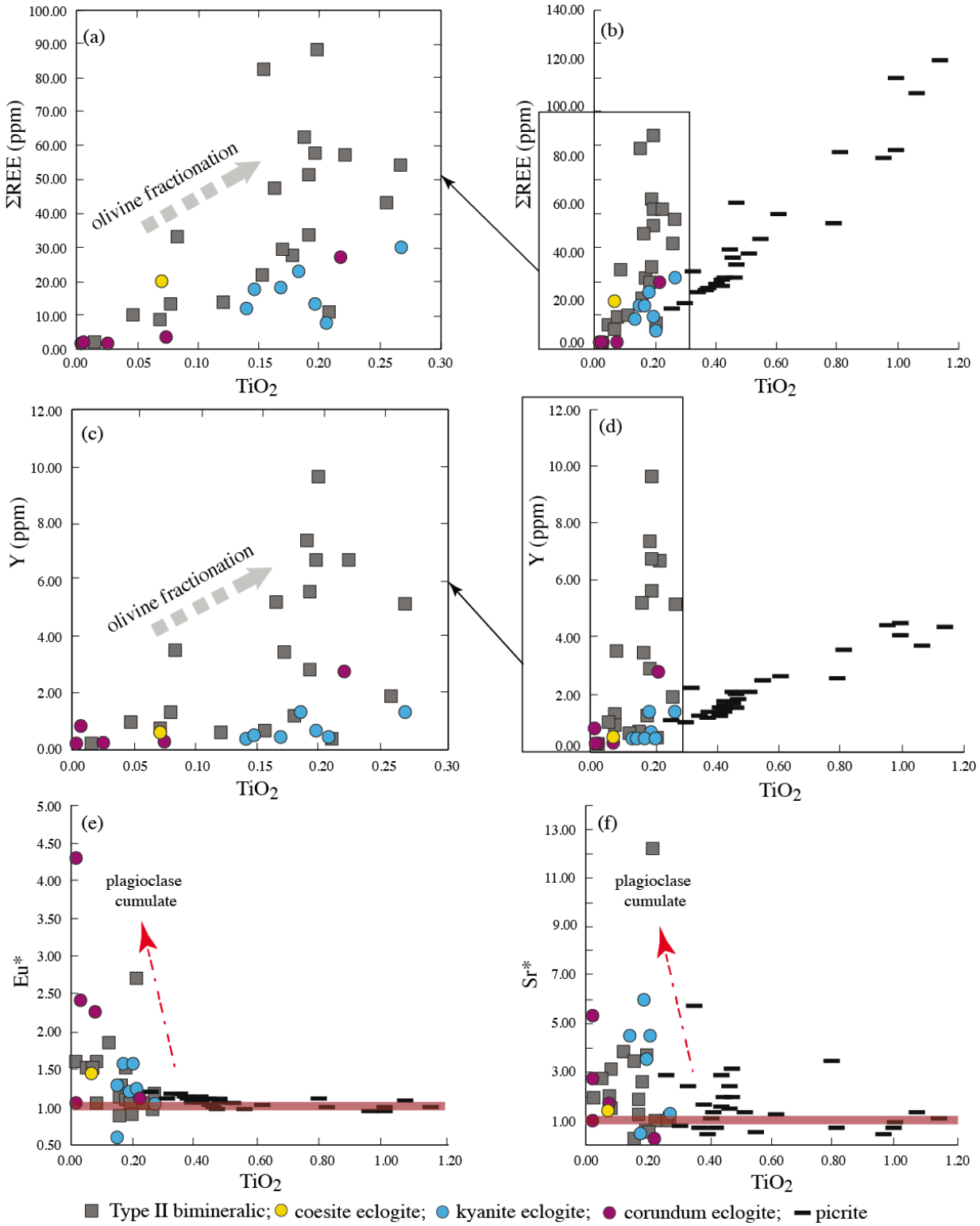

Figure VII—5. Relationships between ΣREE, Y, Eu* and Sr* and TiO2 content in reconstructed whole rock composition of Type II (non-metasomatized) bimineralic, coesite- , kyanite- and corundul-bearing eclogites. Eu* and Sr* values higher than 1 (marked by red line) correspond to positive anomalies.

pyrolite). These compositions are comparable to average picrite content (GEOROC compilation: http://georoc.mpch-mainz.gwdg.de/georoc/) with the exception of Nb, Ta and La. Moreover, Type IIA eclogites show positive correlation between ΣREE and Y concentrations, with respect to TiO_2 content (Figure VII—5 a-d). It is inferred that REE and HFSE enrichment is caused by olivine fractionation (Aulbach and Viljoen, 2015). Nevertheless, all Type IIA eclogites, except sample RV513 (Eu* ~0.99), register positive Eu* (1.06—2.71) and Sr* (1.11—12.21) anomalies, inversely correlated with TiO_2 content (Figure VII—5 e-f). This is in agreement with the previous inference, arguing for the presence of plagioclase in a protolith issued from an evolved picritic liquid for Type IIA eclogites (Aulbach et al., 2016; Jacob and Foley, 1999).

Recalculated bulk-rock $\delta^{18}O$ values vary between 3.0 ‰ and 7.5 ‰. It has been proposed that values lower than average mantle (+5.5±0.4 ‰; Mattey et al. (1994)) reflect high-temperature hydrothermal alteration of the protolith, and higher $\delta^{18}O$ values reflect low-temperature alteration. These would typically be constrained to the lower and upper part, respectively, of an oceanic crustal protolith (Beard et al., 1996; Eiler, 2001; Jacob et al., 1994; Schulze and Helmstaedt, 1988; Shervais et al., 1988). The possibility that Archean oceanic crust had different $\delta^{18}O$ values require oceanic crust with lower $\delta^{18}O$ values than those found in phanerozoic, non-altered ophiolites. The possibility that Archean oceanic crust had different $\delta^{18}O$ values than its more modern counterparts is supported by a recent study on Archean komatiites from Barberton, where based on $\delta^{18}O$ values of fresh olivine crystals it is inferred that mantle-derived magmas in the Archean had significantly lower $\delta^{18}O$ values than the normal mantle today (3.5±0.6 ‰ (Byerly et al., 2017)).

7.2.1.2. Low-Magnesium eclogites

Reconstructed bulk-rock compositions of Type IIB eclogites have low MgO (6.93—10.12 wt.%) and medium to high CaO (10.66—15.54 wt.%), Al_2O_3 (14.26—20.10 wt.%) and Na_2O

(2.58—3.96 wt.%) contents (Figure VII—3). Covering a lower and narrower range of values, MgO content shows a similar positive correlation with Mg# and inverse correlation with Al_2O_3 and Na_2O as for Type IIA eclogites (Figure VII—3a-c, f). It is inferred the progressive enrichment in Al_2O_3 and Na_2O along with MgO depletion is the result of olivine (±pyroxene) fractional crystallization in oceanic crust (Aulbach et al., 2016; Aulbach and Viljoen, 2015), precursory to the eclogite formation. Concurrently, iron oxide crystallization and plagioclase accumulation leads to progressive FeO decrease and CaO increase respectively (Figure VII—3d-e).

REE and extended incompatible elements patterns of reconstructed whole-rock compositions (Figure VII—4c-d), normalized to the primitive mantle (McDonough and Sun, 1995) have strongly fractionated LREE ($(La/Sm)_N$~0.001) and flat to slightly enriched MREE-HREE ($(Sm/Lu)_N$~0.07—0.19) predominantly higher than primitive mantle values (5—10 times pyrolite).

Siberian eclogites are more enriched in LREE ($(La/Sm)_N$ ~0.10) and have less fractionated MREE-HREE ($(Sm/Lu)_N$ ~0.76). The high HREE concentrations higher than primitive mantle, with flat to enriched distribution, are similar to average picrite or tholeiitic basalt compositions (GEOROC compilation: http://georoc.mpch-mainz.gwdg.de/georoc/). Strongly fractionated LREE may be the result of partial melt loss during burial. All samples show negative anomalies in Zr and Hf (Figure VII—4d), which are explained by the presence of rutile needle exsolutions throughout both garnet and clinopyroxene in pristine eclogites. Due to their small size and irregular distribution, they have not been quantified and therefore have not been taken into account for whole-rock reconstruction. Positive correlation between ΣREE and Y concentrations with respect to TiO_2 content (Figure VII—5 a-d) is interpreted as the result of olivine fractionation (Aulbach and Viljoen, 2015). By comparison to Type IIA eclogites, most Type IIB samples have positive Eu* (0.90—1.61), with variable Sr* (0.18—3.78) from negative to positive anomalies, inversely correlated with TiO_2 content (Figure VII—5 e-f). Major and trace

element compositions of Type IIB eclogites are consistent with a picritic to basaltic protolith (Aulbach et al., 2016; Beard et al., 1996; Jacob, 2004; Jacob and Foley, 1999; Taylor and Neal, 1989), which underwent small degrees of partial melting during eclogitization and burial(Schulze et al., 2000; Shervais et al., 1988; Viljoen et al., 2005).

Recalculated bulk-rock $\delta^{18}O$ values vary between 2.3 ‰ and 3.9 ‰. Bulk rock $\delta^{18}O$ values lower than average mantle (+5.5±0.4 ‰; Mattey et al. (1994)) have been attributed to isotopic fractionation during mafic-ultramafic rocks interaction with seawater at high temperatures (Eiler, 2001; Garlick et al., 1971). It is thus inferred that eclogites with low-$\delta^{18}O$ relative to mantle values are derived from an oceanic crustal protolith, subjected to high-temperature seawater alteration prior to burial (MacGregor and Manton, 1986; Riches et al., 2016; Shervais et al., 1988; Vogel and Garlick, 1970).

7.2.1.3. Atypical eclogites

A small set of eclogites, belonging to either of the two previously described groups (Type IIA, IIB) are atypical in terms of major elements content, in that they have reconstructed whole rock compositions significantly more depleted in incompatible elements (Figure VII—6). Type IIA samples (*i.e.* RV174 and RV347) have sub-primitive mantle, fractionated LREE-MREE compostions ($(La/Dy)_N$ 0.06—0.29) and enriched (1.17—1.67 times pyrolite), flat to slightly fractionated HREE ($(Dy/Lu)_N$ 0.69—0.84). Type IIB, RV451 sample, has strongly fractionated LREE ($(La/Sm)_N$ ~0.03) and MREE-HREE flat to slightly fractionated, similarly to the atypical Type IIA eclogites, however with concentrations roughly one order of magnitude lower (Figure VII—6). All samples have positive anomalies in Eu* (1.55—1.62) and Sr* (2.78—3.16) and negative Zr and Hf anomalies. Comparison with a websterite composition (GEOROC compilation: http://georoc.mpch-mainz.gwdg.de/georoc/) as possible protolith (Figure VII—6) cannot satisfactorily account for the high MREE-HREE contents of Type IIA or for the low

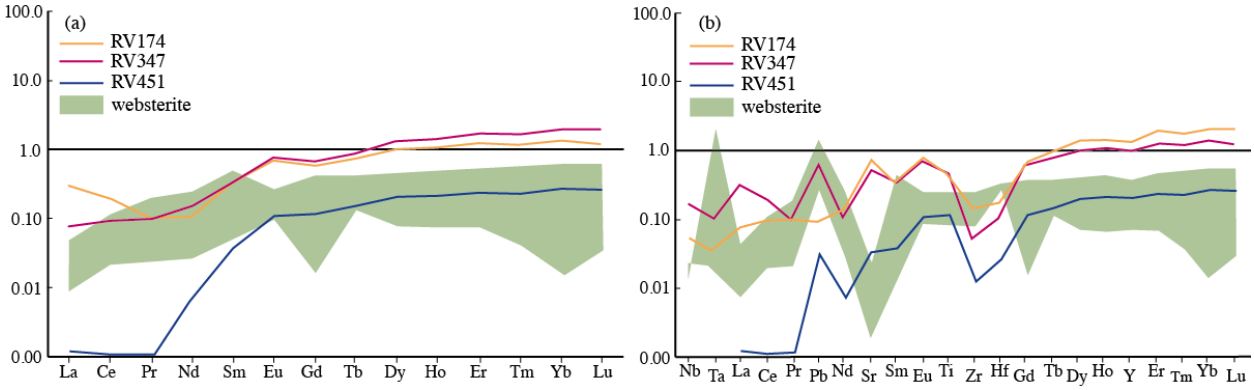

Figure VII—6. Reconstructed whole-rock REE (a) and extended trace elements patterns (b) in atypical bimineralic Type II eclogites from the Kaapvaal craton, compared to websterite composition (GEOROC compilation) reported to the primitive mantle (McDonough and Sun, 1995).

LREE composition of Type IIB atypical eclogites. It is inferred that these eclogitic samples are most likely derived from a basaltic/picritic protolith (Beard et al., 1996), containing a small fraction of plagioclase crystals, which underwent various degrees of partial melting during eclogitization. Pristine bimineralic eclogites typically contain fine rutile exsolutions, which is the main HFSE-bearing phase. Due to their small size, these are not taken into account in the recalculated whole rock and thus the Zr and Hf depletions are most probably mere artefacts of whole rock reconstruction.

Pressure-temperature estimates for Type IIA eclogites show equilibrium conditions at ~2.0—4.5 GPa and ~650—1000° C (based on Fe-Mg exchange; Chapter III) and for Type IIB ~4.5—6.5 GPa and ~1000—1300° C. It is unclear whether the two eclogitic types are derived from fragments of the same oceanic crust, buried at different depths, or whether they have been buried and integrated into the cratonic keel at different stages of craton accretion and crustal thickening.

7.2.2. Coesite-, kyanite-, corundum-bearing eclogites

Reconstructed bulk-rock compositions of coesite-, kyanite and corundum-bearing eclogites have low MgO (5.37—11.47 wt.%),with medium to high CaO (13.03—17.54 wt.%) and Al_2O_3 (22.62—33.34 wt.%) and medium to low Na_2O (1.78—4.56 wt.%) and FeO (1.84—7.43 wt.%)

contents progressively increasing and respectively decreasing from coesite- and kyanite- to corundum-bearing eclogites (Figure VII—3).Similarly, Mg# increases from coesite-, kyanite- (0.34—0.69) to corundum-bearing eclogites (0.71—0.75), except for sample RV344. The progressive enrichment in Mg#, CaO and Al_2O_3 (Figure VII—3a, e-f) and the gradual depletion in FeO and Na_2O (Figure VII—3 c-d) without a strong variation of MgO content, is characteristic for a protolith dominated by plagioclase accumulation possibly concurrent with iron oxides crystallization, without consuming the MgO (Schulze et al., 2000; Shervais et al., 1988; Shu et al., 2016).

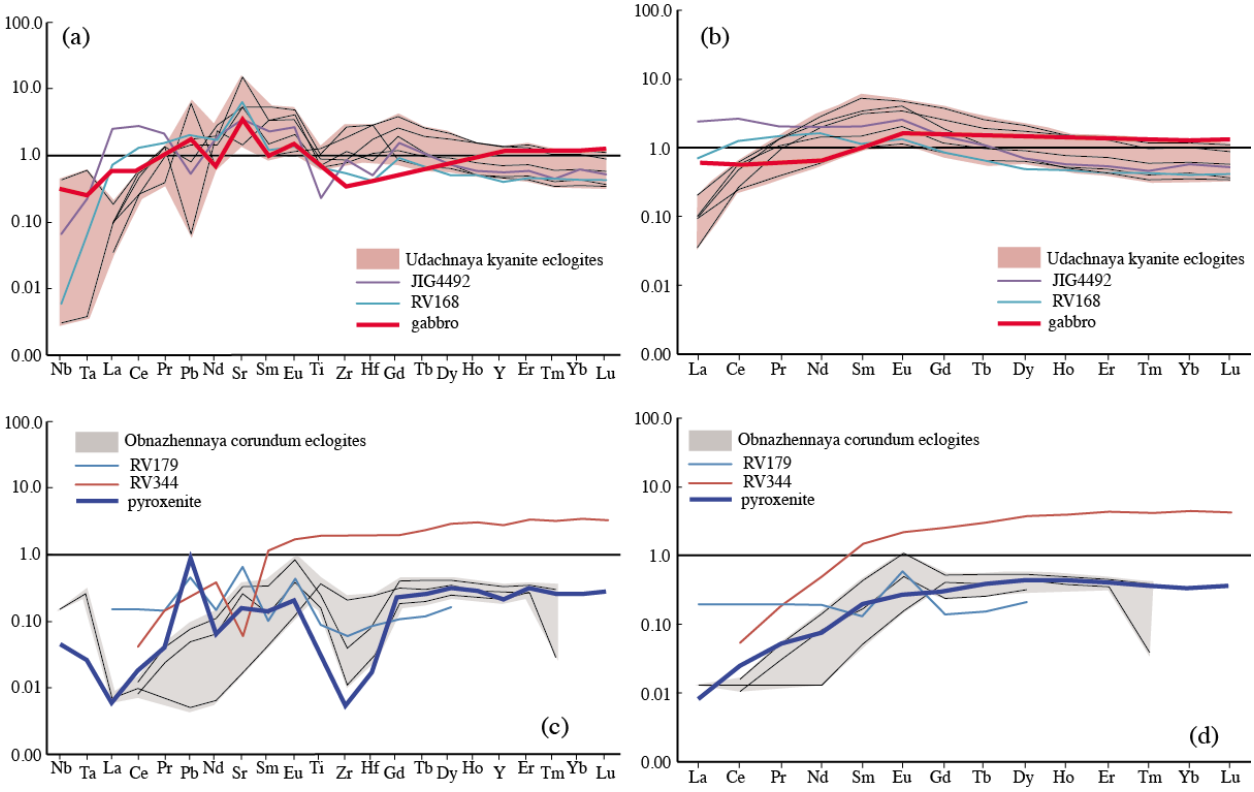

Figure VII—7. Reconstructed whole-rock REE and extended trace elements patterns in kyanite- (a—b) and corundum-bearing eclogites (c—d) from the Kaapvaal and Siberian cratons, compared to the composition of gabbro and pyroxenite respectively (GEOROC compilation) reported to the primitive mantle (McDonough and Sun, 1995).

Reconstructed bulk compositions of coesite- and kyanite-bearing eclogites (Figure VII—7a-b) have fractionated LREE ($(La/Sm)_N$ 0.01—0.09) and flat to slightly fractionated HREE ($(Sm/Lu)_N$ 2.62—9.67), with Roberts Victor eclogites more enriched in La and Ce($(La/Sm)_N$ 0.61—1.18).These incompatible elements concentrations are comparable to a gabbroic

composition (GEOROC compilation: http://georoc.mpch-mainz.gwdg.de/georoc/) and are marked by positive Eu* (1.05—1.59) and Sr* (1.37—6.10) anomalies except for sample UV09-536 (Sr* ~0.52)(Jacob, 2004).

Reconstructed whole-rock compositions of corundum-bearing eclogites (Figure VII—7 c-d) typically have incompatible elements concentrations lower than the primitive mantle. REE and extended incompatible elements patterns have fractionated LREE ($(La/Sm)_N$ ~0.25) and flat to slightly fractionated HREE ($(Sm/Lu)_N$ 0.35—1.47), except for sample RV179 which is LREE-enriched ($(La/Sm)_N$ ~1.52). All samples typically have positive anomalies in Eu* (1.08—4.32) and in Sr* (1.00—5.38) and negative in Zr and Hf. Sample RV344 is an exception, having MREE-HREE concentrations higher than the primitive mantle (~3 times pyrolite), negative Sr* anomaly (~0.09) and not being depleted in Zr and Hf. Recalculated bulk trace elements composition of corundum-bearing eclogites are similar to a pyroxenitic composition (GEOROC compilation: http://georoc.mpch-mainz.gwdg.de/georoc/), whereas sample RV344 is more likely derived from a basaltic protolith which has undergone partial melting (Shu et al., 2016).

Decreasing of TiO_2 with ΣREE and Y (Figure VII—5 a-d) is interpreted as evidence for plagioclase fractionation, whereas the increasing Eu* and Sr*, from negative to positive anomalies, inversely correlated with TiO_2 content (Figure VII—5 e-f), correspond to increasing plagioclase accumulation in the protolith (Aulbach et al., 2016). It is inferred that coesite-, kyanite-bearing eclogites are most likely derived from the gabbro section of a subducted oceanic crust, whereas corundum-bearing eclogites correspond to a pyroxene-dominated cumulate.

Recalculated bulk-rock $\delta^{18}O$ values are estimated at ~7.4 ‰ for the coesite-bearing eclogite, between 5.6 ‰ and 6.7 ‰ for the kyanite-bearing eclogites and are estimated to be between 1.4—4.8 ‰ (Roberts Victor kimberlite) and 5.5—5.9 ‰ (Obnazhennaya kimberlite) for corundum-bearing eclogites. Oxygen isotopic compositions vary from higher to lower than average mantle ($\delta^{18}O = +5.5\pm0.4$ ‰; Mattey et al. (1994)). It is inferred, that as in the case of bimineralic eclogites, coesite- and kyanite-bearing eclogites are derived from an oceanic crustal

protolith that has undergone isotopic exchange during low-temperature alteration in its upper part (Eiler, 2001; Garlick et al., 1971; Schulze et al., 2013). Corundum-bearing eclogites from Obnazhennaya have $\delta^{18}O$ values corresponding to average oceanic crust issued from the primary mantle (Gregory and Taylor, 1981), whereas corundum eclogites from Roberts Victor are interpreted as derived from an oceanic crustal protolith, subjected to high-temperature alteration prior to burial (Shervais et al., 1988; Vogel and Garlick, 1970).

Pressure-temperature estimates (based on Fe-Mg exchange; Chapter III) for coesite-bearing eclogites show equilibrium conditions at ~5.0—7.0 GPa and ~1010—1290°C, for kyanite-bearing at~4.1—5.6 GPa and ~960—1150°C and for corundum-bearing at ~4.0—6.5 GPa and ~950—1300°C. This is coherently sustained by textural arguments: coesite- and kyanite-bearing samples exhibit cloudy clinopyroxene, formed through inner structure breakdown due to fast decompression, as well as by the high-Na, Al- and CaEsk- content. Nevertheless, the connection with the bimineralic eclogites and their geometric relation is not yet clear.

7.3. Inherited oxygen isotope ratio vs. metasomatic imprint

As discussed above, eclogite xenoliths with $\delta^{18}O$ values below or above normal mantle range (+5.5±0.4 ‰; Mattey et al. (1994)) are interpreted as derived from a subducted oceanic crust which has undergone high- to low-temperature fluid interaction and it is inferred they inherit the $\delta^{18}O$ values of their protolith (Jacob, 2004; Jacob and Foley, 1999; Jacob et al., 1994; Jagoutz et al., 1984; MacGregor and Manton, 1986; Riches et al., 2016; Schulze et al., 2000; Viljoen et al., 2005). Nevertheless, an alternative theory has been suggested, which argues that oxygen isotope ratios may reflect secondary overprinting by carbonaceous, hydrous melts or fluids, preceding the kimberlite eruption (Gréau et al., 2011; Huang et al., 2012). In this model, the metasomatic change of $\delta^{18}O$ values in mantle eclogites is said to be supported by intra-sample variability garnet $\delta^{18}O$ value, correlation of $\delta^{18}O$ values with metasomatic tracers (i.e. LREE, HFSE, Sr,

etc.), and a decoupling between the interpretation of oxygen and magnesium isotope values (Huang et al., 2016). This is discussed further in the next section.

7.3.1. Metasomatic influence on oxygen isotope ratios

There are several issues concerning the metasomatic interpretation of oxygen isotope ratio in mantle eclogites that should be addressed. Firstly, if $\delta^{18}O$ values of phenocrysts found in carbonatites from the Dicker Willem complex in Namibia (+7 to +9 ‰) interpreted as primitive compositions (Reid and Cooper, 1992) are considered, an increase in the $\delta^{18}O$ values is to be expected, unable to account for $\delta^{18}O$ values lower than normal mantle found in eclogite xenoliths.

Secondly, intra-sample variability of garnet oxygen isotope ratio and a positive correlation between $\delta^{18}O$ values and metasomatic indices such as Hf and Zr in garnet have been observed on a small set of samples, predominantly showing various degrees of kimberlite-derived metasomatism (Gréau et al., 2011; Huang et al., 2014).

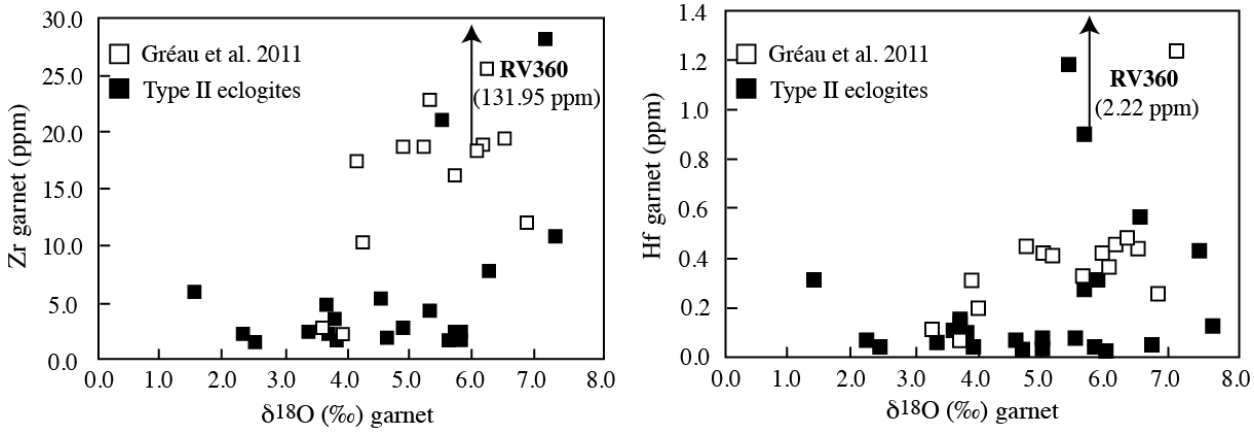

Figure VII—8. $\delta^{18}O$ in garnet vs. Zr and Hf in garnet as trace elements commonly used as indices for kimberlite-derived metasomatism in eclogite xenoliths. Literature data from Gréau et al. (2011) is marked with white solid square symbols and data from non-metasomatized Type II eclogites from this study are marked with black solid square symbols. One sample, RV360 registers values significantly higher in both Zr and Hf with respect to the majority of the dataset and is indicated with an arrow. No positive trend can be seen between the metasomatic tracers and $\delta^{18}O$ values in garnet and moreover the Type II compositions are markedly different to the dataset by Gréau et al. (2011).

No such variability and no correlation is observed in a larger set of non-metasomatized eclogites, showing both lower and higher $\delta^{18}O$ values with respect to normal mantle (Figure VII—8).

According to a recent study coupling oxygen and magnesium isotope analyses in mantle eclogites (Huang et al., 2016), the variable $\delta^{26}Mg$ (-1.09 ‰ to -0.17 ‰) with respect to homogeneous $\delta^{18}O$ values (2.34—2.91 ‰) in three pristine xenoliths is interpreted as evidence for a metasomatic change of oxygen isotope ratios. Furthermore, this implies the $\delta^{26}Mg$ and $\delta^{18}O$ values could not be inherited from an altered oceanic crustal protolith. However, the presumption that hydrothermal alteration processes could not account for the measured $\delta^{26}Mg$ values (-1.09 ‰ to -0.37 ‰) is contradicted by previous studies on both continental (Li et al., 2011; Wang et al., 2014) and cratonic eclogites (Wang et al., 2012). It is argued by these authors that $\delta^{26}Mg$ values in eclogites can be inherited from an oceanic crust which underwent hydrothermal alteration or silicate –carbonate isotopic exchange during subduction (-1.38 ‰ to +0.17 ‰ (Wang et al., 2015)).

Furthermore, attributing low-$\delta^{18}O$ values to mantle metasomatism seems highly unlikely. Oxygen is the most abundant element in mantle rock forming minerals (about 45% by weight). In this case, even a small (*i.e.* <1 ‰) change in the oxygen isotopic ratio of mantle eclogites, with respect to the normal mantle values (+5.5±0.4 ‰; Mattey et al. (1994)) would require substantial amounts of fluids with unrealistically low $\delta^{18}O$ values (Ionov et al., 1994; Riches et al., 2016). Mass balance calculations for a volumetrically significant reactive agent that could change $\delta^{18}O$ values in eclogites without equilibrating with the surrounding mantle, shows that a 1 ‰ change requires a maintained continuous flow from the source and across the upper mantle, of a an extreme-$\delta^{18}O$ fluid, at a ≥ 2:5 fluid-rock ratio (Riches et al., 2016). A metasomatic agent with extremely low $\delta^{18}O$ values, overprinting the lower part of the cratonic root, without re-equilibrating with the surrounding peridotitic mantle seems unlikely. Therefore the simplest explanation is that oxygen isotope ratios in mantle eclogites are inherited from their protolith.

Furthermore, six eclogite xenoliths from Roberts Victor mine (Radu, 2014), were previously investigated with the ^{147}Sm-^{143}Nd and ^{176}Lu-^{176}Hf isotope systematics, values are given in Table 10. Ages were determined using a two-point isochrone (Shu et al., 2014) and the Isoplot software (Figure VII—9). The Type I, metasomatized eclogites yield ages of 122—124 Ma with Sm-Nd and ~110 Ma with Lu-Hf and calculated ε_{Nd} of [-10.2; -6.7] ($\varepsilon_{Nd}=^{143}Nd/^{144}Nd_{initiak}/^{143}Nd/^{144}Nd_{CHUR}-1)*10^4$) and ε_{Hf} of [-8.9] ($\varepsilon_{Hf}=^{176}Hf/^{177}Hf_{initial}/^{176}Hf/^{177}Hf_{CHUR}-1)*10^4$), chondrite values from (Bouvier et al., 2008). These are similar to the age and composition of the host kimberlite estimated at 128 Ma (Smith et al., 1985), [-11,9 ; -11,5] ε_{Nd} and [-14,7;-14,5] ε_{Hf} (Nowell et al., 2004). This is in agreement with the hypothesis of carbonate/kimberlitic metasomatic fluids, reopening the isotopic systems and erasing the original chemical signature in some eclogite xenoliths. The reconstructed whole-rock $\delta^{18}O$ value in one of the Type I samples (RV226) is of 6.1 ‰ and could reflect either the initial ratio of the protolith or a changed composition due to localized metasomatism.

Sample	Type	Sm-Nd Age (Ma)	2σ	Lu-Hf Age (Ma)	2σ	εNd	2σ	εHf	2σ	Bulk $\delta^{18}O$ (‰)
RV179	Cor-bearing	1544	26	-	-	8.40	0.4	-	-	4.84
RV226	Type I	122	7	110	3	-6.71	0.3	-16.01	0.21	6.10
RV233	Type II	886	6	1505	7	120.62	0.4	107.06	0.21	3.60
RV344	Cor-bearing	2204	19	2462	12	33.26	1.0	9.90	0.22	1.37
RV356	Type II	898	6	1698	9	6.16	0.2	15.28	0.21	4.66
RV371	Type I	124	7	-	-	-10.17	0.2	-	-	-

Table 10. Age estimates for eclogites from Roberts Victor mine (*unpublished data*) and reconstructed bulk oxygen isotope ratios.

Type II, non-metasomatized eclogites yield 886—898 Ma and 1.5—1.7 Ga with Sm-Nd and Lu-Hf respectively, [6.2; 120.6] ε_{Nd} and [15.3; 107.1] ε_{Hf}. Although the difference between the two age ranges is significant, this may be due to different closing temperature of the two isotope systematics. The Lu-Hf-determined age is therefore believed to be more accurate, however it must be noted that both ages are much older than of the kimberlite eruption. Any metasomatic agent would have changed the ε values, however these are closely related to the depleted mantle evolution line. It is therefore inferred the eclogite composition most likely reflects the

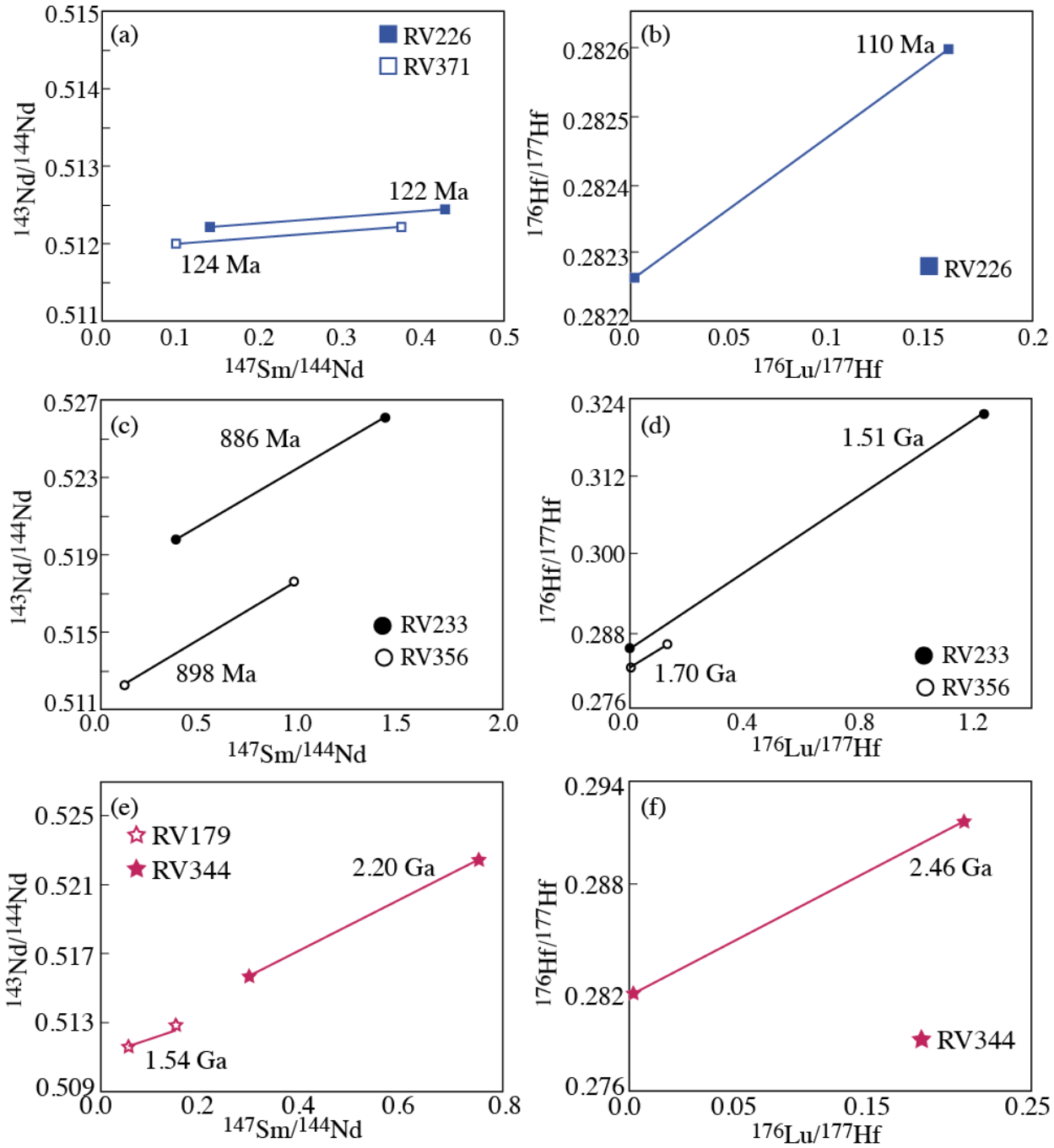

Figure VII—9. Sm-Nd and Lu-Hf ages obtiained by the two-point isochrone method between garnet and clinopyroxene in bimineralic (a-b) Type I, metasomatized; (c-d) Type II, non-metasomatized; and corundum-bearing (e-f) eclogites from Roberts Victor mine.

composition of their protolith. Furthermore, the calculated ages are interpreted as a minimum, corresponding to the last thermal event during or after the eclogitization. The two corundum-bearing eclogites yield older ages (Figure VII—9), of 1.5—2.2 Ga by Sm-Nd and of ~2.4 Ga by Lu-Hf and [8.4; 33.3] ε_{Nd} and [9.9] ε_{Hf}. It is thus inferred that similar to the non-metasomatized bimineralic eclogites, the corundum-bearing eclogites reflect the composition of their protolith.

Furthermore, all calculated ages, significantly older than the kimberlite eruption, support the hypothesis that the reconstructed whole-rock $\delta^{18}O$ values in the Type II bimineralic eclogites (3.6 and 4.7 ‰) and in the corundum-bearing eclogites (1.4 and 4.8 ‰) are inherited from the protolith and not from metasomatic interaction, in agreement with Jacob (2004); Schulze et al. (2000); Viljoen et al. (2005).

7.3.2. Influence of hydrothermal alteration on oxygen isotope ratios

Oxygen isotope ratios in mafic rocks may vary with respect to normal mantle values (+5.5±0.4 ‰; Mattey et al. (1994)) under the effect of fluid-rock interaction at variable temperature (Chapter VI). Consequently, higher than mantle $\delta^{18}O$ values would be caused by low-temperature alteration or fluid exchange from the upper part of an oceanic crust (Bindeman, 2008; Eiler, 2001) and lower $\delta^{18}O$ values by high temperature hydrothermal alteration of the lower section of the crust (McCulloch et al., 1981).

The oxygen isotope ratios measured in the eclogitic garnets from Roberts Victor mine vary broadly from 1.1 ‰ to 7.4 ‰. This partly overlaps previously documented $\delta^{18}O$ values in eclogite suites worldwide (Figure VII—10) and includes values much lower than any previous estimate. Bimineralic eclogites have “typical” $\delta^{18}O$ values according to the majority of the eclogites previously documented (Figure VII—11a-b). Nevertheless, most of the oxygen isotope data on mantle eclogite is based on xenoliths that underwent extensive metasomatism. Conversely, pristine eclogites have been significantly less documented due to their low abundance. Unlike Type I eclogites that typically have mantle or higher than mantle $\delta^{18}O$ values, pristine Type II eclogites have lower values (with ~77% of $\delta^{18}O$ garnet <5 ‰).

The high-Mg, Type IIA eclogites, characterized by lower equilibrium temperatures (Figure VI—5) have a wide range in $\delta^{18}O$ values, from lower to higher than the normal mantle, whereas Type IIB eclogites, with a low-Mg content and high equilibrium temperatures have strictly lower $\delta^{18}O$ values (Figure VII—11d).

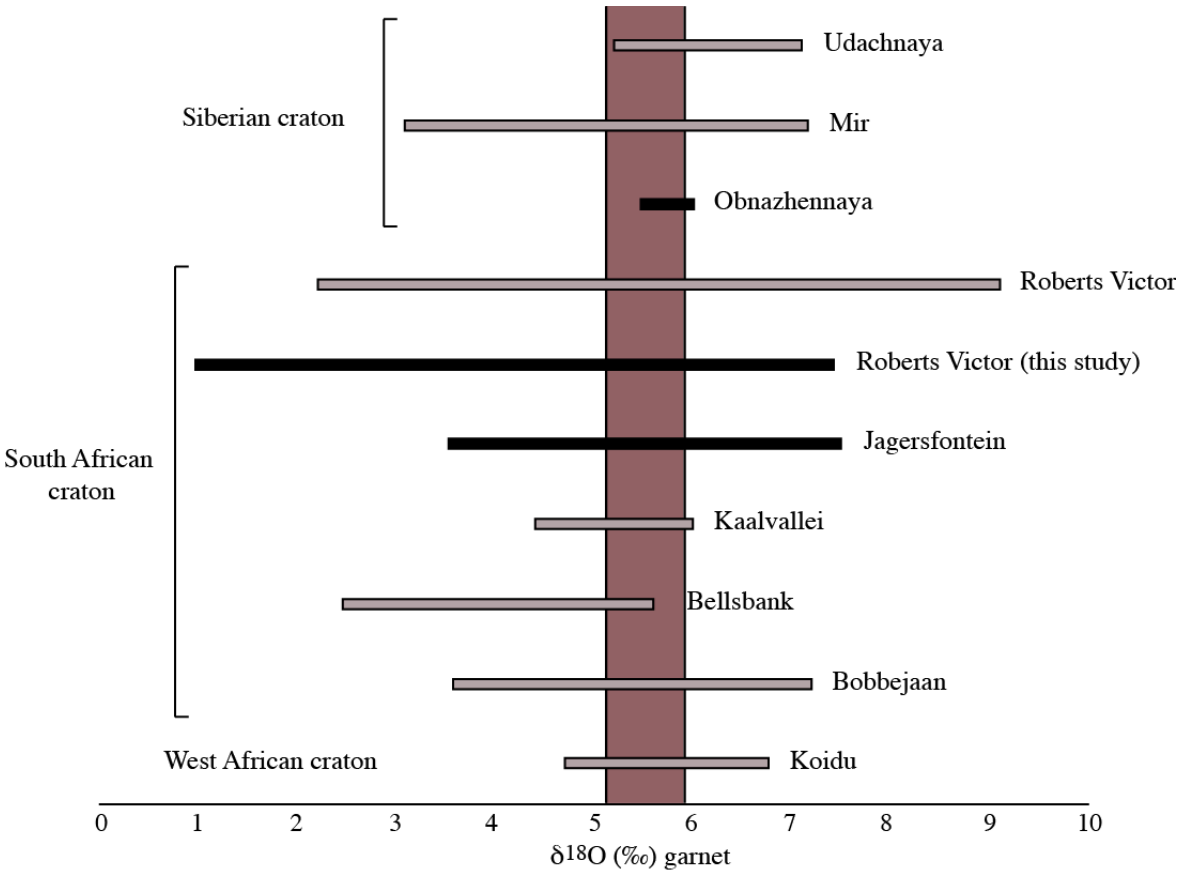

Figure VII—10. Oxygen isotope compositions of eclogite garnets from Obnazhennaya, Jagersfontein and Roberts Victor mines (black bars) analysed in this study and literature data from worldwide eclogite suites (pink bars): Udachnaya (Jacob et al. 1994; Shatsky et al., 2016); Mir (Beard et al., 1996), Roberts Victor (Garlick, 1971; Jagoutz et al., 1984; Ongley et al., 1987; MacGregor & Manton, 1986; Caporuscio, 1990; Schulze et al., 2000; Gréau et al., 2011; Huang et al., 2014, 2016; Riches et al., 2016); Kaalvallei (Viljoen et al., 2005); Bellsbank (Neal et al., 1990; Shervais et al., 1988); Bobbejaan (Caporuscio, 1990); Koidu (Barth et al. , 2001, 2002).

As previously discussed (Chapter 7.3.1), these values are most likely inherited from their protolith and translate the complete range of $\delta^{18}O$ values recorded across an oceanic crust profile (Chapter 6). Taking into account that low- $\delta^{18}O$ values are typically restricted to the lower segment of the oceanic crust and high- $\delta^{18}O$ values to the upper section, it is unclear whether the two eclogite Types (*i.e.* IIA; IIB) are derived from different lithologies of the same oceanic crust, buried at different depths (*i.e.*~150 km; ~210 km).

Coesite- and kyanite-bearing eclogites have $\delta^{18}O$ values within or above the normal mantle range, similar to Type IIA eclogites, whereas the corundum-bearing samples from Roberts

Victor have lower than mantle oxygen isotope ratio. Sample RV344, registers $\delta^{18}O$ values in garnet of 1.1 ‰ in average (n=4, 1σ=0.2), ~1 ‰ lower than any previously recorded sample.

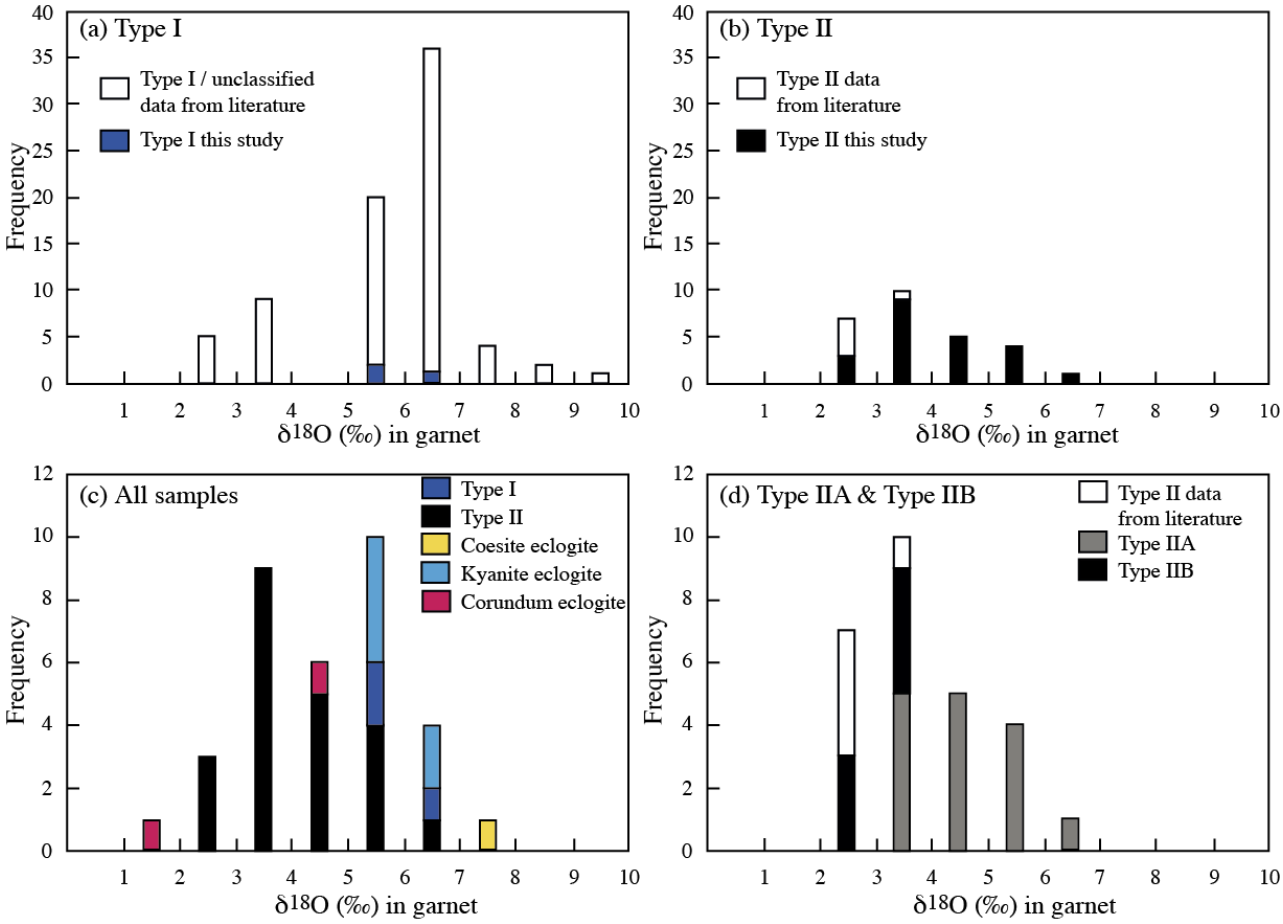

Figure VII—11. Histograms showing oxygen isotope compositions of garnets from Roberts Victor mine from this study, compared to literature data from: Garlick (1971), Jagoutz et al. (1984), MacGregor & Manton (1986), Ongley et al. (1987) Caporuscio (1990), Schulze et al. (2000), Gréau et al. (2011), Huang et al. (2014, 2016), Riches et al. (2016), in (a) Type I (metasomatized) eclogites; (b) in Type II (non-metasomatized) eclogites; (c) in Type II (black), Type I eclogites (dark blue), coesite- (yellow), kyanite- (light blue) and corundum-bearing (violet) eclogite xenoliths; (d) in bimineralic Type IIA (high-Mg) and Type IIB (low-Mg) eclogites.

Phanerozoic conditions for seawater-rock interactions appear unable to account for such low $\delta^{18}O$ values however, in the context of a hotter Earth during the Archean, such values may have been attained through a more extreme hydrothermal regime or a different $\delta^{18}O$ of seawater. A recent study on Archean komatiites from Barberton, gave olivine $\delta^{18}O$ values of 3.5±0.6 ‰ (Byerly et al., 2017). This supports the idea of lower $\delta^{18}O$ values in mantle-derived magmas at that time.

7.4. Mantle cumulate vs. crustal origin

Although a petrogenetic model for mantle eclogites as high-pressure cumulates has been previously suggested (Caporuscio and Smyth, 1990; Hatton, 1978; Hatton and Gurney, 1977; MacGregor and Carter, 1970; O'Hara and Yoder, 1967) these models have been extensively debated, and cannot account for most eclogite compositions. Firstly, as previously discussed, reconstructed whole rock compositions of bimineralic as well as coesite-, kyanite- and corundum-bearing eclogites typically show positive Sr* and Eu* anomalies, most commonly interpreted as evidence for plagioclase accumulation during low-pressure magmatic fractionation. Although it has been suggested that positive Eu anomalies can be produced by changes of redox conditions during metasomatism, this is most commonly associated with intergranular heterogeneity (Griffin and O'Reilly, 2007).All studied samples have homogeneous compositions and show no traces suggesting extensive metasomatism. Moreover, samples exhibiting positive Eu* anomalies systematically correlate with positive Sr* anomalies and increasing CaO, Al_2O_3, and decreasing MgO and FeO compositions. This is coherent with the hypothesis of a plagioclase-rich protolith. Secondly, a more widely accepted and robust argument against a mantle origin for eclogites xenoliths is the wide variability in $\delta^{18}O$ values which cannot be accounted for by fractionation under high-temperature mantle conditions (Shervais et al., 1988). Most recalculated whole rock compositions of non-metasomatized eclogites have values lower than the average mantle (+5.5±0.4 ‰; Mattey et al. (1994)), interpreted as evidence for a “basaltic” protolith which has undergone high-temperature alteration (Shervais et al., 1988). Similarly, some pristine eclogites have higher $\delta^{18}O$ values relative to the mantle, interpreted as low-temperature alteration in the upper part of an oceanic crust, precursory to eclogite formation (Garlick et al., 1971). Although more recently some authors proposed redox-related kinetic fractionation could produce similar $\delta^{18}O$ values, these studies are based on correlations with $\delta^{13}C$ in diamond-bearing eclogites (Griffin and O'Reilly, 2007), which most likely underwent a different history than “barren” eclogites. It is possibly

misleading to extrapolate processes involved in diamond-bearing eclogite formation to the petrogenesis of all mantle eclogites. This is further supported by a $\delta^{13}C$ and $\delta^{18}O$ study of coesite and garnet inclusions in eclogitic diamonds which register anomalously low $\delta^{13}C$ coupled with high $\delta^{18}O$, interpreted as derived from altered seafloor basalt mixed with marine biogenic carbon (Schulze et al., 2013). Isotopic fractionation at mantle conditions could not account for such $\delta^{13}C$ and $\delta^{18}O$ coupled values.

Therefore, based on reconstructed whole rock compositions in major and trace elements as well as $\delta^{18}O$ compositions, it is suggested that mantle eclogites are most likely derived from a subducted oceanic crust.

7.5. Crustal relic vs. crustal residue

Two concurrent models compete for crustal-derived petrogenesis of mantle eclogites (Chapter I): subducted relics of an Archean oceanic crust (Aulbach et al., 2016; Beard et al., 1996; Helmstaedt and Doig, 1975; Jacob, 2004; Jacob and Foley, 1999; Jacob et al., 1994; MacGregor and Manton, 1986; Riches et al., 2016; Schulze and Helmstaedt, 1988; Schulze et al., 2000; Shervais et al., 1988; Shu et al., 2016; Viljoen et al., 2005) or eclogite restite complementary to Archean crust formation (Ireland et al., 1994; Snyder et al., 1993).

The model for mantle eclogites as melt residue requires a common basaltic source for Archean granitoid melts and eclogite xenoliths (Rollinson, 1997). This is based on the complementary compositions of low-Mg eclogites from Koidu kimberlite and Archean TTG with respect to depleted mantle or Bulk Silicate Earth compositions (McDonough, 1991).Similar results have been described for eclogites from the Belomorian Belt of the Baltic Shield (Shchipansky, 2012), compositionally comparable to Koidu eclogites. On this basis, petrogenetic processes yielding Archean eclogites and TTG melts have been extrapolated to the formation of early continental crust and subcontinental lithospheric mantle.

Reconstructed whole rock compositions for eclogites from the four kimberlite pipes from the Kaapvaal (Roberts Victor, Jagersfontein) and Siberian (Obnazhennaya, Udachnaya) cratons do not show the previously detailed complementary compositions to TTG melts (Figure VII—12).

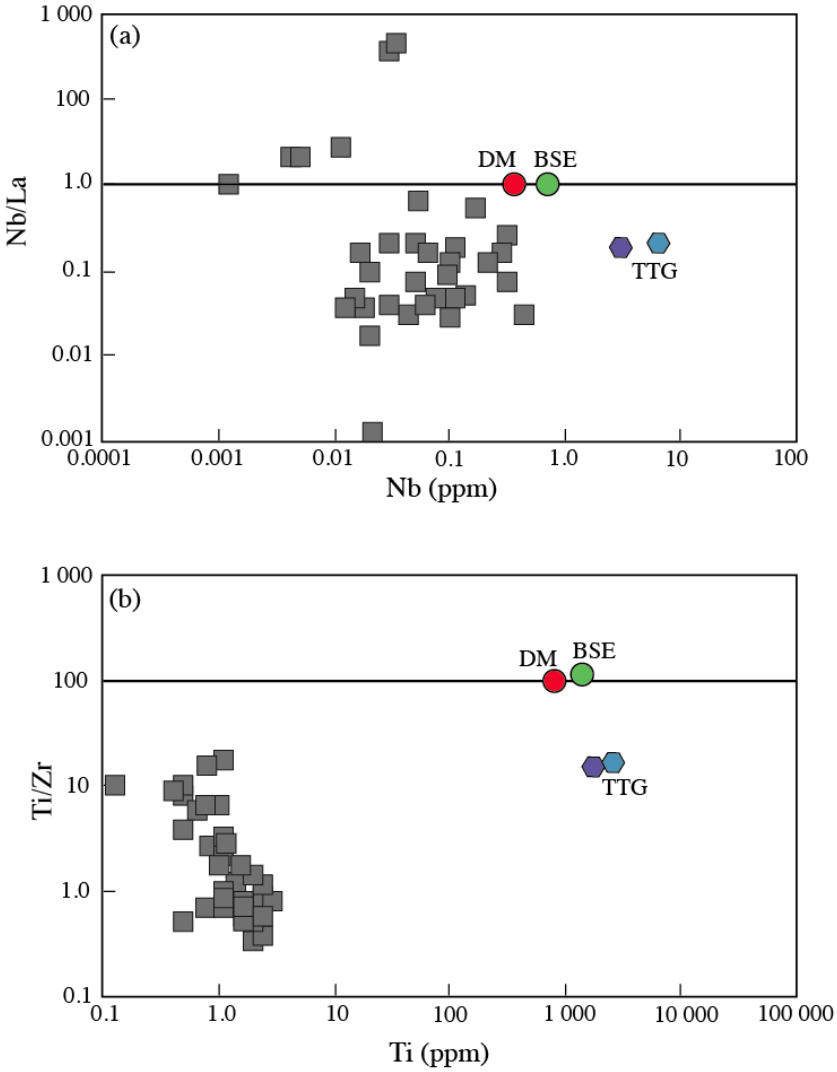

Figure VII—12. Trace element diagrams showing Nb/La versus Nb (a) and Ti/Zr versus Ti (b) in Type II (non-metasomatzed) eclogites from the Kaapvaal and Siberian cratons with respected to Depleted Mantle (DM), Bulk Silicate Earth (BSE) from McDonough (1991) and High to Medium—Low Pressure TTGs from Martin et al. (2014).

All samples show significantly lower Ti (ppm) contents and there is no marked distinction between low- and high-Mg eclogites. Nevertheless, it must be noted that non-metasomatized eclogites typically exhibit needle-like, rutile exsolutions, which have not been quantified in whole rock reconstructed compositions. Considering rutile is the main Ti, Zr and Nb-bearing mineral, this may lead to significant underestimation in the recalculated bulk rock. It is, nonetheless, impossible to quantify rutile contribution to the whole rock estimates for a better compositional constraint.

Moreover, this model cannot account for the general major and trace elements compositions previously described for the studied eclogite suites. It has been shown above, that reconstructed whole rock compositions of type IIA eclogites indicate a plagioclase-bearing protolith derived from an evolving “basaltic” liquid at low pressures, whereas type IIB eclogites seem to be derived from a similar protolith that has undergone partial melting resulting into LREE depletion. Moreover, previous studies arguing for a restitic origin are focused on a very narrow compositional range of eclogite xenoliths, whereas mantle eclogites can register a high variability in composition and textures among samples from the same locality. It is thus inferred that the petrogenetic model for mantle eclogite as subducted relics of an Archean oceanic crust is a more likely hypothesis.

CHAPTER VIII.

WATER IN NOMINALLY ANHYDROUS MINERALS

CHAPTER VIII. WATER IN NOMINALLY ANHYDROUS MINERALS

Throughout Earth's history, water has been of major importance, from influencing the planet's early evolution to the present day tectonics and up to the development of life (Rossman, 1996). Nevertheless, most of the Earth's water is found at trace levels in nominally anhydrous rock forming minerals (NAMs) in the crust and mantle (Peslier et al., 2017). The water solubility in mantle minerals with increasing pressure and temperature is believed to be responsible for localized melts in the asthenosphere (Mierdel et al., 2007) and play an important role on global plate tectonics (Figure VIII —1) (Demouchy and Bolfan-Casanova, 2016; Peslier, 2010).

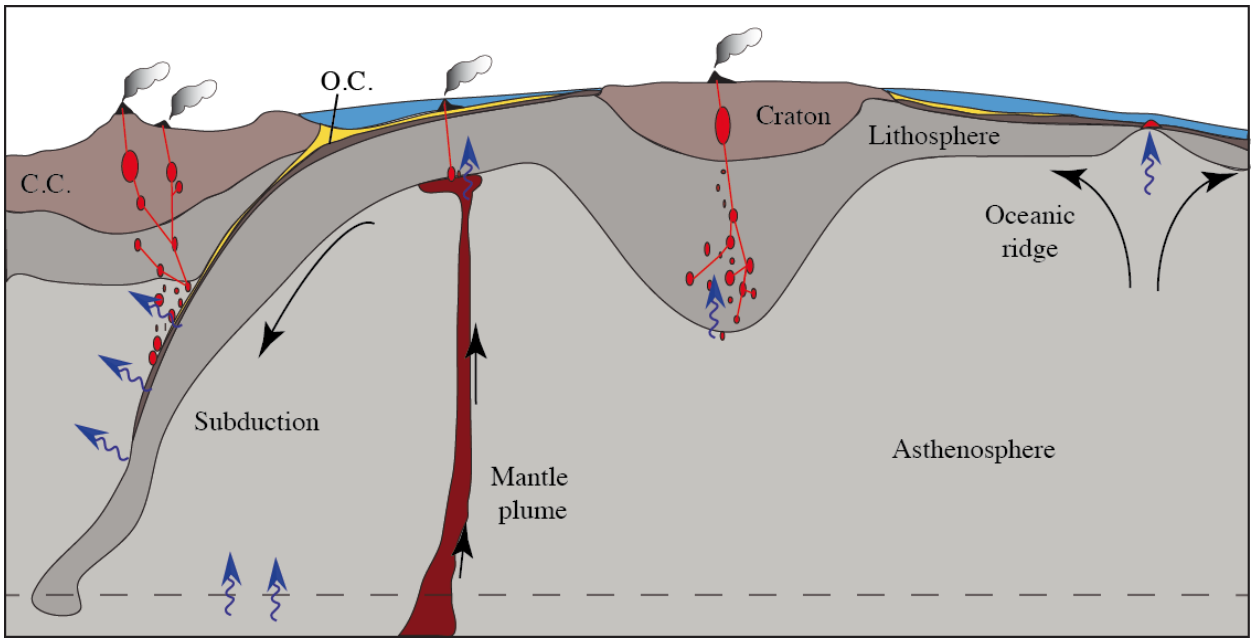

Figure VIII—1. Sketch of the relationship between water global recycling and plate tectonics. Blue arrows indicate water exchange. Crustal thickness is exagerated for clarity, C.C. — continental crust; O.C. — oceanic crust. Figure after Demouchy and Bolfan-Casanova (2016).

Hydrogen may be present in mantle nominally anhydrous minerals as H_2, and OH^- and H_2O (Kovacs et al., 2016). The most documented mechanism is its incorporation as hydroxyl, in structural defects (Figure VIII—2), classified as: point defects (substitution of interstitial or structural atoms, or atomic vacancies), linear defects (dislocations in distorted lattices), planar defects (grain boundaries) and volume defects (inclusions associated with a cluster of point

defects), whereas H_2 could be incorporated only in the latter (Demouchy and Bolfan-Casanova, 2016). What is herein referred to as "water" is to a lesser extent molecular water (H_2O), but more commonly structurally bound OH^-. Hydrogen incorporation under H_2 molecular form in NAMs is still very poorly known. In the context of modern mantle with a sufficiently high oxygen fugacity, hydrogen may be oxidised to OH or H_2O and incorporated accordingly. Nevertheless, under highly reducing conditions, which are believed to have prevailed in a younger Earth (Rubie et al., 2011), hydrogen would have been dissolved in the lattice of mantle NAMs only as H_2 closely related to metamorphic phase changes, stabilizing Fe^{3+} ($2FeO + H_2O = Fe_2O_3 + H_2$) (Yang et al., 2016).

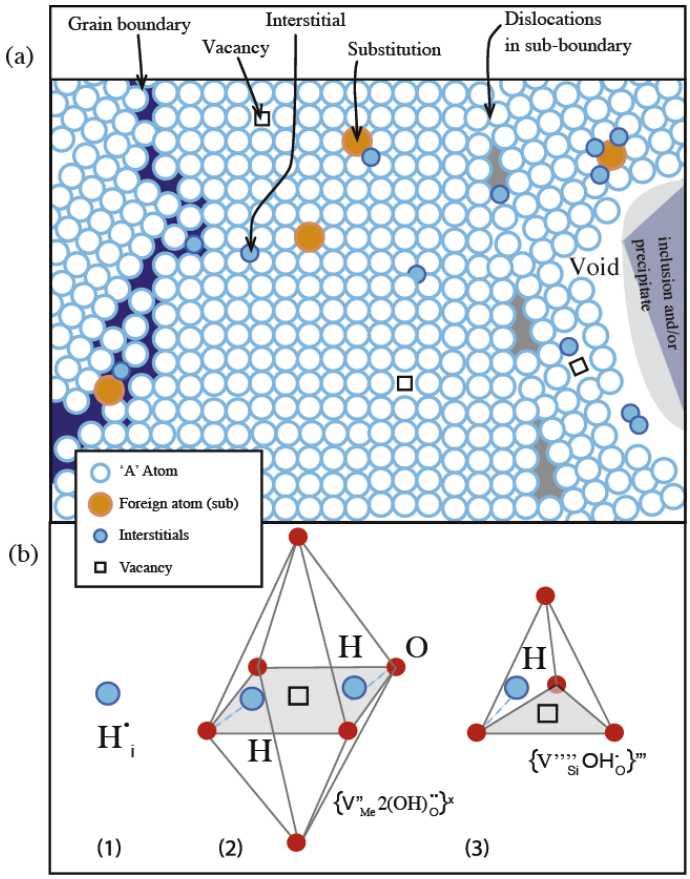

Figure VIII—2. (a)—Sketch showing point defects, line or dislocation defects, plane defects and volume defects in crystalline structure, modified from Darken (1958). (b) _ Theoretical mechanisms for hydrogen incorporation in olivine crystalline structure as (1) interstitial; (2) structurally bound, asociated with a metal vacancy; (3) structurally bound associated with a Si vacancy. Figure from (Demouchy and Bolfan-Casanova (2016).

Due to lack of direct sampling, the only estimates of water in the Earth's interior that can be made are on crustal rocks and upper mantle xenoliths. The latter originate primarily from the subcratonic lithospheric mantle (SCLM) and typically consist of peridotite and eclogite xenoliths. Previous studies on upper mantle NAMs show that clinopyroxene can incorporate significantly more water than garnet, olivine and orthopyroxene (Bell and Rossman, 1992;

Kovacs et al., 2012; Peslier, 2010). Furthermore this implies that despite their comparative low abundance in the upper mantle, eclogites may play a controlling factor in water distribution (Ingrin and Skogby, 2000), cratonic root stability (Li et al., 2008), lithospheric mantle deformation, melting (Hirth and Kohlstedt, 1996) and thermal and electrical conductivity (Karato, 1990). Despite numerous investigations, the limited access to non-metasomatized eclogite xenoliths has left their water storage capacity still poorly constrained.

This chapter aims to quantify water incorporated in non-metasomatized eclogites from the Siberian and Kaapvaal cratons and to investigate the possible substitution reactions that can incorporate hydrogen into the mineral lattice. Furthermore, it sets out to evaluate the differences between distinct analytical methods, correlated to variable water storage mechanisms in omphacite and garnet.

8.1. Fourier Transform Infrared Spectroscopy

The FTIR hydrogen measuring method detects the specific vibration of O-H bonds in different crystallographic configurations. Typically, clinopyroxene is characterized by three hydroxyl absorption bands in the IR un-polarized spectra averaged to 3445—3470cm^{-1}, 3500—3550cm^{-1} and 3600—3635cm^{-1} (Huang et al., 2014; Yang et al., 2008). Previous studies show that hydroxyl absorption bands in omphacite are correlated to the chemistry and the crystallographic orientation of the analyzed grain (Smyth et al., 1991), therefore prone to interference in the un-polarized IR. The 3470cm^{-1} band is strongest when oriented along the γ-polarization direction, corresponding to a preferential accommodation of H by vacancies in the M2 site. The 3650—3540cm^{-1} bands are strongest when oriented along the α- and β-polarization direction (Skogby et al., 2016) where H is accommodated by an Al substituting Si charge-deficiency in the tetrahedral site (Huang et al., 2014; Koch-Müller et al., 2004; Peslier, 2010). Similarly the $H^{+} + Al^{3+} = Si^{4+}$

substitution has been previously described in olivine and orthopyroxenes in peridotite xenoliths (Rauch and Keppler, 2002; Rossman, 1996).

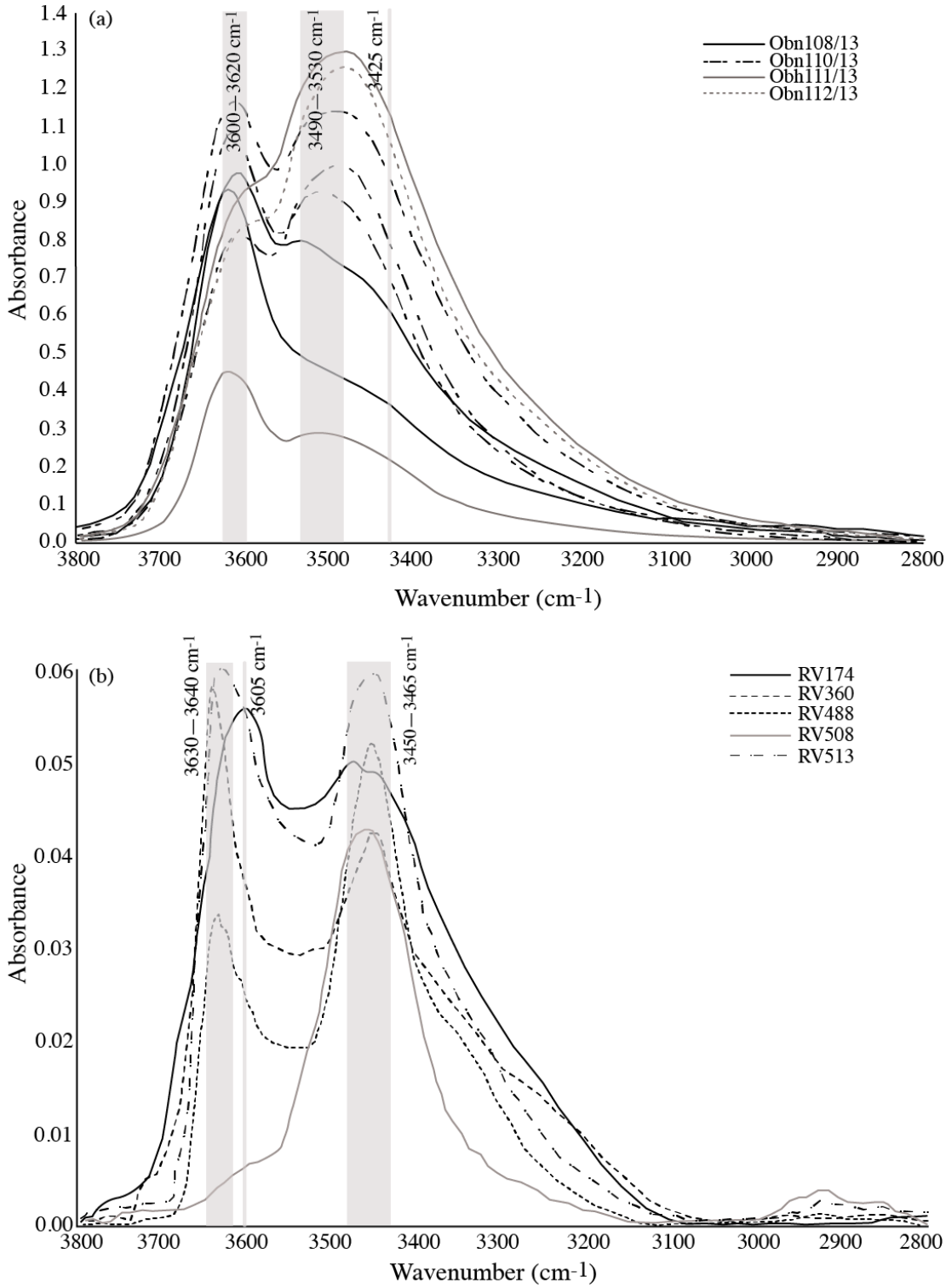

Figure VIII—3. Representative unpolarized IR spectra in omphacite from Obnazhennaya (a) and Roberts Victor (b) eclogites. The main absorption bands are marked in grey.

The Obnazhennaya omphacites show two strong bands at 3490—3530 cm^{-1} and 3600—3620 cm^{-1} and very weak shoulder peaks at ~3425 cm^{-1} (Figure VIII—3a) and Roberts Victor omphacites show two dominating bands at 3450—3465 cm^{-1} and 3630—3640 cm^{-1} (Figure VIII—3b). Variable crystal orientation with respect to the IR beam also leads to variable absorbance for different grains of the same sample. Between 4 and 18 grains have been measured for each sample and large grains have been analysed twice to reduce the uncertainties, with a statistical estimation error within ~20—30% (Kovacs et al., 2008; Xia et al., 2010). Water concentrations differ with the absorption coefficient up to 2x (Table 11). Concentrations calculated with the Koch-Müller et al. (2007) ε for omphacite vary between 929—1413 ppm in Obnazhennaya eclogites and between 124 ppm and 609 ppm for the Roberts Victor eclogites. Water concentrations calculated using the augite coefficient of Bell et al. (1995), vary between 1576—2398 ppm in the Obnazhennaya xenoliths and between 130 and 1191 ppm in Roberts Victor eclogites.

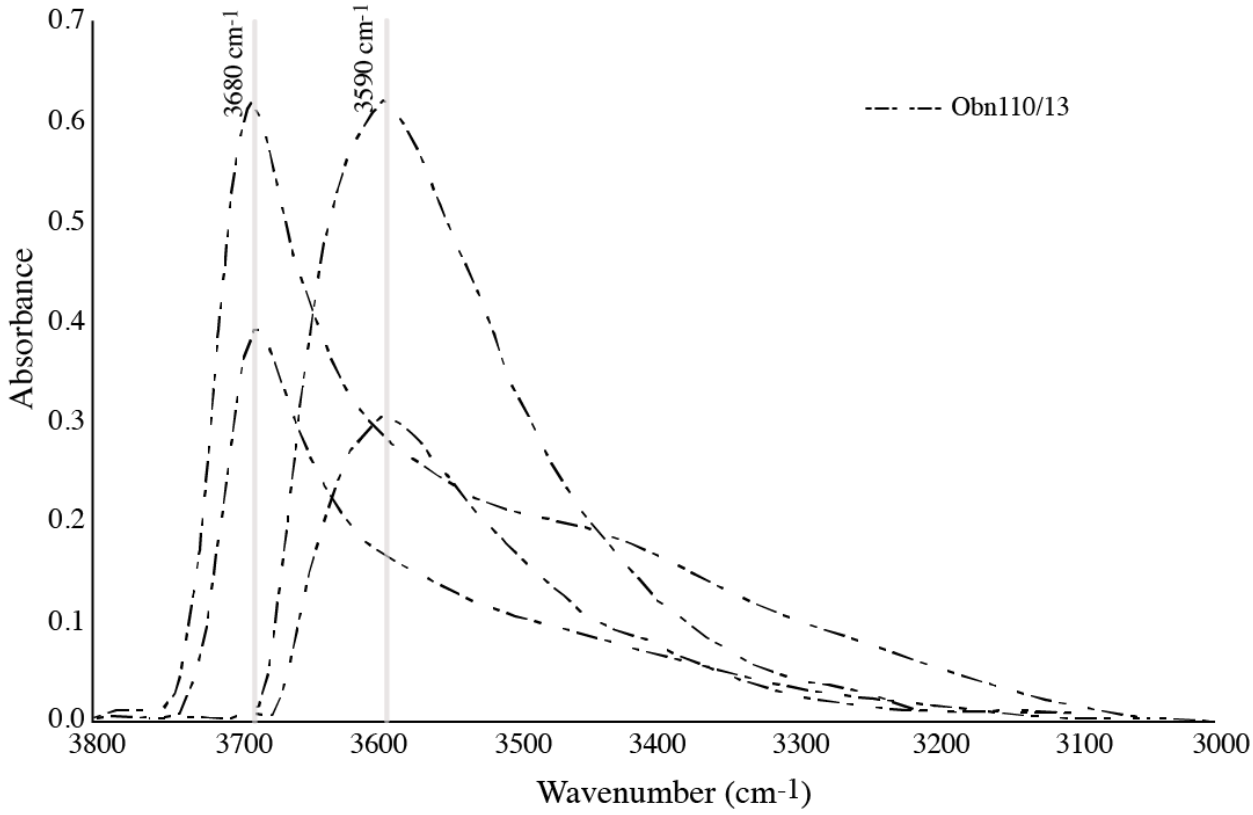

Figure VIII—4. Representative unpolarized IR spectra in coarse garnet exsolution lamellae showing hydrogrossular dominant absorption bands (marked in grey).

Sample	n	Main band	A*i* tot (cm^{-2})	2σ	Thickness (cm)	H_2O ppm wt (Bell et al.,1995)	H_2O ppm wt (Bell et al.,1995) matrix corrected	±30%	H_2O ppm wt (Koch-Müller et al.,2007)	±30%	H_2O ppm wt ERDA	2σ	H_2O ppm wt TC/EA	2σ	H_2O ppm wt SIMS	2σ
Obn108/13 cpx	10	3600—3620cm-1	212	81	0.045	1998	1398	419	1177	353	-	-	2750	160	-	-
Obn110/13 cpx	12	3500—3530cm-1	291	78	0.058	2120	1484	445	1249	375	-	-	4850	420	4738	1623
Obn111/13 cpx	18	3500—3530cm-1	233	215	0.050	2398	1679	504	1413	424	-	-	4650	1080	-	-
Obn112/13 cpx	14	3500—3530cm-1	212	180	0.057	1576	1103	331	929	279	1173	38	5400	680	-	-
RV159	10	3600—3620cm-1	37	40	0.010	1191	834	250	609	183	-	-	5500		-	-
RV174	4	3600—3620cm-1	23	36	0.020	486	340	102	198	59	-	-	-	-	-	-
RV179	8	3450—3465cm-1	9	5	0.010	224	157	47	222	67	-	-	4664		-	-
RV233	11	3600—3620cm-1	14	10	0.010	632	443	133	315	95	795	42	1660	460	-	-
RV360	7	3630—3640cm-1	5	8	0.010	130	91	27	165	49	428	1	2410	380	-	-
RV488	11	3450—3465cm-1	18	15	0.256	301	211	63	177	53	-	-	1230	560	-	-
RV508	10	3450—3465cm-1	7	2	0.020	143	100	30	124	37	-	-	-	-	-	-
RV513	5	3450—3465cm-1	18	4	0.020	441	309	93	254	76	-	-	-	-	-	-

Table 11. Average water estimates based on FTIR, ERDA, TC/EA and SIMS measurements in omphacite from Obnazhennaya (Siberia) and Roberts Victor (Kaapvaal) mines. Samples marked with «Obn» are from Obnazhennaya kimberlite and those marked with «RV» are from Roberts Victor mine.

None of the large garnet grains contain detectable water content (1.3—6.5 ppm) and only few coarse garnet exsolutions from sample Obn110/13 were available for infrared analysis. The spectra show two main peaks at ~3590 cm^{-1} and ~3680 cm^{-1} (Figure VIII—4) previously described in natural hydrogrossular garnets by Rossman and Aines (1991). No bands corresponding to surface or background contamination have been registered (Bell and Rossman, 1992). The water content ranges from ~165 ppm in the grains dominated by the ~3590 cm^{-1} band and 1000—1950 ppm in the grains dominated by the ~3680 cm^{-1} band.

8.2. Elastic Recoil Detection Analysis

The ERDA hydrogen analysis method, quantifies the total hydrogen content, both molecular and structurally bound. As H atoms are ejected from the sample, the alpha particles ejected in the first instance, typically interpreted as "surface water", will arrive at the detectors with high energy and give an intense signal in the 600—850 keV range (Figure VIII—5).

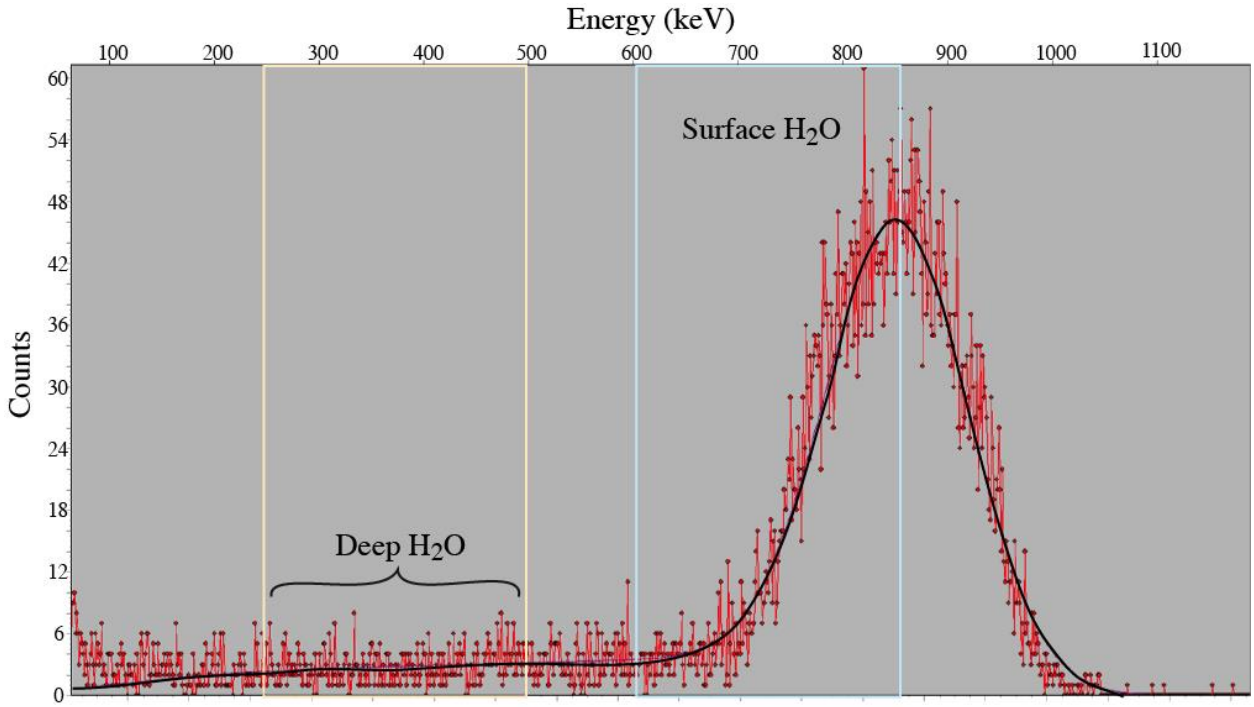

Figure VIII—5. ERDA spectrum of sample Obn112/13. Histogram showing number of counts on the detector as a function of energy (red) and results of SIMNRA model (black solid line). Energy ranges of H atoms ejected exclusively from the deep interior of the sample are considered in the 250-500 keV range (light orange) and from the near surface region between 600 and 850 keV (light blue).

The particles subsequently ejected, typically interpreted as the bulk contribution, corresponding to the deeper levels of the sample, will arrive at the detectors with lower energy, between 250 and 500 keV.

The H contents in omphacites determined using the SIMNRA fitting software are given in Table 11, with average concentrations of 1173±38 ppm wt. H_2O (n=6 fits) in sample Obn112/13, 795±42 ppm wt. H_2O (n=2 fits) in sample RV233 and 428±1 ppm wt. H_2O (n=3 fits) in sample RV360, similar to the FTIR estimates.

8.3. Secondary Ion Mass Spectrometry

The SIMS hydrogen measuring method detects the total hydrogen, both molecular and structurally bound. Two quantifying methods have been used, through H^+ analysis and through H^+/Si^+ respectively.

Water concentrations measured through secondary H^+ ion spectrometry are significantly underestimated, due to matrix differences between the augite standard and the omphacite samples. However, the influence of major element composition on water measurements is still poorly constrained for clinopyroxene.

The water calculation based on H^+/Si^+ measurements is a more precise method, with a quantifiable matrix influence. As inferred by Deloule et al. (1995) on experimental silicate glasses, the effect of different Na^+/Ca^{2+} ratios might result in an up to ~30% overestimation of the water content calculated with respect to the H^+/Si^+ ratio. This method had been applied to sample Obn110/13 and the estimates obtained range from ~3870—6170 ppm water (Table 11).

Sample		n	H_2O ppm (H^+)	2σ	n	H_2O ppm (H^+/Si)	2σ
Obn108/13		4	233	29	-	-	-
Obn110/13		10	224	39	6	4738	1623
Obn111/13	non-exsolved	4	289	76	-	-	-
	exsolved	8	32	19	-	-	-
Obn112/13		22	353	76	-	-	-

Table 12. Average water estimates based on SIMS analyses in omphacite from Obnazhennaya (Siberia) and Roberts Victor (Kaapvaal). Samples marked with «Obn» are from Obnazhennaya kimberlite and those marked with «RV» are from Roberts Victor mine.

The considerable difference between the water content measured by mass spectrometry and by FTIR is to be expected, as infrared water analysis detects the structurally bound H^+ and OH^-. Complementarily, mass spectrometry analyses will preferentially account for molecular water, which is more mobile than the structural hydrogen (Gong et al., 2007). Similar results have been reported by (Kovacs et al., 2016) in clinopyroxene megacrysts, where mass spectrometry analyses provide concentrations two times higher than the infrared estimates.

Water content distribution profiles between two exsolution lamellae hosted in omphacite in sample Obn111/13 show punctual increase in water content at the rims adjacent to the garnet and garnet± zoisite exsolutions (Figure VIII—6) and significantly lower water content in the exsolved clinopyroxene (~9 times lower) than in the non- exsolved grains (Table 12).

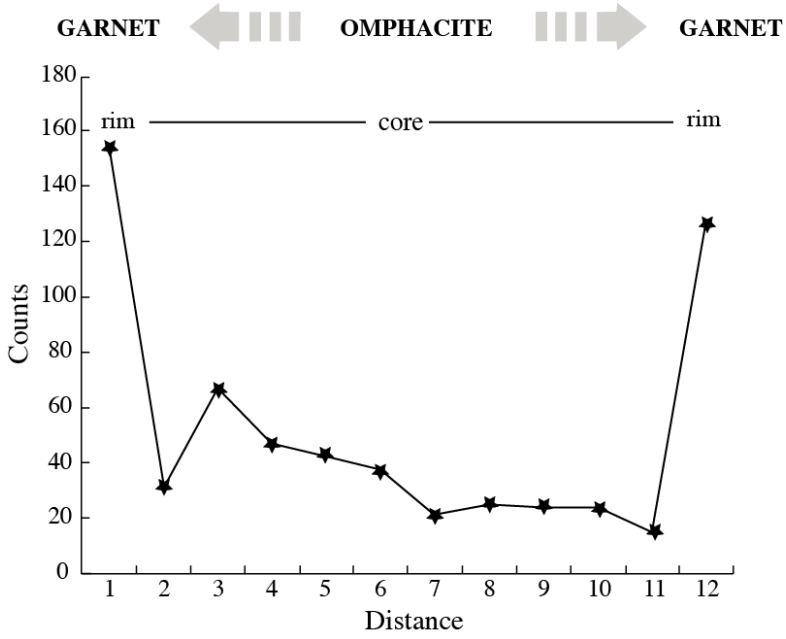

Figure VIII—6. Compositional profile showing number of counts variability as proxy for water content, inbetween garnet exsolution lamellae, in host omphacite (sample Obn111/13). The core has systematically lower content with a 3 to 4 times increase at the rims adjacent to exsolutions.

8.4. High Temperature Conversion Elemental Analysis- Mass Spectrometry

The high-TC/EA-MS hydrogen analysis method, complementary to ERDA and SIMS, quantifies the total hydrogen content (*i.e.* H_2, H_2O, OH^-). The results for the biotite NBS-30 standard (Figure VIII—7 a-b) are in agreement with known calibrations. Bulk 'water' contents are given in Table 11 and the measured hydrogen concentrations and the measurement reproducibility are shown in Figure VIII—7 c-d) for sample Obn108/13. The total water in

omphacites from Roberts Victor eclogites varies from 1230±560 to ~5500 ppm wt. and in omphacites from Obnazhennaya eclogites between 2750±160 and 5400±680 ppm wt. For sample Obn110/13 TC/EA-MS water estimates of 4850±420 ppm are in good agreement with SIMS results, based on the H^+/Si ratio, of 4738±1623 ppm wt.

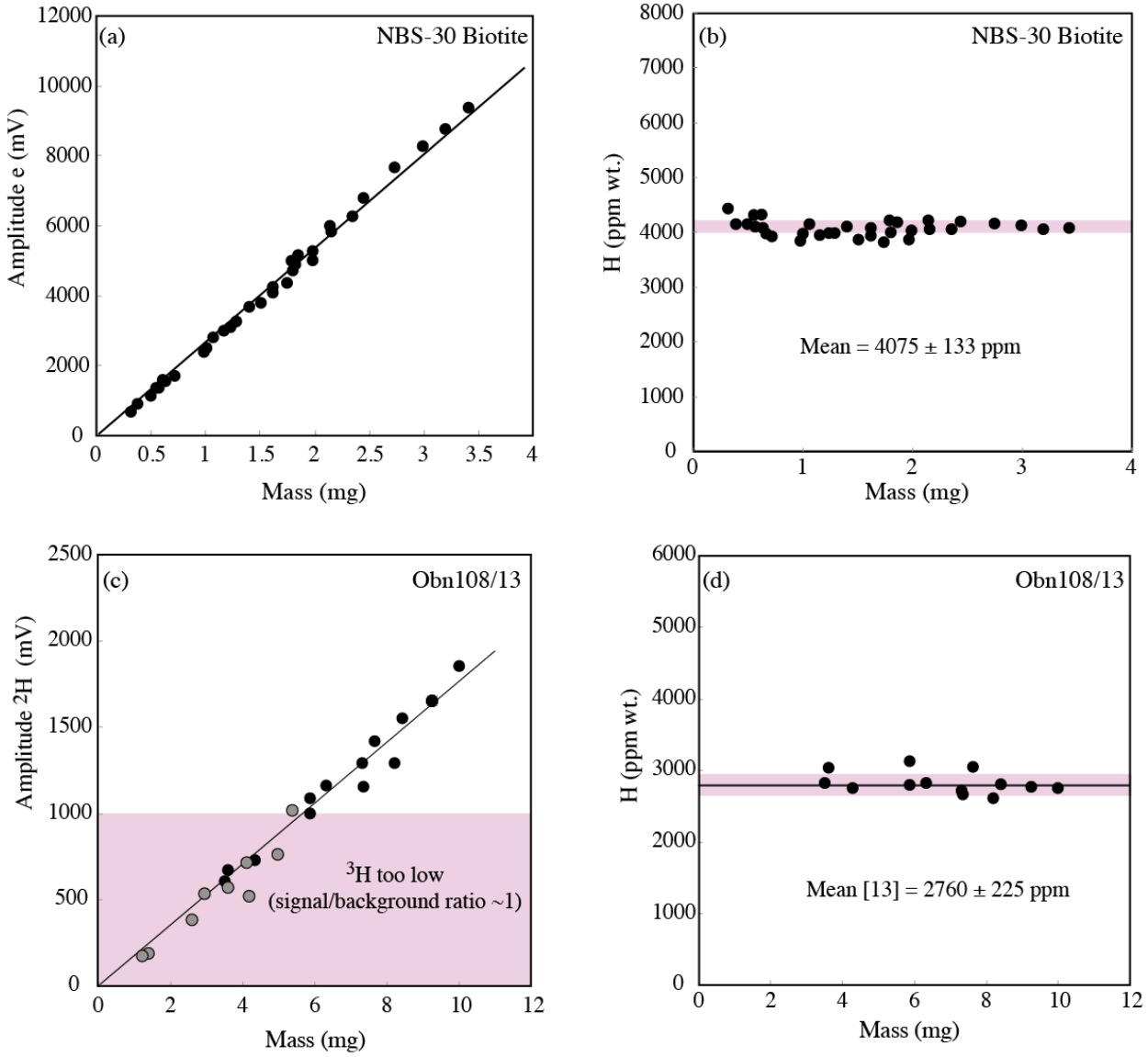

Figure VIII—7. Amplitude vs. Mass and TC/EA-MS measured H2O concentrations for biotite NBS-30 standard (a-b) and Obn108/13 omphacite (c-d). The average water estimate in sample Obn108/13 is over 13 measurements.

Summary: Water can be found in omphacite as structurally bound hydrogen or as H_2O molecules. Different major element composition will play an important role on the crystallographic sites where hydrogen will be incorporated, as well as on water quantification.

Based on FTIR analyses of structural H^+ and OH^-, the calculated water content in Obnazhennaya omphacites varies between 929 and 1413 ppm when using the absorption coefficient by Koch-Müller et al. (2007) and 1576—2398 ppm when using the calibration by Bell et al. (1995). The large garnets analyzed by FTIR do not contain detectable water. Bulk H_2O content measured by ERDA of ~1173 ±38 ppm wt. is within the same range as the FTIR estimate for omphacite from sample Obn112/13. The total 'water' content measured by SIMS, based on the H^+/Si ratio measured in omphacite from sample Obn110/13 varies between ~3870 and 6170 ppm, in close agreement with the results obtained by TC/EA-MS, which give an estimate of 2750—5400 ppm wt. for omphacites from Obnazhennaya.

Omphacite from Roberts Victor eclogites show similar FTIR absorption bands to the Obnazhennaya samples, however they have significantly lower water estimates. Calculated water content varies between 124 ppm and 609 ppm when using the absorption coefficient by Koch-Müller et al. (2007) and between 130 ppm and 1191 ppm when using the calibration by Bell et al. (1995). ERDA bulk 'water' estimates are slightly more elevated (130—632 ppm wt. by FTIR and 428—795 ppm wt. by ERDA), whereas TC/EA-MS bulk estimates are roughly between 2 and 20 times higher (1230—5500 ppm wt.).

It is inferred the difference between the different methods used for hydrogen quantification may be due to the intrinsic nature of each technique and the different amounts of structural and molecular water in the omphacite.

CHAPTER IX.

DISCUSSION PART II

CHAPTER IX. DISCUSSION PART II

9.1. Exsolution

Garnet exsolution in pyroxene has been previously described in eclogites (Caporuscio and Smyth, 1990; Dobosi et al., 2007; Harte and Gurney, 1975; Jagoutz, 1988; Jerde et al., 1993; Lappin and Dawson, 1975; Qi et al., 1997; Schmickler et al., 2004; Smyth and Caporuscio, 1984), grosspydites (Lappin, 1978; Sautter and Harte, 1988, 1990; Smyth et al., 1989; Sobolev et al., 1968), pyroxenites (Xu et al., 2004), peridotites (Dawson, 2004; Spengler et al., 2012) and xenocrysts (Aoki et al., 1980) found in kimberlite pipes from different cratons. The typical textural patterns are defined by parallel lamellae, lenses, blebs and coronae analogous to the ones described in this study. The orientation of the lamellae is crystallographically controlled. Through single crystal X-ray diffraction Aoki et al. (1980) determined topotaxial transition between clinopyroxene and garnet (e.g. $[001]_{Cpx}||\ [111]_{Gt}$) subsequently confirmed by Spengler et al. (2012) through EBSD analysis.

At the core of the garnet-clinopyroxene solid solution is the substitution:

$$2Al^{3+} = Si^{4+} + M^{2+} \qquad 9.1.$$

within a precursor superaluminous (tschermackitic) pyroxene (Spengler et al., 2012). Thus, the main mineral reactions responsible for garnet exsolution can be formulated as:

$$CaMgSi_2O_6 + CaAl_2SiO_6 \Rightarrow Ca_2MgAl_2Si_3O_{12} \qquad 9.2.$$
diopside CaTs grossular-rich garnet

$$CaMgSi2O_6 + 2CaAlSiO_6 + Mg_2Si_2O_6 \Rightarrow CaMg_2Al_2SiO_3O_{12} + Ca_2MgAl_2Si_3O_{12} \qquad 9.3.$$
diopside CaTs MgTs variably grossular-rich garnets

$$2CaMgSi_2O_6 + Al_2Si^{-1}Mg^{-1} \Rightarrow Ca_2MgAl_2Si_3O_{12} \qquad 9.4.$$
diopside grossular-rich garnet

Reactions 2 and 3 are in agreement with the ones suggested by Aoki et al. (1980); Gasparik (1984); Gasparik and Lindsley (1980) and reaction 4 with those by Qi et al. (1997); Sautter and Harte (1990). It is inferred Ca- (grossular-) rich garnet is exsolved at the expense of Tschermak components and aluminium, with limited consumption of Si and Mg (Wood and Banno, 1973) from the host clinopyroxene. The solubility of the Tschermak molecule in clinopyroxene increases with increasing temperature and/or decreasing pressure (Gasparik, 1984; Green and Ringwood, 1967). Due to this compositional dependency, garnet exsolution can result from processes involving temperature decrease, pressure increase or any combination of the two (Jerde et al., 1993; Lappin and Dawson, 1975). However, thermobarometry from previous studies, conducted on the exsolution lamellae, and the reconstructed primary pyroxene and the host pyroxene respectively, show that these exsolution mostly formed through slow cooling (from ~1300—1450°C to ~950—1050°C) at nearly constant pressure (3.5—4.0) GPa (Aoki et al., 1980; Dobosi et al., 2007; Green, 1966; Harte and Gurney, 1975; Sautter and Harte, 1988; Smyth et al., 1989; Spengler et al., 2012; Xu et al., 2004).

9.1.1. Major element diffusion profiles

Composition profiles were determined in the host clinopyroxene perpendicular to the associated lamellae and are shown in Figure IX—1. The Al content decreases towards the interface with the exsolved garnet, as Si and Mg show a complementary evolution, with increasing contents. Na, Ca, Fe do not show diffusion gradients.

Major element point analyses show an increase in the grossular modal abundance between the primary and the exsolved garnet (from ~28% to ~66%), inversely proportional to the CaTschermak component in the host omphacite, which decreases by a factor of 2 (see Table 2). As garnet exsolves, it consumes the Al and Ca, and locally increases the Si and Mg in the host clinopyroxene. This is supported by diffusion gradients still preserved in large clinopyroxene

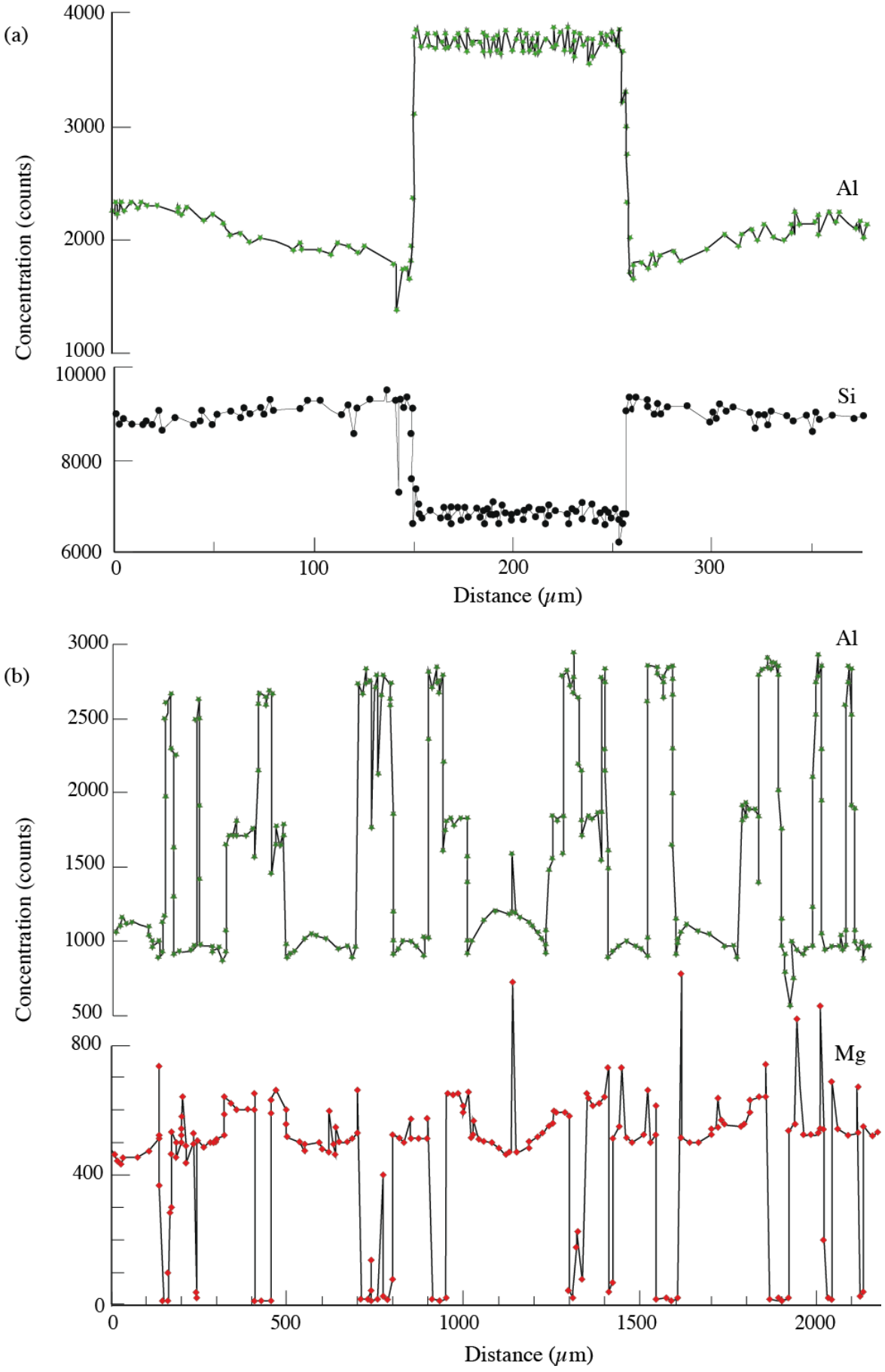

Figure IX—1. Complementary difussion gradients in Al and Si-Mg inbetween lamellar exsolutions preserved in host omphacite in sample Obn108/13 (a) and Obn110/13 (b).

grains (Figure IX—1). Adjacent to the garnet lamellae, the Al content drops significantly, resulting in a concave-downward chemical gradient towards and in-between the exsolution. Less obviously, the Si content slightly increases towards the exsolution, resulting in complementary concave-upward diffusion gradients. Similar trends have been previously described by Dobosi et al. (2007); Jerde et al. (1993); Qi et al. (1997); Sautter and Harte (1988) and Xu et al. (2004). The Aluminium diffusion coefficient in clinopyroxene is lower relative to most other cations. This has allowed the preservation of Al compositional gradients and is furthermore consistent with lamellae nucleation being controlled by Al diffusion in the pyroxene (Sautter and Harte, 1990). We infer the intracrystalline diffusion of Mg, Ca, Fe and, to a lesser extent Si, has continued after the exsolution process has ceased, therefore re-equilibrating inside the lamellae and respectively inside the host clinopyroxene

Garnet-zoisite exsolution in aluminous clinopyroxenes have been previously mentioned by Xu et al. (2004) in garnet-clinopyroxenite xenoliths in the Xuzhou region, China. In the same way as Reaction 1, zoisite nucleation can be written in a very simplified form as:

$$\underset{\text{diopside}}{CaMgSi_2O_6} + \underset{\text{CaTs}}{CaAl_2SiO_6} + \underset{\text{structural water}}{Mg^{1-} + (OH)} \Leftrightarrow \underset{\text{zoisite}}{Ca_2Al_2Si_3O_{12}(OH)} \qquad 9.5.$$

Considering clinopyroxene is a nominally anhydrous mineral, (OH) is not included in the structural formula, but stored as previously discussed in under-bonded sites and in structural defects. Even though a minor phase (<1% modal abundance), zoisite can contain up to ~1.7 wt% water and it is thus very important to constrain the source of the OH. Textural and compositional evidence, coupled with SIMS hydrogen diffusion profiles show that kimberlite contamination is restricted to the rims adjacent to veinlets. We therefore infer all water incorporated in the zoisite exsolution was intrinsic to the precursor clinopyroxene.

In a similar study, Jagoutz (1988) shows that with respect to Sr, Nd as well as to Sm/Nd and Sr/Nd, garnet exsolution from clinopyroxene took place in an intrinsically isochemical system.

Moreover, through the use of Sr isotopes as indicators for kimberlite interaction, it is shown that kimberlite contribution is restricted to minor, interstitial phases at the grain boundaries.

The major element net transfer between the exsolved garnet±zoisite assemblage and the host clinopyroxene is translated into fractioned trace elements patterns with complementary anomalies in Sr, Ti and Pb (e.g. positive in cpx and negative in gt) (Figure V—5). In tandem with the exsolution, the host clinopyroxene becomes depleted in elements compatible in garnet±zoisite (e.g. HREE, Y). Kindred partitioning during garnet exsolution in clinopyroxene has been previously described in Obnazhennaya eclogites by Dobosi et al. (2007), who argued for a diffusion-controlled nucleation in an isochemical system.

Precursor clinopyroxene trace element composition was calculated for sample Obh108/13 using modal abundance and trace element mineral composition. The results were compared with trace element patterns from large, non-exsolved coexisting clinopyroxenes (with garnet±zoisite in solid solution) (Figure IX—2).

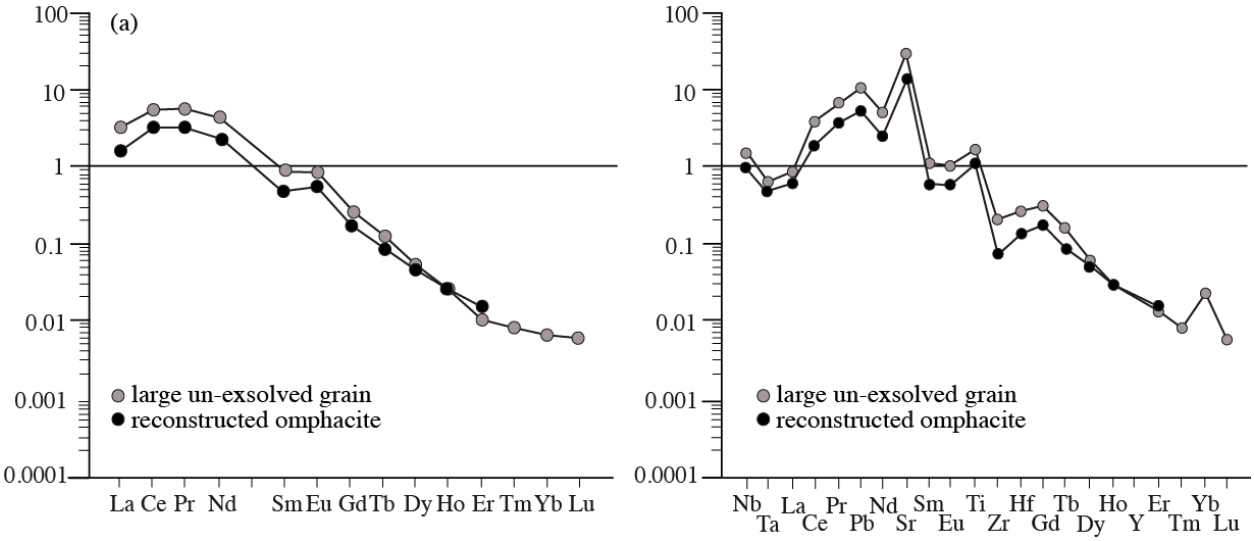

Figure IX—2. Reconstructed omphacite REE (a) and extended trace element patterns (b) compared to non-exsolved large omphacite grains in the Obn108/13 eclogite xenolith.

The two are within error identical, in agreement with the results of Jagoutz (1988). This shows that both garnet and zoisite exsolution formed in an essentially closed chemical system on the xenolith scale, from a superaluminous, water rich primary clinopyroxene.

9.1.2. Stability of zoisite

The intertwined growth of garnet and zoisite as epitaxial lamellae in clinopyroxene (Figure III—10a-b) is consistent with zoisite being stable at the calculated PT equilibrium conditions (3.7—4.1 GPa, 900°—950°C). Zoisite and its polymorphs, although as minor constituents, are primary rock forming minerals at low-pressure eclogite facies conditions, associated with kyanite and/or corundum and high water activity (Deer et al., 1986). In high-pressure xenoliths zoisite has been previously reported in grosspydites(Sobolev et al., 1968) and eclogites (Watson and Morton, 1969) from kimberlites, as a secondary mineral, due to low pressure alteration of pyroxene-kyanite or lawsonite-bearing assemblages. Xu et al. (2004) report garnet, zoisite and amphibole exsolution in clinopyroxene from (garnet-) clinopyroxenite xenoliths in the Xuzhou diorite-monzodiorite intrusions. However, therein it is inferred that the exsolutions formed through cooling from ~950—1000°C to 620°—780°C at ~1.5—2 GPa, at much lower pressures and temperatures than the ones calculated for the Obnazhennaya eclogites.

Multi-anvil experiments coupled with thermodynamic modelling by Schmidt and Poli (1994) show that lawsonite breakdown to zoisite occurs at ~6.8GPa for temperatures of ~950° C (close to the calculated lower temperature limit). Moreover, through further experiments and phase relationship modelling, Poli and Schmidt (1998) show that zoisite can be stable up to a maximum pressure of 7GPa at ~1050°C, for Al_2O_3+H_2O-saturated conditions. This is in agreement with the previously stated hypothesis and observations, where garnet±zoisite exsolutions originate from a precursor superaluminous, water-rich clinopyroxene in the 900°—950°C temperature range at 3.7—4.1 GPa.

9.2. Water incorporation mechanisms in Nominally Anhydrous Minerals

Incorporation of hydrogen in NAMs is controlled by both internal and external factors, such as pressure, temperature, iron content, oxygen and water fugacity (Kolesnichenko et al., 2016;

Peslier et al., 2002; Skogby et al., 2016). It is therefore an intricate ensemble of factors that lead to water storage in nominally anhydrous minerals.

When estimating intrinsic water content several precautions should be taken into account. Firstly a control on the grain properties should ensure no noticeable defects, cracks or inclusions are present on the analyzed surface. Secondly, the collected absorption bands should be examined with caution for any contamination. Submicroscopic amphibole lamellae have been commonly detected in clinopyroxene, with a characteristic OH absorption band at ~3675cm^{-1} (Huang et al., 2014; Skogby et al., 1990), yet no such band has been detected in this study. Nano-inclusions of secondary sheet silicates (clinochlore – $(Mg,Fe^{2+})_5Si_3Al_2O_{10}(OH)_8$ and amesite $Mg_2Al_2SiO_5(OH)_4$) can be present in omphacites, showing a specific hydroxyl absorption band at ~3610 cm^{-1} (Koch-Müller et al., 2004). Unlike samples where such nano-inclusions have been described, we register consistent spectra among different analyses on the same grain. Although clinochlore would be an unusual alteration product in mantle-derived omphacites (Koch-Müller et al., 2004), amesite is common in Al-, Mg-rich rocks and could be exsolved with decompression assisted cooling. If present, such nano-inclusions would have incorporated in part the water initially preserved in the omphacite structure. Therefore, although the data consistency and lack of extensive alteration suggest minor or no contribution in the 3600—3620cm^{-1} band from clinochlore/amesite nano-inclusions, the measured integral absorbance should be interpreted as a minimum for the intrinsic OH content.

In the un-polarized spectra, a good control on the specific absorption bands can be exerted through a statistically sufficient number of analyses (Kovacs et al., 2008). The O2 point position is the most favourable site for the OH incorporation as it is highly underbonded according to its Pauling bond strength (Skogby et al., 2016). The excess charge may be compensated either by cation vacancies in the M2 site or charge-deficient substitutions in the tetrahedral site (Beran, 1976; Ingrin and Skogby, 2000; Skogby et al., 1990). We infer the observed variability of the spectra is given by different orientations of the OH dipole. When oriented in the direction of an

M2 site the ~3475 and ~3535cm^{-1} absorption bands are strong (Ingrin and Skogby, 2000; Smyth et al., 1991) and when oriented towards the O3 position, the dominating band is ~3645cm^{-1} (Beran, 1976; Skogby et al., 1990). Furthermore, the incorporation of OH and the peak heights of the characteristic absorption bands directly correlate with vacancies and the concentration in certain elements (Al, Fe^{3+}, Ti, Na) (Peslier et al., 2002; Skogby et al., 1990). The dominant absorption band in the bimineralic sample Obn108/13 is the 3600—3620cm^{-1} band, correlating with the high total iron content of the omphacite,with shoulder peak at ~3425cm^{-1} (Table 3). We infer this is the effect of trivalent ions (mostly Fe^{3+}) on OH accommodation sites (Skogby et al., 1990). The corundum-bearing eclogites show higher peak variability. The ~3610cm^{-1} band increases with the lamellar exsolutions, while the 3490—3530cm^{-1} absorption band is the strongest. Its intensity has been previously attributed to$^{IV}Al^{3+}$substitution of Si, balanced by H^{+}accommodation (Huang et al., 2014; Koch-Müller et al., 2004). The presence of two differently pleochroic groups of absorption bands indicates that at least two types of hydrogen locations exist simultaneously (Beran, 1976; Ingrin and Skogby, 2000). The registered spectra are nevertheless unusual for omphacites, and the 3490—3530cm^{-1} band might still be poorly constrained.

The discrepancies between water contents calculated with different calibrations are due to significant spectral differences between minerals and to a lesser extent to specific errors in each method. The augite absorption coefficient might be more appropriate for the analyzed omphacites because of the similar hydroxyl bands, however the content might be overestimated by up to 30% (Bell et al., 1995). The inferred water estimates become 1103—1679ppm for the Obnazhennaya omphacites and 91—834 ppm in the Roberts Victor samples. On average these are higher by ~22% than the concentrations obtained using the omphacite calibration of Koch-Müller et al. (2007) for most samples, except RV179, RV360 and RV508 (Table 10).

Similarly, the differences between the composition and structure of the analyzed omphacite and the augite clinopyroxene standard, lead to major underestimates of water quantification

through secondary ion H^+ spectrometry (224±45 ppm to 353±38 ppm, Table 11). More accurate total hydrogen concentrations are calculated on the basis of measured H^+/Si^+ ratio. These range between 3873 and 6170 ppm (4738±1623 ppm average) for sample Obn110/13. Although these concentrations may be slightly overestimated due to different alkali content (Deloule et al., 1995), they are in agreement with TC/EA-MS estimates of 4850±260 ppm.

The only non-standard dependant hydrogen investigation is Elastic Recoil Detection Analysis (Bureau et al., 2009), giving water contents between 1 and 3 times higher than FTIR-determined concentrations, and between 2—20 times lower than to the SIMS and TC/EA-MS estimates (Table 11). The ERDA water content is well correlated with the FTIR estimates (Figure IX—3a) suggesting that most of the water determined by ERDA is as hydroxyl (Aubaud et al., 2009). The higher values measured by elastic recoil analysis may be caused by: surface-adsorbed water; electronic noise of the ERDA detector; other forms of hydrogen than hydroxyl, that are detected by the ERDA (Bureau et al., 2009). Atmospheric contamination was minimized during sample preparation, and the electronic noise of the detector can be estimated during sample analysis, whereas the strong correlation between the ERDA and FTIR estimates are consistent with water incorporation as other forms than hydroxyl (i.e. H_2, mineral inclusions in planar defects), that remain undetected in the expected 2800—3800 cm^{-2} vibration range in the IR spectra (Ingrin et al., 1989; Skogby et al., 1990). Moreover, the extrapolated linear correlation between the two analytical techniques suggests that for no detectable water by FTIR analysis, an estimate of ~398 ppm through ERDA analysis, supporting the hypothesis of hydrogen stored in the omphacite structure in other forms than as hydroxyl (Aubaud et al., 2009).

Structural water (hydroxyl) concentrations decrease with bulk water content for samples dominated by the 3500—3530 cm^{-1} absorption band, showing no other correlation in samples dominated by different IR bands (Figure IX—3b). It is thus inferred conditions suitable for hydrogen incorporation by compensating the deficit in Al – Si substitution in the tetrahedral site (Koch-Müller et al., 2004), are unfavourable for water stored as H_2O or H_2. Furthermore,

hydrogen solubility preferentially as H_2 instead of as OH or H_2O may be controlled by fO_2, believed also to increase with pressure and could be easily accommodate in interstitial position in the mineral lattice, due to its small size, and not related to a specific substitution (Yang et al., 2016).

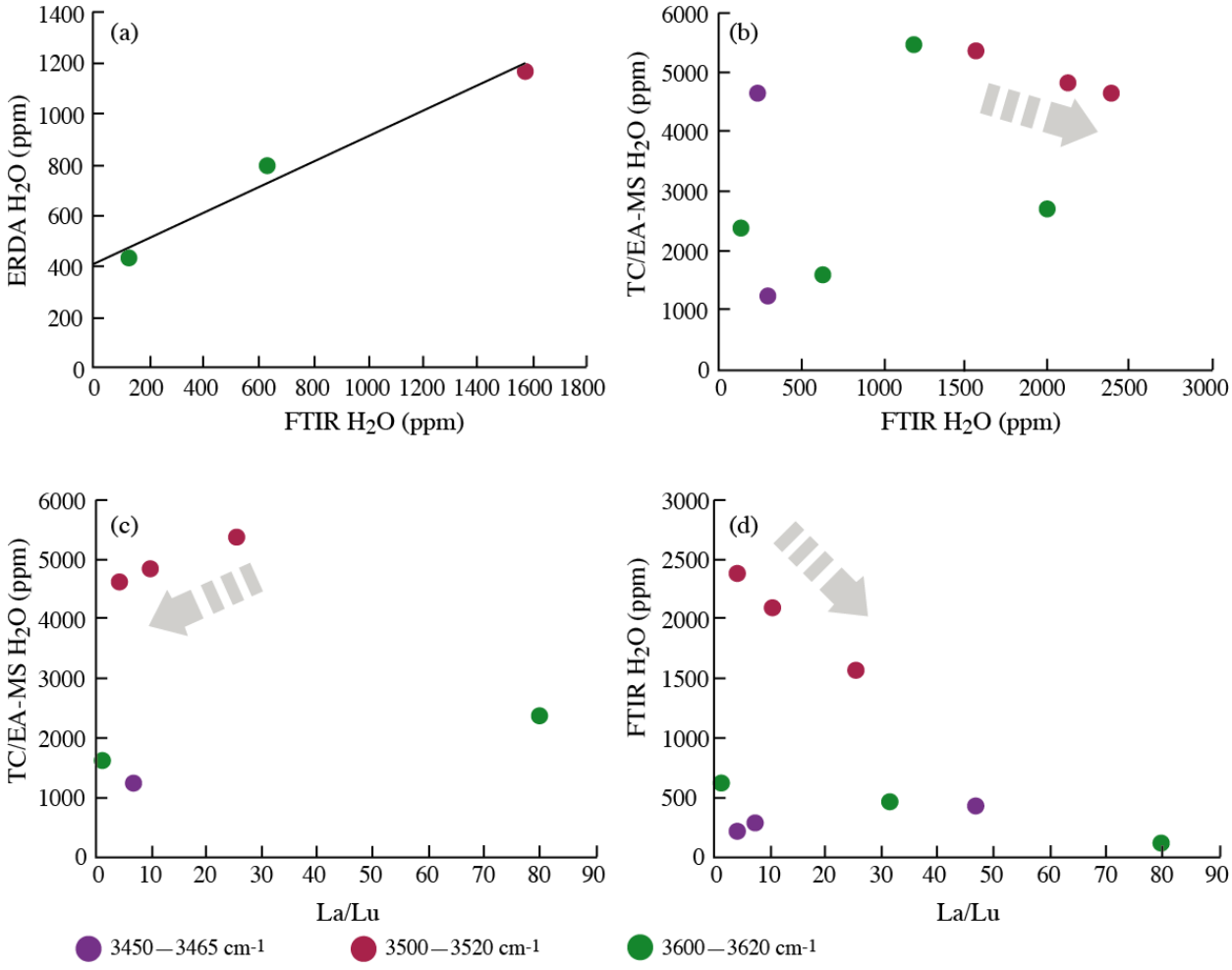

Figure IX—3. Water contents by ERDA (a) and by TC/EA-MS (b) vs. those by FTIR and water contents by TC/EA-MS (c) and by FTIR (d) vs. La/Lu for omphacites dominated by one of the three main IR hydroxyl absorption bands from eclogite xenoliths from Roberts Victor and Obnazhennaya.

There is no significant correlation between major element composition and water content, however La/Lu correlates positively (r = 36) with TC/EA-MS results and negatively with FTIR hydroxyl concentrations (r = -39) in omphacite dominated by the 3500—3530 cm^{-1} absorption band (Figure IX—3c-d). There is no correlation between La/Lu and 'water' estimates by FTIR in samples dominated by the 3450—3465 cm^{-1} and 3600—3620 cm^{-1} IR bands. As the La/Lu ratio

increases, the hydrogen content preferentially accommodated as H^+ balanced by $^{IV}Al^{3+}$ substitution of Si decreases. Nevertheless, this negative correlation is not generated by all hydrogen incorporation mechanisms and more complex processes than fractional crystallisation are required for water incorporation in omphacite. Similar results have been published by Kovacs et al. (2016).

Despite the absorbance and content variability, the results obtained (Table 10) are in general agreement with the previous values calculated in comparable samples 675—1496 ppm (Huang et al., 2014), 43-870 ppm (Peslier, 2010), 31—514 ppm (Koch-Müller et al., 2004).

The primary, coarse garnet is systematically anhydrous (<7 ppm H_2O) and only a few of the exsolutions are variably water-rich (160—2000 ppm). Although studies on both synthetic and natural garnet show it can store structural water at mantle conditions (Ackermann et al., 1983; Aines and Rossman, 1984b; Bell and Rossman, 1992a), mantle-derived garnets typically have much lower water contents compared to clinopyroxene (Bell and Rossman, 1992b). The main mechanism for hydroxyl incorporation in garnet is commonly considered to be the hydrogarnet substitution $H_4O_4^{4-}=SiO_4^{4-}$ (Fyfe, 1970; Rossman and Aines, 1991), nevertheless other mechanisms related to structural defects and/or substitutions should be taken into account (Aines and Rossman, 1984a). Due to a major Si deficit, hydrogarnet total oxides compositions are systematically less than 100 (Birkett and Trzcienski Jr., 1984). Nevertheless, the major element compositions of the analyzed garnet exsolutions give total of oxides close to 100 wt.% and show no major Si-deficiency. This is consistent with the presence of hydrogrossular as nano- to micrometer size crystals within the grossular-rich garnet. The stability of $(OH)_4^{4-}$ clusters in the tetrahedral site at mantle conditions is debatable (Martin and Donnay, 1972), however in such a scenario, the resulting volume increase could locally be accommodated by the surrounding garnet.

Recalculated water content in precursor clinopyroxene in eclogites showing exsolution lamellae, ranges between 1370 ppm and 1767 ppm in sample Obn111 and 4329—4657 ppm in

sample Obn110. This is in agreement with a previous estimates of ~ 4000 ppm by (Smyth et al., 1991). The calculated whole-rock water content ranges between 72 and 953 ppm in Roberts Victor samples and 459—1367 ppm in the Obnazhennaya eclogites, calculated using the absorption coefficient of Bell et al. (1995) and FTIR measurements, or between 241—4400 ppm and 633—3132 ppm respectively, based on the TC/EA-MS bulk measurements. It should be noted that even the lower water estimates (based on FTIR analysis) of mantle eclogites are generally higher than the maximum water content measured in the surrounding peridotites, estimated between <1 and 394 ppm wt. beneath the Siberian craton (Doucet et al., 2014; Kolesnichenko et al., 2016; Matsyuk et al., 1998) and between 0 and 200 ppm wt. beneath the Kaapvaal craton (Peslier, 2010).

9.3. Water content correlation with Ca-Eskola

Experimental studies by Bromiley and Keppler (2004) show that hydroxyl solubility in a solid solution of jadeite and diopside increases significantly with the amount of the Ca-Eskola component ($Ca_{0.5}\square_{0.5}AlSi_2O_6$), to the extent of surpassing pressure and temperature effects. The incorporation of OH in the O2 position, in the direction of the M2 site (Chapter 9.2.), correlate to site vacancies that are consistent with a Ca-Eskola component (Koch-Müller et al., 2004; Skogby et al., 2016; Smyth et al., 1991). An increase in Pressure favours M2 vacancies in the pyroxene structure (Gasparik, 1986) and, consequently, the Ca-Eskola component significantly increases with rising pressure up to 4—6 GPa, above which it slightly decreases at pressures up to ~9—11 GPa (Knapp et al., 2013; Zhao et al., 2011). A positive correlation between water content in omphacite and Ca-Eskola component has been previously described in natural samples by (e.g. Katayama and Nakashima (2003)). Smyth et al. (1991) further show a correlation among structurally bound hydroxyl, Ca-Eskola and crystallographically oriented lamellar exsolution in the clinopyroxene. The reconstructed precursor phase obtained is a high-pressure, water–rich

(~4000 ppm) clinopyroxene. Similar results have been obtained by Terry et al. (2003) in a kyanite-eclogite at ultra-high pressure conditions.

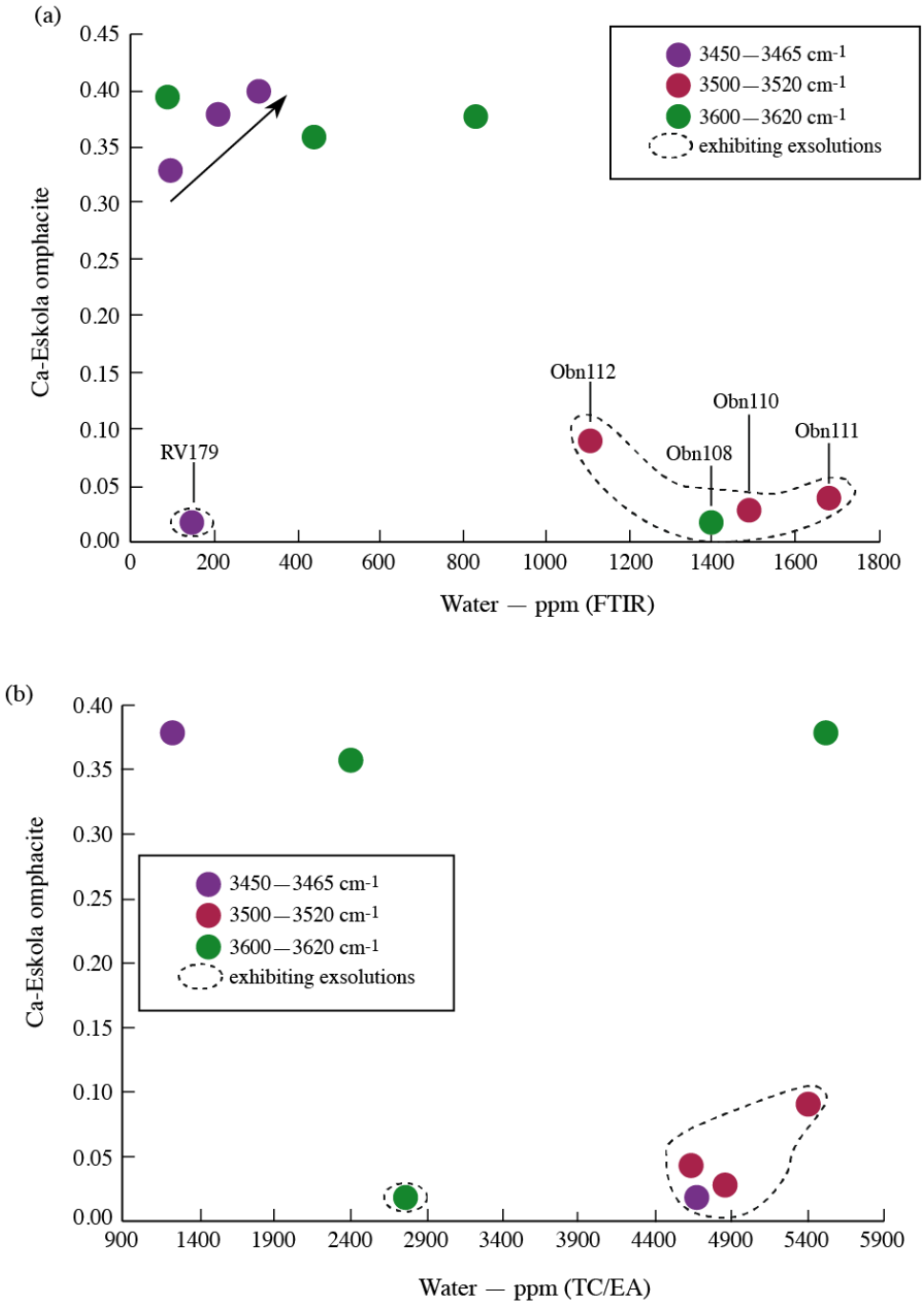

Figure IX—4. Ca-Eskola vs. water content in ppm. (a) measured by FTIR and (b) measured by TC/EA in omphacitic clinopyroxene. Samples dominated by the 3400—3465 cm-1 FTIR absorption band (purple circle solid symbol) show a positive corelation with the Ca-Eskola component and the FTIR measured water content. Samples dominated by the 3500—3520 cm-1 (red circle solid symbol) and 3600—3620 cm-1 (green circle solid symbol) show no apparent correlation. (b) There is no apparent correlation between the Ca-Eskola component and water content measured by TC/EA. All samples exhibiting lamellar exsolution textures in clinopyroxene have significantly lower Ca-Eskola.

Structural water can be incorporated as hydroxyl in different crystallographic sites in the clinopyroxene structure, leading to variable absorption bands in the IR spectra (Chapter 9.2). There is a positive correlation among the samples dominated by the 3450—3465 cm^{-1} absorption band, with 'water' content measured by FTIR increasing with the Ca-Eskola (Figure IX—4a). Samples dominated by the 3500—3520 cm^{-1} and 3600—3620 cm^{-1} bands show no correlation with the Ca-Eskola component.

This is consistent with the incorporation of hydroxyl in the O2 position associated with a cation vacancy in the M2 site, which has been previously interpreted as corresponding to the 3400—3465 cm^{-1} IR absorption band (Ingrin and Skogby, 2000). Garnet-kyanite lamellar exsolutions in omphacite in sample RV179 may have consumed the Ca-Eskola component through a reaction similar to:

$$7CaAl_2SiO_6 + 4Ca_{0.5}\square_{0.5}AlSi_2O_6 = 3Ca_3Al_2Si_3O_{12} + 6Al_2SiO_5 \qquad 9.6.$$
CaTschermak Ca-Eskola Grossular Kyanite

determined by Gasparik and Lindsley (1980). This may have caused the low Ca-Eskola abundance in samples RV179 (~0.02) and RV344 (~0.03). Comparatively low Ca-Eskola values are found in all samples exhibiting lamellar exsolution textures, with a kyanite-absent assemblage. It is inferred the Ca-Eskola component is destabilized and consumed in addition to CaTschermak, during grossular-rich garnet ± zoisite exsolution, however the mineral reaction is unclear in a silica-deficient clinopyroxene (i.e. Obnazhennaya eclogites).

There is no apparent correlation between the proportion of Ca-Eskola component and bulk water content measured through thermal conversion elemental analysis (Figure IX—4b). This indicates molecular water solubility in omphacite is not influenced by structural vacancies in the M2 to site or by increasing pressure.

CHAPTER X.

DISCUSSION

CHAPTER X. DISCUSSION

Earth's evolution as a planet and the development of life were strongly influenced by the presence of 'water'. The current general theory assumes that the origin of water on Earth is derived from the accreted chondritic material, nevertheless, a certain part may have been incorporated from a denser nebular atmosphere and dissolved in silicate minerals under extreme reducing conditions (Yang et al., 2016). It is very important to understand the nature of the water found in the Earth's mantle as well as the amount and mechanisms for its preservation, in order to better understand Earth's evolution and that of other planetary bodies.

10.1. Water preservation

During the high temperature (> 800°C) kimberlite ascent, hydrogen is prone to rapidly diffuse (Mackwell & Kohlstedt, 1990, Peslier, 2010). The exchange between the xenolith and its environment can translate into both water loss (due to decompression) or water gain (from the hosting magmas) and it is important to understand to what extent this affects the measured OH.

An input from the kimberlite melt/fluids would lead to water content decreasing from the rim to the core. However, in the cases where diffusion profiles have been traced, the OH amount decreases from the core to the rim, indicating water loss during ascent. Typically such profiles have been observed in olivine and garnets in peridotite xenoliths, while the associated orthopyroxene and clinopyroxene have homogenous concentrations due to slower diffusion rates (Demouchy et al., 2011, Doucet et al., 2014, Ingrin & Skogby, 2000). It is therefore believed that mantle pyroxenes reflect the 'original' water content of their source region (Sundvall & Stalder, 2011) and that they supply most of the upper mantle water budget (Kovacs et al., 2016). However, if outward diffusion processes have affected the analysed omphacites, it means they

initially stored more water and the calculated values should be taken as a minimum estimate of pre-entrainment water content.

Whether the primary garnet lost its original water content or it was systematically anhydrous it is debatable. The hydroxyl solubility in pyrope and grossular rich garnets increases with pressure up to 5GPa, after which they dehydrate below the detection limit above 7GPa, even under H2O-saturated conditions (Withers et al., 1998). Nevertheless, no intracrystalline variations have been measured and no diffusion profiles have been preserved. The hydrogrossular component integrated in the water-rich clinopyroxene at high-PT conditions, subsequently exsolved with the garnet during (decompression assisted) cooling.

10.2. Origin of water: subduction vs. metasomatism

Hydrogen concentration in mantle xenoliths has been extensively studied in peridotites, as they are significantly more abundant. There has been found no correlation between subduction-zone proximity and the water concentrations in nominally anhydrous minerals (Peslier et al., 2002), and mantle metasomatism precursory to the kimberlite eruption seems a more probable scenario (Doucet et al., 2014). However in the case of eclogites xenoliths, as shown by Katayama et al. (2006) trace amounts of water can be trapped in NAMs and carried by the subducting slab beyond the equilibrating depths of mantle eclogites. Similarly, high-pressure hydrous minerals such as lawsonite, phengite and zoisite-clinozoisite can transport and slowly release water at eclogite conditions (Maruyama & Okamoto, 2007, Poli & Schmidt, 1998). Moreover, pre-subduction faulting and fracturing of the oceanic slab often lead to highly altered hydrous conduits which could have also introduced significant amounts of water into the upper mantle (Li et al., 2008). Solubility of hydrogen has been observed to increase with pressure up to ~3.5—4GPa and afterwards decreases (Xia et al., 2010), conditions in agreement with the estimated equilibration pressures of the Obnazhennaya eclogites. The pressure estimates for Roberts Victor

eclogites, especially Type IIB (Chapter IV) are much higher ~4.5—6.5 GPa and compared to the the Obnazhennaya eclogites, Roberts victor eclogites contain significantly less 'water'. It is observed that the difference between hydrogen stored as OH, and measured by FTIR (130—1190 ppm), and the total water content including hydrogen as H_2 and H_2O, measured by TC/EA-MS (1230—5500 ppm wt.), is higher in samples equilibrated at higher pressures (>4 GPa). This could be due to an increasing hydrogen solubility in mantle minerals as H_2 and instead of OH with increasing pressure, as suggested by Yang et al. (2016). Concurrently, the oceanic protolith of Type IIB eclogites from Roberts Victor is believed to have undergone partial melt loss as shown by the strongly fractionated LREE (Chapter VII), which would further imply a part of their water content was similarly lost.

A rehydration of the mantle is the main competing hypothesis, however, it is unlikely for a metasomatic agent to enrich the lower part of the cratonic root in hydrogen and generate oxygen isotope ratios lower than mantle values as previously discussed in Chapter VII. Nevertheless, this question could be answered through further isotope studies.

10.3. Implication for the Sub-Continental Lithospheric Mantle

Clinopyroxenes are the nominally anhydrous minerals that contain the highest water concentrations in the upper mantle (Bell & Rossman, 1992b, Kovacs et al., 2012, Li et al., 2008, Peslier, 2010) and despite their lower abundance, eclogites might be the major water reservoirs in the SCLM (Ingrin & Skogby, 2000, Sundvall et al., 2008). It is questionable if such high values of >1000ppm wt H2O are representative for the upper mantle.

Water can drastically influence mantle geodynamics (Xia et al., 2010) through changing physical and chemical properties in minerals (Kolesnichenko et al., 2016), the mechanical strength and internal rate of ionic diffusion of the host mineral (Bell & Rossman, 1992b), partial melting (Green, 1973) and deformation as well as mantle rheology (Hirth & Kohlstedt, 1996)

and electrical (Karato, 1990) and thermal conductivity (Katayama et al., 2006). Behaving incompatible during melting (Hauri et al., 2006, Peslier, 2010), the smallest amounts of water can change the depth at which partial melting occurs and extensively the formation of the peridotitic SCLM. Sheared peridotites have higher OH contents than the undeformed ones showing a connection between deformation and water, although the interdependency between the two is unclear (Kolesnichenko et al., 2016). Both water storage as well as subsequent water extraction from NAMs via partial melting, control the viscosity of the upper mantle (Hirth & Kohlstedt, 1996). This rheology changes will further influence the depth of the LAB, leading to significant thinning (by up to ~100km) of the lithosphere beneath ancient cratons (Li et al., 2008). The implications on vertical thermal distribution in such a scenario are still unclear, however this changes in viscosity can lead to lateral pressure gradients controlling melt migration (Hirth & Kohlstedt, 1996).

Moreover, a wet lithosphere raises the question of craton stability. High water content in SCLM is incoherent with a rheologically strong cratonic mantle that can sustain asthenospheric flow (Li et al., 2008). It has been suggested that the hydrous upper mantle is underlined by a highly refractory peridotite layer, which prevents the delamination of the cratonic root (Peslier, 2010). This is further supported by subsequent depletions in iron and incompatible trace elements that would decrease the density and the heat production through radioactive decay, ensuring the buoyancy and longevity of the craton (Doucet et al., 2014, Pollack & Chapman, 1977).

Alternatively, kimberlite sampling could be biased and either the presence of water, or the same mechanisms that lead to water storage, favour the kimberlite path (Doucet et al., 2014). Local changes in the rheology of the mantle can lead to a preferential ascent of the kimberlite. In such a scenario, the water content in the sampled xenoliths is not representative for the upper mantle, but more likely for localized hydrous regions (Peslier et al., 2012). Better constraints

could be applied through a more extensive study of water in eclogite xenoliths from kimberlites, throughout a geographically broader setting.

CHAPTER XI.

CONCLUSIONS and FUTURE WORK

CHAPTER XI. CONCLUSIONS and FUTURE WORK

(1) Bimineralic eclogites from the Kaapvaal and the Siberian cratons, showing little or no interaction with kimberlite-derived metasomatic fluids, can be defined as high-magnesium (Type IIA) and low-magnesium (Type IIB) eclogites. Based on reconstructed whole-rock major and trace element compositions and oxygen isotope ratios, both compositional types are interpreted to be derived from an Archaean oceanic crust issued from an evolved picritic liquid, which underwent low- to high-temperature hydrothermal alteration. Type IIB eclogites are buried at higher depths and have suffered a small degree of melt loss before or during eclogitization. It is still unclear whether both types are derived from the same oceanic crust, or formed during different tectonic events, nevertheless they are believed to represent the precursory rock of metasomatized eclogite xenoliths.

(2) Coesite-, kyanite- bearing eclogites, comparable to bimineralic eclogites, show positive Sr and Eu anomalies and based on resconstructed whole-rock compositions are interpreted to be derived from a gabbroic protolith, whereas corundum-bearing eclogites would correspond to a pyroxene-dominated crustal cumulate.

(3) The studied non-metasomatized eclogites predominantly have oxygen isotope ratios lower than to asthenospheric mantle and one corundum-bearing eclogite from Roberts Victor mine has reconstructed bulk-rock $\delta^{18}O$ values of 1.4 ‰ which is the lowest ratio measured in mantle eclogites. A metasomatic agent with extremely low- $\delta^{18}O$ values overprinting the lower part of the cratonic root, without reequilibrating with the surrounding peridotitic mantle is considered unlikely. It is thus inferred the oxygen isotope ratios in non-metasomatized eclogites are inherited from the Palaeoproterozoic protolith. This implies that in the Archaean, the temperatures of seawater-rock interactions were much higher and/or Archaean mantle had lower $\delta^{18}O$ values than the modern mantle.

(4) Four corundum-bearing eclogite xenoliths from the Obnazhennaya kimberlite show lamellar and lens-shaped exsolutions of garnet, garnet-zoisite and amphibole needles, hosted in

omphacite. Al, Si and Mg diffusion profiles perpendicular to the exsolution and reconstructed trace element composition of precursory clinopyroxene, indicate zoisite was dissolved in the omphacite at higher temperature and an important quantity of hydroxyl can be incorporated by eclogitic clinopyroxene in the upper mantle.

(5) Hydrogen, referred to as 'water' can be incorporated in omphacite as OH^-, H_2 and H_2O. Water stored as hydroxyl is commonly structurally bound, accommodated by point defects (substitution of interstitial or structural atoms, or atomic vacancies), linear defects (dislocations in distorted lattices), planar defects (grain boundaries) and volume defects (inclusions associated with a cluster of point), characterized by different absorption bands in the Infrared Spectra. The incorporation of molecular water (H_2) is still poorly understood and it may be constrained by a highly reducing, primitive environment and the stability of ferric iron.

(6) Water quantification in omphacite is difficult due to discrepancies among different analytical methods. Estimates based on FTIR correspond to hydroxyl water and vary from 124—609 ppm and 130—1191 ppm in Roberts Victor eclogites and between 929—1413 ppm and 1576—2398 ppm in Obnazhennaya eclogites, depending on the absorption coefficient used in the calculus. Bulk water estimates based on ERDA analysis (428—795 ppm for Roberts Victor and ~1173±38 ppm for Obnazhennaya) are within the same range as the FTIR. This is in disagreement with bulk water estimates measured by SIMS and TC/EA-MS, which are roughly between 2 and 20 times higher (1230—5500 ppm for Roberts Victor and 2750—5400 ppm with TC/EA and 3870—6170 ppm with SIMS in Obnazhennaya eclogitic clinopyroxene). The discrepancies between the different measures may be due to the intrinsic nature of each technique.

(7) The associated primary garnets either can't incorporate significant amounts of water or they lose it very rapidly with thermobarometric changes. Grossular-rich garnet lamellae exsolved from the OH-bearing omphacites in the Obnazhennata eclogited, contain up to ~1950 ppm wt. H_2O as hydrogrossular molecules.

(8) The recalculated whole-rock water content varies between 72 and 953 ppm wt. H_2O in Roberts Victor eclogites and 459—1367 ppm in the Obnazhennaya eclogites, calculated using the hydroxyl estimates, or between 241—4400 ppm and 633—3132 ppm respectively, based on the TC/EA-MS bulk measurements. It should be noted that even the lower water estimates (based on FTIR analysis) of mantle eclogites are generally higher than the maximum water content measured in the surrounding peridotites, estimated between <1 and 394 ppm wt. beneath the Siberian craton and between 0 and 200 ppm wt. beneath the Kaapvaal craton.

(9) It is inferred that although eclogites represent a small fraction of the upper mantle, they may be a main water reservoir. The implications of such high water contents in the lithospheric mantle have major consequences on the mechanical strength, element diffusion, deformation, rheology, partial melting and electrical and thermal conductivity, thus influencing the cratonic keel longevity, mantle properties and the global water cycle.

(10) The water found in nominally anhydrous minerals in the upper mantle is most probably incorporated during the subduction of the oceanic crust, as a hydrous metasomatic agent with extremely low $\delta^{18}O$ values seems unrealistic. Nevertheless, future studies of hydrogen and lithium isotopes would be useful tools in answering this question. Furthermore, extensive dating of both Type IIA and Type IIB eclogites are needed in order to better understand the mantle eclogites petrogenesis and the link between the two compositional types.

BIBLIOGRAPHY

CHAPTER XII. BIBLIOGRAPHY

Abouchami, W., Boher, M., Michard, A. and Albarède, F. (1990) A major 2.1 Ga event of mafic magmatism in West Africa: an early stage of crustal accretion. Journal of Geophysical Research 95, 17605-17629.

Ackermann, L., Cemic, L. and Langer, K. (1983) Hydrogarnet substitution in pyrope: a possible location fot "water" in the mantle. Earth Planet. Sci. Lett. 62, 208-214.

Aines, D.R. and Rossman, G.R. (1984a) The hydrous component in garnets: pyralspites. American Mineralogist 69, 1116-1126.

Aines, D.R. and Rossman, G.R. (1984b) Water content of mantle garnets. Geology 12, 720-723

Alifirova, T.A., Pokhilenko, L., Ovchinnikov, Y.I., Donnelly, C.L., Riches, A.J.V. and Taylor, L.A. (2012) Petrologic origin of exsolution textures in mantle minerals: evidence in pyroxenitic xenoliths from Yakutia kimberlites. International Geology Review 54, 1071-1092.

Allègre, C.J. and Rousseau, D. (1984) The growth of the continent through geological time studied by Nd isotope analysis of shales. Earth Planet. Sci. Lett. 67, 19-34.

Aoki, K.-I., Fujimaki, H. and Kitamura, M. (1980) Exsolved garnet-bearing pyroxene megacrysts from some South African kimberlites. Lithos 13, 269-279.

Armstrong, R.L. and Harmon, R.S. (1981) Radiogenic isotopes: The case for crustal recycling on a near-steady-state no-continental growth earth (and dicussion). Philosophical Transactions of the Royal Society of London. Series A, Mathemarical and Physical Sciences 301, 443-472.

Arndt, N.T., Coltice, N., Helmstaedt, H. and Gregoire, M. (2009) Origin of Archean subcontinental lithospheric mantle: Some petrological constraints. Lithos, 61-71.

Ater, P.C., Eggler, D.H. and McCallum, M.E. (1984) Petrology and geochemistry of mantle eclogite xenoliths from Colorado-Wyoming kimberlites: recycled ocean crust?, in: J., K.-P. (Ed.), Kimberlites II: The Mantle and the Crust-Mantle Relationships. Elsevier, Amsterdam, pp. 309-318.

Aubaud, C., Bureau, H., Raepsaet, C., Khodja, H., Withers, A.C., Hirschmann, M.M. and Bell, D.R. (2009) Calibration of the infrared molar absorption coefficients for H in olivine, clinopyroxene and rhyolitic glass by elastic recoil detection analysis. Chemical Geology, 78-86.

Aulbach, S., Massuyeau, M. and Gaillard, F. (2017) Origins of cratonic mantle discontinuities: A view from petrology, gepchemistry and thermodynamic models. Lithos, 364-382.

Aulbach, S., Gerdes, A. and Viljoen, K.S. (2016) Formation of diamondiferous kyanite-eclogite in a subduction mélange. Geochimica et Cosmochimica Acta 179, 156-176.

Aulbach, S. and Viljoen, K.S. (2015) Eclogite xenoliths from the Lace kimberlite, Kaapvaal craton: from convecting mantle source to palaeo-ocean floor and back. Earth Planet. Sci. Lett., 274-286.

Aulbach, S. (2012) Craton nucleation and formation of thick lithospheric roots. Lithos 149, 16-30.

Baertschi, P. (1976) Absolute 18O content of standard mean ocean water. Earth Planet. Sci. Lett. 31, 341-344.

Barth, M., G., Rudnick, R.L., Horn, I., McDonough, W.F., Spicuzza, M.J., Valley, J.W. and Haggerty, S.E. (2002) Geochemistry of xenolithic eclogites from West Africa, part 2: Origins of the high MgO eclogites. Geochimica et Cosmochimica Acta 66, 4325-4345.

Barth, M.G., Rudnick, R.L., Horn, I., McDonough, W.F., Spicuzza, M.J., Valley, J. and Haggerty, S.E. (2001) Geochemistry of xenolithic eclogites from West Africa, Part I: A link between low MgO eclogites and Archean crust formation. Geochimica et Cosmochimica Acta 65, 1499-1527.

Beard, B.L., Fraracci, K.N., Taylor, L.A., Snyder, G.A., Clayton, R.N., Mayeda, T.K. and Sobolev, N.V. (1996) Petrography and geochemistry of eclogites from the Mir kimberlite, Yakutia, Russia. Contribution to Mineral Petrology, 293-310.

Bell, D.R., Ihinger, P.D. and Rossman, G.R. (1995) Quantitative analysis of trace OH in garnet and pyroxenes. American Mineralogist 80, 465-474.

Bell, D.R. and Rossman, G.R. (1992a) The distribution of hydroxyl in garnets from the subcontinental mantle of southern Africa. Contribution to Mineral Petrology, 161-178.

Bell, D.R. and Rossman, G.R. (1992b) Water in Earth's Mantle: The Role of Nominally Anhydrous Minerals. Science 255, 1391-1397.

Beran, A. (1976) Messung des Ultrarot-Pleochroismus von Mineralen. XIV. Der Pleochroismus des OH-Streckfrequenz in Diopsid. Tschermaks Min. Petr. Mitt., 79-85.

Bindeman, I. (2008) Oxygen Isotopes in Mantle and Crustal Magmas as Revealed by Single Crystal Analysis. Rev. Mineral. Geochem. 69, 445-478.

Birkett, T.C. and Trzcienski Jr., W.E. (1984) Hydrogarnet: multi-site hydrogen occupancy in the garnet structure. Canadian Mineralogist 22, 675-680.

Bleeker, W. (2002) Archean tectonics: a review, with illustrations from the Slave craton. Geological Society, London, Special Publication 199, 151-181.

Bleeker, W. and Davis, B.W. (2004) What is a craton? How many are there? How do they relate? And how did they form?, in: American Geophysical Union, S.M. (Ed.), AGU, San Francisco.

Boyd, F.R., Pokhilenko, N.P., Pearson, D.G., Mertzman, S.A., Sobolev, N.V. and Finger, L.W. (1997) Composition of the Siberian cratonic mantle: evidence from Udachnaya peridotite xenoliths. Contribution to Mineral Petrology, 228-246.

Boyet, M. and Carlson, R.W. (2005) 142Nd Evidence for Early (>4.53 Ga) Global Differentiation of the Silicate Earth. Science 309, 576-581.

Bromiley, G.D. and Keppler, H. (2004) An experimental investigation of hydroxyl solubility in jadeite and Na-rich clinopyroxenes. Contribution to Mineral Petrology 147, 189-200.

Brown, M. (2006) Duality of thermal regimes in the distinctive chracteristic of plate tectoinics since the Neoarchean. Geology 34, 961-964.

Bureau, H., Raepsaet, C., Khodja, H., Carraro, A. and Aubaud, C. (2009) Determination of hydrogen content in geological samples using Elastic Recoil Detection Analysis (ERDA). Geochimica et Cosmochimica Acta, 3311-3322.

Bouvier, A., Vervoot, J.D. and Patchett, P.J. (2008) The Lu-Hf and Sm-Nd isotopic composition of CHUR: Constraints from the unequilibrated chondrites and implications for the bulk composition of terrestrial planets. Earth Planet. Sci. Lett., 48-57.

Byerly, B.L., Kareem, K., Bao, H. and Byerly, G.R. (2017) Early Earth mantle heterogeneity revealed by light oxygen isotopes of Archean komatiites. Nature Geoscience 10, 1-5.

Campbell, I.H. (2001) Identification of ancient mantle plumes. Special paper of the Geological Society of America, 1-21.

Caporuscio, F.A. and Smyth, J.R. (1990) Trace elements crystal chemistry of mantle eclogites. Contribution to Mineral Petrology, 550-561.

Carswell, D.A. and Zhang, R.Y. (1999) Petrographic characteristics and metamorphic evolution of untra-high pressure eclogites in plate-collision belts. International Geology Review 41, 781-798.

Cawood, P., Kröner, A., Collins, W.J., Kusky, T.M., Mooney, W.D. and Windley, B.F. (2009) Accretionary orogens through Earth history, in: Cawood, P., Kröner, A. (Eds.), Earth Accretionary Systems in Space and Time. Geological Society, London, pp. 1-36.

Chardon, D., Gapais, D. and Cagnard, F. (2009) Flow of ultra-hot orogens: A view from the Precambrian, clues for the Phanerozoic. Tectonophysics, 105-118.

Clark, J.R. and Papike, J.J. (1968) Crustal-chemical characterization of omphacites. American Mineralogist 53, 840-868.

Coleman, R.G., Lee, D.E., Beatty, L.B. and Brannock, W.W. (1965) Eclogites and eclogites: their differences and similarities. Geological Society of America Bulletin, 483-508.

Condie, K.C. and Kröner, A. (2013) The building blocks of continental crust: Evidence for a major change in the tectonic setting of continental growth at the end of the Archean. Gondwana Research 23, 394-402.

D'Amico, C., Ana, R.C., Felice, G. and Ghedini, M. (1995) Eclogites and jades as prehistoric implements in Europe. A case of petrology applied to Cultural Heritage. European Journal of Mineralogy 7, 29-42.

Darken, L.S. (1958). In The Physical Chemistry of metallic solutions and intermetallic compounds. Her Majesty's Stationary Office, London.

Daudin, L., Khodja, H. and Gallien, J.P. (2003) Development of "position-charge-time" tagged spectrometry for ion beam microanalysis. Nucl. Instrum. Methods Phys. Res. B, 153-158.

Davies, G.F. (1995) Punctuated tectonic evolution of the earth. Earth Planet. Sci. Lett. 136, 363-379.

Davies, G.F. (1979) Thickness and thermal history of continental crust and root zones. Earth Planet. Sci. Lett. 44, 231-238.

Dawson, J.B. (2004) A fertile harzburgite-garnet lherzolite transition: possible inferences for the roles of strain and metasomatism in upper mantle peridotites. Lithos 77, 553-569.

de Wit, M.J., Roering, C., Hart, R.J., Armstrong, R.A., de Ronde, C.E.J., Green, R.W.E., Tredoux, M., Peberdy, E. and Hart, R.A. (1992) Formation of an Archean continent. Nature 357, 553-562.

Deer, W.A., Howie, R.A. and Zussman, J. (1986) Epidote Group, Rock-forming minerals. Longman Group, UK, pp. 4-43.

Deloule, E., Paillat, O., Pichavant, M. and Scaillet, B. (1995) Ion microprobe determination of water in silicate glasses: methods and applications. Chemical Geology, 19-28.

Demouchy, S. and Bolfan-Casanova, N. (2016) Distribution and transport of hydrogen in the lithospheric mantle: A review. Lithos, 402-425.

Demouchy, S., Jacobsen, S.E., Gaillard, F. and Stern, C.R. (2011) Rapid magma ascent recorded by water diffusion profiles in mantle olivine. Geology 34, 429-432.

Dobosi, G., Kurat, G., Wall, F. and Jeffries, T. (2007) Trace element fractionation during exsolution of garnet from clinopyroxene in an eclogite xenolith from Obnazhennaya (Siberia), Goldschmidt. Cambridge Publications, Cologne, Germany.

Dolomieu, D.G. (1794) Mémoire sur les roches composées en général, et particulièrement sur les pétro-silex, les trapps et les roches de corne, pour servir à la distribution méthodique des produits volcaniques (1), in: Lamétherie, J.-C. (Ed.), Journal de Physique, de Chimie, d'Histoire naturelle et des Arts CUCHET, Libraire, Paris, pp. 187-188.

Doucet, L.S., Ionov, D.A. and Golovin, A.V. (2015) Paleoproterozoic formation age for the Siberian cratonic mantle: Hf and Nd isotope data on refractory peridotite xenoliths from the Udachnaya kimberlite. Chemical Geology 391, 42-55.

Doucet, L.S., Peslier, A.H., Ionov, D.A., Brandon, A.D., Golovin, A.V., Goncharov, A.G. and Ashchepkov, I.V. (2014) High water contents in the Siberian cratonic mantle linked to metasomatism: An FTIR study of Udachnaya peridotite xenoliths. Geochimica et Cosmochimica Acta, 159-187.

Eiler, J.M. (2001) Oxygen isotope variations of basaltic lavas and upper mantle rocks. Rev. Mineral. Geochem. 43, 319-364.

Eskola, P. (1920) The mineral facies of rocks. Norsl Geologisk Tidsskrift VI, 143-194.

Fermor, L.L. (1912) Preliminary note on the origin of meteorites. Journal and Proceedings of the Asiatic Society of Bengal (new ser.) VIII, 316-317.

Field, M., Stiefenhofer, J., Robey, J. and Kurszlaukis, S. (2008) Kimberlite-hosted diamond deposits of southern Africa: A review. Ore Geology Reviews, 33-75.

Fyfe, W.S. (1970) Lattice energies, phase transformation and volatiles in the mantle. Phys. Earth Planet. Interiors 3, 196-200.

Garlick, G.D., MacGregor, I.D. and Vogel, D.E. (1971) Oxygen isotope ratios in eclogites from kimberlites. Science 172, 1025-1027.

Gasparik, T. (1984) Experimentally determined stability of clinopyroxene + garnet + corundum in the system CaO-MgO-Al2O3-SiO2. American Mineralogist 69, 1025-1035.

Gasparik, T. (1986) Experimental study of subsolidus phase relations and mixing properties of clinopyroxene in the silica-saturated system CaO-MgO-Al2O3-SiO2. American Mineralogist 71, 686-693.

Gasparik, T. and Lindsley, D.H. (1980) Phase equilibria at high pressure of pyroxenes containing monovalent and trivalent ions, in: Prewitt, C.H. (Ed.), Pyroxenes. Mineralogical Society of America, Washington D.C.

Godard, G. (2001) Eclogites and their geodynamic interpretation: a history. Journal of Geodynamics 32, 165-203.

Goncharov, A.G., Ionov, D.A., Doucet, L.S. and Pokhilenko, L. (2012) Thermal state, oxygen fugacity and COH fluid specification in cratonic lithospheric mantle: New data on peridotite xenoliths from the Udachnaya kimberlite, Siberia. Earth Planet. Sci. Lett. 357-358, 99-110.

Gong, B., Zheng, Y.-F. and Chen, R.-X. (2007a) An online method combining a thermal conversion elemental analyzer with isotope ratio mass spectrometry for the determination of hydrogen isotope composition and water concentration in geological samples. Rapid Communications in mass spectrometry 21, 1386-1392.

Gong, B., Zheng, Y.-F. and Chen, R.-X. (2007b) TC/EA-MS online determination of hydrogen isotope composition and water concentration in eclogitic garnet. Phys Chem Minerals 34, 687-698.

Gréau, Y., Huang, J.-X., Griffin, W.L., Renac, C., Alard, O. and O'Reilly, S.Y. (2011) Type I eclogites from Roberts Victor kimberlites: Products of extensive mantle metasomatism. Geochimica et Cosmochimica Acta, 6927-6954.

Green, D.H. (1973) Experimental melting studies on a model upper mantle composition at high pressures under water-saturated and water-undersaturated conditions. Earth Planet. Sci. Lett. 19, 37-53.

Green, D.H. and Ringwood, A.E. (1967a) An experimental investigation of the gabbro to eclogite transformation and its petrological applications. Geochimica et Cosmochimica Acta 31, 767-833.

Green, D.H. and Ringwood, A.E. (1967b) The stability fields of aluminous pyroxene peridotite and garnet peridotite and their relevance in upper mantle structure. Earth Planet. Sci. Lett. 3, 151-160.

Green, D.H. (1966) The origin of the "eclogites" from Salt Lake crater, Hawaii. Earth Planet. Sci. Lett. 1, 414-420.

Gregoire, M., Mattielli, N., Nicollet, C., Cottin, J.-Y., Leyrit, H., Weis, D., Shimizu, N. and Giret, A. (1994) Oceanic mafic granulite xenoliths from the Kerguelen archipelago. Nature 367, 360-363.

Gregory, R.T. and Taylor, H.P. (1981) An Oxygen Isotope profile in a section of Cretaceous Oceanic Crust, Samail Ophiolite, Oman: Evidence from d18O Buffering in the Oceans by Deep (>5km) Seawater-Hydrothermal Circulation at Mid-Ocean Ridges. Journal of Geophysical Research 86, 2737-2755.

Griffin, W., Belousova, E.A., O'Neil, H.S.C., O'Reilly, S.Y., Malkovets, V.G., Pearson, N.J., Spetsius, S. and Wilde, S.A. (2014) The world turns over: Hadean-Archean crust-mantle evolution. Lithos 189, 2-15.

Griffin, W., Ryan, C.G., Kaminsky, F.V., O'Reilly, S.Y., Natapov, L.M., Win, T.T., Kinny, P.D. and Ilupin, L.M. (1999) The Siberian lithosphere traverse: mantle terranes and the assembly of the Siberian Craton. Tectonophysics, 1-35.

Griffin, W.L. and O'Reilly, S.Y. (2007) Cratonic lithospheric mantle: Is there anything subducted? Episodes 30, 43-53.

Griffin, W., O'Reilly, S.Y., Natapov, L.M. and Ryan, C.G. (2003) The evolution of the lithospheric mantle beneath the Kalahari craton and its margins. Lithos 71, 215-241.

Gurenko, A.A., Bindeman, I. and Chaussidon, M. (2011) Oxygen isotope heterogeneity of the mantle beneath the Canary Island: insights from olivine phenocrysts. Contribution to Mineral Petrology 162, 349-363.

Haggerty, S.E. and Sautter, V. (1990) Ultradeep (Greater than 300 kilometers), Ultramafic upper mantle xenoliths. Science 248, 993-996.

Harris, C. and Vogeli, J. (2010) Oxygen isotope composition of garnet in the peninsula granite, cape granite suite, South Africa: constraints on melting and emplacement mechanisms. South African Journal of Geology 113, 385-396.

Harte, B. and Gurney, J. (1975) Evolution of clinopyroxene and garnet in an eclogite nodule from the Roberts Victor kimberlite pipe, South Africa. Phys Chem Earth, 367-387.

Hatton, C.J. (1978) The geochemistry and origin of xenoliths from the Roberts Victor mine. University of Cape Town, CT, SA, p. 498.

Hatton, C.J. and Gurney, J. (1977) Igneous fractionation trends in Roberts-Victor eclogites., 2nd International Kimberlite Conference.

Hauri, E.H., Gaetani, G.A. and Green, T.H. (2006) Partitioning of water during melting of the Earth's upper mantle at H2O-undersaturated conditions. Earth Planet. Sci. Lett., 715-734.

Haüy, R.J. (1822-1823) Silice combinée avec la magnésie, Traité de minéralogie. Tome 1. Seconde édition, revue, corrigée, et considérablement augmentée par l'auteur. Bachelier, Paris, p. 456.

Hawkesworth, C., Cawood, P., Kemp, T., Storey, C. and Dhuime, B. (2009) A matter of preservation. Science 323, 49-50.

Helmstaedt, H. and Schulze, D.J. (1989) Southern African kimberlites and their mantle sample: implications for Archean tectonics and lithosphere evolution. Kimberlites and related rocks 1, 358-368.

Helmstaedt, H. and Doig, R. (1975) Eclogite nodules from kimberlite pipes of the Colorado plateau - samples of subducted francinsca-type oceanic lithosphere. Phys Chem Earth 9, 95-112.

Hirth, G. and Kohlstedt, D.L. (1996) Water in the oceanic upper mantle: implications for rheology, melt extraction and the evolution of the lithosphere. Earth Planet. Sci. Lett., 93-108.

Hoffman, P.F. (1990) Geological constraints on the origin of the mantle root beneath the Canadian shield. Philosophical Transactions of the Royal Society of London. Series A 331, 523-532.

Huang, J.-X., Xiang, Y., An, Y., Griffin, W., Gréau, Y., Xie, L., Pearson, D.G., Yu, H. and O'Reilly, S.Y. (2016) Magnesium and oxygen isotopes in Roberts Victor eclogites. Chemical Geology, 73-83.

Huang, J.-X., Griffin, W.L., Gréau, Y., Pearson, N.J., O'Reilly, S.Y., Cliff, J. and Martin, L. (2014) Unmasking xenolithic eclogites: Progressive metasomatism of a key Roberts Victor sample. Chemical Geology, 56-65.

Huang, J.-X., Li, P., Griffin, W.L., Xia, Q.-K., Gréau, Y., Pearson, N.J. and O'Reilly, S.Y. (2014) Water contents of Roberts Victor xenolithic eclogites: primary and metasomatic controls. Contribution to Mineral Petrology.

Huang, J.-X., Gréau, Y., Griffin, W.L., O'Reilly, S.Y. and Pearson, N.J. (2012) Multi-stage origin of Roberts Victor eclogites: Progressive metasomatism and its isotopic effects. Lithos, 161-181.

Huang, J., Zhong, S. and van Hunen, J. (2003) Controls on sublithospheric small-scale convection. Journal of Geophysical Research 108, 2405.

Ingrin, J., Latrous, K., Doukhan, J.-C. and Doukhan, N. (1989) Water in diopside: an electron microscopy and infrared spectroscopy study. Eur. J. Mineral. 1, 327-341.

Ingrin, J. and Skogby, H. (2000) Hydrogen in nominally anhydrous upper-mantle minerals: concentration levels and implications. Eur. J. Mineral. 12, 543-570.

Ionov, D.A., Carlson, R.W., Doucet, L.S., Golovin, A.V. and Oleinikov, O.B. (2015) The age and history of the lithospheric mantle of the Siberian craton: Re-Os and PGE study of peridotite xenoliths from the Obnazhennaya kimberlite. Earth Planet. Sci. Lett., 108-119.

Ionov, D.A., Doucet, L.S. and Ashchepkov, I.V. (2010) Composition of the Lithospheric Mantle in the Siberian Craton: New Constraints from Fresh Peridotites in the Udachnaya-East Kimberlite. Journal of Petrology 51, 2177-2210.

Ionov, D.A., Harmon, R.S., France-Lanord, C., Greenwood, P.B. and Ashchepkov, I.V. (1994) Oxygen isotope composition of garnet and spinel peridotites in the continental mantle: Evidence from the Vitim xenoltih suite, southern Siberia. Geochimica et Cosmochimica Acta 58, 1463-1470.

Ireland, T.R., Rudnick, R.L. and Spetsius, Z.V. (1994) Trace elements in diamond inclusions from eclogites reveal link to Archean granites. Earth Planet. Sci. Lett. 128.

Jacob, D.E., Bizimis, M. and Salters, V.J.M. (2005) Lu-Hf and geochemical systematics of recycled ancient oceanic crust: evidence from Roberts Victor eclogites. Contribution to Mineral Petrology, 707-720.

Jacob, D.E. (2004) Nature and origin of eclogite xenoliths from kimberlites. Lithos, 295-316.

Jacob, D.E., Schmickler, B. and Schulze, D.J. (2003) Trace element geochemistry of coesite-bearing eclogites from the Roberts Victor kimberlite, Kaapvaal craton. Lithos, 337-351.

Jacob, D.E. and Foley, S.F. (1999) Evidence for Archean ocean crust with low high field strength element signature from diamondiferous eclogite xenoliths. Lithos, 317-336.

Jacob, D.E., Jagoutz, E., Lowry, D., Mattey, D. and Kudrjavttseva, G. (1994) Diamondiferous eclogites from Siberia: remnants of Archean oceanic crust. Geochimica et Cosmochimica Acta 58, 5191-5207.

Jagoutz, E. (1988) Nd and Sr systematics in an eclogite xenolith from Tanzania: Evidence for frozen mineral equilibria in the continental lithosphere. Geochimica et Cosmochimica Acta 52, 1285-1293.

Jagoutz, E., Dawson, J.B., Hoernes, S., Spettel, B. and Wänke, H. (1984) Anorthositic oceanic crust in the Archean Earth. Lunar Planetary Science 15, 395-396.

James, D.E., Niu, F. and Rokosky, J. (2003) Crustal structure of the Kaapvaal craton and its significance for early crustal evolution. Lithos, 413-429.

Jerde, E.A., Taylor, L.A., Crozaz, G. and Sobolev, N.V. (1993) Exsolution of garnet within clinopyroxene of mantle eclogites: major- and trace-element chemistry. Contribution to Mineral Petrology, 148-159.

Kamenetsky, V.S., Golovin, A.V., Maas, R., Giuliani, A., Kamenetsky, M.B. and Weiss, Y. (2014) Towards a new model for kimberlite petrogenesis: Evidence from unaltered kimberlites and mantle minerals. Earth Science Reviews 139, 145-167.

Karato, S. (1990) The role of hydrogen in the electrical conductivity of the upper mantle. Letters to Nature 347, 272-273.

Katayama, I., Suyama, Y., Ando, J. and Komiya, T. (2009) Mineral chemistry and P-T condition of granular and sheared peridotite xenoliths from Kimberley, South Africa: Origin of the textural variation in the cratonic mantle. Lithos, 333-340.

Katayama, I., Nakashima, S. and Yurimoto, H. (2006) Water content in natural eclogite and implication for water transport into the deep upper mantle. Lithos, 245-259.

Katayama, I. and Nakashima, S. (2003) Hydroxyl in clinopyroxene from the deep subducted crust: Evidence for H2O transport into the mantle. American Mineralogist 88, 229-234.

Khodja, H., Berthoumieux, E., Daudin, L. and Gallien, J.P. (2001) The Pierre Sue Laboratory nuclear microprobe as a multi-disciplinary analysis tool. Nuclear instruments and Methods. Physics Reserch Section B: Beam interactions with Materials and Atoms, 83-86.

Kieffer, S.W. (1982) Thermodynamics and Lattice Vibrations of Minerals: Applications to Phase Equilibria, Isotopic Fractionation, and High-Pressure Thermodynamic Properties. Reviews of Geophysics and Space Physics 20, 827-849.

Knapp, N., Woodland, A.B. and Klimm, K. (2013) Experimental constraints in the CMAS system of the Ca-Eskola content in eclogitic clinopyroxene. Eur. J. Mineral. 25, 579-596.

Kobussen, A.F., Christensen, N.I. and Thybo, H. (2006) Constraints on seismic velocity anomalies beneath the Siberian craton from xenoliths and petrophysics. Tectonophysics 425, 123-135.

Koch-Müller, M., Abs-Wurmbach, I., Rhede, D., Kahlenberg, V. and Matsyuk, S.S. (2007) Dehydration experiments on natural omphacites: qualitative and quantitative characterization by various spectroscopic methods. Phys Chem Minerals, 663-678.

Koch-Müller, M., Matsyuk, S.S. and Wirth, R. (2004) Hydroxyl in omphacites and omphacitic clinopyroxenes of the upper mantle to lower crustal origin beneath the Siberian platform. American Mineralogist 89, 921-931

Kolesnichenko, M.V., Zedgenizov, D.A., Litasov, K.D., Safonova, I.Y. and Ragozin, A.L. (2016) Heterogeneous distribution of water in the mantle beneath the central Siberian Craton: Implications from the Udachnaya Kimberlite Pipe. Gondwana Research.

Komiya, T., Maruyama, S., Masuda, T., Nohda, S., Hayashi, M. and Okamoto, K. (1999) Plate tectonics at 3.8-3.7 Ga: Field evidence from the Isua accretionary complex, Southern West Greenland. Journal of Geology 107, 515-554.

Kovacs, I., Demény, A., Czuppon, G., Lécuyer, C., Fourel, F., Xia, Q.-K., Liu, J., Pintér, Z., Kiraly, E., Török, K., Szabo, A., Deloule, E., Falus, G., Fancsik, T., Zajacz, Z., Sandorné Kovacs, J. and Udvardi, B. (2016) Water concentrations and hydrogen isotope compositions of alkaline basalt hosted clinopyroxene megacrysts and amphibole clinopyroxenites: the role of structural hydroxyl groups and molecular water. Contribution to Mineral Petrology 171.

Kovacs, I., Green, D.H., Rosenthal, A., Hermann, J., O'Neil, H.S.C., Hibberson, W.O. and Udvardi, B. (2012) An experimental study of water in nominally anhydrous minerals in the upper mantle near the water saturated solidus. Journal of Petrology 53, 2067-2093.

Kovacs, I., Hermann, J., O'Neill, H.S.C., Gerald, J.F., Sambridge, M. and Horvath, G. (2008) Quantitative absorbance spectroscopy with unpolarized light: Part II. Experimental evaluation and development of a protocol for quantitative analysis of mineral IR spectra. American Mineralogist 93, 765-778.

Krogh, E. (1988) The garnet-clinopyroxene Fe–Mg geothermometer– a reinterpretation of existing experimental data. Contribution to Mineral Petrology 44-48.

Lacroix, A. (1891) Etude pétrographique des éclogites de la Loire-inférieure. Bulletin de la Societé des Sciences naturelles de l'Ouest de la France I, 81-114.

Lappin, M.A. (1978) The evolution of a grospydite from the Roberts Victor Mine, South Africa. Contribution to Mineral Petrology, 229-241.

Lappin, M.A. and Dawson, J.B. (1975) Two Roberts Victor cumulate eclogites and their re-equilibration. Phys Chem Earth 9, 351-365.

Lee, C.-T.A., Luffi, P. and Chin, E. (2011) Building and destroying continental mantle. Annual Review of Earth and Planetary Sciences 16.

Li, W.-Y., Teng, F.-Z., Xiao, Y. and Huang, J. (2011) High-temperature inter-mineral magnesium isotope fractionation in eclogite from the Dabie orogenm China. Earth and Planetary Science Letters, 224-230.

Li, Z.-X.A., Lee, C.-T.A., Peslier, A.H., Lenardic, A. and Mackwell, S.J. (2008) Water contents in mantle xenoliths from the Colorado Plateau and vicinity: Implications for the mantle rheology and hydration-induced thinning of continental lithosphere. Journal of Geophysical Research 113.

MacGregor, I.D. and Manton, W.I. (1986) Roberts Victor eclogites: ancient oceanic crust. Journal of Geophysical Research 91, 14063-14079.

MacGregor, I.D. and Carter, J.L. (1970) The chemistry of clinopyroxenes and garnets of eclogite and peridotite xenoliths from the Roberts Victor mine, South Africa. Phys. Earth Planet. Interiors, 391-397.

Mackwell, S.J. and Kohlstedt, D.L. (1990) Diffusion of Hydrogen in Olivine: Implications for Water in the Mantle. Journal of Geophysical Research 95, 5079-5088.

Martin, H., Moyen, J.-F., Guitreau, M., Blichert-Toft, J. and Le Pennec, J.-L. (2014) Why Archean TTG cannot be generated by MORB melting in subduction zones. Lithos, 1-13.

Martin, H., Smithies, R.H., Rapp, R., Moyen, J.-F. and Champion, D. (2005) An overview of adakite, tonalite-trondhjemite-granodiorite (TTG), and sanukitoid: relationships and some implications for crustal evolution. Lithos, 1-24.

Martin, R.F. and Donnay, G. (1972) Hydroxyl in the mantle. American Mineralogist 57, 554-570.

Matsyuk, S.S., Langer, K. and Hösch, A. (1998) Hydroxyl defects in garnets from mantle xenoliths in kimberlites of the Siberian platform. Contribution to Mineral Petrology, 163-179.

Maruyama, S. and Okamoto, K. (2007) Water transportation from the subducting slab into the mantle transition zone. Gondwana Research, 148-165.

Mattey, D., Lowry, D. and Macpherson, C. (1994) Oxygen isotope composition of mantle peridotites. Earth Planet. Sci. Lett. 128, 231-241.

Mayer, M. (1999) SIMNRA, Proceedings of the 15th International Conference on the Application of Accelerators in Research and Industry, p. 541.

McCandless, T. and Gurney, J. (1989) Sodium in garnet and potassium in clinopyroxene: criteria for classifying mantle eclogites, in: Ross, J., Jaques, A.L., Ferguson, J., Green, D.H., O'Reilly, S.Y., Danchin, R.V., Janse, A.J.A. (Eds.), Kimberlite and related rocks. Special publication — Geological Society of Australia, Perth.

McCulloch, M.T., Gregory, R.T., Wasserburg, G.J. and Taylor, H.P. (1981) Sm-Nd, Rb-Sr and 18O/16O Isotopic Systematics in an Oceanic Crustal Section: Evidence from the Samail Ophiolite. Journal of Geophysical Research 86, 2721-2735.

McDonough, W.F. and Sun, S.-S. (1995) Composition of the Earth. Chemical Geology, 223-253.

Mrazec, L. (1898) Note sur une jadéite du Piemont. Bulletin de la Societé des sciences de Bukarest 7, 195-196.

McDonough, W.F. (1991) Partial melting of subducted oceanic crust and isolation of its residual eclogitic lithology. Philosophical Transactions of the Royal Society of London. Series A 335, 407-418.

Mierdel, K., Keppler, H., Smyth, J.R. and Langenhorst, F. (2007) Water Solubility in Aluminous Orthopyroxene and the Origin of Earth's Astenosphere. Science 315, 364-368.

Müller, W., Shelley, M., Miller, P. and Broude, S. (2009) Initial performance metrics of a new custom-designed ArF excimer LA-ICPMS system coupled to a two-volume laser-ablation cell. J. Anal. At. Spectrom., 209-214.

Neal, C.R., Taylor, H.P., Davidson, J.P., Holden, P., Halliday, A.N., Nixon, P.H., Paces, J.B., Clayton, R.N. and Mayeda, T.K. (1990) Eclogites with oceanic crustal and mantle signatures from the Bellsbank kimberlite, South Africa, part 2: Sr, Nr and O istope geochemistry. Earth Planet. Sci. Lett. 99, 362-379.

Nowell, G.M., Pearson, D.G., Bell, D.R., Carlson, R.W., Smith, C.B., Kempton, P.D. and Noble, S.R. (2004) Hf isotope systematics of kimberlites and their megacrysts: new constraints on their source regions. Journal of Petrology 45, 1583-1612.

O'Hara, M.J. and Yoder, J.H.S. (1967) Formation and fractionation of basic magmas at high pressures. Scott. J. Geol., 67-117.

Ongley, J.S., Basu, A.R. and Kyser, K.T. (1987) Oxygen isotopes in coexisting garnets, clinopyroxenes and phlogopites of Roberts Victor eclogites: implications for petrogenesis and mantle metasomatism. Earth Planet. Sci. Lett. 83, 80-84.

Pearson, D.G. and Witting, N. (2008) Formation of Archean continental lithosphere and its diamonds: the root of the problem. Journal of the Geological Society 165, 895-914.

Peslier, A.H., Schönbächler, M., Busemann, H. and Karato, S.-I. (2017) Water in the Earth's interior: distribution and origin. Sapce Sci Rev 210, 1-68

Peslier, A.H., Woodland, A.B., Bell, D.R., Lazarov, M. and Lapen, T.J. (2012) Metasomatic control of water contents in the Kaapvaal cratonic mantle. Geochimica et Cosmochimica Acta, 213-246.

Peslier, A.H. (2010) A review of water contents of nominally anhydrous natural minerals in the mantles of Earth, Mars and the Moon. Journal of Volcanology and Geothermal Research, 239-258.

Peslier, A.H., Luhr, J.F. and Post, J. (2002) Low water contents in pyroxenes from spinel-peridotites of the oxidized, sub-arc mantle wedge. Earth Planet. Sci. Lett., 69-86.

Pisarevsky, S.A., Natapov, L.M., Donskaya, T.V., Gladkochub, D.P. and Vernikovsky, V.A. (2008) Proterozoic Siberia: A promontory of Rodinia. Precambrian research, 66-76.

Poli, S. and Schmidt, M.W. (1998) The high-pressure stability of zoisite and phase relationships of zoisite-bearing assemblages. Contribution to Mineral Petrology, 162-175.

Pollack, H.N. and Chapman, D.S. (1977) On the regional variations of the heat flow, geotherms, and lithospheric thickness. Tectonophysics, 279 - 296.

Qi, Q., Taylor, L.A., Snyder, G.A., Clayton, R.N., Mayeda, T.K. and Sobolev, N.V. (1997) Detailed petrology and geochemistry of a rare corundum eclogite xenolith from Obnazhennaya, Yakutia. Russian Geology and Geophysics 38, 247-260.

Radu, I.-B. (2014) A petro-geochemical study of a cratonic eclogite suite - Roberts Victor mine (Kaapvaal, South Africa), Departement de Géologie, Laboratoire Magmas et Volcans. Université Jean Monnet de Saint Etienne, Université Blaise Pascal de Clermont Ferrand, p. 42.

Ragozin, A.L., Karimova, A.A., Litasov, K.D., Zedgenizov, D.A. and Shatsky, V.S. (2014) Water content in minerals of mantle xenoliths from the Udachnaya pipe kimberlites (Yakutia). Russian Geology and Geophysics, 428-442.

Rauch, M. and Keppler, H. (2002) Water solubility in orthopyroxene. Contribution to Mineral Petrology, 525-536.

Reguir, E.P., Chakhmouradian, A.R., Halden, N.M., Malkovets, V.G. and Yang, P. (2009) Major- and trace-element compositional variations of phlogopite from kimberlites and carbonatites as a petrogenetic indicator. Lithos, 372-384.

Reid, D.L. and Cooper, A.F. (1992) Oxygen and carbon isotope patterns in the Dicker Willem carbonatite complex, southern Namibia. Chemical Geology (Isotope Geoscience Section), 293-305.

Riches, A.J.V., Ickert, R.B., Pearson, D.G., Stern, R.A., Jackson, S.E., Ishikawa, A., Kjarsgaard, B.A. and Gurney, J. (2016) In situ oxygen-isotope, major-, and trace-element constraints on the metasomatic modification and crustal origin of a diamondiferous eclogite from Roberts Victor, Kaapvaal craton. Geochimica et Cosmochimica Acta 174, 345-359.

Riches, A.J.V., Liu, Y., Day, J.M.D., Spetsius, Z.V. and Taylor, L.A. (2010) Subducted oceanic crust as diamond hosts revealed by garnets of mantle xenoliths from Nyurbinskaya, Siberia. Lithos.

Rollinson, H. (1997) Eclogite xenoliths in west African kimberlites as residues from Archean granitoid crust formation. Letters to Nature 389, 173-176.

Rosen, O.M. (2002) Siberian craton - a fragment of a Paleoproterozoic supercontinent. Russian Journal of Earth Sciences 4, 103-119.

Rosen, O.M., Condie, K.C., Natapov, L.M. and Nozhkin, A.D. (1994) Archean and early proterozoic evolution of the Siberian craton: a preliminary assesment in: Condie, K.C. (Ed.), Archean Crustal Evolution. Elsevier, pp. 411-460.

Rosen, O.M., Manakov, A.V. and Serenko, V.P. (2005) Paleoproterozoic collisional system and diamondiferous lithospheric keel of the Yakutian kimberlite province. Russian Geology and Geophysics 46, 1237-1251.

Rossman, G.R. (1996) Studies of the OH in nominally anhydrous minerals. Phys Chem Minerals, 299-304.

Rossman, G.R. and Aines, D.R. (1991) The hydrous component in garnets: Grossular-hydrogrossular. American Mineralogist 76, 1153-1164.

Rubie, D.C., Frost, D.J., Mann, U., Asahara, Y., Nimmo, F., Tsuno, K., Kegler, P., Holzheid, A. and Palme, H. (2011) Heterogenous accretion, composition and core-mantle differentiation of the Earth. Earth and Plantetary Science Letters 301, 31-42.

Saleeby, J., Ducea, M. and Clemens-Knott, D. (2003) Production and loss of high-density batholitic root, southern Sierra Nevada, California. Tectonics 22, 1064.

Saussure, H.-B.d.-. (1779-1796) De la cité d'Aoste à Yvrée, in: Fauche (Neuchatel), S. (Ed.), Voyages dans les Alpes. Tome 2 / , précédés d'un Essai sur l'histoire naturelle des environs de Genève, par Horrace-Bénédict de Saussure,... p. 402.

Sautter, V., Harte, B. and Harris, J.W. (1998) Majorite destabilisation on decompression: constrains from natural samples on plume velocity. Mineralogical Magazine 62A, 1320-1321.

Sautter, V. and Harte, B. (1990) Diffusion gradients in an eclogite xenolith from the Roberts Victor kimberlite pipe: (2) kinetics and implications for petrogenesis. Contribution to Mineral Petrology, 637-649.

Sautter, V. and Harte, B. (1988) Diffusion gradients in an eclogite xenolith from the Roberts Victor kimberlite pipe; 1: mechanism and evolution of garnet exsolution in Al2O3-rich clinopyroxene. Journal of Petrology, 1325-1352.

Schmickler, B., Jacob, D.E. and Foley, S.F. (2004) Eclogite xenoliths from the Kuruman kimberlites, South Africa: geochemical fingerprinting of deep subduction and cumulate processes. Lithos, 173-207.

Schmidt, M.W. and Poli, S. (1994) The stability of lawsonite and zoisite at high pressures: Experiments in CASH to 92kbar and implications for the presence of hydrous phases in subducted lithosphere. Earth Planet. Sci. Lett., 105-118.

Schmitz, M.D. and Bowring, S.A. (2003) Ultrahigh-temperature metamorphism in the lower crust during Neoarchean Ventersdorp rifting and magmatism, Kaapvaal Craton, southern Africa. Geological Society of America Bulletin 115, 533-548.

Schulze, D.J., Harte, B., Facility, E.I.M., Page, Z.F., Valley, J., Channer, D.M.D. and Jaques, A.L. (2013) Anticorrelation between low d13C of eclogitic diamonds and high d18O of their coesite and garnet inclusions requires a subduction origin. Geology 41, 455-458.

Schulze, D.J., Valley, J. and Spicuzza, M.J. (2000) Coesite-sanidine eclogites from the Roberts Victor kimberlite, South Africa. Lithos, 23-32.

Schulze, D.J. (1989) Constraints on the abundance of eclogite in the upper mantle. Journal of Geophysical Research, 4205-4212.

Schulze, D.J. and Helmstaedt, H. (1988) Coesite-Sanidine eclogites from kimberlite: products of mantle fractionation or subduction? Journal of Geology 96, 435-443.

Shannon, R.D. and Prewitt, C.T. (1969) Effective ionic radii in oxides and fluorides. Acta Crystallogr. B25, 925-946.

Sharp, Z. (1990) A laser-based microanalytical method for the in situ determination of oxygen isotope ratios of silicates and oxides. Geochimica et Cosmochimica Acta 54, 1353-1357.

Sharp, Z., Atudorei, V. and Durakiewicz, T. (2001) A rapid method for determination of hydrogen and oxygen isotope ratios from water and hydrous minerals. Chemical Geology, 197-210.

Shatsky, V.S., Zedgenizov, D.A. and Ragozin, A.L. (2016) Evidence for a subduction component in the diamond-bearing mantle of the Siberian craton. Russian Geology and Geophysics 57, 111-126.

Shchipansky, A.A. (2012) Subduction geodynamics in Archean and formation of diamond-bearing lithospheric keels and early continental crust of cratons. Geotectonics 46, 122-141.

Shervais, J.W., Taylor, L.A., Lugmair, G.W., Clayton, R.N., Mayeda, T.K. and Korotev, R.L. (1988) Early Proterozoic oceanic crust and the evolution of subcontinental mantle: Eclogites and related rocks from southern Africa. Bulletin of the Geological Society of America 100, 411-423.

Shu, Q., Brey, G.P., Hoefer, H.E., Zhao, Z. and Pearson, D.G. (2016) Kyanite/corundum eclogites from the Kaapvaal Craton: subducted troctolites and layered gabbros from the Mid- to Early Archean. 2016.

Shu, Q., Brey, G.P., Gerdes, A. and Hoefer, H.E. (2014) Mantle eclogites and garnet pyroxenites - the meaning of the two point isochrones, Sm-Nd and Lu-Hf closure temperatures and the cooling of the subcratonic mantle. Earth Planet. Sci. Lett., 143-154.

Skogby, H., Janak, M. and Broska, I. (2016) Water incorporation in omphacite: concentrations and compositional relatios in ultrahigh-pressure eclogites from Phorje, Eastern Alps. Eur. J. Mineral. 28, 631-639.

Skogby, H., Bell, D.R. and Rossman, G.R. (1990) Hydroxide in pyroxene: Variations in the natural environment. American Mineralogist 75, 764-774.

Smelov, A.P. and Zaitsev, A.I. (2013) The Age and Localization of Kimberlite Magmatism in the Yakutian Kimberlite Province: Constraints from Isotope Geochronology - An overview, in: Pearson, D.G., Grütter, H.S., Harris, J.W., Kjarsgaard, B.A., O'Brien, H., Chalapathi Rao, N.V., Sparks, S. (Eds.), Proceedings of 10th International Kimberlite Conference. Spinger, New Delhi, pp. 225-234.

Smith, B., Baziotis, I., Carmody, L., Liu, Y., Taylor, H.P., Pokhilenko, N.P. and Pokhilenko, L. (2012) The subcontinental lithospheric mantle of the NE Siberian craton: peridotites from Obnazhennaya, in: America, G.S.o. (Ed.), GSA Annual Meeting & Exposition, Charlotte, North Carolina, USA, p. 587.

Smith, C.B., Allsop, H.L., Kramers, J.D. and Roddick, J.C. (1985) Emplacement ages of Jurassic-Cretaceous South African kimberlites by the Rb-Sr method on phlogopite and whole-rock samples. Transactions of the Geological Society of South Africa 88, 249-266.

Smyth, J.R., Bell, D.R. and Rossman, G.R. (1991) Incorporation of hydroxyl in upper-mantle clinopyroxenes. Letters to Nature, 732-734.

Smyth, J.R., Caporuscio, F.A. and McCormick, T.C. (1989) Mantle eclogites: evidence of igneous fractionation in the mantle. Earth Planet. Sci. Lett., 133-141.

Smyth, J.R. and Caporuscio, F.A. (1984) Petrology of a suite of eclogite inclusions from the Bobbejaan kimberlite: II. Primary phase compositions and origin, in: Kornprobst, J. (Ed.), Kimberlites II: the mantle and crust-mantle relationship. Elsevier, Amsterdam, pp. 121-131.

Snyder, G.A., Jerde, E.A., Taylor, L.A., Halliday, A.N., Sobolev, V.N. and Sobolev, N.V. (1993) Nd and Sr isotopes from diamondiferous eclogites, Udachnaya Kimberlite Pipe, Yakutia, Siberia: Evidence of differentiation in the early Earth? Earth Planet. Sci. Lett., 91-100.

Sobolev, N.V.J., Kuznetsova, I.K. and Zyuzin, N.I. (1968) The petrology of grospydite xenoliths from the Zagadochnaya kimberlite pipe in Yakutia. Journal of Petrology 9, 253-280.

Spengler, D., Obata, M., Hirajima, T., Ottolini, L., Ohfuji, H., Tamura, A. and Arai, S. (2012) Exsolution of garnet and clinopyroxene from High-Al pyroxenes in Xugou peridotite, Eastern China. Journal of Petrology 53, 1477-1504.

Sundvall, R. and Stalder, R. (2011) Water in upper mantle pyroxene megacrysts and xenocrysts: A survey study. American Mineralogist 96, 1215-1227.

Sundvall, R., Skogby, H. and Stalder, R. (2008) Dehydration-hydration mechanisms in sythetic Fe-poor diopside. Eur. J. Mineral. 21, 17-26.

Taylor, L.A. and Neal, C.R. (1989) Eclogites with oceanic crustal and mantle signatures from the Bellsbank kimberlite, South Africa, Part I: Mineralogy, Petrography and whole rock chemistry. J. Geol., 551-567.

Taylor, L.A., Snyder, G.A., Keller, R., Remley, D.A., Anand, M., Wiesli, R., Valley, J. and Sobolev, N.V. (2003) Petrogenesis of group A eclogites and websterites: evidence from the Obnazhennaya kimberlite, Yakutia. Contribution to Mineral Petrology, 424-443.

Terry, M.P., Bromiley, G.D. and Robinson, P. (2003) Determination of equilibrium water content and composition of omphacitic pyroxene in a UHP kyanite-eclogite, Western Norway, EGS-AGU-EUG Joint Assembly. EGU, Nice.

van Achterbergh, E., Ryan, C.G., Jackson, S.E. and Griffin, W. (2001) Data reduction software for LA-ICP-MS. In Laser ablation-ICPMS in the earth science, in: Sylvester, P. (Ed.), Mineralogical Association of Canada, pp. 239-243.

Van der Meer, Q.H.A., Klaver, M., Waight, T.E. and Davies, G.R. (2013) The provenance of sub-cratonic mantle beneath the Limpopo Mobile Belt (South Africa). Lithos, 90-104.

van Hunen, J. and Moyen, J.-F. (2012) Archean subduction: Fact or Fiction? Annual Review of Earth and Planetary Sciences 40, 195-219.

van Kranendonk, M.J., Collins, W.J., Hickman, A. and Pawley, M.J. (2004) Critical tests of vertical vs. horizontal tectonic models for the Archean East Pilbara Granite-Greenstone Terrane, Pilbara Craton, Western Australia. Precambrian research 131, 173-211.

van Reenen, D.D., Roering, C., Ashwal, L.D. and de Wit, M.J. (1992) Regional geological setting of the Limpopo Belt. Precambrian research 55, 1-5.

Viljoen, K.S., Schulze, D.J. and Quadling, A.G. (2005) Contrasting Group I and Group II Eclogite Xenolith Petrogenesis: Petrological, Trace Element and Isotopic Evidence from Eclogite, Garnet-Websterite and Alkremite Xenoliths in the Kaalvallei Kimberlite, South Africa. Journal of Petrology 46, 2059-2090.

Vogel, D.E. and Garlick, G.D. (1970) Oxygen-isotope ratios in metamorphic eclogites. Contribution to Mineral Petrology 28, 183-191.

Wang, H., van Hunen, J. and Pearson, D.G. (2016) Making Archean cratonic roots by lateral compression: A two stage thickening and stabilization model. Tectonophysics.

Wang, S.-J., Teng, F.-Z., Rudnick, R.L. and Li, S.-G. (2015) Magnesium isotope evidence for a recycled origin of cratonic eclogites. Geology 43, 1071-1074.

Wang, S.-J., Fang-Zheng, T., Li, S.-G. and Hong, J.-A. (2014) Magnesium isotopic systematics of mafic rocks during continental subduction. Geochimica et Cosmochimica Acta 143, 34-48.

Wang, S.-J., Teng, F.-Z., Williams, H.M. and Li, S.-G. (2012) Magnesium isotopic variations in cratonic eclogites: Origin and implications. Earth and Planetary Science Letters, 219-226.

Watson, K.D. and Morton, D.M. (1969) Eclogite inclusions in kimberlite pipes at garnet ridge, northeastern Arizona. American Mineralogist 54.

Werner, A.G. (1817) Abraham Gottlob Werner's lektes Mineral-System, aus dessen Nachlasse aus oberbergamtliche Anordnung herausgegeben und mit Erläuterungen versehen, in: Craz, G., Carl Gerold (Ed.). Gerlach, Freyberg and Vienna, pp. 33-34.

Wiggers de Vries, D.F., Pearson, D.G., Bulanova, G.P., Smelov, A.P., Pavlushin, A.D. and Davies, G.R. (2013) Re-Os dating of sulphide inclusions zonally distributed in single Yakutian diamonds: Evidence for multiple episodes of Proterozoic formation and protracted timescales of diamond growth. Geochimica et Cosmochimica Acta 120, 363-394.

Withers, A.C., Bureau, H., Raepsaet, C. and Hirschmann, M.M. (2012) Calibration of infrared spectroscopy by elastic recoil detection analysis of H in synthetic olivine. Chemical Geology, 92-98.

Withers, A.C., Wood, B.J. and Carroll, M.R. (1998) The OH content of pyrope at high pressure. Chemical Geology, 161-171.

Wood, B.J. and Banno, S. (1973) Garnet-orthopyroxene and orthopyroxene-clinopyroxene relationships in simple and complex systems. Contribution to Mineral Petrology, 109-124.

Xia, Q.-K., Hao, Y., Li, P., Deloule, E., Coltorti, M., Dallai, L., Yang, X.-Z. and Feng, M. (2010) Low water content in the Cenozoic lithospheric mantle beneath the eastern part of the North China Craton. Journal of Geophysical Research 115.

Xia, Q.-K., Dallai, L. and Deloule, E. (2004) Oxygen and hydrogen isotope heterogeneity of clinopyroxene megacrysts from Nushan Volcano, SE China. Chemical Geology, 137-151.

Xu, W., Liu, X., Wang, Q., Lin, J. and Wang, D. (2004) Garnet exsolution in garnet clinopyroxenite and clinopyroxenite xenoliths in early Cretaceous intrusions from the Xuzhou region, eastern China. Mineralogical Magazine 68, 443-453.

Yang, X., Keppler, H. and Li, Y. (2016) Molecular hydrogen in mantle minerals. Geochemical Perspectives Letters, 160-168.

Yang, X.-Z., Xia, Q.-K., Deloule, E., Dallai, L., Fan, Q.-C. and Feng, M. (2008) Water in minerals of the continental lithospheric mantle and overlying lower crust: A comparative study of peridotite and granulite xenoliths fril the North China Craton. Chemical Geology, 33—45.

Zegers, T.E. and van Keken, P.E. (2001) Middle Archean continent formation by crustal delamination. Geology 29, 1083-1086.

Zhao, S., Nee, P., Green, H.W. and Dobrzhinetskaya, L.F. (2011) Ca-Eskola component in clinopyroxene: Experimental studies at high pressure and high temperatures in muntianvil apparatus. Earth Planet. Sci. Lett., 517-524

Zheng, Y.-F. (1993) Calculation of oxygen isotope fractionation in anhydrous silicate melts. Geochimica et Cosmochimica Acta 57, 1079-1091.

ACKNOWLEDGEMENTS

ACKNOWLEDGEMENTS

Words would not suffice if I tried to sum up my PhD experience standing behind this manuscript, however, there are many people without whom I wouldn't have reached this point and my work would have been significantly poorer.

I would like to start by thanking my supervisors, Prof. Jean-Yves Cottin, Prof. Chris Harris and Dr. Bertrand Moine, who have always been there to answer my questions, or to ask me key questions, always understanding and encouraging. Their different styles and approaches have in turn kicked in at the right time, accommodating my needs and making it both possible and easy for me to work at two different universities, in two different countries, on two different continents, in two different hemispheres. I am also grateful to Anne-Marie Avarello, without whom none of my travelling would have gone so smoothly. Furthermore, many thanks go to Gabi Costin, who encouraged my curiosity and ambition in tackling with metamorphic petrology, who first introduced me to mantle eclogites, whose efforts have built up the amazing eclogites collection I have been working on and whose experience helped me have high quality major element compositions of numerous samples.

Keeping this last thought in mind, I would like to thank Jean-Luc Devidal for helping me obtain top notch major and trace elements compositions and to Maud Boyet for her expertise and patience in initiating me in working with radiogenic isotopes. None of this would have been possible without the work of Colette, who made irreproachable thin sections and grain mounts and put up with my many requests.

On a different note I would like to thank all the many people who have helped me throughout my thesis even if in a less obvious way and most probably without even knowing it. I would like to thank Sherissa Roopnarain for teaching me patience in handling oxygen isotope analyses and for all her encouragements; I am grateful to June Chevet for being a friendly ear I could always come and talk to; I would like to thank Jean-François Moyen for encouraging me in unexpected moments. I am grateful to Prof. Acad. Nicolae Anastasiu for helping me develop my analytical

thinking and to learn the importance of doing your work properly and to learn from your mistakes. I am grateful to Prof. Gyuri Ilinca who inspired my passion for mineralogy, who encouraged me from the beginning and whom I appreciate greatly. A huge amount of gratitude, which I find hard to put into words, goes to Prof. Marin Şeclăman, who is an inspiration to me, both scientifically and as a person, maybe the greatest mind I have ever met. I want to thank him for his appreciation and by this motivating me to strive for more. I would like to very much thank the person who, through his passion for fieldwork and the intricate relation between chemistry and mineral properties, involuntarily made me a geologist, Oscar Edelstein. I would like to thank my mom, Livia Ricu, whom everyone thinks is the true responsible for my interest in Geology due to her passion for plate tectonics, field geology and mineralogy. I thank all my family for being supportive and always there for me, to my friends for being such good friends, to Emma for her encouragements, to Simon Schorn for strengthening me, contaminating me with his 'workaholism' and putting up with me, to Lucile for being so in sync with me, to Matthew Mayne for being such a good influence, to Simon Couzinié and Mélodie-Neige for sharing my struggles, to Gautier for being Batman and to everyone else I may be forgetting.

You all have made this better for me and for that I thank you very much!